2014

Modelling of Biomass Gasification Integrated with a Solid Oxide Fuel Cell System

Wayne Doherty
Technological University Dublin, wayne.doherty@tudublin.ie

Funder: Technological University Dublin

Modelling of Biomass Gasification Integrated with a Solid Oxide Fuel Cell System

Wayne Doherty BEng (Hons)

Doctor of Philosophy (PhD)

Dublin Institute of Technology

Supervisors: Dr. Anthony Reynolds and

Prof. David Kennedy

School of Mechanical and Design Engineering

April 2014

ABSTRACT

Biomass is of major interest as a renewable energy source in the context of climate change and energy security. Traditional biomass conversion technologies achieve low electrical efficiencies. Biomass gasification (BG) coupled with fuel cells offer higher efficiencies. Gasification is a process in which a carbonaceous fuel is converted to a combustible gas. It occurs when a controlled amount of oxidant is reacted at high temperatures with available carbon in a fuel within a gasifier. Two technologies (circulating fluidised bed air gasification and dual fluidised bed steam gasification) were modelled. Solid oxide fuel cells (SOFCs) are well suited to integration with gasification due to their high operating temperature and fuel flexibility. They convert the chemical energy contained in a fuel directly to electrical energy via electrochemical reactions, making them highly efficient. The tubular SOFC configuration was selected. The main aim of the research work was to investigate the feasibility of BG-SOFC systems through thermodynamic modelling and economic analyses. Standalone models of the gasification technologies and the SOFC were developed and validated. These models were integrated considering gas cleaning, heat recovery and balance of plant. An engineering economic model was developed and applied to determine the commercial viability of the BG-SOFC systems. The results indicated that these systems are attractive with regard to their operating efficiency; however, they are not yet commercially viable. Capital costs and biomass fuel prices must fall dramatically if these systems are to become competitive. A cathode recycle or electric heater for syngas preheating is not attractive. Thermal integration between the gasifier and fuel cell is desirable. Lowering the syngas preheat temperature is highly recommended. High temperature syngas cleaning reduces plant complexity and improves performance. Gasification air preheating is more attractive than gasification steam superheating.

In memory of my grandmother, Eileen Gartlan (Pembroke)

DECLARATION

I certify that this thesis which I now submit for examination for the award of Doctor of Philosophy (PhD), is entirely my own work and has not been taken from the work of others, save and to the extent that such work has been cited and acknowledged within the text of my work.

This thesis was prepared according to the regulations for postgraduate study by research of the Dublin Institute of Technology and has not been submitted in whole or in part for another award in any Institute.

The work reported on in this thesis conforms to the principles and requirements of the Institute's guidelines for ethics in research.

The Institute has permission to keep, lend or copy this thesis in whole or in part, on condition that any such use of the material of the thesis be duly acknowledged.

Signature _____ Date _____

Candidate

ACKNOWLEDGEMENTS

Firstly, I wish to express my gratitude to my supervisors Dr. Anthony Reynolds and Prof. David Kennedy for their expert guidance and patience throughout this research work. Dr. Reynolds, I am eternally grateful for your belief in my abilities and for helping me to secure funding for this research project; without your support this work would not have been possible.

My appreciation also goes to Dr. Marek Rebow (Head of Research of the College of Engineering & Built Environment) who was always there to lend a helping hand. It was definitely a great advantage to have my desk located in the same office as Dr. Rebow.

Thanks to all of my colleagues in DIT; fellow postgraduates, laboratory technicians: Mr. James Mahon and Mr. Derek Ritchie, IT support: Mr. Simon Farrell, Mr. Michael Faherty and Mr. Allen Brereton, and to all of the undergraduates that I've taught over the years, you made my time at DIT very enjoyable. I would also like to thank my teachers and lecturers throughout my education.

I wish to acknowledge the work of my examiners: Dr. Tim Prescott (confirmation exam), Prof. Tobias Pröll (external examiner) and Dr. Anthony Betts (internal examiner).

Finally, I wish to thank my parents and family; without their support this thesis would not have been possible. I would like to give special thanks to my wife Michelle for her patience and encouragement. She also proof read this thesis and many of the publications. I am delighted to say that you no longer have to tolerate the anti-social working hours.

This research work was funded under the Dublin Institute of Technology ABBEST scholarship programme.

ABBREVIATIONS AND SYMBOLS

Roman letters

A	Constant used in Eq. 5.6 and 5.7
AFC	Alkaline fuel cell
ar	As received
B	Constant used in Eq. 5.7
BFB	Bubbling fluidised bed
BG	Biomass gasification
BG-SOFC	Biomass gasification-solid oxide fuel cell
CAP	Common agricultural policy
CapEx	Capital expenditure, €/kWe or €/MWe or €
CCGT	Combined cycle gas turbine
CEPCI	Chemical Engineering Plant Cost Index
CER	Commission for Energy Regulation
CFB	Circulating fluidised bed
CF_{el}	Electricity capacity factor
CF_{heat}	Heat capacity factor
CGE	Cold gas efficiency
CHP	Combined heat and power
CoE	Cost of electricity, €/MWh
c_p	Specific heat capacity, kJ/kg K
CPI	Consumer price index
CZ	Combustion zone
D	Diffusion coefficient, m^2/s
daf	Dry and ash free

$D_{An(eff)}$	Anode effective diffusion coefficient, m^2/s
db	Dry basis
$D_{Cat(eff)}$	Cathode effective diffusion coefficient, m^2/s
DFB	Dual fluidised bed
D_m	SOFC mean diameter, m
DR	Discount rate
E	Activation energy, J/mol
EPA	Environmental Protection Agency
ER	Equivalence ratio
ESB	Electricity Supply Board
ESP	Electrostatic precipitator
ETS	Emissions trading scheme
EVD	Electrochemical vapour deposition
F	Faraday constant, C/mol
FGD	Flue gas desulphurisation
FICFB	Fast internally circulating fluidised bed
FT	Fischer-Tropsch
GEC	Gross electricity consumption
GFC	Gross final consumption
GHG	Greenhouse gas
GT	Gas turbine
GZ	Gasification zone
$\bar{h}_{f,i}$	Molar enthalpy of formation of gaseous component *i*, J/mol
HHV	Higher heating value, kJ/kg or MJ/kg
HRSG	Heat recovery steam generator

HV	Heating value, kJ/kg
I	Current, A
IEA	International Energy Agency
IGCC	Integrated gasification combined cycle
j	Current density, A/m^2 or mA/cm^2
k	Pre-exponential factor in Eq. 5.10 and 5.11, A/m^2
ktoe	kilotonne of oil equivalent
$LCoE$	Levelised cost of electricity, €/MWh
LHV	Lower heating value, kJ/kg or MJ/kg
LHV_{fuel}	Lower heating value of input fuel gas to SOFC, kJ/kmol
M	Molecular weight, kg/kmol
m	Slope in Eq. 5.10 and 5.11
$\dot{m}$	Mass flow rate, kg/s
MBM	Meat and bone meal
MCFC	Molten carbonate fuel cell
MSW	Municipal solid waste
MWe	Megawatt electrical
MWth	Megawatt thermal
n	Molar flow rate, kmol/s
NO_x	Nitrogen oxides
NPV	Net present value, €
NREAP	National renewable energy action plan
O&M	Operating and maintenance costs, €
ORC	Organic Rankine cycle
P	Pressure, atm

PAFC	Phosphoric acid fuel cell
$P_{biomass}$	Biomass input power, kW
P_{comp}	Electrical power requirement of compressors, kW
PCRW	Post consumer recovered wood
$P_{el,AC}$	Electrical AC power, kW
PEMFC	Polymer electrolyte membrane fuel cell
P_i	Partial pressure of gaseous component *i*, bar
pp	Percentage points
$P_{parasitic}$	Total parasitic power, kW
ppmv	Volumetric parts per million
ppmw	Parts per million by weight
P_{SOFC}	SOFC operating pressure, Pa
PV_{costs}	Present value of net costs, €
PV_{el}	Present value of electricity output, MWh
P^0	Reference pressure, bar
Q	Maximum recoverable heat, kW
r	Electrode pore radius, m
R_{Act}	Specific resistance, Ω m^2
REFIT	Renewable energy feed in tariff
RES-E	Electricity from renewable energy sources
RES-H	Heat from renewable energy sources
RES-T	Transport fuels from renewable energy sources
R_g	Universal gas constant, J/mol K
RME	Rapeseed oil methyl ester
R_z	Net revenue over time period, €

SCR	Selective catalytic reduction
SEAI	Sustainable Energy Authority of Ireland
$\bar{s}_i$	Molar entropy of gaseous component *i*, J/mol K
SNG	Synthetic natural gas
SOFC	Solid oxide fuel cell
SO_x	Sulphur oxides
SPGI	Siemens Power Generation Inc.
SRC	Short rotation coppice
ST	Steam turbine
STBR	Steam to biomass ratio
STCR	Steam to carbon ratio
T	Temperature, °C or K
t	SOFC component thickness, m
TPER	Total primary energy requirement, ktoe
U_a	Air utilisation factor
U_f	Fuel utilisation factor
V	Voltage, V
v	Fuller diffusion volume
wb	Wet basis
w_{Int}	Interconnection width, m
y_i	Molar fraction of gaseous component *i*
YSZ	Yttria stabilised zirconia
y^0_i	Molar fraction of gaseous component *i* in bulk flow
z	Time period
ZnO	Zinc oxide

Greek letters

$\Delta\bar{g}_f$	Molar Gibbs free energy of formation, J/mol
$\Delta\bar{h}_f$	Molar enthalpy of formation, J/mol
$\Delta\bar{s}$	Molar entropy, J/mol K
ΔT	Temperature difference
δ_{O2}	Constant in Eq. 5.13
ε	Electrode porosity
η	Efficiency
$\eta_{CHP,net}$	Plant net AC CHP efficiency (LHV basis)
$\eta_{el,net}$	Plant net AC electrical efficiency (LHV basis)
$\eta_{SOFC,gross}$	Gross SOFC AC efficiency (LHV basis)
$\eta_{SOFC,net}$	Net SOFC AC efficiency (LHV basis)
ξ	Electrode tortuosity
ρ	Resistivity, Ω m

Subscripts

A	Anode
a	Air
Act	Activation
avg	Average
C	Cathode
Conc	Concentration
E	Electrolyte
(eff)	Effective

flue	Flue gas
fuel	Input fuel
g	Gasification
gas	Gas
i	Gaseous component
ideal	Ideal or maximum
Int	Interconnection
K	Knudsen
k	Second gaseous component in a binary mixture
N	Nernst
Ohm	Ohmic
op	Operating

TABLE OF CONTENTS

TABLE OF FIGURES

TABLE OF TABLES

PUBLICATIONS

Peer reviewed journal articles

1. W. Doherty, A. Reynolds, D. Kennedy. Process Simulation of Biomass Gasification Integrated with a Solid Oxide Fuel Cell Stack. *Journal of Power Sources* (under review).
2. W. Doherty, A. Reynolds, D. Kennedy. Simulation of a Tubular Solid Oxide Fuel Cell Stack Operating on Biomass Syngas Using Aspen Plus. *Journal of The Electrochemical Society*. 2010;157:B975-B981.
3. W. Doherty, A. Reynolds, D. Kennedy. Computer Simulation of a Biomass Gasification-Solid Oxide Fuel Cell Power System Using Aspen Plus. *Energy*. 2010;35:4545-4555.
4. W. Doherty, A. Reynolds, D. Kennedy. The Effect of Air Preheating in a Biomass CFB Gasifier Using ASPEN Plus Simulation. *Biomass and Bioenergy*. 2009;33:1158-1167.

Peer reviewed book chapter

5. W. Doherty, A. Reynolds, D. Kennedy. Aspen Plus Simulation of Biomass Gasification in a Steam Blown Dual Fluidised Bed. Book Chapter: *Materials and processes for energy: communicating current research and technological developments*, A. Méndez-Vilas (Ed.), Formatex Research Centre, 2013.

Peer reviewed conference articles

6. W. Doherty, A. Reynolds, D. Kennedy. Computer Simulation of a Biomass Gasification-Solid Oxide Fuel Cell Power System Using Aspen Plus. *Proc. 3rd International Conference on Sustainable Energy & Environmental Protection*, Dublin, Ireland, 2009.

7. W. Doherty, A. Reynolds, D. Kennedy. Modelling and Simulation of a Biomass Gasification-Solid Oxide Fuel Cell Combined Heat and Power Plant Using Aspen Plus. *Proc. 22nd International Conference on Efficiency, Cost, Optimization, Simulation and Environmental Impact of Energy Systems*, Foz Do Iguaçu, Brazil, 2009.

8. W. Doherty, A. Reynolds, D. Kennedy. Simulation of a Tubular Solid Oxide Fuel Cell Stack Operating on Biomass Syn-gas Using Aspen Plus. *ECS Transactions*. 2009;25:1321-1330 (presented at: *216th ECS Meeting: Solid Oxide Fuel Cells, Eleventh International Symposium (SOFC-XI)*, Vienna, Austria, 2009).

9. W. Doherty, A. Reynolds, D. Kennedy. Simulation of a Circulating Fluidised Bed Biomass Gasifier Using ASPEN Plus – A Performance Analysis. *Proc. 21st International Conference on Efficiency, Cost, Optimization, Simulation and Environmental Impact of Energy Systems*, A. Ziebik, Z. Kolenda, and W. Stanek (Ed.), Krakow, Poland, 2008, 1241-1248.

Abstract: poster presentation

10. W. Doherty, A. Reynolds, D. Kennedy. Techno-Economic Modelling of Biomass Gasification Integrated with Advanced Power Systems. *Proc. Sir Bernard Crossland Symposium*, Limerick, Ireland, 2008.

11. W. Doherty, A. Reynolds, D. Kennedy. Simulation and Parametric Analyses of a Tubular Solid Oxide Fuel Cell Stack Using Aspen Plus. *Proc. Fuel Cells Science & Technology*, Copenhagen, Denmark, 2008.

12. W. Doherty, A. Reynolds, D. Kennedy. Techno-Economic Modelling of Biomass Gasification Integrated with Advanced Power Systems. *Proc. Irish Society for Scientific and Engineering Computation Symposium*, Dublin, Ireland, 2007.

1 INTRODUCTION

1.1 Chapter Introduction

This chapter provides an introduction to the thesis. Firstly, some background information is presented on biomass and its conversion. Secondly, the motivation and reasons for conducting the research are given. Then the research aim, objectives and the methodology for achieving them are described. Finally, the contribution to knowledge and significance of the work is highlighted and then the structure of the thesis is discussed briefly.

1.2 Background and Motivation for Research

1.2.1 Background

Biomass is of major interest as a renewable energy source in the context of both climate change mitigation and energy security. Biomass energy can be defined as the energy contained in plants and non-fossil organic matter. The most commonly used form of biomass energy is wood, which also includes wood wastes like sawdust, forest residues and energy crops such as willow. The efficient utilisation of biomass resources is of utmost importance if it is to replace a significant proportion of fossil fuels. Traditional biomass combustion based technologies achieve low electrical efficiencies at small scale (20-25%) and therefore cannot compete with fossil fuels. Scale is limited by biomass supply logistics. Biomass gasification (BG) coupled with advanced power generation systems such as gas turbines or fuel cells offer much higher efficiencies. Reported electrical efficiencies for biomass gasification-solid oxide fuel cell (BG-SOFC) systems range from 23-50% [1]. These systems offer highly efficient renewable energy, are modular in nature making them ideal for decentralised combined heat and

power (CHP) applications and as a result have recently gained much attention [2-11]. The two technologies (BG and SOFC) are well matched as they are thermally compatible (similar operating temperatures ~800 to 1,000 °C) and thus offer many integration options. Figure 1.1 displays a simplified block diagram of a BG-SOFC CHP system. These plants are still being developed and there is a need for accurate computer simulation models that can aid in the design and understanding of these systems. Moreover, BG-SOFC system models should have short computational times and be easily calibrated to match the continuous and rapid technological advances in the field.

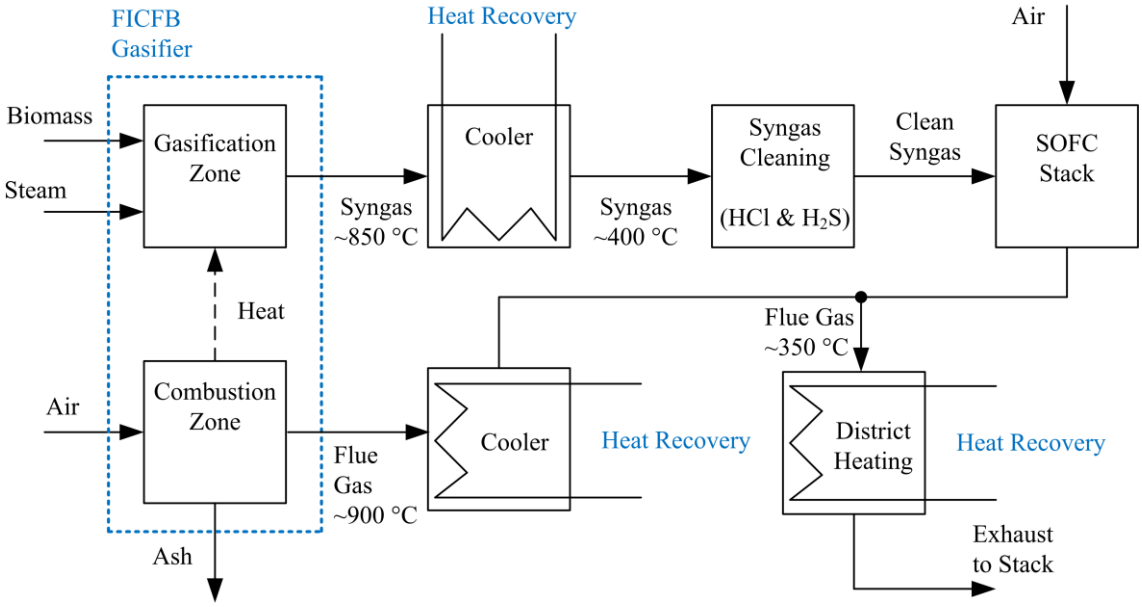

Figure 1.1 Simplified block diagram of a BG-SOFC CHP system

Stoichiometric combustion occurs when all the carbon in a fuel is converted to carbon dioxide (CO_2) and there is no excess oxygen (O_2). The basis of gasification is to supply less oxidant than would be required for stoichiometric combustion of a fuel. Gasification is a thermochemical process in which a carbonaceous fuel is converted to a combustible gas. This combustible gas is known as syngas (from synthetic or synthesis gas) and consists of hydrogen (H_2), carbon monoxide (CO), methane (CH_4), CO_2, water

vapour (H_2O), nitrogen (N_2), higher hydrocarbons and impurities such as tars, ammonia (NH_3), hydrogen sulphide (H_2S) and hydrogen chloride (HCl). The process occurs when a controlled amount of oxidant (e.g. pure O_2, air, steam) is reacted at high temperatures with available carbon in a fuel within a gasifier. Air gasification produces a syngas with low energy content, around 4-7 MJ/m^3 higher heating value (HHV), while pure O_2 and steam blown processes result in a syngas with a heating value in the range of 10-18 MJ/m^3 (HHV) [12]. Gasification with pure O_2 is not practical for BG due to prohibitively high costs for O_2 production using current commercial technology (cryogenic air separation). The gasification process may be split into steps: drying (at 100-200 °C), pyrolysis (at 200-500 °C), gasification and combustion. These steps are frequently modelled in series but there is no sharp boundary dividing them and they often overlap [13]. Combustion is necessary to supply the heat required for the endothermic gasification reactions.

Fuel cells convert the chemical energy contained in a fuel directly to electrical energy via electrochemical reactions, making them a highly efficient energy conversion device. SOFCs can utilise a wide spectrum of fuels (natural gas, coal and biomass syngas, liquid fuels including methanol and kerosene) due to their high operating temperature. It has been shown that CO-rich gases (i.e. biomass and coal syngas) are attractive and useful fuels for SOFCs exhibiting excellent power generation characteristics comparable to those for H_2-based fuels [14].

1.2.2 Motivation for Research

The main reasons for conducting this research were environmental considerations, energy security and to improve conversion efficiency (make biomass more attractive for power generation).

Climate change caused by global warming is a critical issue. The consensus among the scientific community is that it is caused by the release of CO_2 and hydrocarbons, so called greenhouse gases (GHGs), into the atmosphere. The International Energy Agency (IEA) reports that the energy sector accounts for two thirds of global GHG emissions [15]. It predicts that energy related CO_2 emission will increase 20% by 2035 eventually leading to an average temperature rise of 3.6 °C (well above the 2 °C target). The electricity sector accounts for ~40% of CO_2 emissions [15]. These figures highlight the importance of research into alternative power generation technologies such as BG-SOFC systems. Gasification offers potential for the generation of electricity, heat and the production of hydrocarbon liquids via Fischer-Tropsch synthesis, in a manner that allows environmental impacts to be kept to a minimum. Emissions can be reduced because the fuel input has been converted to gaseous form, which makes it possible to remove the contaminants that cause the emissions prior to combustion. It is possible to incorporate CO_2 capture into gasification systems; however, because these technologies are relatively new, they would increase costs substantially. For BG, CO_2 emission is of no great concern because it is considered a low carbon technology. The CO_2 released upon burning the syngas will be absorbed by growing new biomass. There will be some CO_2 emission due to planting, harvesting, processing and transporting the biomass, hence the term low carbon as opposed to carbon neutral.

Energy security is of utmost importance and is vital for any country's continued economic growth. Currently, Ireland imports 90% of its energy [16]. This high dependency on energy imports puts the country at risk. Rising energy demand, instability in the Middle East and decreasing fossil fuel supplies could result in dramatic increases in oil and gas prices. The IEA forecast an increase in global energy demand of

one third from 2011-2035, driven by emerging economies (China, India, Southeast Asia and the Middle East). The electricity sector will account for over half of this increase [15]. Biomass gasification coupled with other renewable energy options would cut Ireland's dependency on imported energy and would help to ensure energy security.

Currently, energy is primarily recovered from biomass through combustion (either mono or co-firing) in a boiler to generate steam which is then used to generate electricity by means of a steam turbine. Co-firing of biomass in peat stations is one of the Irish government's initiatives. The efficiency of these conventional direct combustion plants is limited and therefore they cannot compete with fossil fuels. Gasification is a more energy efficient method than conventional combustion in a boiler. Gasification will make the utilisation of biomass for electricity generation a more feasible option. Energy efficiency improvements could mitigate high energy costs, energy security and environmental concerns [15].

In addition to the main reasons presented above for carrying out this research, in the author's opinion, the Irish government has put too much focus on wind electricity generation (over 4,600 MWe planned for 2020 [17]) and not enough on other sources such as biomass (only 153 MWe planned for 2020 [17]), ocean, etc. This policy is difficult to justify as wind generation requires expensive backup natural gas peaking power plants and energy storage systems due to its intermittence and unpredictability. In contrast, biomass is capable of generating dispatchable base load electricity and Ireland has exceptional potential for bioenergy due to its favourable growth climate. The following is a list of some of the advantages/benefits related to the exploitation of biomass as an energy resource:

- Biomass is a sustainable resource unlike finite fossil fuel resources.
- Biomass fuels are environmentally beneficial because they are considered low carbon fuels and lead to reductions in other harmful emissions (e.g. nitrogen oxides and sulphur oxides). In addition, their utilisation lowers CH_4 emission, which would have resulted from the natural decomposition of organic wastes.
- Economic development through the creation of green jobs (biomass must be grown, harvested, processed, transported to the end user and converted to a useful form of energy). Biomass utilisation presents new opportunities for farmers, such as the growing of energy crops.
- Biomass is an indigenous resource and thus reduces dependence on imported energy and increases energy security.
- The exploitation of biomass can contribute to all three types of renewable energy targets, i.e. heat, electricity and transport.
- Biomass usage contributes to waste management, which in Ireland is becoming an increasing problem.
- In terms of renewable electricity biomass is capable of generating dispatchable base load electricity, in contrast to highly unpredictable wind generated electricity.

Finally, BG-SOFC CHP systems satisfy many EU and national objectives including increasing the contribution of renewable energy, improving energy efficiency, security of supply, raising the level of CHP and reduction of GHG emissions.

1.3 Aim and Objectives

The aim of this research work was to investigate the feasibility of BG-SOFC CHP systems through thermodynamic modelling and economic analyses. Within this aim there are a number of objectives:

- To determine the state of the art of biomass gasification, SOFCs and syngas conditioning (cleaning and reforming) equipment.
- To review Irish and EU energy policy and energy trends in Ireland.
- To assess Ireland's biomass resources.
- To establish the current capabilities and limitations of process simulation.
- To develop process simulation models and investigate the effect of important operating parameters and integration options at various scales.
- To perform economic analyses of the modelled systems.
- To analyse the results and draw conclusions as to the feasibility of the investigated systems and make recommendations.

1.4 Methodology

The methodology employed to achieve the research aim and objectives described above was as follows:

- The available literature on pertinent technologies, energy trends, energy policy and biomass resources was reviewed.
- The BG-SOFC systems were modelled utilising the process simulation software package Aspen Plus.

- Standalone technical models of various biomass gasifiers and the chosen SOFC technology were developed.
- The standalone technical models were validated against actual plant or experimental data.
- Sensitivity analyses using the standalone technical models were conducted to investigate the influence of the main operating parameters. For example, investigation of the effect of varying the level of moisture contained in the biomass fuel on gasifier performance.
- The standalone models were integrated considering syngas conditioning, heat recovery and balance of plant components and various system configurations were evaluated (e.g. thermal integration between the gasifier and SOFC).
- Options to improve combined system performance were identified and explored.
- Sensitivity analyses of the main operating parameters were carried out for the best performing combined system configuration.
- Plant scale up was investigated.
- A spreadsheet based engineering economic model for the BG-SOFC systems was developed.
- Sensitivity analyses of engineering economic model inputs were conducted.

1.5 Knowledge Contribution and Significance

There is a lack of research on integrated gasification fuel cell systems. To date, the bulk of modelling work has focussed on biomass gasification or fuel cells alone. This research project aims to address this knowledge gap. New standalone technical models of the fast internally circulating fluidised bed (FICFB) and circulating fluidised bed (CFB) biomass gasifiers and tubular SOFC have been developed. No Aspen Plus

model of the FICFB biomass gasifier could be found in the literature; therefore, the model conceived in this work is original. Novel combined system (BG-SOFC) models were developed and extensive sensitivity analyses and investigations (e.g. integration options and ways to increase system performance) were conducted. All computer simulation models have short computational times and can be easily adapted to match technological advances in the field.

The engineering economic model of the BG-SOFC CHP systems allowed identification of the main economic barriers to the deployment of the technology and it is hoped that this will aid in their removal in the future.

Conclusions were drawn from analysis of the model results and recommendations were made in an Irish context. Biomass resources in Ireland were also assessed with those suitable for gasification identified (considering fuel properties and availability).

This research work is topical and relevant; the IEA identified biomass gasification integrated with high temperature fuel cells, process modelling and techno-economic analysis as important research areas [18]. Moreover, the research is in line with developments in the BG industry. SOFC testing has been carried out onsite at the Güssing biomass gasification CHP plant in Austria over the period 2007 to 2010 [19, 20]. Further experiments are planned using larger scale SOFCs (0.2 to 1 kW) [21].

1.6 Thesis Structure

This thesis consists of seven chapters. Chapter two provides details on energy trends (national), energy policy (EU and national) and Ireland's biomass resources. Particular attention is paid to renewable energy targets and CHP. Information on the state of the art of biomass gasification, SOFC and syngas conditioning technologies is presented in chapter three. Pertinent modelling and simulation work by other

researchers is also reviewed in this chapter. Chapters four and five present the details of all developed technical models (standalone and combined system) and results through their application. Model validation details are provided along with in depth discussion of the results. All details pertaining to the engineering economic model are given in chapter six. A description of the methodology employed and an explanation of all model inputs and assumptions is provided. In addition, the model results are presented and discussed. The final chapter, chapter seven summarises important results and conclusions drawn from them, presents the main findings and recommendations of the thesis and lists potential areas of further research.

2 ENERGY TRENDS, POLICY AND BIOMASS IN IRELAND

2.1 Chapter Introduction

This chapter presents information on Ireland's energy requirements; then the most important energy policy legislation and documents are discussed. A section dedicated to electricity generation in Ireland is included. The next section outlines Ireland's progress in relation to structure of the electricity market, measures in place to promote renewable energy, renewable energy targets, Kyoto Protocol commitments and increasing the level of CHP. Biomass is defined and its composition and properties are discussed. Various types of biomass available in Ireland are listed and described. The next section presents an in-depth review of Ireland's biomass resources with only the types deemed suitable discussed (considering fuel properties and availability). The final section compares the available quantities of suitable biomass with the estimated demand by 2020.

2.2 Ireland's Energy Requirements

Figure 2.1 illustrates Ireland's energy requirements in terms of total primary energy requirement (TPER) over the period 1990 to 2008. TPER is defined as the total amount of energy consumed. The data used to plot Figure 2.1 was reported by the Sustainable Energy Authority of Ireland (SEAI) [22]. The total TPER has increased substantially over the period (approximately 72%) and reached 16,356 ktoe in 2008. As a result of the economic downturn, Ireland's TPER has decreased by approximately 12.4% according to provisional data for 2009 [23]. Figure 2.1 indicates Ireland's high dependence on fossil fuels, particularly oil (mainly in transport) and natural gas with the

importance of coal and peat decreasing over the period. The level of renewables, although low in comparison with fossil fuels, has risen by approximately 247% (168 ktoe in 1990 to 581 ktoe in 2008).

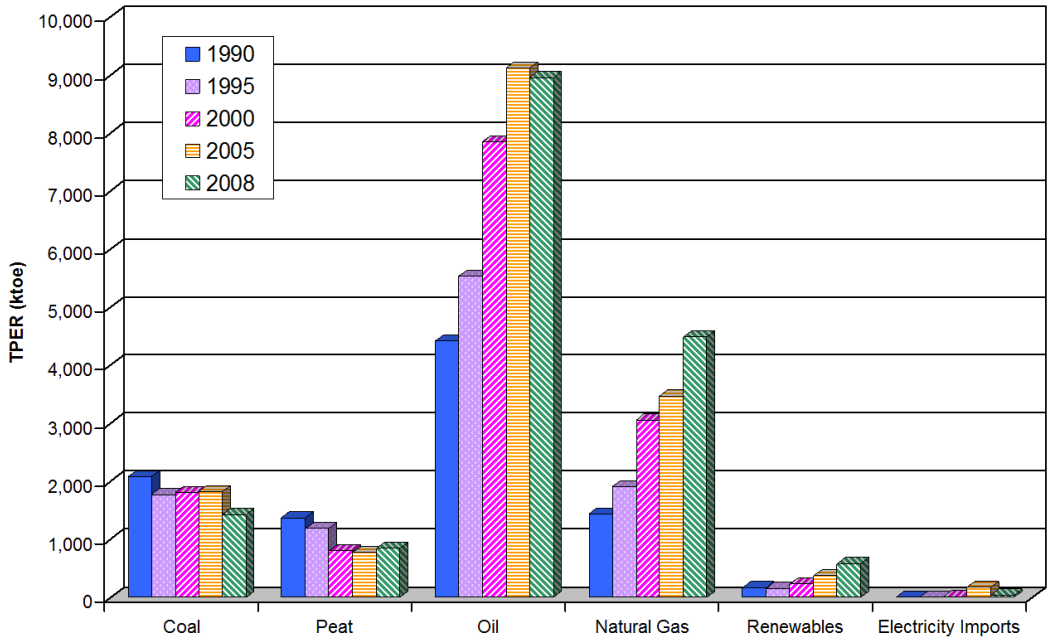

Figure 2.1 Ireland's TPER by fuel over the period 1990 to 2008

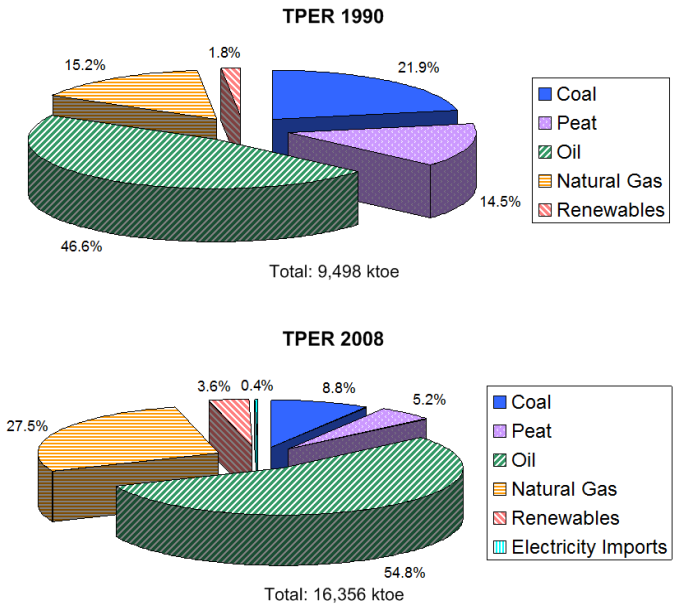

Figure 2.2 Ireland's TPER by fuel (% share) in 1990 and 2008

Figure 2.2 displays how the TPER fuel mix has changed over the period (data from SEAI report [22]). The contribution of coal and peat has dropped from 36.4% in 1990 to 14% in 2008; however, reliance on oil and natural gas has heightened with oil alone making up 55% of Ireland's TPER in 2008. The level of renewables has doubled from 1.8% in 1990 to 3.6% in 2008. Provisional 2009 data puts the contribution of renewables at 4.4% of TPER.

2.3 Energy Policy

In the context of climate change, energy security and economic recovery the development of renewable energy is a key objective of the European Union (EU). The European Parliament and Council published EU Directive 2009/28/EC on the promotion of the use of energy from renewable sources [24]. The directive emphasises the importance of energy savings through increased energy efficiency in order to increase the share of energy from renewable sources. Mandatory national targets were set consistent with the EU target of 20% share of energy from renewables by 2020. Ireland's target was set at 16% of gross final consumption (GFC) from renewables. In addition, each member state must achieve 10% share of renewable energy in transport. Finally, under the directive all member states were required to submit a national renewable energy action plan (NREAP) detailing how they will meet the 2020 targets. The EU Climate and Energy Package set out the following targets to be achieved by 2020 [25]:

- 20% of GFC from renewable sources (10.3% in 2008 [26]).
- 20% reduction in GHG emissions compared to 1990 levels.
- 20% decrease in primary energy use through efficiency measures.

In line with European energy policy the Irish government published the White Paper on Energy in 2007 [16]. This paper was based on three objectives; environmental sustainability, energy security and economic competitiveness. Renewable energy contributes to meeting all of these objectives. With little or no GHG emissions renewables help to accomplish environmental sustainability, they also increase energy security as they are largely indigenous and therefore reduce reliance on imported fossil fuels. In 2008 Ireland imported 89% of its energy mainly in the form of oil, natural gas and coal [27]. In comparison, the EU-27 average import dependency in 2007 was 53.1% [28]. Renewables enhance economic competitiveness through the stimulation of economic development and reduction in dependence on fossil fuels (highly volatile costs). The White Paper sets out actions, timeframes and targets to achieve the objectives. Ireland's targets for renewable energy supply electricity (RES-E), heat (RES-H) and transport (RES-T) are as follows:

- RES-E target of 15% (EU mandatory target of 13.2%) by 2010 and 40% by 2020.
- RES-H target of 5% by 2010 and 12% by 2020.
- RES-T target of 3% by 2010 and 10% by 2020.

In addition, the White Paper established targets of 500 MWe from ocean energy by 2020, 30% co-firing at the three peat fired power stations by 2015, 400 MWe of CHP by 2010 and 800 MWe by 2020 with particular emphasis on biomass. Finally, a target of 20% energy savings through efficiency measures by 2020 was set.

Another important Irish energy policy document is the National Climate Change Strategy [29]. This document presented a strategy for Ireland to meet its Kyoto Protocol commitment of limiting GHG emissions to 13% above 1990 levels over the period 2008

to 2012. This document reported that electricity generation accounted for 96% of energy sector emissions with the energy sector responsible for ~23% of the total emissions in 2005, which demonstrates the importance of meeting the RES-E targets. The Irish government also published a number of action plans related to renewable energy and efficiency [17, 30, 31]:

- Bioenergy Action Plan – This document presented pertinent information related to biofuels and biomass for heat and electricity production in Ireland. It made numerous recommendations such as expanding the renewable energy feed in tariff (REFIT) to facilitate biomass co-firing at peat plants and support mechanisms for energy crop establishment.
- National Renewable Energy Action Plan – This document sets national RES-E, RES-H and RES-T targets for 2020 in line with the mandatory 16% RES target for Ireland and details the steps towards accomplishing them. The SEAI has predicted Ireland's energy consumption for the period 2010-2020 and in light of these projections the RES-E target has been increased from 40% to 42.5%. The RES-H and RES-T targets remain unchanged. Two scenarios with respect to RES-E were examined. The modelled scenario predicts that onshore wind will dominate the RES-E contribution with low levels of biomass RES-E and less developed technologies (offshore wind and ocean). The export scenario, considers a much greater penetration of RES-E with a much more significant contribution from offshore wind, biomass and ocean technologies. This scenario would require considerable grid investment to accommodate the much greater RES-E penetration. In the modelled scenario it is envisaged that 153 MWe will come from biomass by 2020, whereas in the export scenario 400 MWe is projected. For

RES-H it is predicted that solid biomass will account for 77% of the RES-H target in 2020. These figures indicate that it would be wise to utilise biomass through CHP, which would contribute to RES-E and RES-H targets simultaneously.

- Energy Efficiency Action Plan – It is predicted that gains in efficiency will have the most significant savings in GHG emissions. This action plan identifies policies and measures to reach the 2020 target of 20% reduction in energy demand (compared to average energy demand over the 2001-2005 period). Greater energy efficiency can be realised in the electricity sector through improvements in how it is generated and distributed. This document recommends prioritising efficiency in investment decisions for new generation plant and recognises the potential that distributed generation, more than likely in the form of CHP, has to reduce the efficiency losses associated with transmission and distribution. It is estimated that 8.3% of the electricity generated in Ireland is lost through transmission and distribution [32]. The investigated systems in this work (BG-SOFC systems) fit with these priorities as they are highly efficient and are suitable for distributed CHP applications.

2.4 Electricity Generation in Ireland

In 2008 electricity generation accounted for 31% of the TPER. The quantity of each fuel used for electricity generation in Ireland over the period 1990 to 2008 is presented in Figure 2.3 (data from SEAI [22]). The dominance of natural gas is the most striking feature and Figure 2.4 shows that it accounted for 54.7% of the electricity generation fuel mix in 2008 increasing from 27.3% in 1990. This dominance is mainly due to the move away from inefficient and more polluting oil power generation. The contribution of coal and peat has dropped; however, the level of usage in terms of ktoe

has not changed significantly. The level of peat usage has actually increased in recent years for reasons of fuel diversity and security of supply. There has been a considerable increase in renewables in the fuel mix. Electricity demand fell by 6% in 2009 based on provisional data [23]. This was the first drop in electricity usage in Ireland in decades and was due to the economic downturn. The transmission system operator (EirGrid) forecasts that electricity demand will not reach 2008 levels until 2012-2014, depending on economic recovery [32].

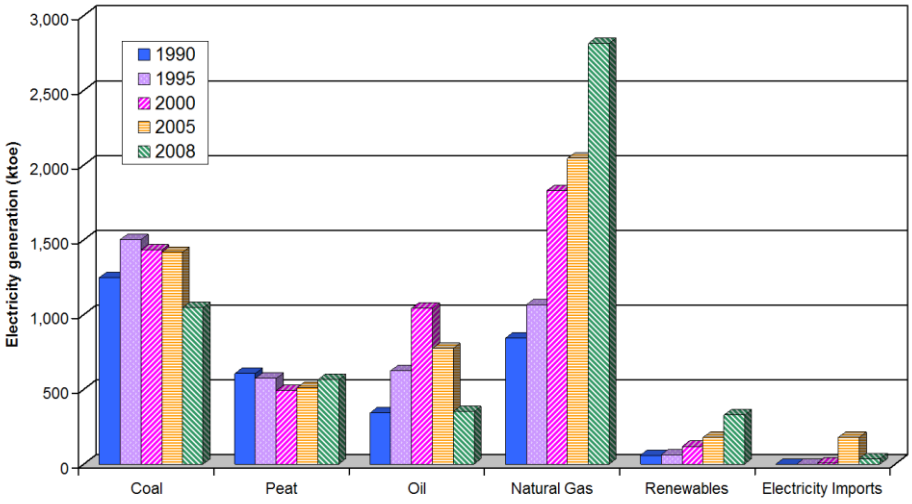

Figure 2.3 Electricity generation fuel mix 1990 to 2008

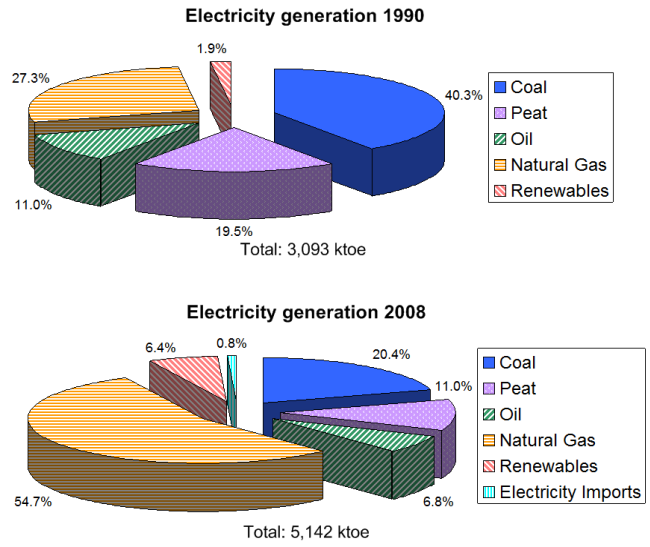

Figure 2.4 Electricity generation fuel mix (% share) in 1990 and 2008

Table 2.1 reports the export capacity of all conventional and renewable installed electricity generators that are connected to the Irish electricity grid. The capacities are reported on a plant type or fuel used basis. The data presented is accurate as of 2010. The total export capacity is 7,759.3 MWe of which 6,127.1 MWe is generated from fossil fuels and 1,632.2 MWe from renewables (landfill gas, wind, hydro, biogas and solar). These are only approximate values because a certain proportion of the CHP, which was assumed to be completely from fossil fuels, is generated from renewables, e.g. using waste sawdust at sawmills. In addition, EirGrid has not considered the biomass co-firing that is taking place at the 121.5 MWe peat fired Edenderry power plant, which stands at 7% of fuel input from biomass [33].

Table 2.1 Connected electricity generators in Ireland [34]

Plant Type/Fuel	**Units**	**Export Capacity (MWe)**
Natural gas	5	1841.0
Natural gas/distillate oil[a]	7	1114.3
Natural gas/heavy fuel oil[b]	3	461.0
Heavy fuel oil[c]	7	805.4
Coal	3	862.5
Peat	3	356.5
Distillate	4	207.6
Landfill gas	15	35.8
CHP	18	186.8
Wind	123	1358.6
Hydro	66	237.5
Pumped storage hydro	4	292.0
Biogas	1	0.2
Solar	1	0.1
Total Export Capacity		**7759.3**

[a] The Electricity Supply Board (ESB) has closed the 27 MWe Marina plant steam turbine unit reducing the plant's capacity to approximately 85 MWe [32].

[b] The three units at Poolbeg were closed at the end of March 2010 [35].

[c] All heavy fuel oil plants were sold by the ESB to Spanish electric utility company Endesa in 2008. These units were to be upgraded to natural gas combined cycle gas turbine (CCGT) [36].

There is a move away from high emission fossil fuel plants (closing of Poolbeg units, etc.). However, for reasons of fuel diversity and security of supply this does not extend to coal and peat. It is envisaged that the coal fired Moneypoint plant (862.5 MWe) will continue to operate beyond 2020. For this reason the ESB launched a retrofit project (€368 million) to satisfy EU nitrogen oxides (NO_x) and sulphur oxides (SO_x) emission regulations [37]. The project involves the installation of flue gas desulphurisation (FGD) and selective catalytic reduction (SCR) technologies to limit SO_x and NO_x emission respectively. In the last ten years old inefficient peat fired power plants have been replaced by three highly efficient plants based on fluidised bed boiler technology. Bord na Móna reported that they burned 68,598 tonnes of biomass displacing 66,663 tonnes of peat in 2009 at their Edenderry peat power plant [38]. The Irish government has set a target of 30% co-firing at the three peat plants by 2015. Electricity generated from peat and renewables is supported under the public service obligation levy, which covers additional costs incurred in generating or purchasing electricity from these sources. As a result of the closure of old inefficient plants and the commissioning of new efficient natural gas CCGT and fluidised bed peat plants the electricity supply efficiency in Ireland has increased from ~33% in 1990 to ~42% in 2008 [22]. There has been low uptake of CHP in Ireland despite the government target of 400 MWe by 2010 and 800 MWe by 2020. This is discussed in more detail in section 2.5.5. Wind on the other hand, has seen considerable uptake with an export capacity of 1,358.6 MWe. Wind alone accounted for 10.5% of gross electrical consumption in 2009 (provisional data) [23]. Ireland does not have a significant hydro resource and it is exploited to near its full potential. Pumped storage hydro, however, is likely to play a role as it is seen as a means of storing intermittent wind energy. Biogas and solar contribute very little to the total connected export capacity (0.3 MWe).

By the end of 2010 323.6 MWe of new wind capacity and 900.3 MWe of new non-wind capacity (876 MWe from natural gas, 21 MWe from biomass and 3.3 MWe from landfill gas) should be installed. The planned 21 MWe biomass plant is a waste-to-energy incinerator. In addition, there are many electricity generators seeking connection. In order to cope with the high volume of renewable generator applications (mainly wind) the Commission for Energy Regulation (CER) developed the group processing approach where grid connection applications are grouped together and processed simultaneously as opposed to the traditional method of examining applications on a case by case basis. Grid connection applications are processed within 'Gates' (e.g. Gate 3). The CER believes that there is a public interest in connecting certain renewable and low carbon generators (bioenergy and CHP) outside the group processing approach [39]. EirGrid will issue connection offers for 1,717.8 MWe of conventional generation (including natural gas peaking plants, pumped storage hydro, etc.), 168.33 MWe of renewable and low carbon generators outside the group processing approach (CHP, waste-to-energy, biogas, etc.) and 3,990.31 MWe of wind generation [40].

The Irish electricity grid must be reinforced and upgraded to accommodate the large amounts of RES-E that will be connected in the future. EirGrid have developed the Grid 25 strategy [41] based on the findings of the All Island Grid Study [42]. The Grid 25 strategy is a €4 billion grid development programme to build a cost effective and efficient system to cater for planned and prospective RES-E.

2.5 Progress Towards Targets

2.5.1 Electricity Market Reform and RES Policy and Support Measures

The Irish electricity market has undergone significant changes in the last ten years following the creation of the CER. It has gone from a market dominated by the semi-state owned ESB electric utility company to an open liberalised market with greater levels of competition. The small size of the electricity market in Ireland (~1.8 million customers) was recognised as a significant barrier to foreign investment and competition [43]. Consequently, the Irish government encouraged other semi-state owned companies to enter the electricity market. A significant action to liberalise the market was the creation of the all island single electricity market in 2007. This has increased the size of the market to ~2.5 million electricity customers (~1.8 million in the Republic of Ireland and ~0.7 million in Northern Ireland) and allows for greater competition and security of supply [44]. Interconnection between Ireland and the UK (500 MWe East-West interconnector) will allow greater penetration of RES-E in Ireland due to the possibility of exporting excess generation. Ireland will also be able to import electricity from the UK if the need arises, thus increasing security of supply. Table 2.2 lists some of the most important renewable energy policy and support measures in existence in Ireland. For a complete list of measures refer to Ireland's NREAP [17].

2.5.2 RES-E Share of Gross Electricity Consumption

Figure 2.5 presents the contribution of each fuel to Ireland's gross electricity consumption (GEC) from 1990 to 2009 (provisional data for 2009). The data used to plot Figure 2.5 was reported by the SEAI [23]. Similar trends exist to those seen in Figure 2.3 for electricity generation in Ireland, such as the increasing dominance of natural gas with diminishing use of oil, reduction in the contribution of coal and peat,

and the growing importance of renewables. RES-E accounted for 11.9% and 14.4% of the GEC in 2008 and 2009 (provisional) respectively, which indicates that Ireland surpassed the EU 2010 target of 13.2%.

Table 2.2 Renewable energy policy and support measures in Ireland

Name of measure	Description
Renewable Energy Feed in Tariff (REFIT)	A financial incentive to encourage the building of new RES-E generation plants. The categories supported are as follows: large wind (> 5 MWe), small wind (< 5 MWe), hydro, landfill gas, biomass, ocean, offshore wind, anaerobic digestion (CHP and non-CHP), biomass CHP.
Gate 3 Process	Improved grid connection process for RES-E generation plants through group processing of connection applications.
CER Decision Paper CER/09/099	Due to the high volume of grid connection applications for wind the CER believes that there is a public interest in connecting certain renewable and low carbon generators outside the group processing approach. The CER identified bioenergy, CHP, autoproducers, hydro, ocean, wave, solar, geothermal and experimental/emerging technologies as meeting the public interest criteria for an alternative processing approach, which would increase the speed of connection for projects based on these technologies.
EU Emissions Trading Scheme (ETS)	This is a financial incentive to encourage reductions in emissions and applies to large installations in the industrial and energy sectors. These installations must return emission allowances equivalent to their emissions. The scheme operates on a cap and trade basis.
Bioenergy Scheme for Willow and Miscanthus	Grant support for the planting of energy crops in order to contribute to the biomass needs of the energy sector. There were 2,500 hectares (ha) planted in 2009 and a further 1,000 ha of planting was to be supported under the scheme in 2010 [45].
CHP Deployment Programme	Grant support to assist the deployment of CHP (< 1 MWe for fossil fuel fired CHP with no cap for biomass fired CHP). The grant covers 30% of the cost of equipment or 40% of the cost of feasibility studies.
Accelerated Capital Allowance Scheme	This scheme is a type of corporation tax relief. It allows businesses to write off the cost of certain energy efficient technologies in the first year of purchase.

The contribution of the individual renewable energy sources is shown in Figure 2.6. It is clear that the bulk of Ireland's RES-E is from wind (68% of the 11.9% of GEC achieved in 2008 was from wind). The next most significant renewable source is hydro, followed by landfill gas and then small contributions from solid biomass and biogas. Ireland is not utilising solid biomass to its full potential even though it has numerous advantages over other renewables such as wind (see chapter one). The European Commission see solid biomass as one of the main alternatives to fossil fuels; therefore, they published a biomass action plan [46]. The Commission's 2009 renewable energy

progress report shows that electricity from solid biomass has grown considerably and that the combined contribution of solid biomass, biogas and bio-waste is comparable to that of wind [47]. The accompanying staff working document revealed that the growth in RES-E from solid biomass was attributable to the development of biomass CHP in a small number of EU member states (Germany, Finland and Sweden) [48]. This demonstrates that Ireland is lagging behind other member states with respect to biomass RES-E, even though it has been reported that Ireland's potential to develop biomass for energy is exceptional as it has the best growth climate in Europe [49].

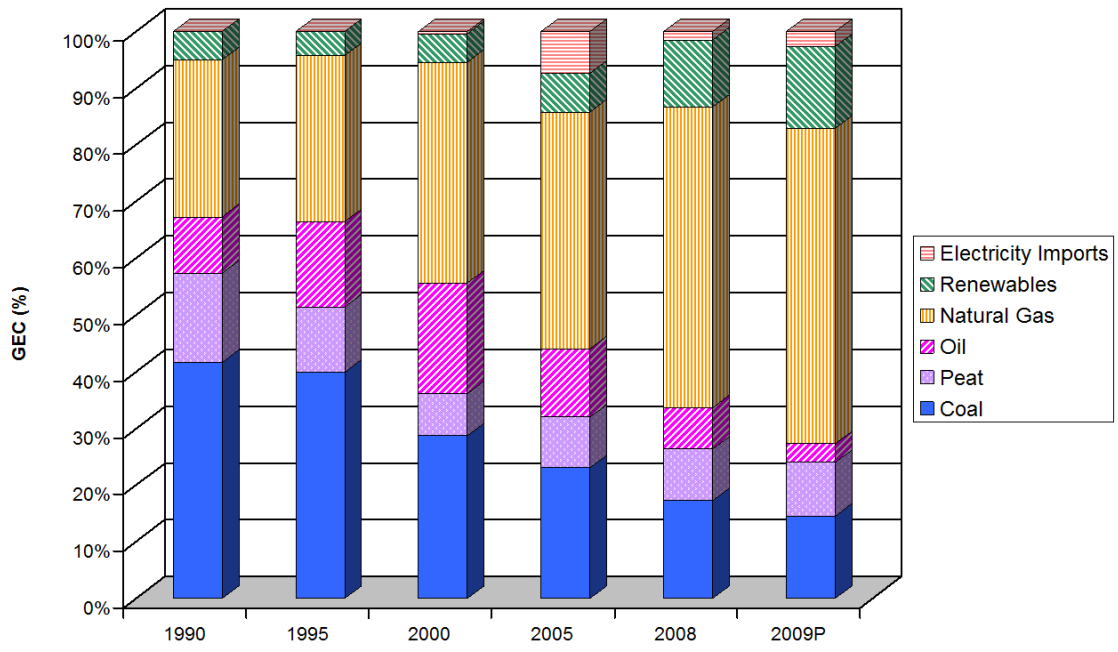

Figure 2.5 Ireland's GEC by fuel over the period 1990 to 2009

Denmark, which has an energy market of similar size to Ireland, generated 29% of its electricity from renewables in 2007, with 18.8% coming from wind, 10.1% from biomass and the balance from hydro and solar [28]. In addition, by 2010 1,017 MWe of renewable electricity will be generated from biomass (991 MWe from solid biomass

and 26 MWe from biogas) and by 2020 this will have risen to 2,779 MWe (2,404 MWe from solid biomass, 349 MWe from biogas and 26 MWe from bioliquids) [50]. Given that Ireland has almost twice the land area and a more favourable growth climate it is clear that Ireland's planned biomass 2020 targets, as outlined in Ireland's NREAP (153 MWe for the 'modelled scenario' and 400 MWe for the 'export scenario'), are not ambitious enough.

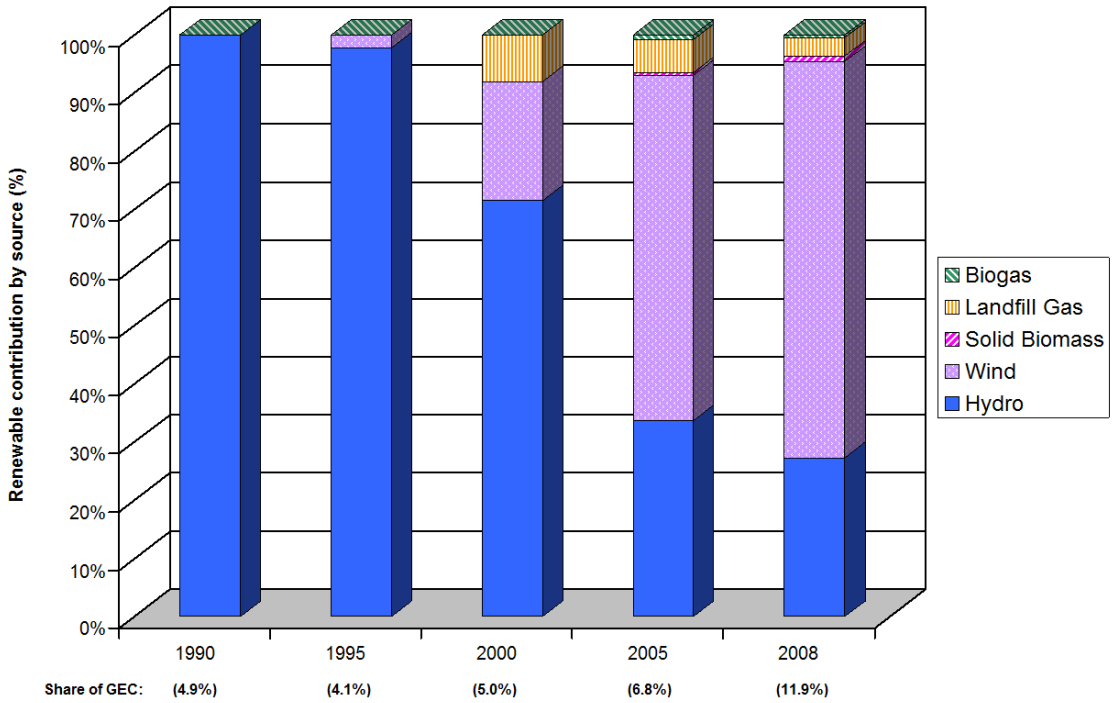

Figure 2.6 Renewable contribution by source

2.5.3 RES Share of Gross Final Consumption

Figure 2.7 illustrates Ireland's progress towards its mandatory target of 16% of GFC from renewables (RES-E, RES-H and RES-T). It is evident from Figure 2.7 that the contribution of renewable energy to GFC has grown steadily since 2003. It reached 3.9% (558 ktoe) in 2008 and provisional data for 2009 indicates that 4.7% (607 ktoe) has been achieved. The greatest contribution is from wind followed by biomass, which

is mainly in the form of RES-H as RES-E generated using biomass is currently very low. In 2008 RES-E accounted for approximately 55% of the GFC contribution from renewable energy, while RES-H and RES-T were responsible for ~35% and ~10% respectively. The progress with respect to the RES-E, RES-H, RES-T and the overall GFC targets are summarised in Table 2.3.

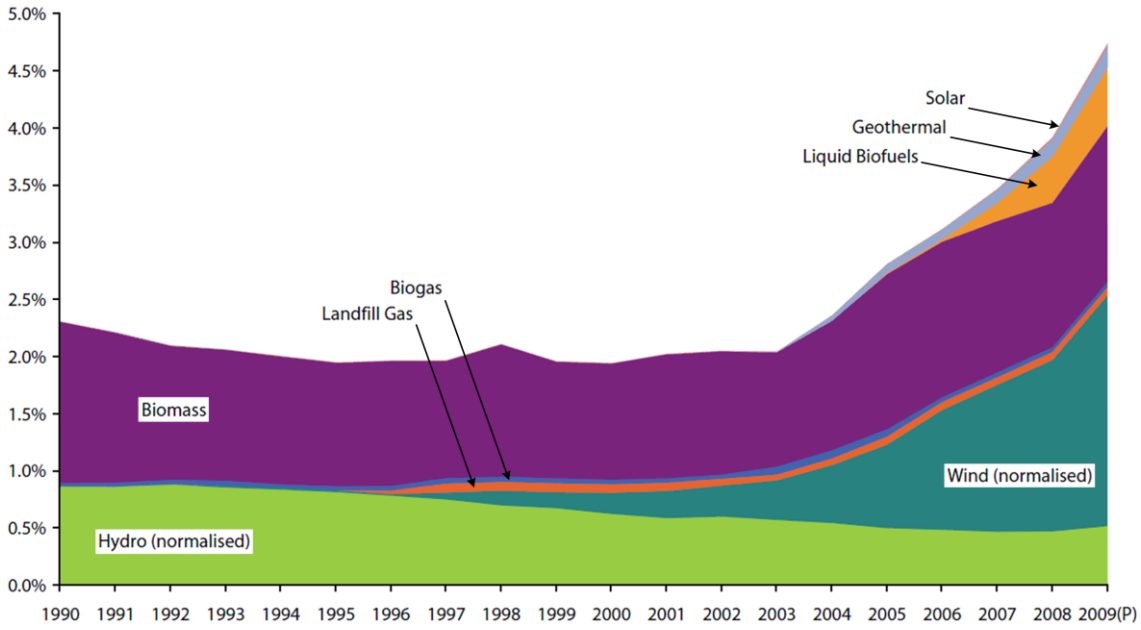

Figure 2.7 Renewable contribution to GFC by source over the period 1990 to 2009 [23]

In 2008 energy use for thermal purposes accounted for 34% of TPER [22]. The RES-H contribution is dominated by biomass with low levels of solar and geothermal. The bulk of the biomass RES-H stems from the use of wood waste at wood processing plants to meet their energy needs with lesser amounts of wood being utilised in the residential and commercial/services sectors [23]. Biogas contributes to RES-H at food processing and waste water treatment plants. The dominance of industry, which was responsible for 70% of the total RES-H in 2008, and its decline in recent years meant

that growth in RES-H was slow. Ireland failed to achieve the 5% 2010 target (4.4% achieved) [51]. Ireland also failed to reach the 3% RES-T target (2.4% achieved) [51].

Table 2.3 Ireland's progress to RES targets summary

	2008	2009 (Provisional)	2010 Target	2020 Target
RES-E	11.9%	14.4%	15% (EU 13.2%)	40% (NREAP 42.5%)
RES-H	3.6%	3.9%	5%	12%
RES-T	1.2%	1.5%	3%	10%
RES (% GFC)	3.9%	4.7%	-	16%

2.5.4 Greenhouse Gas Emissions

The EU Kyoto Protocol commitment (EU-15) was to lower GHG emissions by 8% compared to 1990 levels over the period 2008 to 2012. Ireland's commitment was to limit GHG emissions to 13% above 1990 levels over the period. Assuming 1990 levels of 55.61 Mt CO_2 equivalent, this translates to 314.2 Mt CO_2 equivalent over the period or 62.8 Mt CO_2 equivalent per annum [52]. Furthermore, the EU as part of the Climate and Energy Package has agreed to reduce GHG emissions by 20% by 2020 based on 1990 levels. Regarding this EU 2020 target, Ireland must ensure that ETS participants lower their GHG emissions by 21% and non-ETS by 20% below 2005 levels by 2020 [27, 52].

In 2008 the EU-15 achieved a reduction of 6.9% on 1990 GHG levels [53]. Ireland's GHG emissions, excluding carbon sinks, were 21.3% above 1990 levels at 67.4 Mt CO_2 equivalent [52-54]. It is estimated that renewable energy (RES-E, RES-H and RES-T) avoided 2.83 Mt CO_2 emissions in 2008 [23]. In an effort to reduce GHG emissions from the non-ETS sector, which was 4.4 Mt above target in 2008, the Irish government introduced a carbon tax [54].

The Irish Environmental Protection Agency (EPA) reported that Ireland was on track to meet its Kyoto commitments [55]. The reduction in emissions was primarily

due to the economic recession and the EPA warns of the challenges that Ireland faces to meet its 2020 targets. The GHG emissions over the 2008 to 2012 period on a sectoral share basis were as follows: Energy (21%), Transport (20%), Agriculture (30%), Industry/Commercial (15%), Residential (12%) and Waste (2%) [55].

2.5.5 CHP in Ireland

CHP is the simultaneous generation in one process of electrical/mechanical and thermal energy. In conventional electricity generation much of the input energy is lost as heat; in Ireland 55% of the input energy is lost with 45% being transformed into electricity [56]. In CHP systems this heat is recovered for useful purposes, which increases the efficiency of the process (> 75%). CHP is recognised as a means of meeting the goals of the EU Climate and Energy Package by increasing the efficiency of electricity and heat supply and by lowering GHG emissions, especially in the case of biomass CHP. Frequently the electricity is consumed onsite, which reduces transmission and distribution losses. The IEA in their energy policy country review of Ireland recommended the deployment of distributed generation, such as CHP in order to reduce high network losses [43]. The European Parliament and Council published EU Directive 2004/8/EC on the promotion of cogeneration based on a useful heat demand in the internal energy market [57]. The term cogeneration is equivalent to CHP. Fuel cells were listed as a cogeneration technology covered by the directive.

The 400 MWe 2010 target for CHP was not met. At the end of 2010 the installed capacity was 307 MWe (284 MWe operational) [58]. It appears highly unlikely that the 2020 800 MWe target will be achieved. An average annual growth rate of 11% would be required over the period 2010 to 2020. This compares to a reduction of 1.3% in 2010 (compared to 2009) and an average annual growth rate of 5% between 2006 and 2010

[58]. In 2008 there were 11 CHP units exporting electricity to the grid growing to 18 units in 2010 as presented in Table 2.1 and it was reported that 6.3% of the GEC was generated using CHP plants [56]. Moreover, 4% of Ireland's total thermal energy demand was met by CHP installations. Ireland's CHP capacity is well below the EU average; for comparison the CHP share of electricity in Denmark is ~55% and ~38% of thermal energy demand [59]. It has been reported that Ireland has one of the lowest CHP deployment levels of all IEA countries [43].

Natural gas fuelled CHP made up approximately 94% of the installed units with solid biomass and biogas only accounting for 3.5% of the units (12.5 MWe) [60]. By the end of 2008 there was 5.13 MWe of biomass CHP installed at two wood processing sites and a planned 3 MWe plant at a third. The White Paper stated that there should be particular emphasis on biomass CHP in meeting the 2010 and 2020 targets [16]. Clearly there has not been sufficient uptake of biomass CHP, which indicates that barriers exist. Additional categories, including biomass CHP (≤ 1.5 MWe €140/MWh and > 1.5 MWe €120/MWh), were added to the REFIT in the hope of increasing its uptake [61]. On a sectoral basis in 2008, the industrial sector dominated installed capacity (~80% of total) with a relatively low number of units (~14% of total), whereas the commercial/services sector accounted for ~18% of installed capacity and ~83% of the total number of units [60]. There was virtually no CHP in the residential sector in 2008. The following is a list of some of the most significant barriers to CHP that exist in Ireland:

- CHP Economics – Substantial investment is required resulting in long payback periods, which are unattractive to corporations. The CHP Deployment Programme ceased in 2010 [58].

- Socio-Economic Structure of Ireland – There is a lack of heavy industry with high heat loads in Ireland, which would offer opportunities for large scale CHP. In addition, Ireland is sparsely populated with low population density making the development of district heating challenging. The slowdown in the construction industry presents fewer opportunities for district heating schemes as the economics of retrofit are unfavourable compared to new build. Ireland is therefore not in a good position regarding CHP as future CHP potential is mainly dependent on developments in district heating and industrial applications [59].
- Technological – Micro-CHP units suitable for the residential market have been subject to field trials. Bord Gáis Éireann (semi-state owned natural gas and electric utility company) have signed an agreement with UK based SOFC company Ceres Power regarding their residential scale natural gas fuelled SOFC CHP units [62].
- Fuel Availability – Ireland's low population density means that there are large areas of the country that do not have access to the natural gas grid, which presents a barrier given that natural gas is the most popular fuel for CHP units. Presently, biomass supply chains for the energy industry are not yet well established and strong competition exists with other biomass applications, such as co-firing at peat power plants, etc.

Sectors that have been identified as growth areas for CHP include the industry, commercial/services and residential sectors [60]. The wood processing plants within the industry sector are of particular importance for biomass CHP. Two wood processing sites have biomass CHP systems installed (5.13 MWe) with a third site planned (3 MWe). With at least ten companies in the Irish sawmilling industry (~100 sawmills in

Ireland [63]) and four wood based panel board manufacturers [64] plenty of scope for additional biomass CHP exists. There are at least two wood processing sites that are interested in installing gasification based biomass CHP systems [60]. There are opportunities for additional CHP in hospitality, healthcare (13 of 49 hospitals have CHP units installed [60]) and waste management. The residential sector offers considerable potential for CHP due to very limited uptake to date. Suitable micro-CHP units are beginning to come on to the market and there should be growth in district heating schemes in the medium to long term in high population density areas. In light of the information available on the status of CHP in Ireland the following recommendations are made:

- Specific targets to 2020 for biomass and fossil fuel fired CHP should be set, i.e. sub-targets of the national 2020 CHP target of 800 MWe.
- The CHP Deployment Programme should be re-established.
- District heating schemes should be supported in order to provide large heat loads for CHP.
- Biomass availability should be enhanced through continuation of the Bioenergy Scheme for Willow and Miscanthus and support should be provided to private forest owners to stimulate thinning operations.

2.6 Ireland's Biomass Resources

2.6.1 Biomass Definition

The EU Directive 2009/28/EC defines biomass as the biodegradable fraction of products, waste and residues from biological origin from agriculture (including vegetal and animal substances), forestry and related industries including fisheries and

aquaculture, as well as the biodegradable fraction of industrial and municipal waste [24]. Plant biomass is derived from the reaction between CO_2 in air, water and sunlight via the process of photosynthesis, which produces O_2 and the organic compounds that make up plant biomass. As a result of this process, solar energy is stored in biomass as chemical energy. Despite fossil fuels originating from biomass they cannot be considered renewable as they were formed over millions of years and the conversion of these fuels releases carbon that has been out of the atmosphere for a very long time. The use of more recent biomass as fuel contributes no new CO_2 to the atmosphere as the CO_2 released will be absorbed through the growing of new biomass. Consequently, biomass is considered by many to be carbon neutral. In practice, there will be CO_2 emission due to planting, harvesting, processing, etc.; therefore, a more accurate description of biomass would be to describe it as a low carbon fuel.

2.6.2 Biomass Properties

The main organic components that make up biomass are cellulose, hemicellulose and lignin. Cellulose is the chief constituent of many types of biomass. Biomass typically contains 40 to 50 weight per cent (wt. %) dry basis (db) cellulose [65, 66]. Hemicellulose ranges from 20 to 40 wt. % db [66]. Lignin accounts for about 20 to 30 wt. % db of most biomass [65]. On a microscopic scale, wood cells are composed of microfibrils, bundles of cellulose molecules coated with hemicellulose, with lignin deposited between the microfibrils [67]. Cellulose, hemicellulose and lignin represent 95 to 98 wt. % db of woody biomass with the balance consisting of extractives and ash [68]. The ash content of wood is composed of inorganic compounds: alkali metals, heavy metals, sulphur, chlorine and silicates.

The proximate analysis of a fuel provides an indication of the fuel quality and therefore its suitability to a particular application. It determines the moisture, volatile matter, fixed carbon and ash in the fuel. Methods have been standardised by major standards institutions (ASTM, ISO, etc.). The moisture content is determined by weighing before and after drying. The volatile matter is found by heating the fuel in a covered crucible for a defined time at a defined temperature. The loss in mass of the fuel sample, taking any moisture into account, is equivalent to the volatile matter. The ash content is determined by complete combustion of the sample. Finally, fixed carbon is calculated by subtracting from 100 the mass percentages of moisture, volatile matter and ash [69].

Table 2.4 Proximate and ultimate analyses of selected biomass and coal [66]

	Unit	Wood (average)	Barley Straw	Bituminous Coal
Ultimate Analysis (db)				
Carbon	wt. %	51.6	45.7	73.1
Hydrogen	wt. %	6.3	6.1	5.5
Oxygen	wt. %	41.5	38.3	8.7
Nitrogen	wt. %	0.0	0.4	1.4
Sulphur	wt. %	0.1	0.1	1.7
Ash	wt. %	1.0	6.0	9.0
Proximate Analysis				
Volatile Matter	wt. %	82.0	46.0	35.0
Fixed Carbon	wt. %	17.0	18.0	45.0
Ash	wt. %	1.0	6.0	9.0
Moisture	wt. %	20.0	30.0	11.0
LHV[a] (db)	MJ/kg	18.6	16.1	34.0

[a] LHV = Lower Heating Value.

The ultimate analysis provides information about the elemental composition of a fuel. The percentages of carbon, hydrogen, oxygen, nitrogen, and other components, including sulphur, chlorine, potassium and sodium are determined. Trace elements are usually included with the ash. Proximate and ultimate analyses may be reported on a dry

basis (db), a dry and ash free basis (daf), or on an as received basis (ar). Proximate and ultimate analyses of selected biomass and coal are given in Table 2.4.

In comparison to coal, biomass is a highly volatile fuel. During thermal conversion biomass will, at relatively low temperatures, give off ~80% of its weight as gaseous components, whereas coal only releases ~35% of its weight. Biomass has lower carbon content than coal, both fixed carbon (~15 wt. % versus ~45 wt. %) and elemental carbon (~50 wt. % versus ~75 wt. %), which negatively impacts the LHV. As a result of their low carbon content, biomass fuels have higher hydrogen and oxygen levels compared to coal (e.g. oxygen: ~40 wt. % versus ~10 wt. %). The high oxygen content of biomass fuels also lowers their LHV. The higher proportion of oxygen and hydrogen in biomass, compared with carbon, reduces the fuel energy value due to the lower energy contained in carbon-oxygen and carbon-hydrogen bonds than carbon-carbon bonds [66]. The significance of the carbon, oxygen and hydrogen content on the heating value is illustrated using a Van Krevelen diagram in Figure 2.8.

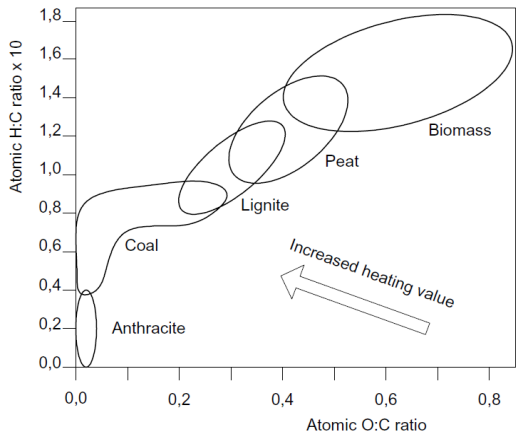

Figure 2.8 Van Krevelen diagram for various solid fuels [68]

As can be seen from Table 2.4, nitrogen and sulphur fractions in biomass are very low in comparison to coal. The low sulphur content is a distinct advantage for biomass

over coal as candidate fuel for fuel cell based systems as sulphur species are poisonous to fuel cells. The sulphur contained in fuels lead to SO_x emission. As was discussed in section 2.4, an expensive FGD system was installed at Ireland's Moneypoint coal power plant in order to comply with EU SO_x emission regulations. Consequently, low sulphur biomass fuels are very attractive. The same applies to fuel bound nitrogen, which causes NO_x emission. Similar to SO_x emission, NO_x emission is strictly regulated within the EU, which led to the retrofit of a costly SCR system at Moneypoint coal power plant.

Ash requires capture and disposal and as a result contributes to the overall cost of the conversion system. Moreover, the amount of energy available decreases with increasing ash content. The low ash content in certain biomass species, e.g. wood, is therefore advantageous. An important parameter, especially for fluidised bed gasifiers, is ash softening temperature, which is dependent on ash composition. Biomass ash composition differs greatly to that of coal ash and results in much lower softening temperatures. For example, the ash softening temperature may be as low as 800 °C for some straws in contrast to ~1,300 °C for coals. Fuel ashes that contain high silica and/or alumina have high softening temperatures, whereas ashes that contain high alkali metals (e.g. sodium, potassium, etc.) have low softening temperatures. Biomass ash can contain high levels of these alkali metals, which can cause serious problems for fluidised beds, i.e. slagging and agglomeration resulting in defluidisation. Care must be exercised when utilising high alkali containing biomass fuels, such as miscanthus and straw. Siedlecki et al. reported that agglomeration and defluidisation occurred during miscanthus and straw gasification experiments at temperatures as low as 800 °C and consequently, they reduced reactor temperature to ~750 °C [70].

Moisture content, which is the mass percentage of water within a fuel, is of paramount importance. The level of moisture in a fuel has a strong influence on the

heating value of the fuel, i.e. the amount of energy that may be recovered through conversion of the fuel. Fuel heating value decreases with increasing moisture content. Moreover, since vaporising water requires energy, fuel moisture will lower the conversion efficiency of any system. Biomass fuels have high moisture and hence low heating values compared to coal (see Table 2.4). The moisture content reported for wood fuel in Table 2.4 (20 wt. %) is for wood after drying because fresh forest wood contains at least 50 to 60 wt. % moisture [71]. Thermochemical conversion systems (combustion, gasification, etc.) require low moisture content fuels (typically < 50 wt. %), while biochemical conversion systems (anaerobic digestion, etc.) can utilise high moisture fuels.

Heating value may be expressed in two forms depending on the phase of the water in the products: the higher heating value (HHV) or the lower heating value (LHV). HHV is used when the water in the products is in liquid form with the latent heat of vaporisation recovered. LHV is used when the water in the products is in vapour form. The difference between them is equal to the product of the amount of water and the enthalpy of vaporisation of water at room temperature [72]. The HHV represents the maximum amount of energy potentially recoverable from a particular fuel. Normally the latent heat of vaporisation of the product water cannot be utilised and therefore the LHV is most appropriate [66]. The heating value of fuels is determined experimentally using a bomb calorimeter; however, numerous empirical correlations have been developed that predict the heating value based on composition.

2.6.3 Biomass Classification

The types of biomass that are available in Ireland are discussed briefly in the following paragraphs.

Wood from the forest, usually in the form of small diameter pulpwood (7 to 14 cm) made available through forest thinning operations, will be a very important biomass resource as the supply is set to outstrip the demand for current uses. Another source of woody biomass is forest residues (tree tops, branches, stumps, etc.), which result from forest thinning and clear felling. In the past, these residues were typically left in the forest as no market for them existed. The energy market offers foresters additional income for this unexploited resource; however, there are constraints on the amount of residues that should be removed from the forest during thinning operations. These residues give important nutrients back to soil and are also used as a brash mat in order to protect the soil from the harvesting machinery [63, 73]. Sawmill residues (sawdust, chips, bark, etc.) can also be used as a fuel. The bulk of these residues serve as feedstock to the panel board mills and have other uses such as in horticulture; therefore, the energy potential of this resource is limited. Post consumer recovered wood (PCRW) (e.g. pallets, construction and demolition waste wood) is also considered promising. Energy crops, i.e. crops specifically grown for energy generation, will become increasingly important as the bioenergy sector develops. Two promising crops are short rotation coppice (SRC) willow, which is a fast growing tree, and miscanthus a perennial grass.

Agricultural residues such as straw, poultry litter and spent mushroom compost have potential as biomass fuels in Ireland [74]. Straw, which is a by-product of cereal production, is used for animal bedding, feed supplement and production of mushroom compost with a large portion of the resource simply ploughed back. This surplus straw could be used as a fuel; however, it is a widely dispersed resource and its level of utilisation for energy will depend on the economics of collection and transportation. A

considerable amount of poultry litter and spent mushroom compost remains unused and is disposed of by land spreading.

Food processing wastes such as meat and bone meal (MBM) and tallow (animal fat) also hold potential as biomass fuels. MBM is currently being investigated as a potential fuel for co-firing with peat at the Edenderry power station [75].

Wet organic residues such as agricultural slurry, sewage sludge, certain food processing wastes and the biodegradable fraction of municipal solid waste (MSW) are considered suitable for anaerobic digestion [74].

2.7 Biomass Availability

This section presents a more in-depth review of Ireland's biomass resources. Only those types of biomass considered suitable for thermochemical conversion and available in sufficient quantities are discussed. The biomass fuels considered are as follows: small diameter pulpwood, forest residues, wood processing residues, PCRW, energy crops and straw. These biomass fuels are considered suitable for thermochemical conversion mainly because they contain relatively low levels of moisture. Biomass gasification systems are considered fuel flexible; however, the fuel type will affect the conversion efficiency of the system, e.g. high moisture fuels will lower efficiency as a result of the energy required to evaporate the moisture. In addition to adverse effects on conversion efficiency, it is not economically feasible to transport high moisture biomass and therefore these fuels are typically collected and converted on the same site at small scale, e.g. a farm based anaerobic digester utilising agricultural slurry that was generated on site. Based solely on moisture content, wet agricultural slurry, sewage sludge, food processing waste and MSW were excluded. Other fuel properties that were considered when determining the suitable biomass types were nitrogen and sulphur

content, ash content and the level of alkali metals present in the ash. Spent mushroom compost was deemed unsuitable because it contains high moisture, nitrogen, sulphur (comparable to coal) and very high ash content (35%) containing high levels of alkali metals [71]. Poultry litter was ruled out due to its high ash and nitrogen content and because it is regarded as a problematic fuel that causes frequent downtime [71]. The food processing wastes MBM and tallow may not be available in sufficient quantities as a biomass fuel [60]. These biomass resources are currently fired in boilers located at the rendering plants. Moreover, MBM is being considered as a candidate co-firing fuel at Edenderry [75] and the available quantity of MBM is forecasted to drop dramatically in the future (149,656 tonnes in 2006 compared to 46,000 tonnes in 2020) [17]. MBM also contains very high nitrogen and ash. Tallow is not suitable for gasification based systems and is currently utilised for biodiesel production or in combustion based systems.

2.7.1 Pulpwood and Forest Residues

The total forested area in the Republic of Ireland is ~765,000 ha, which is ~10.9% of the total land area. The total forested area is composed of public and private forest estate. The public forest estate, which is owned by Coillte (state owned), totals 445,000 ha [76, 77] and the private forest estate equates to 320,000 ha (300,000 ha in 2006 plus 20,000 ha planted since 2006) [78, 79]. The Irish government's afforestation policy is to increase forest cover to at least 17% of total land area by 2030 [78]. This translates into an annual afforestation rate of at least 10,000 hectares per annum (ha/a). If annual afforestation rates continue to fall below 10,000 ha/a, wood fuel supply will not be sustainable in the long term and government biomass targets will not be attained [79]. The wood fuel supply would be unsustainable due to the fact that small diameter

pulpwood, which accounts for up to 50% of timber from first thinnings, decreases as the crop gets older [80]. An afforestation rate greater than 10,000 ha/a was achieved over the period 1990 to 2002, with a peak of ~24,000 ha achieved in 1995 [81]. More recently, planting rates have fallen below 10,000 ha/a in 2003 to 2004 and 2006 to 2009 (slightly above 10,000 ha of new forest was planted in 2005). Private forest planting has been dominant over the past two decades, with no public planting since 2004 and no significant public planting since the mid nineties.

Figure 2.9 presents the forecasted quantities of roundwood in the Republic of Ireland over the period 2010 to 2028. The data plotted was published by Coillte (public forest data) and COFORD (private forest data).

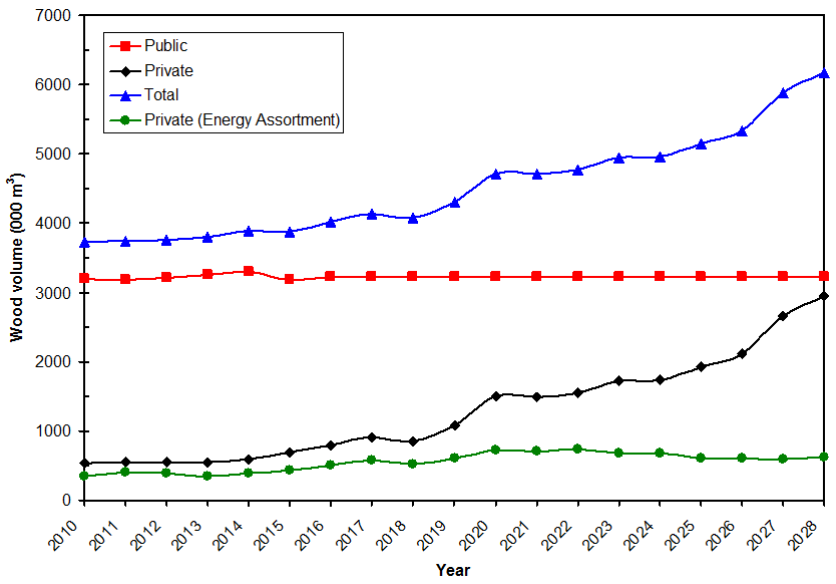

Figure 2.9 Forecasted roundwood production in the Republic of Ireland 2010 to 2028 [78, 82]

From Figure 2.9 it is evident that the public wood supply remains fairly static over the forecast period (~3.2 million m^3). The Coillte forecast only gave data up to the year 2020; it was assumed that the public forest output remained constant out to 2028. This

assumption is supported by data presented by COFORD [83]. The potential output from the private forest estate shows a strong increasing trend over the forecast period, rising from 535,000 m^3 in 2010 to 2.95 million m^3 in 2028. In Figure 2.9 the series labelled 'Total' is simply the sum of the public and private supply data. In 2010 Coillte will supply ~86% of the total roundwood, dropping to ~68% by 2020 and ~52% by 2028. It has been reported that the private forest estate is the most realistic source of wood for the energy market, given that much of Coillte's wood supply is destined for wood processing [30]. As a result, in this work it is assumed that all of the traditional public forest supply (large sawlog, small sawlog and pulpwood) goes to the wood processing industry, with only wood supply from new operations (i.e. gathering forest residues) considered available to the energy market. Furthermore, it was assumed that the energy market would not draw wood away from existing non-energy markets [73] and that the consumption of the wood processing industry remains constant [71]. Based on these assumptions, the potential wood fuel available to the energy market is equal to the sum of the small diameter wood from private forests and forest residues collected from the public forest estate. The energy assortment shown in Figure 2.9 is defined as the theoretical amount of wood available to the energy market from private forests. It includes all of the private forest pulpwood and forest residues [78]. The quantity of energy assortment wood increases up to 2020 remains stable and then drops slightly after 2024 (341,000 m^3 in 2010 growing to 626,000 m^3 by 2028). The slight drop is due to the increasing age of the private sector forests, which results in lower levels of small diameter wood.

Figure 2.10 displays the forecasted roundwood production from the Irish private forest estate by wood size category (see Appendix A for details on wood size categories). The quantity of small diameter timber (suitable for energy) compared to

larger diameter sawlog (suitable for wood processing) produced from forests decreases with time. This trend is evident in Figure 2.10, with pulpwood accounting for the majority of the total output up to the year 2022 after which the small sawlog size category is dominant until 2025 when large diameter sawlog becomes the dominant category. Small diameter wood accounts for a higher proportion of the total output from private forests compared to public forests simply because they are younger. Most of the private forest estate was established over the past two decades with many areas now entering the first thinning stage [79].

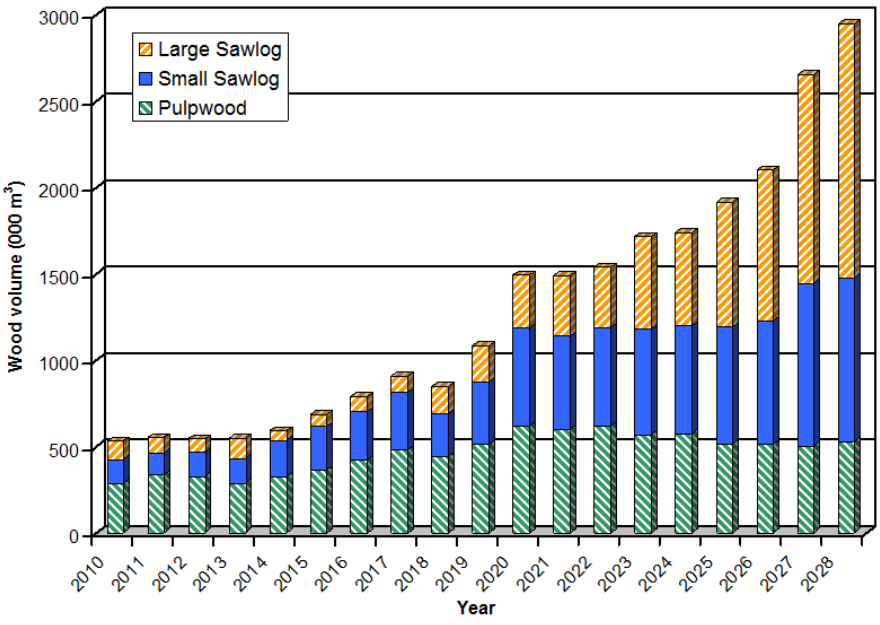

Figure 2.10 Forecasted roundwood production from private forests in the Republic of Ireland 2010 to 2028 [78]

Forest residues, defined as all above ground material removed from marketable trees and including tops, branches, foliage and unmarketable stems [71], are an untapped resource suitable for the energy market. There are constraints on the level of forest residue removal as they give important nutrients back to soil and are used as a

brash mat during harvesting. The most common tree species in Ireland is spruce (72% of public forest and 78% of private forest [71, 78]), which produces about twice the amount of forest residues as pine or birch [63]. This implies that there are significant quantities of forest residues available. Coillte estimate the potential supply of forest residues from the public forest estate to be 450,000 tonnes per annum (t/a) with the likely available supply being ~150,000 t/a [84, 85]. This is in addition to the forest residue output from the private forest estate, which is forecasted to increase from 50,000 m^3 in 2010 to 96,000 m^3 by 2028 (calculated using COFORD forecast data by subtracting the total pulpwood volume from the energy assortment volume).

Freshly felled forest wood in Ireland typically contains ~60% water. Not only is transportation of this water uneconomical but this level of moisture content may render the wood fuel unsuitable for certain applications. Most biomass gasification based systems require relatively dry fuels (< 30% moisture content) in order to achieve acceptable conversion efficiencies. Stacking and storage of the freshly felled logs will lower the moisture content. Various methods have been investigated in Ireland, such as storage within the forest, outside the forest on open exposed land, in containers, covered or uncovered, etc. Covered stacks in an exposed location can achieve a moisture content of ~45% after six months and 25 to 30% after twelve to eighteen months [80]. The lower the moisture content of the wood the higher the price that can be charged by the grower.

The scale of thinning required to realise the potential increase in roundwood production from the private forest estate represents a significant challenge and considerable capital investment will be needed (roads, harvesting equipment, etc.); therefore, strong government support will be necessary. In addition, considerable investment is required to achieve afforestation targets.

2.7.2 Energy Crops

It is unlikely that the necessary quantities of biomass will be available to the bioenergy sector and therefore significant areas of energy crops in addition to conventional forestry will be needed [86]. It is forecasted that at least 3.6 million m^3 of woody biomass will be required to meet Ireland's 2020 bioenergy targets [87]. Considering that the total roundwood production for 2010 is forecasted to be ~3.7 million m^3 (Figure 2.9), a substantial increase in woody biomass production is needed. The woody energy crop SRC willow can fill this supply gap.

In Europe much attention has been focussed on woody energy crops (fast growing trees) especially willow and poplar. Extensive research has been conducted on SRC willow (16,000 ha planted in Sweden [87]) mainly because it thrives in temperate wet conditions, which makes willow a very promising energy crop in Ireland. There are only minor differences between the fuel properties of willow and forest wood, none of which will have any impact on conversion systems [87]. Of the herbaceous species, miscanthus a perennial grass has attracted considerable interest. Miscanthus is regarded as an ideal fuel crop: annual, easy to grow/harvest, dry when harvested and has high energy yield per ha [66].

The total land area of the Republic of Ireland is ~7 million ha, 60% of which (~4.2 million ha) is used for agriculture. Ninety per cent of the farmed land is grassland, which supports livestock and the remaining 10% is used for crop production. Table 2.5 presents land use data for the Republic of Ireland. This data reveals the reason why agriculture contributes such a large proportion of the country's total GHG emission (30% see section 2.5.4); it is due to the dominance of livestock production. Livestock agricultural activity results in the release of CH_4 and nitrous oxide into the atmosphere.

Table 2.5 Land use in Ireland June 2009 [88]

Land Use		Hectares
Total Cereals		293,300
of which:		
Wheat	83,000	
Oats	20,100	
Barley	185,900	
Other	4,300	
Other Crops		108,800
Grassland		3,787,800
of which:		
Pasture	2,092,400	
Silage	1,033,900	
Hay	220,300	
Rough Grazing	441,200	
Total		**4,189,900**

Irish agricultural policy changed with the EU Common Agricultural Policy (CAP) reform in 2005. With the CAP reform production based subsidies were replaced by production decoupled single farm payments. This system promotes innovation by farmers in that their basic income is secure through the single farm payment and they may become more market oriented in choosing what crops to grow to best supplement this income, thus presenting opportunities for energy crops [74]. In the context of the CAP reform livestock numbers were expected to decline thus freeing up grassland for other uses, furthermore cereal production was predicted to fall as a result of reduced livestock numbers because a large proportion of the cereals produced in Ireland is used as animal feed [30, 89]. In addition, in 2006 the EU adopted reforms to the sugar production regime, which resulted in the end of sugar production in Ireland and a sharp drop in the area under sugar beet [88]. Considering these changes to the Irish agricultural sector the amount of land potentially available to energy crops was estimated to be ~141,000 ha (100,000 ha of converted grassland, 10,000 ha of set aside land and 31,000 ha of land previously used for sugar beet production) [30]. Livestock numbers fell and consequently the total grassland dropped (~108,700 ha lower in 2009 compared to 2007 [88]). The land area dedicated to sugar beet production fell by 22,700

ha to 8,300 ha in 2009 compared to 2005 [88]. The level of cereal production dropped after CAP reform but has grown again in recent years. Energy crop planting has been low considering the amount of land that has been freed up since the CAP reform, Teagasc report that as of the end of 2009 there were 2,500 ha of energy crop (willow or miscanthus) planted under the Bioenergy Scheme for Willow and Miscanthus with a further 1,000 ha planned for 2010 [45]. It has been reported elsewhere that there are 500 ha of willow planted in Ireland [87], which implies that the majority (~2,000 ha) of the total energy crop planted under the scheme is miscanthus. The likely reasons for farmers' preference to growing miscanthus over willow are discussed later in this section. Considering the information presented, it may be stated that the cultivation of energy crops not only reduces GHG emission through displaced fossil fuels in the energy sector but also through the reduction in high GHG emission agricultural activity, i.e. livestock production.

Table 2.6 Willow and miscanthus crop cycle [89, 91, 92]

Year	Willow	Year	Miscanthus
0	Herbicide Ploughing	0	Herbicide Ploughing
1	Fertiliser and herbicide Soil rotovation Planting 15,000 plants per ha	1	Fertiliser and herbicide Soil rotovation Planting 20,000 rhizomes per ha
2	Cutback/coppicing[a] Fertiliser and herbicide	2	Fertiliser First year growth not harvested
5	Harvest Fertiliser and herbicide	3	Fertiliser and herbicide (if required)
8	Harvest		Harvest
9-20[b]	Repeat year 5-8 rotation	4-15[c]	Repeat year 3

[a] Cutback/coppicing is cutting the willow stems to initiate the development of multiple shoots [90].

[b] The willow plantation will last indefinitely; however, after 16 to 20 years it may be worthwhile planting new higher yielding willow varieties [91].

[c] The miscanthus crop will last at least 15 years [92].

As mentioned earlier, Irish farmers seem to have a preference for planting miscanthus over willow. Under the Bioenergy Scheme for Willow and Miscanthus only

357 ha of willow has been established compared to 2,100 ha of miscanthus as of year ending 2009 [90]. Some likely reasons for this trend are that miscanthus is an annual crop whereas willow can only be harvested every three years (Table 2.6), miscanthus is considered easy to grow and harvest as it is similar to other crops grown in Ireland and therefore conventional farm machinery may be used throughout the crop cycle. Finally, miscanthus is much drier than willow when harvested (possible 20% moisture content compared to ~55% for willow), which means less storage time and no need for expensive drying systems.

A major obstacle to the uptake of energy crops is the high initial establishment/planting costs (~€2,900 per ha) [30, 91]. In spite of these establishment costs, it has been reported that cultivation of both willow and miscanthus in Ireland is profitable compared to conventional land uses, including cattle rearing, sugar beet, wheat and barley [89]. In the UK willow chips are being sold at lower prices than forest wood chip [91]. In addition, the establishment/planting costs are expected to fall with experience by as much as 50% [66]. Intensive research and development into increasing biomass yields using hybrid willow and miscanthus varieties is being conducted, which will lead to increased profitability and thus decrease payback periods. Farmers are reluctant to invest in energy crops before an established biomass market in Ireland emerges and in turn, potential biomass consumers are reluctant to invest in biomass conversion systems because a guaranteed biomass supply does not yet exist. This highlights the need for strong financial incentives. Another aspect of energy crop cultivation that would deter new growers is the relatively long establishment periods compared to traditional crops (three years for miscanthus and four years for willow). Finally, the economically viable transport distance for energy crops presents a barrier (energy crops should be grown within a ~50 km radius around the end user).

2.7.3 Wood Processing Residues and PCRW

Wood processing residues, a waste product in the form of chips, sawdust and bark from the processing of sawlog at sawmills and manufacture of panel board at panel board mills is considered a suitable biomass fuel. The bulk of the sawmill residues serve as feedstock to the panel board mills (73% of total in 2008 see Figure A.1) and if it is assumed that the panel board mills demand for these residues remains constant [71, 85] any increase in processed sawlog will increase the level of sawmill residues available for energy purposes. The amount of sawlog processed at sawmills is expected to rise in the future as a result of increased roundwood production from the private sector forests. However, the wood processing residues due to this increased activity is not expected to be available as biomass fuel outside of the wood processing industry as it is likely to be utilised within the industry for own use energy purposes. The wood processing sector has the view that biomass availability is quite tight and it would therefore be difficult to source the quantities needed for new biomass CHP plants [60]. They would not be self-sufficient in supplying biomass if they were to install CHP and are therefore not in a position to supply other biomass plants.

PCRW, i.e. waste wood from construction/demolition and packaging, may be used as a fuel. Greater than 95% of this resource is already recovered and therefore potential for any additional bioenergy from this resource is very limited [85]. As a fuel PCRW may present some problems, contaminants such as glue and paint could result in slagging/agglomeration and harmful emissions.

With reference to Figure A.1, in 2008 a total of 758,000 m^3 of sawmill residues were produced, which consisted of 62% chip, 20% sawdust and 18% bark. None of the wood chip was used for energy purposes, with 96% of the chip used at the panel board mills and the balance exported. 67% of the sawdust also went to the panel board mills,

with 26% utilised for energy and 7% exported. The majority of the bark (63%) was used as CHP/boiler fuel with the remaining 37% used for horticultural purposes. The entire amount of panel board mill residues (106,000 m^3) were used for energy generation purposes, which consisted of 63% bark and 37% sawdust. Finally, a total of 208,000 m^3 of PCRW was recovered in 2008 with 59% used as feedstock in the panel board mills and 41% used as CHP/boiler fuel.

2.7.4 Straw

Straw, a dry agricultural residue and by-product of cereal production (wheat, barley and oats), has high potential as a biomass fuel in Ireland. The total resource has been estimated to be in the range of 1.1 to 1.4 Mt (16 to 20 PJ) [30]. After considering current uses (animal bedding, feed supplement and mushroom compost production) and the economics of collection and transport, it has been predicted that 10% (1.8 PJ) of the total resource could be utilised for energy production [30]. The total straw resource was expected to fall post CAP reform due to a reduction in land under cereal production [71, 74]. The land under cereal production did drop after CAP reform; however, it has increased in recent years, e.g. in 2008 the land under cereal production (wheat, barley and oats) reached 309,400 ha, which is higher than in 2004 prior to CAP reform [88].

Straw may be harvested and baled using conventional machinery after the cereal grains have been harvested. The straw is dry when harvested with a moisture content of 15 to 25% and therefore storage/drying is not necessary before being transported to the end user. As a fuel straw can be problematic. Its low ash softening temperature and high alkali content can cause major problems for fluidised bed systems. In addition, the high chlorine and potassium content in straw make it a difficult fuel [71]. The long particles

and low density can lead to difficulties during fuel feeding but this problem could be overcome by pelleting the material (also applies to miscanthus).

The major barrier to the uptake of straw as a fuel is the fact that it is a widely dispersed resource, which means that its level of utilisation will depend on the economics of collection and transportation. The price that end users are prepared to pay for the fuel must be high enough to account for these costs to encourage farmers to harvest the resource as opposed to simply ploughing it back.

2.8 Biomass Supply and Demand

Table 2.7 compares the existing and future available supply of biomass with the estimated minimum demand by 2020 that will be necessary to meet Ireland's bioenergy targets (i.e. RES-H, co-firing and CHP targets). A biomass demand equivalent to 3.6 million m^3 of roundwood or ~4 million wet tonnes was assumed [79, 87]. It has been suggested that the forest sector could only supply up to half of the required biomass [79], highlighting the importance of energy crops. Co-firing alone will require ~1 million wet tonnes or 7.1 PJ per annum [38]. As discussed previously, spruce (more specifically Sitka spruce) accounts for a large proportion of the national forest estate [71, 78]; therefore, all calculations for forest wood were carried out using data for Sitka spruce. To convert volume to mass and vice versa a density of 420 kg/m^3 db was assumed [93] and for the calculation of the fuel energy a LHV of 18.246 MJ/kg db was used [94]. Using this data the estimated demand by 2020 on an energy basis was found to be 27.59 PJ. Furthermore, ~1 million wet tonnes (60% moisture content) of Sitka spruce amounts to 7.1 PJ on an energy basis, which is consistent with Bord na Móna's calculations for co-firing demand.

Table 2.7 Biomass supply and demand with estimated electricity production potential

	Fuel Volume (m^3)	Fuel Mass (t)	Fuel Energy (PJ)	Electricity (MWe)
Demand				
Biomass				
2020	3,600,000	3,780,000[a]	27.59	-
Total demand by 2020	**-**	**-**	**27.59**	**-**
Supply				
Existing supply of wood fuel[b]				
2008 to 2020	586,000	351,600[c]	4.49	45.03
Private forest				
2010	341,000	204,600[c]	2.61	26.21
2015	435,000	261,000[c]	3.33	33.43
2020	725,000	435,000[c]	5.56	55.72
Public forest				
2010 to 2020	142,860[d]	150,000[a]	1.09	10.98
Energy crop[e]				
2010	-	56,000[f]	0.77	7.69
Willow energy crop				
2015	-	98,304[f]	1.35	13.55
2020	-	331,093[f]	4.55	45.64
Miscanthus energy crop				
2015	-	42,667[f]	0.58	5.84
2020	-	69,333[f]	0.95	9.49
Wood processing residues and PCRW				
2010	0	0	0	0
2015	264,000	158,400[c]	2.02	20.29
2020	543,000	325,800[c]	4.16	41.73
Straw				
2010	-	107,000[g]	1.5	15.08
2015	-	143,000[g]	2.01	20.15
2020	-	765,000[g]	10.75	107.79
Total supply by 2020[h]	**-**	**-**	**31.55**	**316.38**

[a] Assuming 60% moisture content.

[b] Includes wood used for heating (commercial and residential), the wood utilised at wood processing plants for process drying, heat and electricity and wood co-fired with peat at the Edenderry power station.

[c] Assuming 30% moisture content.

[d] Calculated using a conversion factor of 0.9524 m^3/t for wood containing 60% moisture.

[e] Willow and miscanthus contribution unknown; therefore, average values for energy crop yield and LHV were used to calculate the fuel energy.

[f] Assuming 25% moisture content.

[g] Assuming 20% moisture content.

[h] Assuming 25% straw collection efficiency, the total supply in PJ drops to 25.19 PJ and the total potential electricity production decreases to 252.62 MWe.

Under the heading supply in Table 2.7, the first biomass source listed is the existing biomass used for energy in Ireland, which consists of the wood used for fuelling heating systems, wood utilised at wood processing plants for process drying, heat and electricity and wood co-fired with peat at the Edenderry power station. The quantity used in 2008 was 586,000 m^3 [79] and this amount of roundwood was assumed to remain available annually over the period 2008 to 2020. Using data for Sitka spruce the mass at 30% moisture content, which is a moisture content considered acceptable for many biomass conversion systems (combustion and gasification), and the fuel energy in petajoules were determined. The potential electricity production was determined assuming a net electrical efficiency of 25.3% and a capacity factor of 80% (typical for BG-SOFC plants).

The private forest supply data presented in Table 2.7 for the years 2010, 2015 and 2020 are the same data plotted in Figure 2.9 (energy assortment series). The mass and fuel energy were calculated using properties for Sitka spruce assuming a moisture content of 30%. The potential electricity production was calculated using the same plant performance data as described above. As discussed in section 2.7.1, only forest residues are considered available to the energy market from the public forest estate. The quantity of 150,000 tonnes, estimated based on field trials undertaken by Coillte [84, 85], was assumed to be for Sitka spruce with a moisture content of 60%. The amount of forest residue available from public forests was assumed constant to 2020.

The biomass source entitled energy crop represents the 3,500 ha of energy crops that will be planted by the end of 2010 (see section 2.7.2). The fuel mass in tonnes (25% moisture content) was computed assuming an average energy crop yield of 12 tonnes per hectare (t/ha) db and the fuel energy was determined considering an average LHV of 18.25 MJ/kg. Average values for energy crop yield and LHV were used in the

calculations because the individual contribution of willow and miscanthus was not known. The full energy yield of 0.77 PJ may not be available for a number of years, considering the establishment period of energy crops (three to four years). The figures presented in Table 2.7 for willow and miscanthus in 2015 and 2020 were determined using data presented in Ireland's NREAP [17]. The moisture content of the biomass is not reported in the NREAP; however, considering the energy production values that are reported the forecasted quantities of willow and miscanthus appear to be for a moisture content of ~20%. In this work it was assumed that both willow and miscanthus contain 25% moisture when purchased as a biomass fuel. Therefore, the values presented in Table 2.7 are slightly greater than those published in the NREAP because the higher moisture content has been accounted for. Using lower heating values of 18.326 and 18.205 MJ/kg db for willow and miscanthus respectively [94] the fuel energy yields were computed and utilising the same power plant performance data as for the other biomass fuels the potential electricity production was determined. Considering energy crop yields of 10 and 14 t/ha db for willow and miscanthus respectively [89] the amount of agricultural land needed to grow the forecasted quantities of willow and miscanthus are 24,832 and 3,714 ha respectively by 2020.

Energy crop yield per ha has a very strong influence. Willow yield has been reported to range from 10 to 15 t/ha db [66]. The lower yield of 10 t/ha db was assumed in this work; however, the effects of increasing the yield to 15 t/ha db were investigated. The land area required to achieve the 331,093 tonnes (25% moisture content) of willow in 2020 dropped from 24,832 ha to 16,555 ha. In addition, the energy yield per ha increased (183.3 GJ/ha to 274.9 GJ/ha) and thus the land required to fuel a 1 MWe BG-SOFC plant (net electrical efficiency 25.3% and capacity factor 80%) fell from 544.1 ha to 362.8 ha. Miscanthus yield can range from 12 to 30 t/ha db [66]. A conservative yield

of 14 t/ha db was assumed in this work. Increasing the yield to 30 t/ha db was found to have significant influence on required land area and energy yield per ha. The required land area fell by over 50% and the energy yield per ha more than doubled (254.9 GJ/ha to 546.2 GJ/ha).

Wood processing residues and PCRW utilised for energy production were included in the existing supply category in Table 2.7. This was accounted for by subtracting the existing supply from the forecasted supply for the period 2010 to 2020. For 2010 it was assumed that there was no change in the amount of wood processing residues and PCRW used for energy production (compared to 2008) and therefore the 2010 supply is zero after accounting for the existing supply. For 2015 and 2020 the figures published in Ireland's NREAP were used [17]. The existing supply was accounted for by subtracting 317,000 m^3 (refer to Figure A.1) from the forecasted figures. Considering a moisture content of 30%, the mass of the fuel was determined. The fuel energy and potential electricity production were computed using the properties and parameters described previously for the private forest wood supply.

The final biomass type listed in Table 2.7 is straw. The data for straw available for energy production in 2010 was taken from a report published by the SEAI [71]. The authors of the report assumed that ~8% of the total straw resource was available to the energy sector after considering other uses (animal bedding, etc.) and the economics of collection and transportation. The quantities listed in Table 2.7 for 2015 and 2020 were published in Ireland's NREAP [17]. A moisture content of 20% was assumed, which is typical for straw (the calculated fuel energy content was found to match those reported in the NREAP and thus the assumed moisture content is accurate). As shown in Table 2.5, barley is the most widely grown cereal crop in Ireland and therefore the LHV of barley straw (17.563 MJ/kg db [94]) was used in the calculation of the fuel energy. The

potential electricity was determined using the same plant performance data as for the other fuels. Considering that the total straw resource has been estimated to be 1.25 Mt (20% moisture content) [30], the quantity of available straw for 2020 (765,000 tonnes) is very high (61.2% of total resource) and may be over predicted. As mentioned previously, straw is widely dispersed and its level of utilisation for energy will depend on the economics of collection and transportation. It is highly unlikely that 61.2% of the total resource will be used for energy purposes by 2020. A conservative estimate of 25% utilisation leads to a reduction in the fuel energy to 4.39 PJ and potential electricity to 44.03 MWe, which lowers the total 2020 supply to 25.19 PJ and potential electricity to 252.62 MWe.

From Table 2.7 it appears that the forecasted demand to meet the 2020 targets can be met by existing and forecasted supply (forecasted 2020 supply is 3.96 PJ higher than the demand). However, when the unrealistically high level of straw utilisation (10.75 PJ by 2020) is decreased to a more conservative level (4.39 PJ) there is a supply deficit of 2.4 PJ. In addition, it is highly unlikely that the full potential output from the private forest estate will be achieved, increasing the supply deficit even further. This would also affect the level of wood processing residue available, as the forecasted increase in residue is a direct result of a rise in private forest output. In contrast, energy crops have enormous potential. If all agricultural land in Ireland (~4.2 million ha) was used to grow energy crops the potential energy yield would be 920 PJ, assuming an average energy crop yield of 12 t/ha db and LHV of 18.25 MJ/kg db. This energy yield is approximately 1.34 times Ireland's TPER in 2008. If all of the land potentially available to energy crops ~141,000 ha (see section 2.7.2) was used, ~2.3 Mt (25% moisture content) of biomass fuel with an energy content of 30.9 PJ would be produced, which alone would be sufficient to meet Ireland's 2020 bioenergy targets. It is acknowledged

that energy crops are the only realistic method of generating sufficient additional indigenous supply to meet the 2020 targets [75].

The main barrier to further development of the bioenergy sector in Ireland is therefore insufficient biomass supply. There are a number of projects underway to address this issue. The 'Forestry Energy Research Programme 2010-2014' aims to investigate cost effective wood fuel supply chains in order to meet the growing demand [95]. Supply chains for wood fuel from private forest thinning and forest residues are two areas that will be investigated under the programme. Another project aims to develop a geographic information system that supports the development of the bioenergy sector via the cataloguing of current bioenergy resources and through modelling potential bioenergy output [96]. The country was divided into cells and each cell was given a suitability rating for each energy crop. This biomass resource mapping system is also important considering the relatively short economically viable transportation distance for biomass.

2.9 Chapter Summary

This chapter highlighted Ireland's dependence on fossil fuel energy imports and the need to develop an indigenous bioenergy sector to decrease this dependence. A strong case for biomass CHP over other renewable energy options such as wind was made (chapters one and two). The potential for bioenergy in Ireland is exceptional but to date its uptake has been very low. Insufficient biomass supply was identified as the main barrier. Measures that have been taken to increase biomass supply to date include: financial incentives through grants for forestry and energy crop growers, stimulating demand by setting co-firing targets, new biomass REFIT categories and financial incentives through grants for the installation of biomass conversion technologies. These

and new incentives are of paramount importance for the future development of the bioenergy sector in Ireland.

In conclusion, it will be necessary to increase the establishment of energy crops, ensure that private forest owners thin their forests and that an annual afforestation rate of at least 10,000 ha/a is achieved if Ireland is to meet its bioenergy targets and establish a sustainable biomass supply for the future.

3 LITERATURE REVIEW: GASIFICATION, FUEL CELLS, SYNGAS CONDITIONING AND MODELLING

3.1 Chapter Introduction

This chapter presents pertinent information available in the literature. Firstly, biomass conversion is discussed. Secondly, information on biomass gasification regarding history, theory and technologies is presented. The next section provides details on fuel cells under similar criteria. Then a description of syngas cleaning and reforming in terms of impurities and their impact, removal/conversion technologies, carbon deposition, etc., is provided. Based on the literature review, a syngas cleaning and reforming system suitable for BG-SOFC applications is proposed. Finally, existing biomass gasification, SOFC and combined BG-SOFC models available in the literature are described. The reader is referred elsewhere for a review of biomass pre-treatment (chipping, drying), handling and feeding as it is beyond the scope of this work but is of great importance for biomass plants [97-101].

3.2 Biomass Conversion

There are two major conversion routes for biomass as shown in Figure 3.1; biochemical and thermochemical. Both digestion (anaerobic and aerobic) and fermentation are examples of biochemical processes. The thermochemical conversion route is applicable to this research work, i.e. processes that are driven by thermal energy. Combustion involves complete conversion of biomass in excess oxidant (usually air) to CO_2 and H_2O at high temperature. In contrast, gasification involves biomass conversion in an O_2 deficient environment. Pyrolysis takes place at a relatively

low temperature in the total absence of O_2 [97]. The liquefaction process, which is the only thermochemical process that is irrelevant to this work, breaks down the large biomass molecules into liquids (oily compounds) having smaller molecules [97, 102]. This occurs in the presence of a catalyst at low temperature and high pressure.

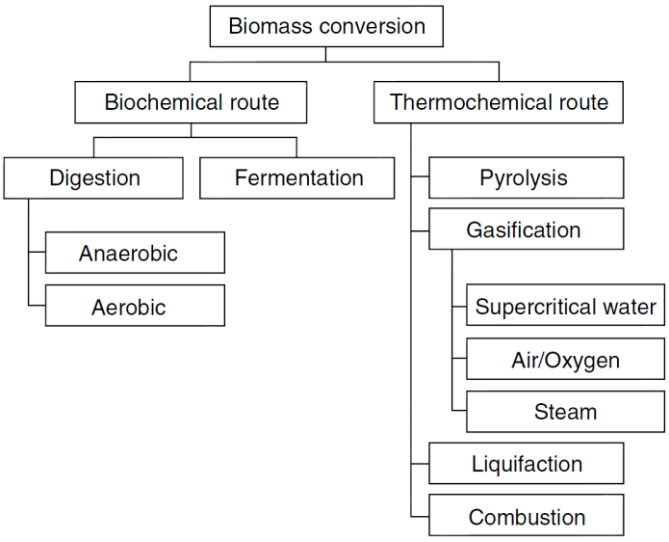

Figure 3.1 Biomass conversion routes and processes [97]

Gasification is a thermochemical process in which a carbonaceous fuel is converted to a combustible gas known as syngas, consisting of H_2, CO, CH_4, CO_2, H_2O, N_2, higher hydrocarbons and impurities (e.g. tars, NH_3, H_2S and HCl). The process occurs when a controlled amount of oxidant (pure O_2, air, steam) is reacted at high temperatures with available carbon in a fuel within a gasifier. Gasification converts biomass to a gas, which can then be utilised in advanced power generation systems such as fuel cells thus achieving higher electrical efficiencies compared to combustion based technologies. For this reason, gasification is considered the enabling technology for modern biomass use [103]. Furthermore, it offers greater flexibility in terms of applications (electricity, heat, transport fuels and chemicals) as depicted in Figure 3.2.

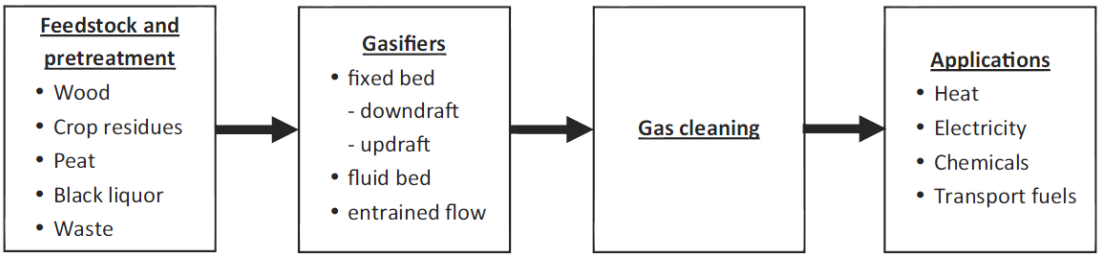

Figure 3.2 Flexibility of gasification process [103]

In Ireland, the main focus is on combustion based systems for biomass power generation. Currently, the largest biomass to electricity application is co-firing at the Edenderry peat power station (see chapter two). Additionally, biomass is converted to heat and power at Irish wood processing plants by means of low electrical efficiency combustion systems at small scale [60]. A 15 MWe straw fuelled CHP plant (combustion technology) is planned and should be fully operational by 2016 [104].

3.3 Biomass Gasification

Gasification has a long history. Coal syngas (town gas) was used for lighting in the 19th and early 20th century. The discovery of natural gas decreased interest in gasification [97]. During the Second World War the shortage of liquid fuels led to the installation of biomass/coal gasifiers in automobiles [105]. The wider availability of natural gas in the 1950s dampened the development of coal and biomass gasification (BG) [97]. The oil crisis of the 1970s renewed interest and resulted in the installation of fixed and fluidised bed biomass (heat) gasifiers at paper mills in Finland and Sweden in the 1980s [105, 106]. Work was also conducted on highly efficient integrated gasification combined cycle (IGCC) technology (see section 3.3.4). More recently, environmental considerations and energy security have been the driving forces for interest in gasification (biomass and coal). Despite the years of work, BG is still

considered to be at an early stage of development [103]. CHP has become the main application for BG (heat was in the past) but deployment has been limited due to high costs [103, 107].

3.3.1 Gasification Theory

The following fundamental reactions occur during pyrolysis and gasification respectively of biomass or coal [108]:

$$\text{Biomass} \xrightarrow{Heat} \text{Char} + \text{Liquids} + \text{Gases} \qquad \text{Eq. 3.1}$$

$$\text{Char} + \text{Gasification Medium} \xrightarrow{Heat} \text{Gases} + \text{Ash} \qquad \text{Eq. 3.2}$$

The gasification process may be split into steps: drying (at 100-200 °C), pyrolysis (at 200-500 °C), gasification and combustion. As the biomass enters the gasifier, it is first dried. Then pyrolysis occurs during which char, H_2, CO, CH_4, CO_2, H_2O, tars and hydrocarbons are produced. The char is a carbon rich solid residue [109]. For modelling purposes, it was assumed in this research work that char was 100% carbon (graphite). Demirbaş reported the elemental analysis of various wood chars and the carbon content ranged from 90.5 to 92.1 wt. % [109]; therefore, this assumption is valid. The char is gasified or burnt via heterogeneous reactions (Table 3.1). Gaseous phase reactions also take place (homogeneous reactions in Table 3.1). These steps are frequently modelled in series but there is no sharp boundary dividing them and they often overlap [13]. Combustion is necessary to supply the heat required for the endothermic gasification reactions (Table 3.1). Pyrolysis depends on process variables such as heating rate, particle size and volatile content of the fuel, hundreds of pyrolysis products may be formed [67]. There is neither a unified approach nor an overall kinetic equation

describing the pyrolysis step for all possible biomass under all possible circumstances [110]. Therefore, pyrolysis is very difficult to model and is a source of high uncertainty [97, 111]. Some researchers resort to using empirical data to set the yields of pyrolysis. For engineering design purposes, the black box approach can be useful [97]. The black box approach to pyrolysis was applied in this research work. These gasification steps are illustrated in Figure 3.3.

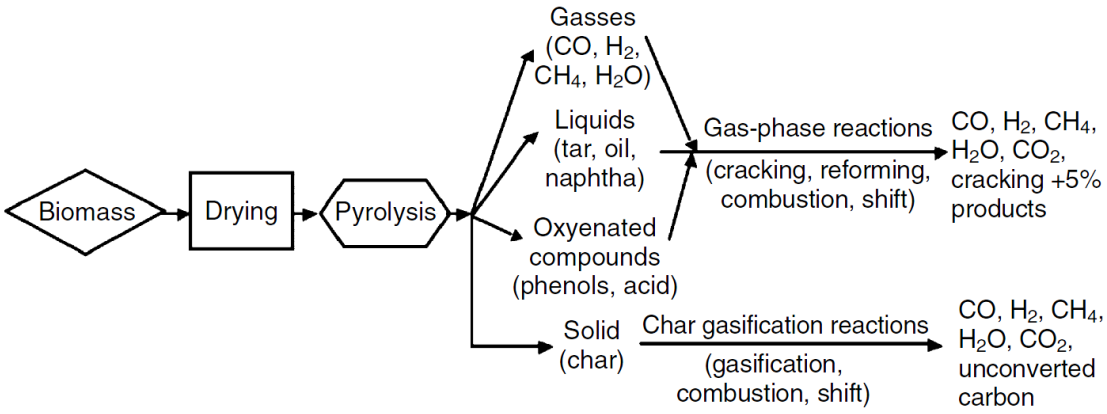

Figure 3.3 Biomass gasification steps and reaction pathways [97]

The modelling approach in this research work, assumes that BG can be represented by a limited number of chemical reactions (Eq. 3.3-3.13), i.e. the main gasification reactions provided in Table 3.1. Hundreds or even thousands of chemical reactions may occur during BG [65, 67]. It is common in modelling and simulation to consider the main reactions only [108]. Pyrolysis plays a major role in biomass gasification as biomass contains a high level of volatile matter (see section 2.6.2); therefore, the syngas composition depends strongly on pyrolysis. The combustion reactions listed in Table 3.1 are the fastest and are thus of great importance [97]. However, in the case of dual fluidised bed steam gasification the combustion and gasification steps occur in separate reactors (see section 3.3.2); therefore, the

combustion reactions Eq. 3.7 and 3.8 do not take place and the char partial combustion reaction (Eq. 3.3) does not compete with the other heterogeneous reactions (Eq. 3.4-3.6). The water-gas reaction (Eq. 3.5) is the key gasification reaction followed by the slower Boudouard reaction (Eq. 3.4) [97]. Both the Boudouard and water-gas reactions are several orders of magnitude faster than the methanation reaction (Eq. 3.6) [69, 97]. The CO-shift reaction (Eq. 3.9) is the most important homogenous reaction followed by steam-methane reforming (Eq. 3.10) [97].

Table 3.1 Main gasification reactions [69, 97]

Reaction	Heat of reaction[a]	Reaction name	Reaction number
Heterogeneous reactions:			
$C + 0.5O_2 \rightarrow CO$	(-111 MJ/kmol)	Char partial combustion	Eq. 3.3
$C + CO_2 \rightleftharpoons 2CO$	(+172 MJ/kmol)	Boudouard	Eq. 3.4
$C + H_2O \rightleftharpoons CO + H_2$	(+131 MJ/kmol)	Water-gas	Eq. 3.5
$C + 2H_2 \rightleftharpoons CH_4$	(-75 MJ/kmol)	Methanation	Eq. 3.6
Homogeneous reactions:			
$CO + 0.5O_2 \rightarrow CO_2$	(-283 MJ/kmol)	CO combustion	Eq. 3.7
$H_2 + 0.5O_2 \rightarrow H_2O$	(-242 MJ/kmol)	H_2 combustion	Eq. 3.8
$CO + H_2O \rightleftharpoons CO_2 + H_2$	(-41 MJ/kmol)	CO-shift	Eq. 3.9
$CH_4 + H_2O \rightleftharpoons CO + 3H_2$	(+206 MJ/kmol)	Steam-methane reforming	Eq. 3.10
NH_3, H_2S and HCl formation reactions:			
$0.5N_2 + 1.5H_2 \rightleftharpoons NH_3$	nr[b]	NH_3 formation	Eq. 3.11
$H_2 + S \rightleftharpoons H_2S$	nr	H_2S formation	Eq. 3.12
$Cl_2 + H_2 \rightleftharpoons 2HCl$	nr	HCl formation	Eq. 3.13

[a] Negative sign indicates an exothermic reaction and a positive sign indicates an endothermic reaction.

[b] nr = not reported.

Gasification is heavily dependent on the employed gasifying medium (pure O_2, air or steam). Air gasification produces a low energy content syngas, around 4-7 MJ/m^3 (HHV), while O_2 and steam blown processes result in a syngas with a heating value of 10-18 MJ/m^3 (HHV) [12]. Gasification with pure O_2 is not practical for BG due to

prohibitively high costs for O_2 production using commercial technology (cryogenic air separation). According to Higman and van der Burgt O_2 supply to the gasifier is one of the most expensive parts of any gasification project [69]. Higman and van der Burgt concluded that O_2 gasification should only be used for plants > 50 MW [69]; therefore, it is not suitable for BG. In the long term, new technologies such as ion transport membranes may decrease O_2 production costs and thus make it attractive for BG.

Cold gas efficiency (*CGE*) is a means of indicating the performance of a gasifier and is defined as:

$$CGE = \frac{\dot{m}_{gas} \cdot HV_{gas}}{\dot{m}_{fuel} \cdot HV_{fuel}} \times 100 \qquad \text{Eq. 3.14}$$

where $\dot{m}_{gas}$ and $\dot{m}_{fuel}$ are the mass flow rate in kg/s of syngas and biomass respectively and HV_{gas} and HV_{fuel} are the heating value in kJ/kg of the syngas and biomass respectively (LHV or HHV basis). A high *CGE* is desirable, the higher the *CGE*, the greater the fraction of energy in the syngas, which leads to higher system efficiency.

3.3.2 Gasifier Types

There is a broad range of gasifier types in existence. Differences between classifications are in the movement of the fuel through the vessel, the operating pressures and temperatures and the size and condition of the raw fuel [112]. Furthermore, in this section it will be apparent that gasifier classification depends on direction of flow (e.g. downdraft or updraft fixed bed), the gasification medium (pure O_2, air, steam), the flow rate of the gasification medium and the method of gasifier heating (direct/autothermal or indirect/allothermal). The primary configurations are

moving/fixed bed, fluidised bed and entrained flow. For a comprehensive list of gasification technologies and suppliers, refer to Kirkels and Verbong [103], Olofsson et al. [113] and Austermann and Whiting [107].

Fixed bed

Fixed bed (also known as moving bed) gasifiers are the oldest type and are considered simple and robust [113]. These gasifiers operate with counter-current or co-current movement of fuel and oxidant through the vessel. The fixed bed gasifiers counter-current and co-current flow are known as updraft and downdraft gasifiers respectively (see Figure 3.4). Examples of commercial updraft fixed bed gasifiers are the Sasol-Lurgi dry bottom process and the British Gas/Lurgi slagging process [114]. Due to the simplicity of the design, it is easy to distinguish the steps of the gasification process (drying, pyrolysis, gasification and combustion) and therefore the fixed bed gasifier may be split into zones as shown in Figure 3.4.

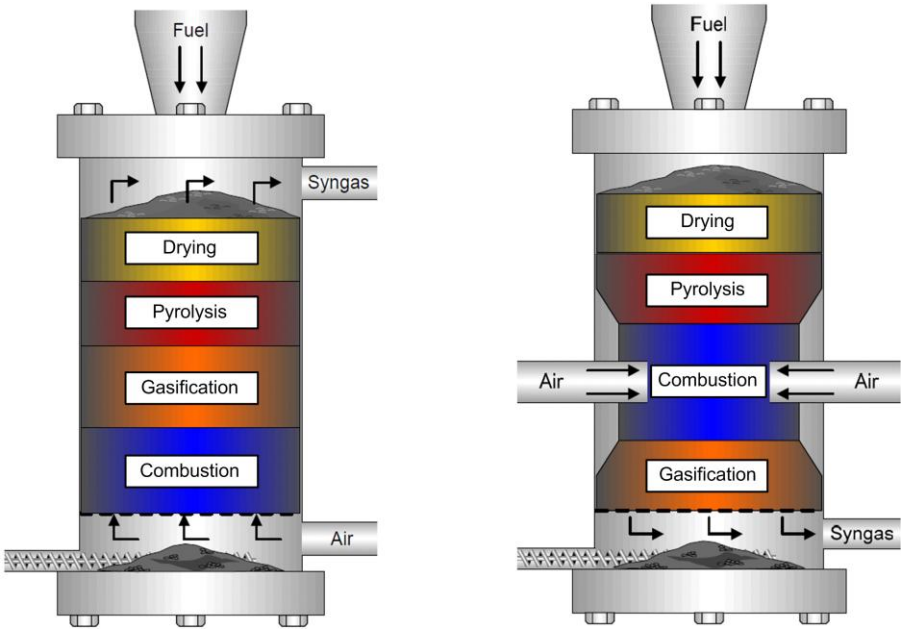

Figure 3.4 Simplified schematics of updraft (left) and downdraft (right) fixed bed gasifiers [113]

In updraft gasifiers, the syngas is cooled to a low temperature in the pyrolysis and drying zones before it exits. This results in very high syngas tar content [69, 97]. It has been reported that > 20% of the energy content of the syngas from updraft gasifiers is contained in the tar [107]. Considering that most commercial plants use filters and scrubbers to remove tar, this energy is usually lost. This is a major disadvantage of updraft gasifiers. There are over 100 fixed bed biomass gasifiers installed in Europe and the USA and hundreds installed in developing countries for rural electrification; however, the technology for power generation is still not considered to be commercial and is seen as unreliable [115]. Most updraft biomass gasifiers have been decommissioned due to environmental issues [102]. The downdraft design overcomes the tar problem, producing syngas with the lowest tar content of all biomass gasifiers [97]. This is accomplished by passing the pyrolysis products through the high temperature combustion zone prior to leaving the gasifier. Both mixing and heat transfer within the fixed bed are poor, which makes it difficult to achieve uniform distribution of fuel, temperature and gas composition across the cross-section of the gasifier [97]. This limits the scale of downdraft gasifiers.

Both fixed bed gasifier types have strict feed requirements in comparison to fluidised beds. They necessitate feed in the range of 6-50 mm and excessive fines in the feed will cause operational problems [69]. Downdraft gasifiers require relatively low moisture fuels; many manufacturers specify a maximum moisture content of 15% [107]. This is a major drawback for biomass applications as drying to this level is usually uneconomical. Both fixed bed designs achieve high *CGE*, in the range of 80-90%, which is the reason that interest in the technology continues. Recent research has been carried out on a new downdraft design called Viking [9, 116]. It is a two stage gasification process with drying and pyrolysis occurring in a separate screw conveyer

unit prior to gasification in the downdraft gasifier unit. The Novel updraft fixed bed gasifier is another example of recent work on fixed bed gasification; a 7.2 megawatts thermal (MWth) CHP plant based on the technology was built in Finland (see Appendix B for further details).

Fluidised bed

A fluidised bed is made of granular solids (bed material) that are kept in a semi-suspended condition (fluidised state) by the passage of the gasification medium through it at an appropriate velocity [97]. The velocity of the gasification medium determines whether the fluidised bed is a bubbling fluidised bed (BFB) or a circulating fluidised bed (CFB) (refer to Figure 3.5). CFB gasifiers have higher gas velocity than BFB gasifiers. Commonly employed bed materials include sand, dolomite and olivine. The bed material enhances heat exchange and increases mixing and kinetics, thus increasing overall gasifier efficiency and fuel throughput [113]. The bed materials immediately disperse the heat released by the chemical reactions to the entire fluidised bed [97]. As a result, fluidised bed gasifiers are noted for their excellent mixing and temperature uniformity. A major advantage over fixed bed gasifiers is the uniform distribution of temperature within the reactor [102].

The fuel (particles of 6-10 mm) is fed into or above the bed. It is then suspended in continuous random motion by the gasification medium, introduced near the bottom of the vessel. When the syngas is to be used for power generation, gasification with air may be applied and in the case of BG, it often is [69]. Recently, there has been a lot of interest in using steam instead of air in order to produce a higher quality syngas suitable for many applications (e.g. conversion in fuel cells or production of chemicals).

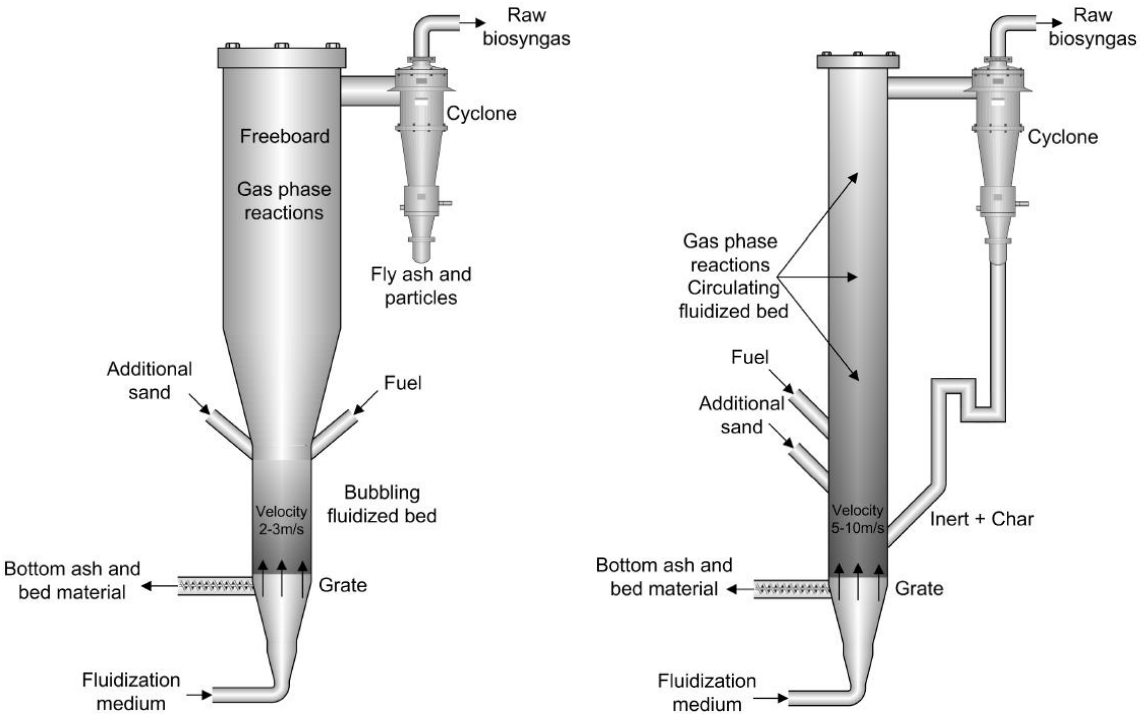

Figure 3.5 Simplified schematics of BFB (left) and CFB (right) gasifiers [113]

For both BFBs and CFBs, un-reacted char becomes entrained in the syngas exiting the gasifier along with bed material and fly ash. A cyclone separates out the bulk of these solid particles and in the case of a CFB gasifier they are recycled to the bottom of the gasifier, which improves carbon conversion and efficiency. The operating temperature is restricted to temperatures below the ash softening temperature of the fuel (800-1000 °C for biomass) in order to avoid agglomeration and defluidisation [69]. This low temperature operation means that fluidised bed gasifiers are best suited to gasifying reactive feedstocks, such as biomass [69, 97]. Biomass char is more porous and therefore more reactive than other fuel char (e.g. coal char). Unlike fixed bed gasifiers, fluidised bed gasifiers are tolerant of fines and fuel moisture. Moreover, they have high fuel flexibility, which is advantageous for biomass plants as biomass availability can determine what fuel is utilised, i.e. it may be necessary to switch between biomass fuels. There is no real scale up limit; however, scale is dependent on biomass availability and

transport distance. The tar content in the syngas is much lower than updraft gasifiers but substantially greater than downdraft gasifiers. It is possible to add catalytically active material to the bed to reduce tar level. This has been done very successfully at the Güssing CHP plant (olivine bed material).

Fluidised beds have some disadvantages. The syngas has relatively high particulate loading meaning cyclones and filters are required. Carbon conversion is limited to about 97%, whereas fixed bed and entrained flow gasifiers can achieve 99% conversion [69]. As a consequence, the *CGE* of fluidised beds are in the range of 70-80%, i.e. significantly lower than fixed beds. Examples of current research on fluidised bed gasification include the work done on the HoSt CFB gasifier; a 3 MWth CHP plant was constructed in Tzum (Netherlands) but the project was put on hold due to fuel supply issues [117]. Siedlecki carried out experimental and simulation work on CFB steam-O_2 blown BG at TU Delft (Netherlands) [118].

Entrained flow

Entrained flow gasifiers are the preferred technology for coal gasification. Reactors of this type typically operate at 1,400 °C and 20-70 bar, where powdered fuel is entrained in the gasifying medium [97]. The prevailing high temperatures (~1,400 °C) compensate for the very short residence times (~1 second) of carbonaceous feed to achieve faster kinetic rates while promoting tar cracking [114]. A negative effect of the high reactor temperature is a high O_2 requirement, which results in high operating costs. Powdered fuel is injected into the reactor chamber along with O_2 and steam (air rarely used). To facilitate feeding into the reactor the fuel may be mixed with water to make slurry. The gas velocity in the reactor is sufficiently high to fully entrain the fuel particles [97]. Entrained flow gasification is only suitable for large scale applications (>

50 MWth). As a result of the high operating temperature a very high quality syngas is produced with low CH_4 content and no other hydrocarbons, the high temperature destroys all tars and oils. A properly designed and operated entrained flow gasifier can have carbon conversion close to 100% [97].

According to Basu, the suitability of entrained flow gasification for biomass is questionable [97]. Owing to a short residence time, the fuel needs to be very fine, and grinding fibrous biomass into such fine particles is difficult and expensive. Also, molten biomass ash is highly aggressive (due to high alkali content), which greatly shortens the life of the gasifier's refractory lining. In addition, biomass is not suited to the large scales required for these systems. Furthermore, the relatively high moisture content of biomass makes it a difficult fuel for entrained flow gasification. Finally, pressurised BG is generally not attractive due to high costs associated with biomass pressurisation using commercial technology (lock hopper system) [119-121].

The production of biomass powder suitable for entrained flow gasification from different feed stocks is an extra cost, but may be reduced by an initial torrefaction process [113]. Torrefaction is a mild form of pyrolysis that makes the biomass brittle and easier to grind into small particles. An example of a biomass entrained flow gasification process is the Choren process. It is a three stage process; the fuel is first pyrolysed and the gases and char are separated. The gases are combusted in the second stage. In the final stage, the char is gasified along with the gases from the second stage [113]. Olofsson et al. reports that the Choren process is likely to be too complex and expensive and also implies that there are several severe issues not openly discussed by the technology developer [113].

Dual fluidised bed

As mentioned in the fluidised bed gasifier section, there has been a lot of interest in using steam as gasification medium in order to produce high quality syngas suitable for applications such as fuel cells. A special type of fluidised bed gasifier known as the dual fluidised bed (DFB) utilises steam as gasification medium. A DFB gasifier is based on the principle that separation of the gasification and combustion zones (GZ and CZ) will avoid N_2 dilution of the syngas (due to combustion of fuel with air) and thus a high quality gas will be produced without the need for an expensive air separation unit, which would be required for O_2 blown gasification. These gasifiers are also known as indirectly heated or allothermal gasifiers as the GZ and CZ are separated and heat is transferred between them by means of circulating bed material, heat pipes or some alternative method. Examples of these gasifiers include the Pyrox DFB, Silvagas DFB, MILENA, Heatpipe Reformer and fast internally circulating fluidised bed (FICFB). Refer to Corella et al. [122] and Göransson et al. [123] for a review of the various DFB gasifier technologies.

A detailed description of the FICFB technology will be presented as it was modelled in this research work. This technology has been under development since the early 1990s at TU Wien and has been demonstrated at industrial scale (8 MWth fuel input) in Güssing (Austria) since 2002 [124, 125]. Due to its significance, this plant is discussed in detail in Appendix B. The fundamental idea of this system is to physically separate the gasification and combustion reactions in order to gain a largely N_2 free syngas [126, 127]. With reference to Figure 3.6, the biomass fuel enters a BFB reactor (GZ) where it is dried, pyrolysed and gasified with steam [128]. Char leaves the GZ with bed material through an inclined chute and enters a CFB riser (CZ) where it is combusted with air. After separation from the flue gas in a cyclone, the heated bed

material flows back to the GZ via a loop seal [128]. This bed material provides the heat required to drive the endothermic steam gasification reactions which produce the syngas. The FICFB gasifier operates at atmospheric pressure. The syngas is of high quality and is characterised by low N_2 content, high H_2, low tar level and high energy content. These characteristics make the syngas suitable for many applications, including CHP using gas engines, gas turbines or fuel cells, as an intermediate product for chemical synthesis or synthetic natural gas (SNG) production [129]. Moreover, the FICFB gasifier has been described as the most suitable gasification technology for integration with fuel cells [130].

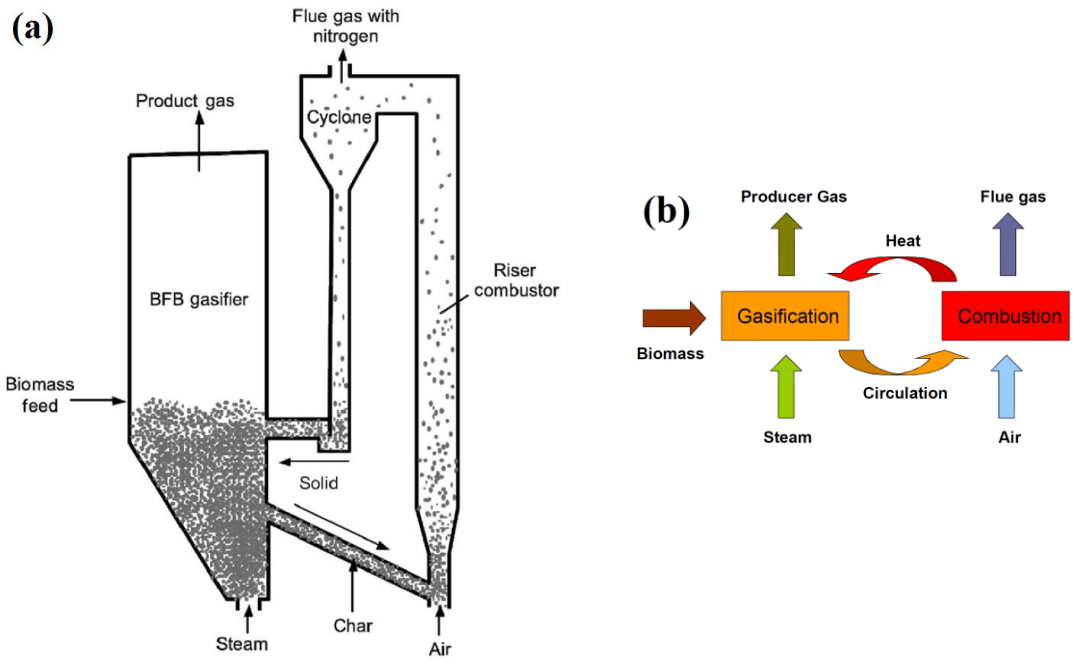

Figure 3.6 (a) FICFB gasifier schematic [97] and (b) FICFB gasifier operating principle [131]

The FICFB technology was successfully scaled up from laboratory to industrial scale within ten years [131, 132]. The scale up process was as follows: cold flow model and simulation → 10 kWth test rig → 100 kWth pilot plant → 500 kWth pilot plant →

8 MWth demonstration plant [124, 133]. The cold flow model was built to study and optimise the fluid mechanics of the process [124]. The 10 kWth test rig design was very different to the current FICFB gasifier design. It consisted of an annular BFB reactor with a CFB riser in the centre [124]. Based on experience with the test rig, the first 100 kWth pilot plant was built and experiments conducted over the period 1995 to 1999. In 1999 a new 100 kWth pilot plant was commissioned which included design changes to enhance operational performance. A third 100 kWth pilot plant was built in 2003 with minor design changes and is still in use today [124]. Experiments were conducted using different bed materials (sand, olivine, etc.) and various fuels (wood pellets, wood chips, straw, willow, etc.) and parameter studies were carried out [124, 126, 131]. The FICFB technology was scaled up to 500 kWth within the framework of an EU project (1998-2001) [134]. The pilot plant is located at the ENEA Trisaia Research Centre (Italy). Construction of the plant was completed in 2000 [130]. Finally, the 8 MWth demonstration plant was constructed and has been in operation since 2002. In Oberwart (Austria) the second CHP plant based on the FICFB technology was realised and has been operational since 2008 [135]. In addition, two more FICFB based facilities began operating in the period 2010-2011 (one located in Villach, Austria and another in Ulm, Germany) [136]. However, it has been reported that the Villach plant has been put on hold or has become insolvent [137]. Current FICFB gasification research efforts include: production of Fischer-Tropsch (FT) fuels from syngas, upgrading syngas to SNG and mixed alcohols and conversion in a fuel cell [137, 138]. A 20 MW SNG plant (based on FICFB technology) is in commissioning in Sweden [137].

This paragraph gives a brief summary of the latest developments regarding other DFB gasifiers. The Pyrox DFB gasifier was demonstrated at a scale of 150 tonnes per day (t/d) at three plants in Japan from 1983 to 1989 [122]. Work on this technology

ceased until recently with the installation of a 5 t/d unit at University of California (USA) [139]. The Silvagas DFB technology was acquired by Rentech in 2009 and there have been no operating units since the Vermont plant shut down in 2001 (see Appendix B); however, Rentech have a number of projects in planning [139]. The MILENA DFB gasifier has been tested at pilot scale and efforts are ongoing to realise an 11.6 MWth demonstration plant [140]. There are concerns about the lifetime of the wall separating the two fluidised beds as it would experience severe redox conditions during normal operation [122]. A successful demonstration plant would help to allay these concerns. The Heatpipe Reformer technology has been proven at pilot scale (500 kWth). Two commercial plants, one in Germany and another in Italy, have been built but were closed when the Heatpipe Reformer supplier (Agnion) became insolvent [141]. Agnion has been acquired by ENTRADE Group and the two plants should be fully operational in early 2014 [141].

3.3.3 Gasifier Selection

Gasification technologies were selected for this study and the main reasons for the selections are outlined as follows. Firstly, entrained flow gasification was considered unsuitable for reasons of feed requirements, cost, complexity, scale, etc., (see section 3.3.2 for full details). Fixed bed gasification was also ruled out. Updraft gasifiers produce a syngas with extremely high tar content, making them unsuitable for most power applications (gas engines, gas turbines and fuel cells). Some researchers have argued that updraft gasification is suitable for integration with SOFCs because the tars remain in the gaseous phase if the syngas is kept at elevated temperature [11]. However, problems due to the high tar content are likely using current syngas cleaning technologies which are limited to an operating temperature of ~400 °C (see section

3.5.1). In addition, further research must be done in order to prove that SOFC operation on high tar syngas is feasible before updraft gasification can be considered attractive. Downdraft gasifiers are limited to small scale and require low moisture fuels. Furthermore, fixed bed gasifiers have strict feed requirements in comparison to fluidised beds and cannot handle excessive fines.

According to Iliuta et al., fluidised bed technology has reached a high level of reliability [114]; numerous commercial plants have operated for many years since the 1980s. Fluidised bed gasification is well proven, fuel flexible and suitable for a wide range of scales. In addition, fluidised bed gasifiers are tolerant of fines in the fuel feed and do not require very low moisture fuels. Fluidised bed gasifiers are commercially available, e.g. Foster Wheeler CFB and BFB. The FICFB gasifier will also be considered commercial if the recently constructed plants operate successfully over an extended period of time. Figure 3.7 affirms the arguments made regarding gasifier selection. It shows that fluidised bed gasification is more attractive for power applications than both entrained flow and fixed bed gasification.

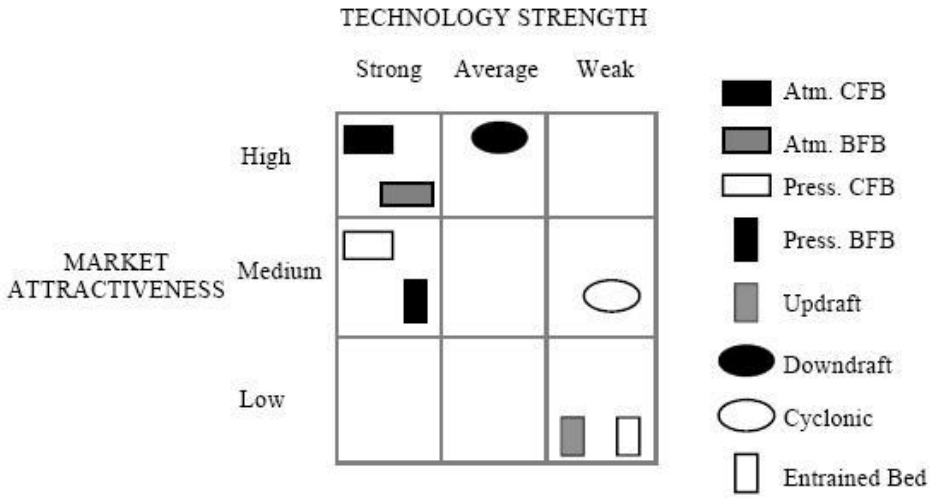

Figure 3.7 Technology strength and market attractiveness of biomass gasification technologies for power applications [142]

The CFB and FICFB gasifiers were chosen for this research work. As described in section 3.3.2, DFB gasifiers produce high quality syngas (high energy content, high H_2 and N_2 free) well suited to fuel cells. The FICFB gasifier was selected over alternative indirect gasification technologies as it is the most proven. Furthermore, research work on integration of the FICFB gasifier and fuel cells is ongoing. An EU project (2001-2004) on integration of FICFB technology with high temperature gas cleaning and molten carbonate fuel cell (MCFC) technology was completed [130]. A 125 kWe MCFC was to be installed at the Trisaia 500 kWth FICFB pilot plant. This does not appear to have been accomplished during the project timeframe as more recent publications reported that the MCFC was under construction [143]. The latest project 'HotBiocell' (2011-2014) aims to investigate the integration of the 500 kWth pilot plant with high temperature fuel cells (MCFC and SOFC) [138]. Additionally, SOFC testing has been carried out onsite at the Güssing FICFB gasifier [19, 20, 144].

3.3.4 Gasification Plants

According to the US Department of Energy '2010 Worldwide Gasification Database', total gasification capacity is 70,817 MWth of syngas, consisting of 144 plants with 412 gasifiers [145]. In addition, there are 48 plants under construction or planned to be operational by 2016, 40 of which will be coal fed. Coal is the most popular gasifier feedstock (51%), followed by petroleum (25%), natural gas (22%), petcoke (1.3%) and biomass/waste (0.5%) [145]. Product distribution from the installed gasification capacity is as follows: chemicals (45%), liquid transport fuels (38%), electricity (11%) and gaseous fuels (6%). Interest in electricity from gasification is growing rapidly as it accounts for 38% of the planned new capacity by 2016. The majority of these power plants will be coal fed IGCC. An IGCC plant consists of the

following main components: the gasifier, an air separation unit if pure O_2 is used as oxidant, gas processing system, gas turbine (GT), heat recovery steam generator (HRSG) and steam turbine (ST). A conceptual diagram for an IGCC power plant is shown in Figure 3.8. The fuel is fed into the gasifier along with oxidant. The raw syngas leaving the gasifier contains unwanted contaminants that must be removed prior to combustion in the GT. Due to limits on the cleaning technologies available, the raw syngas must be cooled before it is cleaned. After cooling and cleaning, the syngas is combusted. The products of combustion are expanded through the GT producing electricity. The GT exhaust is directed to the HRSG, which generates steam. The steam is expanded in the ST, generating additional electricity.

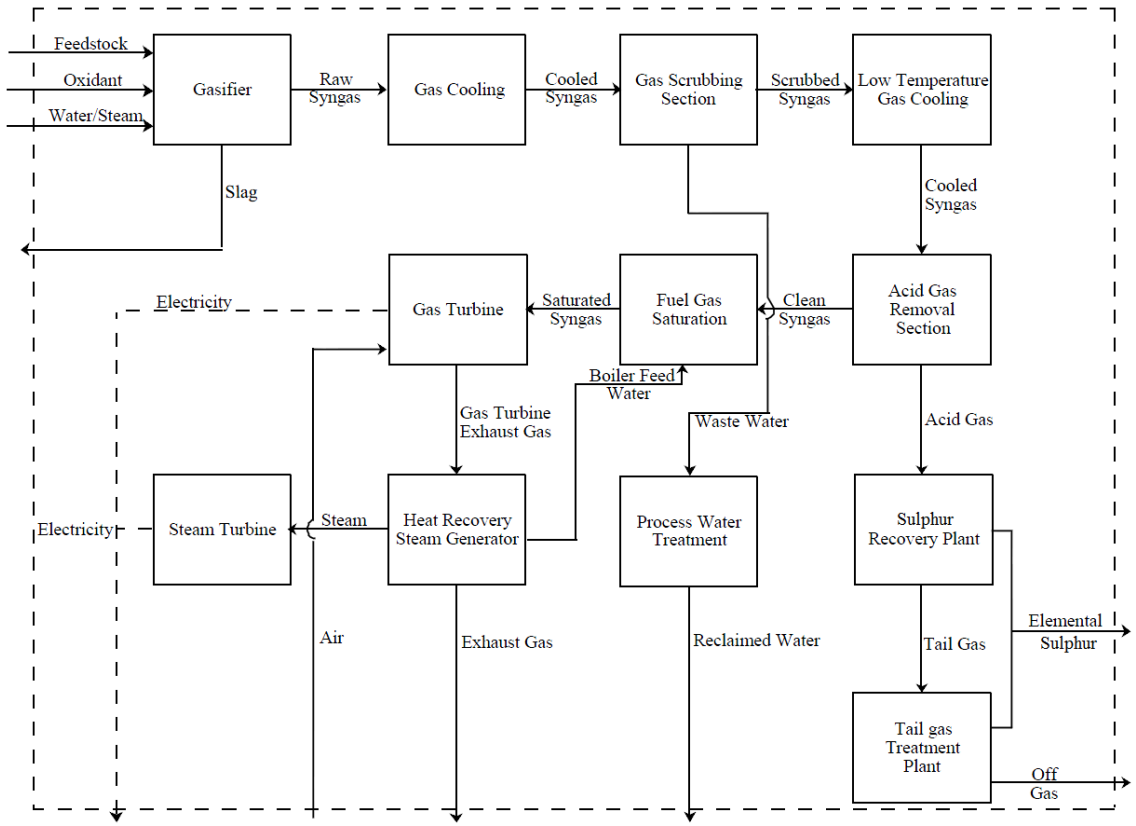

Figure 3.8 Conceptual diagram for an IGCC plant [146]

Table 3.2 presents details on various BG plants. The plants listed in Table 3.2 are described in Appendix B and considered the most relevant to this work; for a comprehensive review of BG facilities the reader is referred to the IEA Bioenergy Task 33 website [117].

Table 3.2 Biomass gasification demonstration and commercial plants

Name/Location	Gasifier	Plant Type	References
Nuon Buggenum IGCC (NL)	Shell Entrained Flow	IGCC 85 MWth Biomass Fuel	[140, 143]
Elcogas Puertollano IGCC (Spain)	Prenflo Entrained Flow	IGCC 10% of Fuel Input	[147]
Värnamo Biomass IGCC (Sweden)	Foster Wheeler/ Sydkraft Pressurised CFB	IGCC 18 MWth Fuel	[120, 148]
ARBRE Plant Yorkshire (UK)	TPS CFB	IGCC 25 MWth Fuel	[149, 150]
BCL/FERCO Demo Vermont (USA)	BCL/FERCO/Rentech SilvaGas DFB	Boiler 44 MWth Fuel	[119, 151]
Hawaii Renugas Demo (USA)	GTI Renugas Pressurised BFB	Gas Flared 15 MWth Fuel	[65, 119, 152]
Renugas Pilot Plant Tampere (Finland)	Metso/Carbona/GTI Pressurised BFB	Boiler 15 MWth Fuel	[119, 149]
Carbona CHP Skive (Denmark)	Carbona/GTI Pressurised BFB	Gas Engine or Boiler 20 to 28 MWth Fuel	[153]
Biomass CHP Güssing (Austria)	TU Wien DFB (FICFB)	Gas Engine 8 MWth Fuel	[154, 155]
Energie Oberwart (Austria)	TU Wien DFB (FICFB)	Gas Engine/ORC[a] 8.5 MWth Fuel	[154, 155]
Kymijärvi CHP Plant Lahti (Finland)	Foster Wheeler CFB	Boiler 60 MWth Fuel	[119, 156]
BioCoComb Plant Zeltweg (Austria)	CFB	Boiler 10 MWth Fuel	[119, 157]
Electrabel Ruien (Belgium)	Foster Wheeler CFB	Boiler 50 MWth Fuel	[65, 157]
Amer/Essent CHP Geertruidenberg (NL)	Lurgi CFB	Coal Bolier 85 MWth Fuel	[105, 140]
Greve-in-Chianti Waste Plant (Italy)	TPS/Ansaldo CFB	Boiler 30 MWth Fuel	[149, 157]
Värö Paper Mill (Sweden)	Metso CFB	Lime Kiln 35 MWth Fuel	[149, 157]
Harboøre CHP (Denmark)	Vølund Updraft Fixed Bed	Gas Engine 5 MWth Fuel	[158, 159]
Kokemäki Novel CHP (Finland)	Condens/VTT Novel Updraft Fixed Bed	Gas Engine 7.2 MWth Fuel	[105, 156]

[a] Organic Rankine cycle (ORC).

The experience gained to date suggests that relatively small scale CHP BG projects (e.g. based on gas engines or fuel cells) are more likely to succeed than large scale biomass IGCC projects. Only one of the many biomass IGCC projects discussed in Appendix B is considered a success, i.e. the Värnamo plant, and it was shut down after the demonstration phase due to poor economics. Furthermore, the plant capacity was said to be too small for commercial operation. In order to minimise costs biomass IGCC plants should be up scaled to 30-200 MWe [103]. Increasing the plant size means higher feedstock costs because longer transport distances are involved [160]. This mismatch between scale and the dispersed biomass resource could be dealt with by converting the biomass to an intermediate product in small scale facilities (e.g. oil/char slurry by fast pyrolysis or torrefied pellets) and then transporting the fuel to the large scale gasification plant. This approach however would require significant investment. In conclusion, it is recommended that Ireland focus on small scale CHP BG, especially considering the country's underdeveloped biomass supply chains.

3.4 Fuel Cells

Fuel cells convert chemical energy contained in a fuel directly to electrical energy via electrochemical reactions. The principle of the fuel cell was proposed by Christian F. Schönbein in 1838 and was demonstrated by Sir William R. Grove ca 1839-1842 [161]. Walther H. Nernst is credited with conducting the first work on SOFCs (basic principle and materials) in ca 1890. However, it wasn't until the 1950s that detailed SOFC experiments took place [162]. The first application of fuel cells was during the 1960s when alkaline fuel cells (AFCs) were employed by NASA to produce electricity and drinking water on board space crafts [11]. The SOFC is the fuel cell with the longest continuous development period, starting in the late 1950s [163]. Westinghouse

began developing SOFCs in 1962 and started work on tubular SOFCs in 1978 [162]. Development work on SOFCs continues to this day as they are considered one of the most promising fuel cell types.

Fuel cells are highly efficient (direct conversion of chemical energy to electrical energy) and conversion efficiency is less dependent on scale in contrast to conventional power generation technologies, i.e. small scale fuel cell systems operate nearly as efficiently as large scale ones [163]. They are quiet (no moving parts, no vibrations), can achieve high plant availability (low operating and maintenance costs), are modular (small units combined to achieve desired scale) and show good part load (off design) performance [163-166]. In addition, fuel cells have very low environmental impact with low emissions. Disadvantages or challenges include: fuel cell costs are still considerably higher than conventional technologies; fuel cells require a relatively clean fuel (adds complexity and cost); durability and fuel cell lifetime (long term demonstration needed); technical issues for some designs (e.g. sealing problems for planar SOFCs) [163, 165].

3.4.1 Fuel Cell Theory

Principle of operation

A fuel cell consists of two electrodes separated by an ion conducting electrolyte [165, 167]. Figure 3.9 depicts the working principle of a SOFC. Fuel is supplied to the negative electrode (anode) and oxidant to the positive electrode (cathode) [163]. In the case of a SOFC, O_2 at the cathode is ionised and ions migrate through the electrolyte to the anode side. The ions combine with fuel to produce electrons and product (H_2O for H_2 fuel). Electrons travel around a circuit through a load (doing useful work) to the cathode side. At the cathode electrons combine with O_2 producing ions; the process repeats for as long as fuel and oxidant are supplied.

Both electrodes are porous and electron conducting to allow the transfer of gases and electrons respectively. The electrolyte is an ion conductor only, i.e. it does not conduct electrons. Electrochemical conversion of CO and CH_4 in high temperature fuel cells (SOFCs and MCFCs) is possible. However, it is common to assume that CO is shifted to H_2 and CH_4 is reformed to H_2 via Eq. 3.9 and 3.10 respectively and thus only H_2 participates in the electrochemical reaction [163]. Equations 3.15 and 3.16 represent the electrochemical conversion of H_2 in a SOFC.

Cathode half reaction: $0.5O_2 + 2e^- \rightarrow O^{2-}$ Eq. 3.15

Anode half reaction: $H_2 + O^{2-} \rightarrow H_2O + 2e^-$ Eq. 3.16

On the cathode side, O_2 is reduced to oxide ions (O^{2-}), consuming two electrons [167]. On the anode side, the ions combine with H_2 releasing two electrons and forming H_2O. The overall process may be represented by Eq. 3.8 ($H_2 + 0.5O_2 \rightarrow H_2O$).

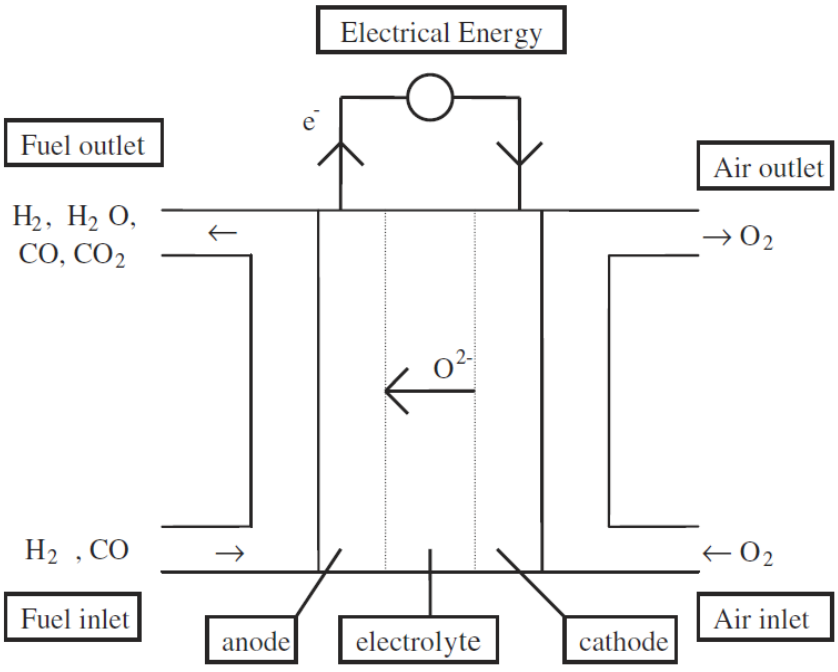

Figure 3.9 Working principle of a SOFC [168]

Ideal performance and Nernst equation

The fuel cell is considered to be H_2 fuelled in the following analysis. The initial step in understanding the operation of a fuel cell is to define its ideal performance. Then losses arising from non-ideal behaviour can be calculated and deducted from the ideal performance to describe the actual operation [163]. For a fuel cell, it is the change in Gibbs free energy of formation ($\Delta\bar{g}_f$) that is converted to electrical energy [165]. $\Delta\bar{g}_f$ represents the maximum electrical energy produced by a fuel cell assuming no losses (i.e. reversible process) [163, 169]. Gibbs free energy and the ideal cell voltage (V_{ideal}) are related by [170]:

$$V_{ideal} = \frac{-\Delta\bar{g}_f}{2 \cdot F} \qquad \text{Eq. 3.17}$$

where V_{ideal} is the ideal voltage (i.e. the maximum cell voltage assuming no losses), $\Delta\bar{g}_f$ is the molar Gibbs free energy of formation (J/mol) at standard pressure (1 bar), 2 represents the number of moles of electrons produced per mole of H_2 fuel reacted and F is the Faraday constant. V_{ideal} is temperature dependent because $\Delta\bar{g}_f$ varies with temperature. For a description of how $\Delta\bar{g}_f$ is calculated refer to Appendix C. V_{ideal} is also known as the standard potential (i.e. voltage at standard pressure).

The Nernst equation (Eq. 3.18) outlines how ideal cell voltage varies as a function of species concentration, gas pressure, etc., and is the centrepiece of fuel cell thermodynamics [170]. This equation is employed to calculate the Nernst voltage (V_N), which is also known as the equilibrium potential or reversible potential. V_N is more realistic and practical than V_{ideal} ($V_N < V_{ideal}$, i.e. V_N will be closer to the actual cell voltage). In Eq. 3.18, T is temperature (K), R_g is the universal gas constant and P_i is the

partial pressure (in bar) of gaseous component *i*. See section 5.2.1 for additional details on the calculation of V_N.

$$V_N = V_{ideal} + \frac{R_g \cdot T}{2 \cdot F} \ln \frac{P_{H_2} \cdot P_{O_2}{}^{0.5}}{P_{H_2O}} \qquad \text{Eq. 3.18}$$

It can be useful to examine theoretical maximum efficiency of an energy conversion device. The efficiency of a fuel cell operating reversibly is [163, 169]:

$$\eta_{ideal} = \frac{\Delta \bar{g}_f}{\Delta \bar{h}_f} \qquad \text{Eq. 3.19}$$

where $\Delta \bar{h}_f$ is the molar enthalpy of formation (J/mol); the calculation of which is described in Appendix C. The actual fuel cell efficiency will be much lower due to irreversible losses (see next section) and because the fuel utilisation is kept below 100% (see temperature and gas concentration section).

Actual performance

Actual fuel cell performance (cell voltage and efficiency) will be lower than values predicted by Eq. 3.17-3.19. Figure 3.10 displays the relationship between voltage and current for a SOFC. The characteristic shape of this graph is the result of three voltage losses; activation, ohmic and concentration losses. The activation loss is due to reaction kinetics and is less important at high temperatures. Therefore, the concave portion of the curve (small initial fall in voltage on the left side of Figure 3.10) is hard to distinguish for high temperature fuel cells [163]. SOFC performance is dominated by ohmic and concentration losses [170]. The linear portion of the graph is attributed to the

ohmic loss, caused by ionic and electronic resistance in the fuel cell components. At high load (or high fuel/air utilisation), mass transport effects become important and results in a rapid drop in voltage. In chapter five these voltage losses and their calculation are discussed in detail as well as the determination of the actual cell voltage. Voltage losses lead to production of heat (instead of electricity); the rest of the generated heat is due to entropy change during the process (see Appendix C).

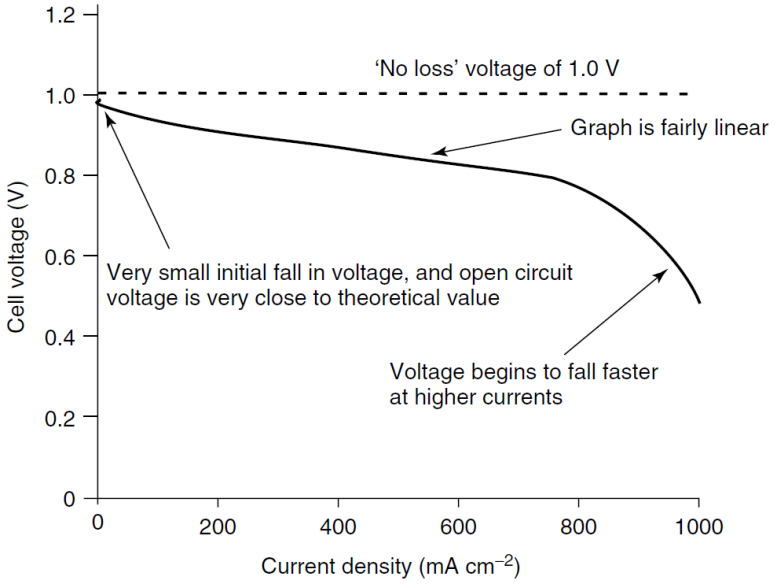

Figure 3.10 Typical voltage-current density curve for a SOFC [169]

Temperature and gas concentration

$\Delta\bar{g}_f$ drops as temperature rises (see Eq. C.1) and in turn causes V_{ideal}, V_N and η_{ideal} to decrease [171]. Considering this fact, it would appear that fuel cells should be operated at low temperature to ensure high performance. It has been widely reported however that elevated temperature actually increases cell voltage [163, 169, 172]. Actual operating cell voltage increases with temperature because the activation loss decreases due to higher reaction rates and the ohmic loss drops as a result of lower resistance (ceramic based fuel cells, e.g. SOFCs) [163].

With reference to Eq. 3.18, increasing reactant partial pressure (H_2 and O_2) increases V_N; in contrast, increasing product partial pressure (H_2O) reduces V_N. Fuel cell voltage is strongly influenced by reactant concentrations; maximum performance is achieved when reactants at the anode and cathode are pure [163]. This proves that fuel dilution with inert gas such as N_2 is highly undesirable; therefore, steam gasification is much more attractive than air gasification for integration with fuel cells. Fuel and air utilisation factors (U_f and U_a) are of great importance in this respect. They are defined in chapter five (see Eq. 5.2 and 5.4). If U_f is too high fuel concentration becomes low, which leads to an increase in the concentration loss and low cell voltage. For high temperature fuel cells, U_f ranges from 50-90% and U_a = ~25% [163, 167, 172]. U_a is low for high temperature fuel cells because excess air is used to control temperature [162, 173]. This method of cooling means that the fuel cell air blower is a significant power consuming component and thus has a strong impact on net electrical efficiency.

Fuel cell stack

A single fuel cell produces ~0.7 V. For practical applications, cells are connected in series or parallel to achieve the voltage and power output level required for the application [163, 165, 174]. This multiple cell assembly is known as a fuel cell stack and may contain tens, hundreds or thousands of cells. Cells are connected via electrically conductive interconnects or bipolar plates, which serve to conduct electrons through the external circuit. The stack arrangement for the Siemens Power Generation Inc. (SPGI) tubular SOFC (originally developed by Westinghouse) is given in Figure 3.11.

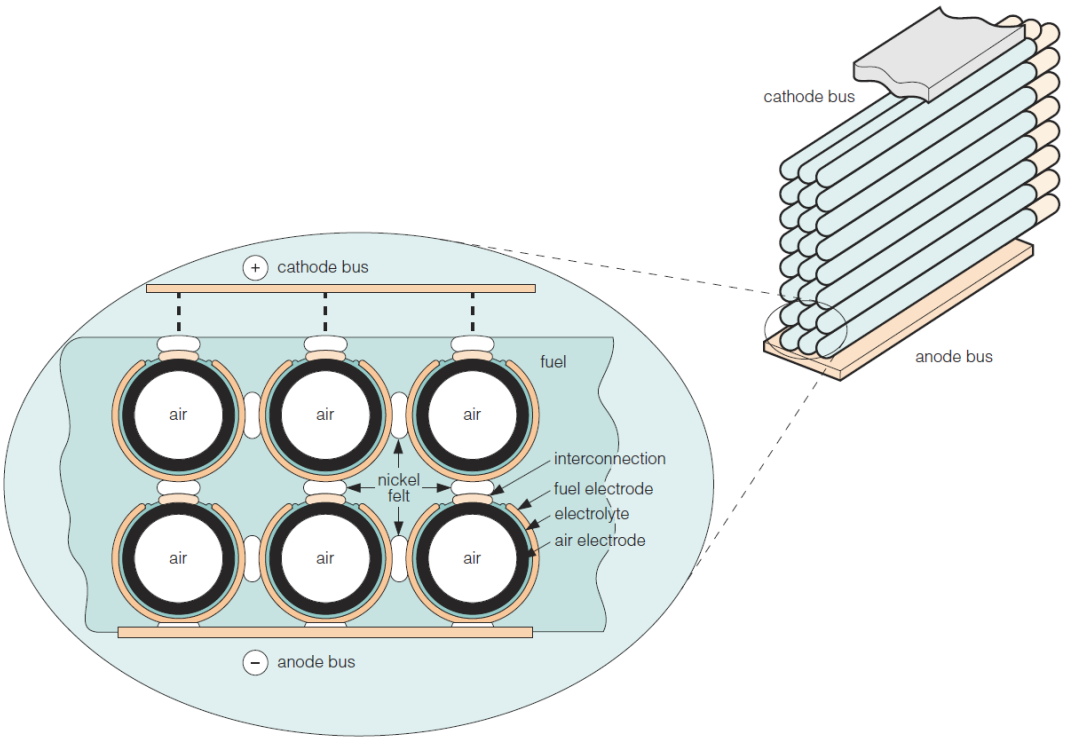

Figure 3.11 Tubular SOFC stack arrangement [174]

3.4.2 Fuel Cell Types and Selection

Five classes of fuel cell have emerged as viable systems for the present and near future, AFC, proton exchange membrane fuel cell also known as polymer electrolyte membrane fuel cell (PEMFC), phosphoric acid fuel cell (PAFC), MCFC and SOFC. These fuel cells may be categorised according to their electrolyte or operating temperature. AFCs, PEMFCs and PAFCs are considered low-medium temperature fuel cells (40-220 °C); whereas, MCFCs and SOFCs are high temperature fuel cells (600-1000 °C). SOFCs can be classified further as planar or tubular design (see Figure 3.12). The solid electrolyte used in SOFCs allows the manufacture of differently shaped cells.

AFCs are intolerant of CO_2, even the low amount present in air causes problems (pure O_2 usually employed as oxidant) [161, 164]. CO_2 is a major component of syngas and pure O_2 is not considered feasible for economic reasons; therefore, AFCs are not suitable for BG applications. Low-medium temperature fuel cells (PEMFC and PAFC)

require pure H_2 fuel and have little or no tolerance to CO [163, 170]. CO intolerance is due to the use of expensive platinum catalysts (needed at low-medium temperature) [174]. PEMFCs are very promising for automotive applications due to their rapid start-up (low temperature operation) and high power density [161, 163]. The fuel requirements of low-medium temperature fuel cells make them unsuitable for BG applications. Benson stated there is little interest in the integration of low temperature fuel cells with solid fuel gasification [174]. High temperature fuel cells are more attractive as they are able to utilise CO as fuel and their operating temperature closely matches that of the gasifier, offering better opportunities for thermal integration and hence higher efficiencies [174].

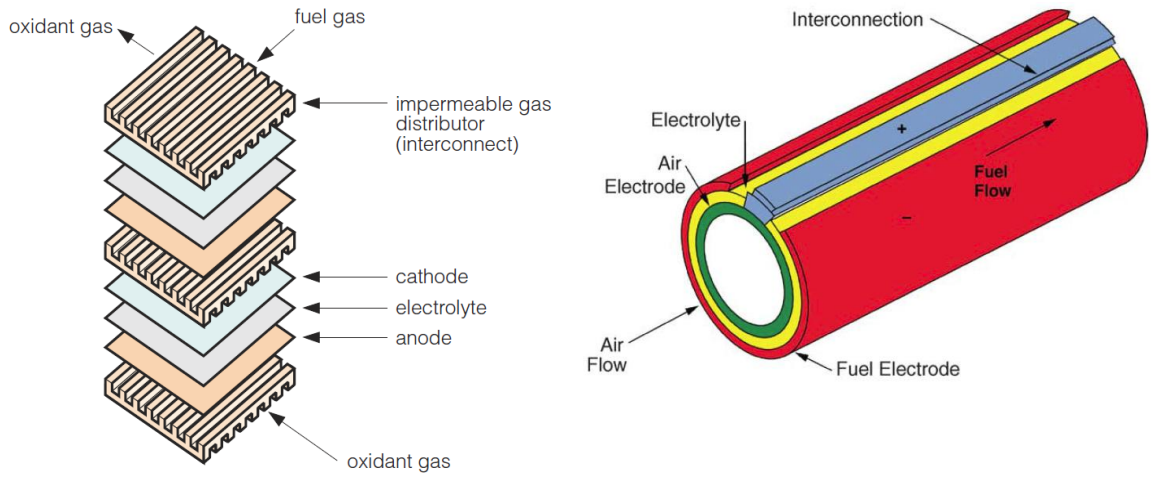

Figure 3.12 SOFC designs: planar (left) and tubular (right) [172, 174]

High temperature fuel cells do not require the use of platinum catalysts (inexpensive nickel catalysts are sufficient) and thus can tolerate CO. Moreover, they can utilise CO and hydrocarbons as fuel; usually via the CO-shift and reforming reactions (described previously). This high fuel flexibility makes these fuel cells especially suited to integration with gasifiers. The high temperature operation also

makes them suitable for integration with gas turbines and for CHP applications. MCFCs and SOFCs have the greatest potential as their development was focused on reformed natural gas as fuel which exhibits similar properties to syngas [11]. The SOFC was selected for this research work instead of the MCFC for the following reasons:

- CO_2 must be supplied to the cathode of the MCFC (usually by means of an anode recycle), which adds complexity [163-165, 174].
- MCFCs employ a liquid electrolyte [163-165, 170]. Thermal cycling of the MCFC gives rise to leakage and loss of the highly corrosive electrolyte [174]. The use of a solid electrolyte like in SOFCs avoids these problems.
- SOFC stack lifetime is reported to be better than that of MCFCs [163]. Molino et al. reported that MCFC stack lifetime is currently 20,000 hours [175]. SOFCs (tubular design) have a stack lifetime of at least 40,000 hours [176]. A low performance degradation rate of < 0.1% per 1,000 hours of operation has been achieved for tubular SOFCs [166, 172].
- SOFCs have the highest fuel flexibility of all fuel cells [168].
- The SOFC is the most tolerant of any fuel cell type to sulphur [165]. MCFC sulphur tolerance has been reported to be as low as 0.1 ppmv (volumetric parts per million) [174].

SOFCs however have disadvantages. High temperature operation is necessary (700-1000 °C) to achieve adequate ionic conductivity in yttria stabilised zirconia (YSZ) electrolytes [162-165, 174]. High temperature operation can lead to thermal stress and sealing issues [165]. It also limits the materials that can be used and therefore the fabrication methods (expensive materials and fabrication) [163, 170, 174]. Start-up

times can be in the order of 18-24 hours (SPGI tubular SOFC stack) [174, 177]. Finally, SOFCs achieve relatively low power densities compared to other fuel cells [163]. Table 3.3 summarises the main characteristics of the fuel cell technologies described in this section.

Table 3.3 Main characteristics of fuel cell technologies [11, 161, 163-165, 168, 170, 174]

	PEMFC	**PAFC**	**MCFC**	**SOFC**
Temperature	40-120 °C	150-220 °C	600-700 °C	700-1000 °C
Electrolyte phase	Solid	Liquid	Liquid	Solid
Catalyst	Platinum	Platinum	Nickel	Nickel
Fuel gases	Pure H_2	Pure H_2	H_2, CO, CH_4	H_2, CO, CH_4, higher hydrocarbons
Advantages	Rapid start-up, high power density, solid electrolyte	Mature technology, commercially available	High fuel flexibility, inexpensive catalyst, CHP applications	Highest fuel flexibility, inexpensive catalyst, CHP applications, solid electrolyte, most tolerant type to sulphur, long stack life (tubular design)
Disadvantages	Expensive catalyst, low fuel flexibility, CO poisoning	Low power density, expensive catalyst, low fuel flexibility, CO poisoning, liquid electrolyte (mobile and corrosive)	Slow start-up, CO_2 recycle, liquid electrolyte (mobile and corrosive), degradation / lifetime issues	Low power density, slow start-up, thermal stress, sealing issues (planar design), expensive materials and fabrication

The main SOFC geometries are planar and tubular [161, 163, 164, 166]. The tubular SOFC design (SPGI) was chosen over the planar design for the following reasons:

- The SPGI tubular SOFC is at an advanced stage of development [163, 174, 178]. It has been demonstrated up to a scale of 250 kWe; whereas, planar SOFCs have

been tested at smaller scale [166]. At present, the tubular SOFC is the most reliable and robust design [11].

- The SPGI tubular SOFC is well proven. A 100 kWe unit was operated for over 36,000 hours on natural gas (see section 3.4.3). Operational data from these demonstrations is widely available (needed for model validation).
- As discussed earlier, the SPGI tubular SOFCs have demonstrated low performance degradation and therefore can achieve long stack lifetimes. In addition, their durability and robustness has been proven as they have shown the ability to be thermally cycled to room temperature from 1,000 °C over 100 times without mechanical damage or performance loss [172].
- Planar SOFCs suffer from sealing problems (difficult at high temperatures) [163, 174, 179]. A major advantage of the tubular design is that seals are not required (see section 3.4.3 for details on construction) [162, 163, 169].
- Thermal stress is also a major issue for planar SOFCs [162, 169, 174, 179]. A challenge with the planar geometry is obtaining a mechanically stable structure, as thin layer ceramics are susceptible to failure when subjected to moderate stresses [161].
- Planar SOFCs have stacking and scale limitations [163, 180]. The issue of thermal stresses and fabrication of very thin components places constraints on scale [169].

There are a number of drawbacks to the tubular design. Tubular SOFCs suffer from low power densities caused by long current flow paths (see Figure 3.13) which result in high ohmic loss [11, 161, 169, 171]. Low power density means large plant footprint and weight, e.g. the SPGI 100 kWe unit has a 16 m^2 footprint and is 9.3 tonnes [162]. In contrast, planar SOFCs achieve more favourable power densities and are

therefore more compact [161, 166, 169, 174]. The cost of fabrication is the other major issue with the tubular design [162, 169, 171]. Cost efficient production methods are possible for the planar design [11, 163, 166, 169].

3.4.3 Solid Oxide Fuel Cells: Status

Recent trends

The main barriers to SOFC commercialisation are high costs due to expensive materials/fabrication and low power density [162, 163, 172, 174]. Low cost conventional fabrication techniques such as screen printing may be employed for manufacturing planar SOFCs [166, 169]. Cheaper fabrication and higher power density (in comparison to tubular technology) explains why most manufacturers are concentrating on the development of planar cells [161]. A recent report by the IEA on the status of SOFC deployment confirms this trend [181]. Companies such as Bloom Energy, Delphi, Versa Power Systems, Ceramic Fuel Cells Limited and many others are working to commercialise planar SOFCs. In contrast, only a small number of companies are developing the tubular design, e.g. Mitsubishi Heavy Industries (segmented tubular SOFC), LG Fuel Cell Systems (flattened segmented tubular SOFC) and TOTO Ltd. (tubular SOFC similar to SPGI design) [163, 181-183]. Mitsubishi Heavy Industries have made great progress; a 200 kWe SOFC-GT unit has been demonstrated for over 3,000 hours with no performance degradation [184]. Testing is underway on a 250 kWe unit (3,000 operating hours as of July 2013) and commercialisation is planned for 2015 [185].

The US Department of Energy SECA program is the main SOFC development program. Fuel cell manufacturers such as SPGI are heavily involved and one of the main goals is to reduce the cost of SOFC production to 400 $/kWe [180]. It was

recognised that the standard SPGI tubular SOFC could not meet the cost and performance targets of SECA [186]. A new flattened tube design was investigated [162, 171]. Higher power density is realised because the ribs act as bridges for current flow, shortening the current flow path and reducing ohmic loss (see Figure 3.13) [167]. In 2008 SPGI began working on the next generation of high power density tubular SOFC, the delta (triangular tube) SOFC [11, 187]. Demonstration of a MWe class module based on the delta SOFC was planned for 2012 but it appears that all work has stopped. SPGI ceased work on the development of their tubular SOFC technology ca 2010. SPGI found the timeframe to bring the technology to commercialisation did not fit with its profit targets [188]. Details on state of the art materials and processes (applicable to tubular SOFCs) are provided hereafter to give some insight into possible reasons why SPGI halted their fuel cell operations.

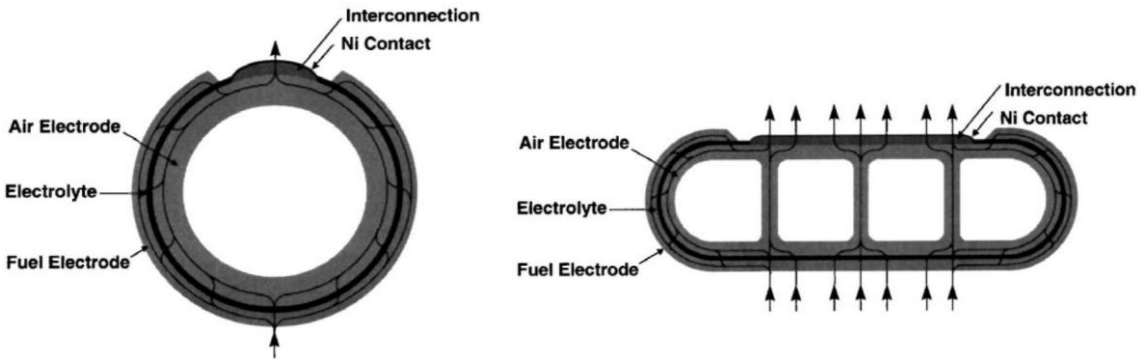

Figure 3.13 Current flow path for the standard (left) and flattened (right) tubular SOFC [167]

The SPGI tubular SOFC is displayed in Figure 3.12 (right) and Figure 3.13 (left). The single cell consists of four components; cathode (oxidant electrode), electrolyte, anode (fuel electrode) and interconnection. The cathode tube, made from doped lanthanum manganite, is fabricated by extrusion and sintering and must be relatively

thick compared to other cell components as it is the cell support [163, 166]. A YSZ electrolyte is deposited on the cathode using a manufacturing technique known as electrochemical vapour deposition (EVD) [162]. The nickel/YSZ cermet anode is deposited on the electrolyte by nickel slurry application followed by EVD of YSZ [163, 166]. Finally, the doped lanthanum chromite interconnection is deposited by plasma spraying [163, 172]. It is clear from the foregoing description that high costs are a major issue for this technology due to expensive ceramic materials and complex fabrication methods. The EVD process is time consuming and expensive making it impractical for commercial application [162, 179]. Therefore, SPGI were investigating alternative techniques in an attempt to reduce costs [172].

Lower temperature operation (< 800 °C) would enable the use of metallic interconnections, which would decrease material and machining costs significantly [162, 171]. However, alternative electrolyte materials (to YSZ) must be found that show adequate ionic conductivity at lower temperatures [163]. Finally, alternative anode materials are under investigation in order to increase their tolerance to fuel gas impurities such as H_2S. Another objective is to develop anodes with greater resistance to carbon deposition caused by reforming of hydrocarbons on the anode. The most widely researched materials in this regard are doped ceria materials such as GDC [168, 170, 189, 190].

SPGI tubular SOFC stack

A detailed description of the SPGI tubular SOFC stack (standard cylindrical tube design) is provided as this system was modelled in this research work. The power rating of the stack is ~100 kWe (AC). Fuel cells produce DC power; therefore, an inverter is necessary to convert it to AC power for most applications [174]. This stack has been

operated very successfully for over 36,000 hours on natural gas [191]. It employs 1,152 cells in 48 bundles of 24 cells each [178]. A cell bundle consists of eight cells connected in series and three in parallel (see Figure 3.11). As shown in the Figure, nickel felt is used to ensure good contact between the cells [163]. The bundles are vertically aligned in twelve bundle rows (four bundles in each row) [178].

A simplified stack flow diagram is provided in Figure 3.14. The oxidant stream is fed via injector tubes, placed centrally in each SOFC, to the closed end of the cells. SPGI tubular SOFCs have a closed end, which eliminates the need for gas seals [163]. The oxidant then flows back through the annular space formed by the cathode surface and the injector tube to the open end. The oxidant is electrochemically reacted with the fuel supplied to the anode as it flows over the cathode surface. Fuel gas is supplied to the ejector where it is mixed with depleted fuel from the recirculation plenum. This anode recycle loop provides the steam and heat required for the steam reforming process. The mixed fuel then passes through the pre-reformers which convert the higher hydrocarbons and a small portion of the CH_4 to H_2 and CO. The partially reformed fuel enters the internal reformers and using the heat generated by the exothermic electrochemical reactions occurring in the SOFC stack it is reformed further. An internal reformer is located between each bundle row [178]. The fuel then flows along the anode surface from the closed end to the open end, parallel to the direction of the oxidant flow and is electrochemically oxidised, generating electricity and increasing the temperature of both streams. A portion of the depleted fuel is recycled and the remainder is reacted with the depleted oxidant in the combustion plenum. The generated heat serves to preheat the incoming oxidant stream in the injector tubes.

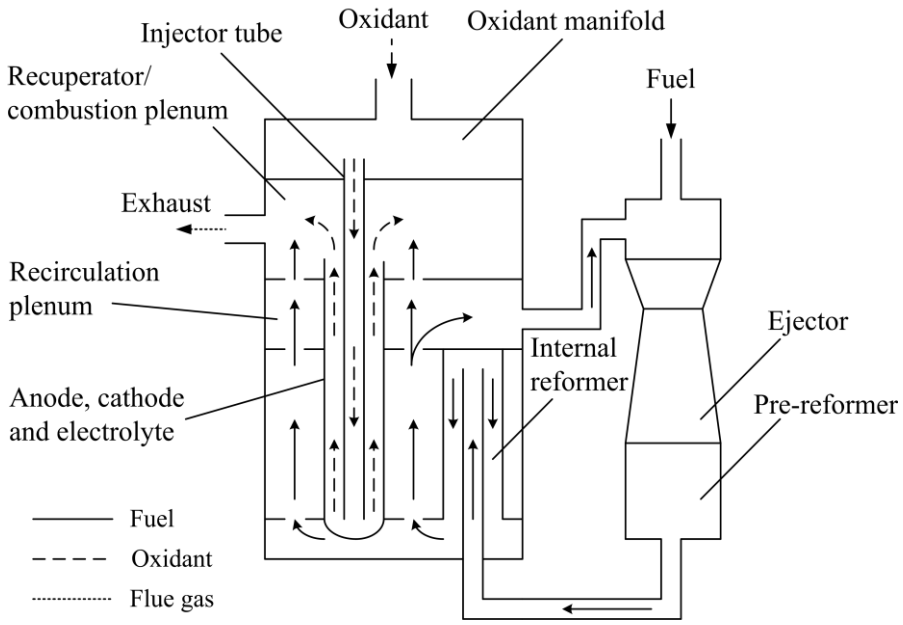

Figure 3.14 SPGI tubular SOFC stack flow diagram

3.5 Syngas Cleaning and Reforming

The greatest challenge for BG may be the cost of syngas cleaning equipment [192]. A reliable and effective syngas cleaning system is one of the main criteria for the successful operation of BG-SOFC systems [193]. Aravind and de Jong recently conducted a comprehensive review of syngas cleaning technologies with regard to BG-SOFC applications [168]. They concluded that additional experimental investigations are required to obtain detailed information on contaminant tolerance of SOFCs so that financially viable BG-SOFC systems may be realised. These recent articles highlight the importance of syngas cleaning equipment selection and the need for continued research and development of more efficient and cost effective cleaning technologies. Syngas produced by gasification of biomass may contain the following impurities/contaminants that must be removed or converted:

- Particulates – Particulates are solid phase materials entrained in the syngas as it exits the gasifier [194]. They include fly ash, un-reacted char and gasifier bed

material. They can cause erosion and blocking of downstream equipment and are subject to emission limits [11]. Particulates can clog the pores of SOFC anodes and negatively affect performance [168, 195-197].

- Alkali – The presence of alkali metals in biomass (such as potassium and sodium) was discussed in chapter two. Alkali can deposit on equipment surfaces, cause corrosion and may deactivate catalysts [194]. According to Benson, alkali would degrade ceramic components in SOFCs [174].
- Chlorides – The chlorine in biomass is converted to hydrogen chloride (HCl) during gasification [168, 198]. HCl may cause corrosion and is a poison to sulphur removal catalysts such as zinc oxide (ZnO) [8, 168, 174]. For this reason it must be removed upstream of any sulphur removal process [8, 11, 174].
- Sulphur compounds – Sulphur in biomass fuels is converted to hydrogen sulphide (H_2S) and lower amounts of carbonyl sulphide (COS) during gasification [11, 168, 199]. These compounds are strong poisons to catalysts such as nickel used in tar reforming reactors and SOFC anodes [11, 174, 194-197]. In addition, they may be converted to SO_x which are subject to strict emission regulations.
- Tars – Tar is a complex mixture of condensable hydrocarbons [97, 174]. There is no unique definition of the term, but there is a broadening consensus in defining tar as organic contaminants with a molecular weight greater than benzene (78.11 kg/kmol) [97, 168, 194, 200]. Below the tar dew point, they condense and form droplets which accumulate as sticky films on cold surfaces, e.g. inside pipes and heat exchangers [11, 98, 194, 198]. Tars also lead to carbon deposition problems in components such as reformers and SOFCs (see section 3.5.2).
- Nitrogen compounds – Ammonia (NH_3) is the most important nitrogen containing impurity in syngas [168, 194, 198, 200]. In most cases it must be removed as it

leads to NO_x in combustion based power generation systems (gas engines/turbines); however, it has been proven that SOFCs can convert NH_3 as a fuel with very little or no NO_x formation [11, 201, 202]. The reverse NH_3 formation reaction (Eq. 3.11) is promoted by nickel catalysts [198, 203]. Nickel is commonly used in SOFC anodes and reformers; therefore, removal of nitrogen compounds is not considered necessary in this research work.

The level of impurities contained in the syngas will depend on many factors (biomass fuel, gasifier type, operating conditions, etc.). Typical impurity levels for fluidised bed BG found in the literature will now be presented. Particulates range from 2-35 g/m^3 [107, 204], alkali and H_2S are 1 ppmw (parts per million by weight) and 50-200 ppmv respectively [204], HCl can be in the range of a few ppmv [204]; however, it has been reported to be 100 ppmv for the FICFB pilot gasifier at Trisaia [134]. Published values for tars range from 1-20 g/m^3 [97, 107, 204]. Finally, NH_3 can reach 4,000 ppmv [204] but has been reported to be in the range 1100-1700 ppmv for the FICFB gasifier [205].

The tolerance of SOFCs to the aforementioned impurities is generally not well understood and additional research is required to confirm tolerance limits [168]. H_2S is the exception as its impact has been well studied (due to the presence of sulphur in natural gas); standard nickel/YSZ based SOFCs can tolerate fuel gas containing $H_2S \leq 1$ ppmv [4, 163, 168, 194, 195, 198, 204]. Data on HCl tolerance is limited but values of 1 ppmv have been reported [4, 163, 195]. The limit on particulates and alkali is likely to be low at 1 ppmw and 1 ppmv respectively [168]. Aravind and de Jong stated that, although there are several indications that tar might not affect SOFC performance and might even become reformed on the anode, such arguments have not yet been solidly

proven for long duration operation [168]. Therefore it is assumed that tar must be at low ppmv level prior to the SOFC anodes [168, 204]. As discussed previously, NH_3 reacts as a fuel in SOFCs.

3.5.1 Syngas Cleaning: Temperature and Technologies

In this thesis the term cold syngas cleaning refers to those systems with operating temperatures of < 100 °C. Warm syngas cleaning systems are assumed to operate at temperatures in the range 200-500 °C. Hot syngas cleaning processes are those with temperatures > 500 °C where minimal syngas cooling has occurred. These temperature ranges were defined by Stevens [194]. A major advantage of biomass gasifier SOFC integration is that they operate at comparable temperatures; therefore, syngas cooling to low temperature would have considerable efficiency penalty. Thus hot and warm syngas cleaning technologies are of interest for BG-SOFC systems. Hot syngas cleaning is considered to be expensive and less reliable, compared to cold syngas cleaning systems [168]. For other conversion technologies such as gas engines, cold syngas cleaning is attractive as the engine requires a cold fuel gas. Similarly, gas turbines necessitate the compression of the syngas (most biomass gasifiers operate at atmospheric pressure) and therefore cooling to low temperature is desirable.

The cleaning temperature of BG-SOFC systems is limited to ~400 °C. This is because SOFCs require sulphur removal to ≤ 1 ppmv and current sulphur removal technologies capable of achieving this level of cleaning are limited to this temperature (see section on sulphur removal). In addition, the complexity of alkali cleaning is increased at temperatures above their condensation temperature (~600 °C) and chloride removal is limited to ~600 °C (see sections on alkali and chloride removal respectively). Finally, unless cold syngas cleaning, i.e. scrubber technologies are to be employed, the

syngas must be kept above the tar dew point temperature (~400 °C considered safe) to prevent tar condensation and associated problems.

Scrubbers for cold syngas cleaning are capable of removing all impurities including sulphur compounds [8, 105, 200]. These scrubbers use water (Harboøre and Skive plants) or oil such as rapeseed oil methyl ester (RME) (Güssing plant) [117, 121]. Tar contaminated water is considered hazardous waste and its disposal incurs high costs [97]. Water scrubbers shift the tar problem to expensive wastewater treatment [121]. The oil based scrubbers do not have this problem; however, they do increase plant complexity as tar must be recycled to the gasifier. For RME scrubbers the oil loaded with tar is recycled and in the case of the OLGA oil scrubber system, tar is stripped from the oil and then recycled (lowers oil consumption) [121]. As these cleaning systems are not attractive for BG-SOFC applications they will not be discussed further. Details on removal/conversion technologies for each impurity are provided in the following sections. As NH_3 is a fuel for SOFCs, options for its removal are not discussed.

Particulates

Cyclone filters serve as the initial particulate removal step; removing the bulk of coarse material (fine particulates remain) [194]. They are inexpensive and an integral part of many fluidised bed gasifier designs. They operate efficiently over a wide range of temperatures even at typical gasifier temperatures (no cooling needed). Filters for fine particulates removal include candle (ceramic and sintered metal), bag, packed bed and electrostatic precipitator (ESP). Bag filters are made of woven material and operate at relatively low temperature < 250 °C [8, 11]; therefore, they are not attractive for BG-SOFC systems. There may also be clogging issues related to tar and alkali condensation

[194]. Packed bed filters operate with the gas passing through a bed of packed material such as sand or ceramic spheres [200]. They have operational problems related to cleaning and waste disposal [121, 194, 200]. Wet and dry ESPs are not practical for BG applications due to capital and operational costs [97, 168]. Candle filters are made of porous rigid materials that allow gas to pass through while blocking particulates. Both ceramic and sintered metal candle filters can operate close to the gasifier temperature [200]. In practice, these filters are operated at much lower temperatures ~350-500 °C. Even at these reduced temperatures problems were encountered with ceramic candle filters. At the Värnamo plant ceramic candles broke due to thermal stress and had to be replaced with sintered metal candles (see Appendix B) [194]. Martini et al. have tested a sintered metal candle filter downstream of the Güssing FICFB gasifier and upstream of a SOFC [20]. Over 200 hours the filter achieved 99.98% separation efficiency for particulate loads of 20-100 g/m^3. Hofmann et al. also employed a sintered metal candle filter for BG-SOFC experiments [196, 197]. They tested the cleaning unit and SOFC at a 100 kWth CFB gasifier, a downdraft gasifier and a Heatpipe Reformer gasifier. Stable continuous operation of the SOFC was achieved with no carbon deposition or other contamination [196, 197]. This suggests that sintered metal candle filters are adequate for BG-SOFC applications.

Catalytic filtration (ceramic candles impregnated with catalyst) for the combined removal of particulates and conversion of tars is under investigation [168]. If nickel catalyst is used, sulphur poisoning will be an issue as the sulphur cannot be removed at high temperature upstream of the filter. In addition, alkali will remain in the gaseous phase and pass through the filter so an additional unit will be needed downstream for its removal at high temperature (i.e. alkali getter see next section).

Alkali

Alkali metals condense below ~600 °C [97, 98, 121, 174]. They are removed by cooling the syngas below 600 °C to allow condensation of the material into solid particulates, which are subsequently removed using filters [8, 11, 97, 121, 194]. Syngas cooling with particulate matter removal in cyclones and filters has proved to be successful in removing alkali and chlorides [105]. If the syngas remains above the alkali condensation temperature and particulates are removed at elevated temperature; the alkali will pass through the particulate removal unit and remain in the syngas. In this case, a separate alkali removal step is necessary. An alkali getter such as activated bauxite may be used; these units can operate at temperatures between 650-725 °C [97, 194, 200]. The regeneration process for bauxite is simple (using boiling water); this and its performance make it very promising [98].

Chlorides

Two types of adsorbents are commercially available for HCl removal; sodium carbonate and calcium oxide. Calcium oxide is less suitable for syngas applications as it reacts with CO_2 [121]. Moreover, Fiorenza et al. tested a calcium oxide unit at the Trisaia FICFB gasifier and reported a HCl removal efficiency of 70% at ~500 °C [134]. A higher HCl removal efficiency would be needed for SOFC applications. In contrast, sodium carbonate is not affected by CO_2 and is capable of cleaning to below 1 ppmv at 400-500 °C [121]. Aravind and de Jong described sodium carbonate as one of the best options and predicted ~1 ppm HCl could be achieved at 600 °C [168].

Sulphur compounds

Conventional desulphurisation processes operate at low temperature, e.g. physical washes like the Purisol, Selexol and Rectisol processes [69]. These processes are

usually followed by sulphur recovery (Claus process). These methods of sulphur removal and recovery are only economical for high sulphur fuels (e.g. coal); therefore, they are not considered suitable for biomass applications [11, 121].

Metal oxide sorbent beds (also known as sulphur guards) are better suited to BG-SOFC systems; due to the low sulphur content and because they can operate at much higher temperature ~400 °C. ZnO is among the best metal oxide sorbents and therefore one of the most commonly used [8, 11, 199]. COS is converted to H_2S and subsequently adsorbed in ZnO beds [121, 168]. They can reduce H_2S concentration to below 1 ppmv [168, 174, 199]; removal to 0.3 ppmv has been reported [121]. Operating temperature is limited to ~400 °C to ensure good removal efficiency and because at higher temperatures zinc will undergo volatilisation [8, 11]. A ZnO bed for H_2S removal downstream of the Güssing FICFB gasifier and upstream of a SOFC was tested and achieved less than 1 ppm H_2S at 450 °C [20]. Hofmann et al. also employed ZnO beds for BG-SOFC testing and post experiment examination of the SOFC revealed no damage [196, 197]. This shows that ZnO beds are adequate for BG-SOFC applications.

The temperature limitation for ZnO beds has led to research on alternative metal oxides such as zinc titanate. Zinc titanate beds are capable of sulphur removal at temperatures of 540-760 °C [199]. However, they can only reduce H_2S to 4-10 ppm [168, 198], which is above that allowable for SOFCs (1 ppmv). New sorbents capable of sulphur cleaning to the level required by SOFCs at higher temperatures are needed as this cleaning step is limiting the efficiency of BG-SOFC systems (see cleaning temperature sensitivity analysis section 5.3.4).

Tars

As discussed previously, tars may not be an issue for SOFCs; they may simply pass through the SOFC and be burned in the post combustor or they may be reformed

and oxidised contributing to electricity production [11, 20, 168]. Liu et al. found tar had a positive impact on SOFC performance and recommended that tars should not be removed [189]. If tars remain in the syngas, humidification will be necessary to inhibit carbon deposition and a pre-reforming step should be employed prior to the SOFC anodes (see section 3.5.2). In addition, the syngas temperature should be kept above the tar dew point temperature (~350 °C) to prevent tar condensation and fouling of equipment [20, 97, 121, 190].

Tar formation occurs during pyrolysis and is highly dependent on the conditions inside the gasifier. It is widely known that raising the gasifier temperature lowers tar level [97]. Li stated that the most effective and economic way of reducing tar yield is by increasing the gasifier operating temperature [206]. If this fails to decrease tar content to the required level, further action will be necessary to convert or remove the tars. Tars may be removed via scrubbers and wet ESPs at low temperature. Removal leads to a loss in syngas energy content and produces hazardous waste that must be disposed of at high cost [98, 200, 207]. Torres et al. stated that physical strategies (i.e. removal strategies) are not attractive because of their costs and because these methods only transfer the tars into liquid or solid phase, where the environmental hazard posed by these compounds remains [198]. Therefore, tar removal will not be discussed further. Tar conversion is more attractive as the energy content in the tars is retained in the syngas [97, 107, 198]. Tars may be converted by thermal or catalytic methods.

Thermal conversion of tars is not appealing for a number of reasons. High temperatures (> 1,000 °C, i.e. above biomass gasifier temperature) are needed to convert the tars, usually achieved by partial oxidation, which results in an energy penalty. Furthermore, the high temperature means expensive materials must be used and soot is formed, which may be even more problematic than tars [98, 200, 207]. Catalytic

tar conversion processes can be operated at lower temperatures hence eliminating the heating and material requirements of thermal processes and avoiding soot problems [200]. Catalysts are mineral (calcined dolomite, olivine, etc.) or metal based (e.g. nickel). The catalyst may be added to the bed of a fluidised bed gasifier (in situ tar conversion) or a separate downstream unit (usually a fixed bed, fluidised bed or monolith). Calcined dolomites ($CaMg(CO_3)_2$) are the most widely employed mineral catalyst for tar conversion in BG [203]. They are inexpensive, disposable and achieve high conversion rates; however, they have poor mechanical properties and quickly become entrained in the syngas if used for in situ tar conversion [121, 168, 198]. Therefore, they are not suitable as in situ catalyst but have found use in downstream catalyst beds [203]. The BG company TPS applied this technology commercially (ARBRE plant, etc.); their system consisted of a calcined dolomite CFB situated downstream of the CFB gasifier [168]. Olivine ($(Mg, Fe)_2SiO_4$) is a suitable in gasifier bed catalyst due to its hardness and attrition resistance; however, it has been found to be less effective than calcined dolomite at converting tars [121, 198]. It has been used as gasifier bed material at the Güssing plant for many years and reduces tar content in the syngas to 2-5 g/m^3 [125, 208]. It is well known that tar can be decomposed catalytically with nickel catalysts [190]. Commercial nickel catalysts have been widely used for BG tar conversion [198, 203]. Nickel catalysts are not utilised in gasifier bed tar conversion because they are expensive and are deactivated by sulphur, chlorine and alkali [121, 200]. These catalysts are employed downstream in secondary beds and achieve very high tar conversion. Carbon deposition can be a problem and steps must be taken to avoid it (see section 3.5.2). It has been reported, that the best option for tar conversion is to employ a calcined dolomite guard bed followed by a fixed bed nickel catalyst reactor [105, 200, 203]. Hofmann et al. successfully utilised this type of two step tar reformer

for BG-SOFC experiments [196, 197]. The guard bed can be eliminated, simplifying the system, if olivine bed material is used in the gasifier [203].

3.5.2 Syngas Reforming: Carbon Deposition and Technologies

Steam reforming of natural gas or CH_4 is well established and is one of the most inexpensive and energy efficient ways of producing syngas [11]. The general steam-hydrocarbon reforming and CO-shift reactions (Eq. 3.20 and 3.9 respectively) occur during steam reforming [8, 174, 203].

$$C_xH_y + xH_2O \rightleftharpoons xCO + (y/2 + x)H_2 \qquad \text{Eq. 3.20}$$

Methane as well as tars (higher hydrocarbons and oxygenated hydrocarbons) are reformed [11]. Nickel catalysts are employed to promote these reactions at relatively low temperatures (< 800 °C) [11, 198, 203]. As discussed previously, nickel catalysts are poisoned by sulphur and other impurities and therefore the syngas must be thoroughly cleaned prior to reforming. Moreover, carbon deposition is a major problem for nickel catalysts; especially when the fuel gas contains tars [194]. Nickel catalysts are commonly used for SOFC anodes. Direct use of hydrocarbon fuels results in deactivation from carbon deposition, which can hinder fuel transport, block active sites on the anode and as a consequence reduce the electrical efficiency and durability of the fuel cell [190]. Carbon deposition occurs via the reverse Boudouard reaction (Eq. 3.4), methane decomposition reaction (i.e. reverse methanation Eq. 3.6) and the reverse water-gas reaction (Eq. 3.5) [144, 189, 209]. Higher hydrocarbons and tars are decomposed in a similar way to methane [189]. Liu et al. investigated the impact of temperature on the carbon deposition reactions [189]. They found that methane and

higher hydrocarbon decomposition reactions were favoured at high temperature; whereas, the reverse Boudouard and reverse water-gas reactions became less important. Thus, carbon deposition is due primarily to methane and higher hydrocarbon (i.e. tar) decomposition at typical SOFC operating temperatures (800-1000 °C). At lower temperatures (600-700 °C), the reverse Boudouard and reverse water-gas reactions play an important role and the total amount of carbon deposition increases. Suwanwarangkul et al. published experimental results that agree with these findings [210]. The amount of carbon deposited via the reverse Boudouard reaction increased as temperature decreased. These results suggest temperature should be kept high in order to inhibit carbon deposition. Other measures are necessary to decrease carbon deposition from tar and hydrocarbons. Syngas humidification in order to increase its H_2O content is the simplest and most effective way; however, a rise in H_2O content decreases the partial pressure of the fuel gases and lowers SOFC performance [14, 144, 209, 211, 212].

In SOFC systems, steam reforming may take place outside or inside the fuel cell stack (external or internal reforming). The steam reforming process is highly endothermic (see steam-methane reforming heat of reaction Table 3.1); therefore, external reforming is not attractive as it requires an external heat source. Internal reforming utilises the heat generated inside the SOFC stack, which aids stack thermal management and increases efficiency as it lowers the amount of cooling air [174]. Internal reforming may be further classified as direct or indirect internal reforming. Direct internal reforming is tar and hydrocarbon reforming directly on the SOFC anodes. This approach is not recommended due to the risk of carbon deposition and also because the highly endothermic reactions will cause thermal stress in the SOFCs, which could lead to mechanical failure. These problems have occurred during BG-SOFC experiments [144]. Indirect internal reforming (pre-reforming) is preferred; SPGI

employed this method for their natural gas fuelled SOFCs (see section 3.4.3). The experimental results of Dekker et al. and Mermelstein et al. provides further evidence that a pre-reforming step is needed [211, 213]. In both works tars resulted in carbon deposition on the SOFC anode and performance degradation. Mermelstein et al. varied the syngas H_2O content over a wide range and found that carbon deposition still occurred [211].

3.5.3 Proposed Syngas Cleaning and Reforming System

Based on the information presented in the preceding sections, a syngas cleaning and reforming system configuration suitable for BG-SOFC applications is proposed (Figure 3.15). The proposed system employs warm syngas cleaning technologies. Cold syngas cleaning technologies, although more developed and reliable, are not attractive for BG-SOFC applications. Hot syngas cleaning technologies are not yet sufficiently developed to meet the strict SOFC cleaning requirements.

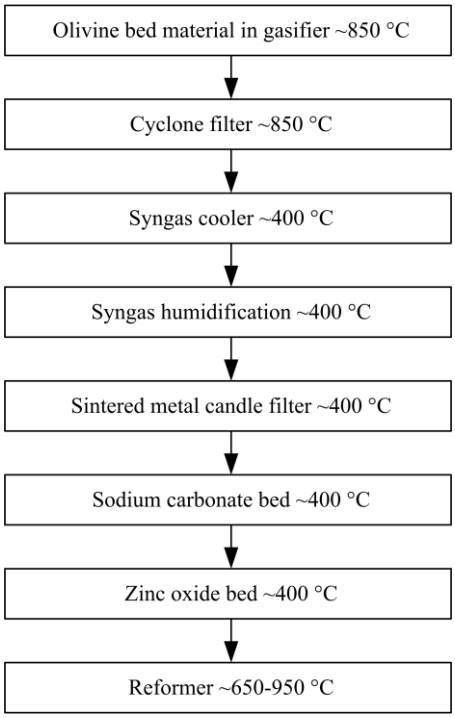

Figure 3.15 Proposed syngas cleaning and reforming system

The first step is tar reduction within the gasifier, which is achieved through temperature control (sufficiently high at ~850 °C) and the use of catalytically active bed material (olivine). Next the syngas passes through a cyclone filter for removal of coarse particulates at high temperature. The syngas is then cooled to a temperature suitable for fine particulates, alkali, HCl and H_2S cleaning (~400°C). A robust syngas cooler will be required for smooth operation as alkali will condense to form particulates that may deposit and cause blockage/corrosion problems within the cooler. Experience has shown robust heat exchangers are required, i.e. corrosion resistant and designed so that particulates pass through and do not lead to blockage [105]. The major difficulties encountered at the Amer plant (refer to Appendix B) were caused by particulates and alkali in the gas cooler [105, 214]. An additional cyclone filter may be needed after cooling prior to the candle filter in order to prevent plugging (coarse particulates may have formed due to alkali condensation). To inhibit carbon deposition in pipes and downstream equipment the syngas is humidified with steam. Fine particulates and alkali are removed by means of a sintered metal candle filter. An alkali getter such as bauxite should not be necessary as the syngas is cooled to 400 °C and therefore the alkali should condense out. The next step is HCl cleaning in a sodium carbonate bed, followed by H_2S removal in a ZnO bed. Finally, the syngas enters the SOFC stack where internal reforming occurs (nickel catalyst bed); converting the tars, hydrocarbons and decomposing the NH_3 prior to the SOFC anodes.

3.6 Modelling and Simulation

This literature review section focuses on modelling and simulation of BG and SOFCs, which is of great importance to the advancement of BG-SOFC systems. Equally important is experimental work on BG-SOFC. A lot of these works have been

referred to in the preceding sections; however, they are listed here for convenience. A small number of research works on SOFCs operated on actual biomass gasifier syngas have been published [19, 20, 144, 195-197]. The majority of experimental research to date has been on SOFCs operated on simulated syngas (i.e. mixed bottled gases) [7, 14, 68, 189, 190, 204, 211-213, 215, 216]. Saule et al. described short term experimental work as a first step to a BG-SOFC system [217]. They claim the next step is to integrate the two units in an optimal way. This highlights the need for modelling and simulation of BG-SOFC systems. A major limitation of experimentation in comparison to modelling is that if one variable of the original process changes the identified optimum operating conditions are no longer valid [218]. Modelling or simulation can [97]:

- Reveal optimum operating conditions or design (plant layout).
- Identify areas of concern/danger in operation.
- Provide information over a much wider range of conditions, e.g. extreme conditions (conditions at which experimentation is not possible or advised).
- Assist in scale-up.
- Do all of the above without involving large capital investments.

3.6.1 Biomass Gasification Modelling

Numerous CFB biomass gasifier models can be found in the literature and a review of them is beyond the scope of this work. Discussion of these models and different modelling techniques can be found elsewhere [219, 220].

In contrast, DFB biomass gasifier technology is at a much earlier stage of development and therefore few models exist. Kaushal et al. developed a complex one-dimensional (1-D) model of the FICFB gasifier [111]. Both reaction kinetics and bed hydrodynamics were considered. The model predicted the syngas composition profile

(i.e. variation in composition in the axial direction) and the results indicated that most of the biomass conversion takes place in the bottom zone of the gasifier with little change in syngas composition in the freeboard (area above the fluidised bed). This finding shows that zero-dimensional (0-D) models, like the one developed in this research work (see section 4.3), are sufficient to simulate the FICFB process. Gassner and Maréchal presented a Belsim model of the FICFB gasifier [221]. They applied the temperature approach method to adjust the predicted syngas composition (see section 4.3 for details on method). They investigated ways to improve the efficiency of the process and predict a ~10% increase in *CGE* if the biomass is pyrolysed before feeding to the FICFB reactor. Pröll et al. reported work on an IPSEpro model of the FICFB gasifier [128, 129]. It is described as a black box model with functional equations for parametric modelling [129]. Reaction kinetics were not considered and some empirical equations were used in the model calculations. A pure equilibrium FICFB model was developed by Schuster et al. using IPSEpro [12]. It is clear from the results of this simulation that the real FICFB process is far from equilibrium as the predicted H_2 and CO contents are well above measured FICFB gasifier values and CH_4 and CO_2 contents are well below measured levels. Two ChemCAD FICFB models have been published by an Italian research group [134, 175]. The models are based on the 500 kWth FICFB pilot plant operating at the ENEA Trisaia Research Centre. The results for both models do not show good agreement with the reported syngas composition for the FICFB pilot plant.

Abdelouahed et al. simulated the Silvagas and TNEE DFB gasification processes [222]. The model is a semi-kinetic Aspen Plus simulation that incorporates Fortran subroutines. A pyrolysis correlation was implemented and both tar and char were considered. Bed hydrodynamics were neglected. Jie He et al. presented an Aspen Plus model of a 150 kW DFB gasifier (MIUN gasifier) [223]. They applied the Gibbs free

energy minimisation with temperature approach method and empirical equations were used to predict the products of pyrolysis including char and tar. De Kam et al. developed a process simulation model of the Silvagas DFB gasifier using Aspen Plus [224]. The Gibbs free energy minimisation with temperature approach method was also applied by these authors. An Aspen Plus heat stream was used to simulate the transfer of heat from the gasifier CZ to the GZ via bed material. The amount of char directed to the CZ was set at 19.7%; this constraint reduces the model prediction capability. An Aspen Plus model of the Silvagas process was published by Cohce et al. [225]. The model uses National Renewable Energy Laboratory correlations to adjust the syngas composition.

3.6.2 Solid Oxide Fuel Cell Modelling

A multitude of SOFC models have been developed and a detailed review of them is beyond the scope of this work. Comprehensive reviews of these models and different modelling approaches have been published [161, 226-229].

The most relevant tubular SOFC models are discussed briefly in the following. Examples of 0-D tubular SOFC models include [230-238]. More complex 1-D and 2-D tubular SOFC models capable of predicting temperature distribution, gas concentration along the SOFC axis, etc., have also been developed [6, 7, 239-253]. The 0-D tubular SOFC model proposed in this research work (see section 5.2) was based on the models developed by Zhang et al. and Campanri [231, 232]. Campanari modelled the SPGI tubular SOFC stack [231]. The model was 0-D and voltage was calculated employing semi-empirical correlations developed using a reference polarisation curve (i.e. a voltage versus current density graph for an actual SOFC operated on reference fuel at reference conditions). Zhang et al. adopted the same approach [232]. The semi-

empirical correlations and other model equations were implemented in Aspen Plus (Fortran code). Sensitivity analyses of the main operating parameters such as current density were carried out using the Aspen Plus 0-D model. It has been reported that semi-empirical correlations may not be valid for other fuels [163]. For this reason a very different method of voltage calculation has been applied in this work; the equations employed consider changes in temperature, pressure, gas molar fractions, etc., and therefore may be applied to diverse fuels.

Campanari and Iora published a complex model, which considered ohmic, activation and concentration voltage losses, kinetics of hydrocarbon reforming and heat transfer [240]. They employed the equivalent circuit method for ohmic loss computation taking into account realistic current paths. Other researchers have opted to simplify this calculation by assuming a current flow length equal to the cell component thickness neglecting current flow in the circumferential direction [233, 236, 242]. Accurate calculation of the ohmic loss is of utmost importance when simulating tubular SOFCs due to complicated current flow paths (see Figure 3.13); therefore, the cell component thickness simplification is not recommended. A simplified method, but one that considers realistic current paths, was applied in this work (see section 5.2). Campanari and Iora applied the Butler-Volmer equation to determine activation loss [240]. This equation must be solved numerically [254] and therefore would be difficult to implement using Aspen Plus and would increase computational time. Calise et al. have reported a computational time of four hours for a 1-D tubular SOFC Matlab model employing the Butler-Volmer equation, the equivalent circuit method for computing ohmic loss and the same method applied in this research work for concentration loss calculation (see section 5.2 for details) [241]. Considering this and the fact that activation loss is less important for high temperature SOFCs, semi-empirical

correlations were utilised in the model developed during this research (see section 5.2). Hernández-Pacheco et al. found that the correlations show reasonable accuracy in comparison to the Butler-Volmer equation for temperatures of 900-1473 °C [254].

3.6.3 BG-SOFC Modelling

A review of the available literature on BG and SOFC integration was conducted by Seitarides et al. [1]. Modelling studies predict efficiencies of 23-50% for BG-SOFC systems [1]. A recent publication from the same research group stresses the importance of thermal integration [255]. Zabaniotou claims that the heat generated inside the process (SOFC) could cover the heat demands of gasification and reforming stages and allow the production of extra electrical power using a conventional heat engine [255].

A number of works have been published where SOFCs were modelled and their performance on biomass syngas investigated, i.e. the biomass gasifier was not modelled and a typical syngas composition was assumed [6, 7, 11, 250, 251, 256]. It is essential to model both processes (BG and SOFC) as integration options strongly affect plant performance. Thermal integration, steam generation, preheating requirements, syngas cleaning and parasitic power demand are of utmost importance and therefore both processes should be simulated to obtain meaningful results. Omosun et al. developed two gPROMS models; one for a planar SOFC operating on syngas from a fixed bed gasifier with cold gas cleaning and the other from a fluidised bed gasifier with hot gas cleaning (both air blown) [256]. Limitations of the models include: SOFC voltage and biomass syngas compositions were model inputs. The main finding was that hot gas cleaning is preferred in terms of system efficiency. Suwanwarangkul et al. presented a detailed 2-D tubular SOFC FEMLAB model [7]. Predicted performance on syngas was lower than that on pure H_2. Biomass syngas composition was a model input and the

syngas was assumed to be free of CH_4 and other hydrocarbons. A comparison to performance on natural gas instead of pure H_2 would be more meaningful as pure H_2 fuel is currently not a practical option. A 1-D SOFC-GT (SPGI design) model was employed by Sucipta et al. to investigate performance when fuelled with biomass syngas compositions typical of air, pure O_2 and steam blown gasification [6, 250, 251]. All syngas compositions resulted in reduced performance compared to pure CH_4 due to lower energy content and the impact of inert gases [250]. The greatest efficiency was predicted for steam gasification, followed by pure O_2 and then air. The main limitation of this work was that gasification was not modelled. Biomass syngas fuelled SOFC-GT systems are not appealing (presently) as the GT would increase plant complexity and cost. Furthermore, pressurised BG is not attractive (see section 3.3.2); meaning syngas cooling and compression would be needed, lowering system efficiency. Nagel et al. modelled BG-SOFC systems based on fixed bed (updraft and downdraft) and fluidised bed BG [257, 258]. Complex 1-D models of planar and tubular SOFC designs were developed and Aspen Plus was utilised to execute mass and energy balances for the examined systems. A surprising result was that the air blown updraft gasifier based systems yielded greater efficiencies than the steam fluidised bed systems (due to higher *CGE*). This result is based on the assumption that tars have no adverse impact on system components, which has yet to be proven (see section 3.5). A major limitation of the work was that the BG processes were not simulated, i.e. typical syngas compositions were entered as model inputs.

Other research works detailing the simulation of both BG and SOFC have been published [2-5, 8-10, 176, 193, 259-268]. Recent work will be discussed here; for a description of earlier works such as Panopoulos et al. and Pröll et al. [4, 5], the reader is referred to Nagel [11].

Arteaga-Pérez et al. developed a quasi-equilibrium BG (air blown) model based on empirical equations to set carbon conversion and tar formation and employing the temperature approach method [260]. The SOFC appears to be of planar design based on the operating temperature and support (650 °C and anode supported). The models are 0-D developed using Aspen Plus. The investigated scale of 1,000 kg/h (biomass feed) is impractical and the authors neglected syngas impurities such as H_2S and HCl. Di Carlo et al. investigated a 100 kWth BG-SOFC-GT system [10]. They developed complex 1-D ChemCAD models considering reaction kinetics and fluid dynamics. The SOFC was anode supported planar type. It operated at low U_f and therefore low efficiency to ensure adequate heat was available to drive the BG process (anode exhaust burned to provide heat to gasifier). Impurities such as H_2S and HCl were ignored. Morandin et al. studied systems such as BG-SOFC, BG-SOFC-GT and BG-SOFC-ST [263]. They utilised Belsim models of the FICFB and Viking BG processes developed by others [221]. The scale of the studied systems was limited to 100 kWe by the chosen anode supported planar SOFC. The authors assumed wet biomass (50% moisture) could be dried onsite; a biomass dryer would be impractical at this scale. The authors concluded that the FICFB process is the most promising in terms of cost and system performance since it allows better thermal integration and has higher H_2 yield in contrast to the Viking process. Bang-Møller et al. published two articles on 0-D models of the Viking biomass gasifier and anode supported planar SOFC [9, 261]. BG-SOFC, BG-GT and BG-SOFC-GT systems were analysed in the 2010 article [9]. The SOFC was found to be more efficient converting the syngas than the GT. In the 2013 article only the BG-SOFC system was studied [261]. The authors state that a GT would add complexity and cost and therefore BG-SOFC systems are more realistic in the short term. The CH_4 bypass method was applied in the BG model to adjust the syngas composition to match data

(CH_4 separated prior to chemical equilibrium block and then mixed back in). This method is not as rigorous as the temperature approach method as the syngas CH_4 content is fixed; however, it has been used by others [4, 8, 259]. The model predicted a high net electrical efficiency of ~45% (LHV basis) [261]. An efficiency of this magnitude is unrealistic considering that low temperature cleaning (50 °C) and air-steam blown BG (high N_2/low LHV syngas) was employed. An extremely high gasifier *CGE* of 99.9% was assumed, which may explain the inflated efficiency. The models developed by Bang-Møller et al. were used by other researchers to investigate the inclusion of an ORC [262]. Two articles on the integration of BG and an electrolyte supported planar SOFC were published by Colpan et al. [193, 264]. The effect of gasification agent (air, enriched air and steam) was studied in the 2010 article [264]. The highest electrical efficiency was predicted for steam blown BG-SOFC. The BG model was pure equilibrium and 0-D; however, a detailed 2-D model was used to simulate the SOFC. A BG-SOFC system very similar to the one analysed by Bang-Møller et al. [9, 261] was studied in the 2012 article [193]. The BG process is very like the Viking system (separate pyrolysis unit), cold gas cleaning was chosen and the syngas is converted in a planar SOFC. The same basic BG model (described in the 2010 article) was employed along with a 1-D pyrolysis model and 2-D SOFC model. Low efficiencies were predicted even when 0% biomass moisture was assumed (electrical efficiency = 25% and CHP efficiency = 44%, net and HHV basis). This is in stark contrast to the high efficiencies reported by Bang-Møller et al. for a very similar BG-SOFC system [261]. BG-SOFC-GT system models were developed at TU Delft [8, 259]. In-house process simulation software (Cycle-Tempo) was employed to simulate the systems based on various BG technologies (steam blown FICFB and air blown Värnamo CFB, etc.). The impact of BG technology, cleaning temperature and scale

(100 kWe and 30 MWe) was studied. Built-in 0-D models (Gibbs free energy minimisation equilibrium blocks) were used to simulate the BG processes and the SOFC. Toonssen modelled the FICFB gasifier; however, syngas composition predictions do not show good agreement with published data for the Güssing gasifier (CH_4 over predicted, H_2 under predicted and 3.8% N_2 in syngas) [8]. The discrepancies appear to be due to the use of a CH_4 and CO_2 bypass and mixing of the CZ flue gas with the syngas, which explains the high level of N_2 in the syngas. Moreover, a low steam to biomass ratio (0.32) and high CZ temperature (~1,050 °C) were assumed (typical values 0.75 and 905 °C respectively, see section 4.3). Toonssen found that BG technology had little influence on system performance (steam versus air BG). This surprising result may be due to the following: the atmospheric pressure FICFB gasifier and pressurised Värnamo gasifier means that the systems are not comparable (FICFB system requires inefficient syngas pressurisation), the SOFC model predicts a negligible drop in cell voltage (16 mV) when operated on high N_2 (~50%) syngas compared to undiluted high H_2 syngas from the FICFB gasifier (an actual SOFC would experience a much greater drop in performance). Finally, the proposed 30 MWe scale systems are not feasible considering biomass availability/transport distance and SOFC technology (enormous plant footprint, e.g. Toonssen reports a required SOFC active area of 14,290 m^2 for the FICFB based system). BG-SOFC-GT systems in general are not attractive as discussed previously (complexity, cost, pressurisation, etc.). Sadhukhan et al. modelled a conceptual DFB gasifier integrated with a SOFC and ST using Aspen Plus (100-1000 kWe scale) [265]. The SOFC anode exhaust was fed to the gasifier GZ (steam) and the cathode exhaust was directed to the gasifier CZ (oxidant). The Rectisol cleaning process and wastewater treatment system were also simulated (not attractive for biomass systems, see section 3.5.1). Extremely high net electrical efficiencies (LHV basis) were

predicted (64.4% for 600 kWe system). An efficiency of this magnitude is unrealistic especially considering the low temperature cleaning at 25 °C. A possible reason for the over predicted efficiency is that the power required to compress the syngas to the SOFC operating pressure (5 bar) was neglected. Other limitations/issues include: carbon deposition would be a major problem as the syngas H_2O content is lowered to 3% during cleaning (another reason for the inflated efficiency because SOFC performance increases with decreasing H_2O), the cathode exhaust contains only 3% O_2 meaning it would not be an efficient oxidant for the gasifier CZ, it also suggests that the SOFC operates at high air utilisation and therefore SOFC cooling may be an issue (greater SOFC air flow would decrease predicted efficiency dramatically).

3.7 Chapter Summary

Interest in electricity from gasification is growing rapidly as it accounts for a large proportion of the planned capacity (by 2016) and CHP has become the main application for BG. Based on the experience to date (international) and biomass availability within Ireland it is recommended that Ireland focus on relatively small scale BG CHP projects.

The available literature on BG technologies was reviewed and technologies considered most suitable for BG-SOFC applications were selected (FICFB steam blown gasifier and CFB air blown gasifier). The tubular SOFC technology was chosen based on a fuel cell technology literature review. The main challenges for SOFC developers were identified: high costs and low power density. A syngas conditioning system suitable for BG-SOFC applications was proposed. Warm syngas cleaning technologies (~400 °C) were selected. Relevant modelling and simulation work was reviewed and no Aspen Plus models of the FICFB process were found.

4 BIOMASS GASIFICATION MODELLING

4.1 Chapter Introduction

This chapter provides details on the developed biomass gasification models and the results from those models. Firstly, a description of the employed computer simulation software is provided. Then the DFB gasifier model is presented along with model validation and results from sensitivity analyses. The next sections describe the CFB gasifier model including validation details and results.

4.2 Computer Simulation Software

Aspen Plus was selected for modelling the gasifiers, SOFC, syngas cleaning and balance of plant components in this research work. This simulation package has been used for modelling coal and biomass power generation plants in many studies [146, 269-273] and for modelling fuel cell power generation systems [3, 4, 7, 176, 232, 260, 265, 274, 275]. It is a steady state chemical process simulator, which was developed at Massachusetts Institute of Technology for the US Department of Energy, to evaluate synthetic fuel technologies [146]. It uses unit operation blocks, which are models of specific process operations (reactors, heaters, pumps, etc.). The user places these blocks on a flowsheet, specifying material and energy streams. An extensive built-in physical properties database is used for the simulation calculations. The program uses a sequential modular approach, i.e. solves the process scheme module by module, calculating the outlet stream properties using the inlet stream properties for each block. Aspen Plus has the capability to incorporate Fortran code, written by the user, into the model. This feature is utilised for the definition of non-conventional fuels, e.g. biomass, MSW, specific coals, for ensuring the system operates within user defined limits and

constraints (design specifications and calculator blocks) and for calculating performance indicators such as syngas LHV, gasifier *CGE*, system efficiencies, SOFC current and voltage, etc.

Before a detailed description of the models some Aspen Plus terms will be explained. One of the first things that must be done when modelling with Aspen Plus is stream class specification. There are seven different stream classes to choose from and the one best suited for this research work is called 'MIXCINC'. This stream class allows the user to model with three substreams 'MIXED', 'CISOLID' and 'NC'. The 'MIXED' substream is used to model conventional components in the gaseous phase that are in the Aspen Plus database and the 'CISOLID' substream is used to model conventional solid components (e.g. carbon and sulphur). The 'NC' substream is used to model non-conventional components, i.e. components that are not in the Aspen Plus database (e.g. the biomass feed).

There is no standard or universally accepted composition for biomass. There are many different kinds of biomass; even woody biomass covers a vast range of woods with varying composition and properties (see chapter two). Therefore, Aspen Plus does not have anything in its database that can represent this kind of feed. The user must define the feed as a non-conventional component and provide analyses, such as the ultimate and proximate analyses. Non-conventional components do not take part in the Aspen Plus phase and equilibrium calculations. Therefore, it is necessary to convert the non-conventional feed to carbon, hydrogen, oxygen, nitrogen, sulphur, chlorine, moisture and ash. These components, which make up any fuel, are in the Aspen Plus database and are therefore classed as conventional components, with the exception of ash; however, ash is inert and simply passes through the system with no impact.

The user must also select a property method. Selecting a property method defines how thermodynamic properties are calculated within the simulation. The Peng-Robinson equation of state with Boston-Mathias modifications was selected as the property method for all models [112, 276-278]. It is recommended for synthetic gas and fuel applications, power generation systems and coal gasification, liquefaction and combustion plants [279].

4.3 DFB Gasifier Model

All details regarding the DFB gasifier model are presented in this section. A DFB gasifier known as the FICFB was selected (see section 3.3.3). The model is based on Gibbs free energy minimisation. At equilibrium there is no change in gas concentration and the Gibbs free energy of the system is at a minimum [97]. It is clear from Eq. C.1 that Gibbs free energy will be at its minimum when system entropy is at its maximum. Actual BG processes do not reach equilibrium; therefore, it is necessary to employ methods to restrict equilibrium. The temperature approach method is well established and has been used by numerous researchers [221, 223, 224, 260]. The chemical reaction equilibrium constants are adjusted, which allows the model to be calibrated against published data. Others have used the CH_4 bypass method to adjust syngas composition, as described in section 3.6.3.

4.3.1 Model Description

The Aspen Plus flowsheet of the FICFB gasifier is depicted in Figure 4.1. Table 4.1 presents a brief description of the unit operation blocks shown in Figure 4.1. It gives the Aspen Plus name, i.e. the name given to each unit operation block by the software

developers, the block ID, which is the name given to each block by the user and a short description. For comparison to the actual system, refer to Figure 3.6.

The model is based on the following main assumptions: isothermal and steady state operation; zero-dimensional (0-D); operation at atmospheric pressure (~1 bar); pressure drops are neglected; char is 100% carbon (see section 3.3.1); all fuel bound nitrogen is converted to NH_3 [12, 135, 224, 280]; all fuel bound sulphur is converted to H_2S [12, 135, 224]; all fuel bound chlorine is converted to HCl [224]; tar formation is not considered [12, 175]; a heat stream is used to simulate the heat transferred by the circulation of bed material between the gasifier CZ and GZ [223-225]; heat loss from the gasifier is neglected [222].

With reference to Figure 4.1, the stream 'BIOMASS' was specified as a non-conventional stream and the ultimate and proximate analyses, given in Table 4.2, were entered. The biomass LHV was also specified with the HCOALGEN and DCOALIGT property models chosen to estimate the biomass enthalpy of formation, specific heat capacity and density based on the ultimate and proximate analyses. Finally, the stream thermodynamic condition (1 bar and 25 °C) and mass flow rate were inputted. The pressure of all feed streams and unit operation blocks were set to 1 bar. The mass yields of the RYield reactor 'BRKDOWN', which converts the non-conventional biomass into conventional components, are determined and set using a calculator block. The calculator block uses the ultimate and proximate analyses to calculate these yields.

The outlet stream 'ELEMENTS' is fed to a separator block 'CHARSEP' whose purpose is to separate out a portion of the char and all of the ash. The char split fraction is set using a design specification; the block split fraction is varied until the gasification temperature (T_g) of 850 °C is achieved [5, 221]. The char and ash are directed to the gasifier CZ, simulated by an RStoic reactor titled 'COMB'.

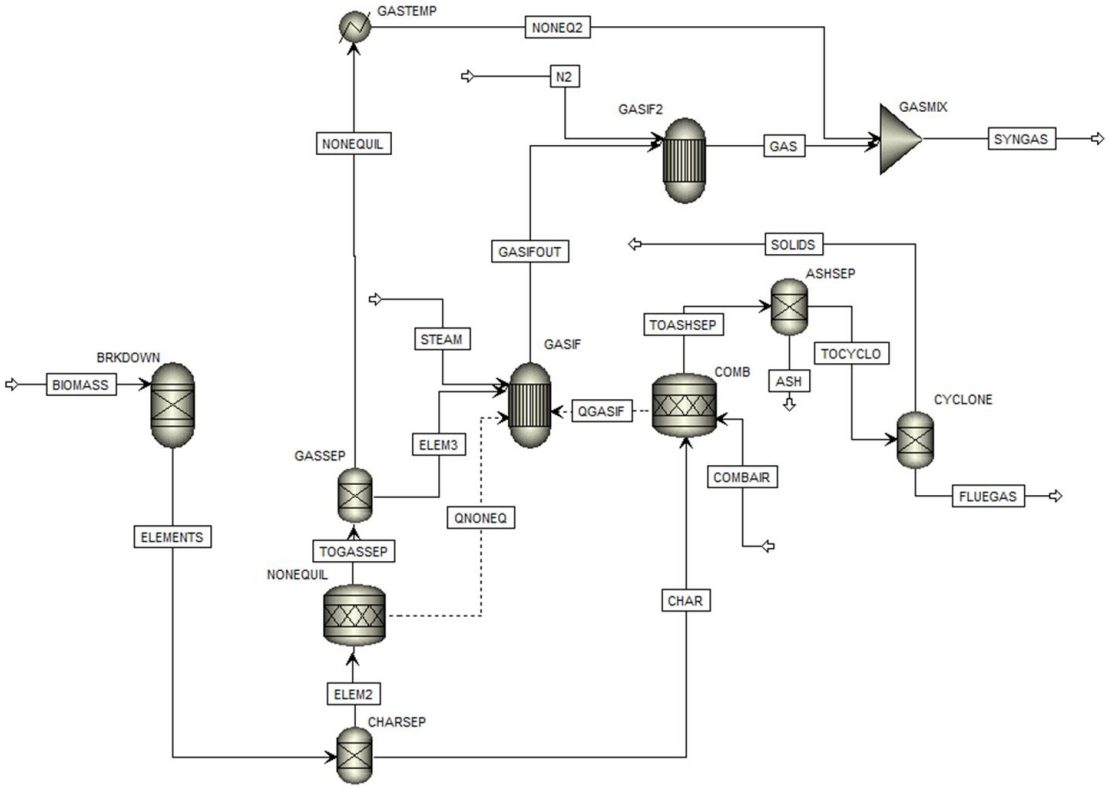

Figure 4.1 FICFB gasifier Aspen Plus flowsheet

Table 4.1 Description of FICFB gasifier Aspen Plus flowsheet unit operation blocks presented in Figure 4.1

Aspen Plus name	Block ID	Description
RYield	BRKDOWN	Yield reactor – converts the non-conventional stream 'BIOMASS' into conventional components
Sep2	CHARSEP	Separator – extracts a portion of the carbon (char) contained in the fuel and all of the ash
	ASHSEP	Separator – separates the ash from the CZ flue gas
	CYCLONE	Separator – simulates the FICFB cyclone by separating out a specified percentage of unburned char
	GASSEP	Separator – separates the impurities (NH_3, H_2S and HCl) from the main fuel stream
RStoic	NONEQUIL	Stoichiometric reactor – simulates the conversion of fuel N_2, S and Cl_2 to NH_3, H_2S and HCl
	COMB	Stoichiometric reactor – simulates the complete combustion of char with air in the gasifier CZ
RGibbs	GASIF	Gibbs free energy reactor – simulates steam gasification of the biomass in the gasifier GZ
	GASIF2	Gibbs free energy reactor – restricts chemical equilibrium of the specified reactions to adjust the syngas composition
Heater	GASTEMP	Heater – brings the impurities up to the gasification temperature
Mixer	GASMIX	Mixer – mixes the impurities into the syngas stream

Table 4.2 Biomass (wood chip) composition, heating value and flow rate

	Unit	Value	Source
Ultimate Analysis (db)			[205]
Carbon	wt. %	51.19	
Hydrogen	wt. %	6.08	
Oxygen	wt. %	41.3	
Nitrogen	wt. %	0.2	
Sulphur	wt. %	0.02	
Chlorine	wt. %	0.05	
Ash	wt. %	1.16	
Proximate Analysis (db)			
Volatile Matter	wt. %	80	[12]
Fixed Carbon	wt. %	18.84	Calculated by difference
Ash	wt. %	1.16	[205]
Moisture	wt. %	20	[5, 129]
LHV (db)	MJ/kg	19.09	[205]
Thermal power input	MW	8	[128, 129]
Mass flow rate	kg/h	1508.64	Calculated

The air stream 'COMBAIR' is also fed to this block. The mole fraction of the air was specified as 0.79 N_2 and 0.21 O_2 and its temperature (T_a) was set to 450 °C [205]. The air mass flow rate is computed and set using a calculator block; air mass flow rate equals biomass mass flow rate multiplied by an assumed air-fuel ratio of 1.12 [205]. The air and char react to produce the heat required for gasification, represented by the heat stream 'QGASIF' connecting the block 'COMB' to 'GASIF'. No chemical reactions were specified; the generate combustion reactions option was selected. The combustion temperature is set by a calculator block and was assumed to be 55 °C above T_g [128]. The chosen air-fuel ratio ensures complete combustion of the char; therefore, the stream 'TOASHSEP' contains only CO_2, O_2, N_2 and ash.

The separator 'ASHSEP' simulates ash removal from the gasifier. The stream 'TOCYCLO' made up of CO_2, O_2 and N_2 enters a separator titled 'CYCLONE' where any un-reacted char is separated out and recycled to the gasifier. The block split fraction was specified as 0.85 (typical cyclone separation efficiency [281]). In a real FICFB gasifier entrained bed material and fly ash would also be separated from the exhaust gas

and recycled but this has not been modelled. As mentioned, combustion is complete; therefore, the 'SOLIDS' stream has zero mass flow rate. 'FLUEGAS' represents the final exhaust from the gasifier CZ.

The material stream 'ELEM2' is directed to the RStoic reactor 'NONEQUIL' where 100% of the fuel bound nitrogen, S and Cl_2 are converted to NH_3, H_2S and HCl respectively via Eq. 3.11-3.13. The enthalpy change due to this process is accounted for by the heat stream 'QNONEQ' fed to 'GASIF'. The NH_3, H_2S and HCl are removed from the main fuel stream using the separator 'GASSEP'.

The main fuel stream 'ELEM3' is fed to the gasifier GZ simulated using an RGibbs reactor named 'GASIF'. The other feed stream is the steam needed to gasify the biomass and fluidise the bed. The steam temperature was set to 450 °C and its mass flow rate depends on the gasifier steam to biomass ratio (STBR). STBR is defined as the mass flow rate of biomass moisture plus the injected steam divided by the dry biomass mass flow rate. The injected steam mass flow rate is set by a design specification block employing the wet biomass mass flow rate, the specified moisture content and a STBR of 0.75 in its calculations [5]. In order to maintain good fluidisation, a steam flow rate higher than that required stoichiometrically is chosen [135]. In the block 'GASIF' the gasification reactions Eq. 3.4-3.6 and Eq. 3.9 and 3.10 were specified with zero temperature approach for each reaction (i.e. the chemical equilibrium constant for each reaction is calculated at the reactor temperature). In Aspen Plus the temperature approach for a reaction is defined as the difference between the temperature at which the chemical equilibrium constant is calculated and the reactor temperature. Thus a negative temperature approach is specified if it is desired to ensure that the chemical equilibrium constant of the reaction in question is calculated at a temperature below the reactor temperature.

The function of the next block ‘GASIF2’, which is another RGibbs reactor, is to adjust the gas composition to match data reported in the literature. The block temperature is set to the ‘GASIF’ block temperature by means of a calculator block. Two reactions Eq. 3.9 and 3.10 were entered and equilibrium was restricted by inputting temperature approach values (-90 °C and -265 °C respectively). These temperature approach values ensure that the model outputs a realistic syngas composition (see Table 4.3). This block is also used to inject a small amount of N_2, which is present in the syngas produced by FICFB gasifiers because it is utilised as purge gas in the fuel feeding system [135].

The final block ‘GASMIX’ simply mixes back in the NH_3, H_2S and HCl, separated prior to the RGibbs reactors. However, before this can be done, these impurities must be brought up to the same temperature as the ‘GAS’ stream (i.e. T_g). This is accomplished by means of the heater block ‘GASTEMP’ and a calculator block is used to set the temperature to T_g. The exit stream from ‘GASMIX’ represents the final output syngas from the gasifier.

4.3.2 Model Validation

The DFB gasifier model was validated against published data for the FICFB gasifier operating at the 8 MWth Güssing CHP plant and pilot FICFB plants. The model inputs were the same as those presented in section 4.3.1. As seen in Table 4.3, the model results are in very good agreement with actual plant data. The percentage error for the syngas composition is 9.26% for CH_4, 4.75% for CO_2 and 0% for H_2, CO and N_2. The model LHV value is 2.75% higher than the reported syngas LHV value. The model prediction for the gasifier *CGE* (Eq. 3.14) is within the range reported in the literature for the FICFB gasifier. In addition, the level of syngas impurities NH_3, H_2S

and HCl are predicted quite accurately. Finally, the amount of char directed to the gasifier CZ is within the published range for the FICFB gasifier.

Table 4.3 DFB gasifier model results compared to literature

	Literature	Source	Model results
Syngas composition (vol. %[a] db and NH_3, H_2S, HCl free)	H_2 45.8, CO 21.6, CH_4 10, CO_2 21.2, N_2 1.4	[5]	H_2 45.8, CO 21.59, CH_4 11.02, CO_2 20.19, N_2 1.4
Syngas LHV (db at 0 °C and 1 atm[b])	11.3 MJ/m^3	[5]	11.6 MJ/m^3
CGE (LHV and mass basis)	71.5-78.4%	[129, 221]	76.7%
Impurities (ppmv db)	NH_3 1100-1700, H_2S 21.5-170, HCl 100	[134, 135, 205]	NH_3 1514, H_2S 66.12, HCl 149.5
Char combusted (mass basis)	10-15%	[5, 12]	12.93%

[a] Volume per cent.

[b] One atmosphere pressure.

4.3.3 Sensitivity Analyses Results and Discussion

The validated model was employed to perform sensitivity analyses of the main operating parameters with respect to gasifier performance. Parameters including T_g, biomass moisture content, STBR, air-fuel ratio, steam temperature and T_a were varied over a wide range. During the sensitivity analyses the input data was kept the same as described in section 4.3.1 with a single parameter being varied at any given time.

Gasification temperature

The influence of T_g on syngas composition is shown in Figure 4.2 (a). T_g is varied from 650 to 1,050 °C and Figure 4.2 (a) shows that it has a very strong influence on syngas composition. Fluidised bed biomass gasifiers should operate below 1,000 °C to ensure that ash softening does not occur, which would cause agglomeration and defluidisation [69]. Over the T_g range 650-950 °C H_2 increases 46.65 percentage points (pp) (9.15% to 55.8%) and CO rises 27.04 pp (2.03% to 29.07%). Both CH_4 and CO_2

decrease; CH_4 drops from 44.03% to 1.45% and CO_2 from 43.15% to 12.35%. A reduction in the level of H_2O in the syngas is seen (36.39-21.06%). T_g has little impact above 950 °C; H_2O reverses its trend and increases slightly. This is most likely due to the decline in CH_4, i.e. the other reactant required for steam-methane reforming (Eq. 3.10). The variation in syngas composition with T_g can be understood by considering that rising temperature favours the products of endothermic gasification reactions (Eq. 3.4, 3.5 and 3.10) and simultaneously the reactants of exothermic reactions (Eq. 3.6 and 3.9). The temperature approach values for the CO-shift and steam-methane reforming reactions (see section 4.3.1) were held constant during this sensitivity analysis. This appears to have led to the over-prediction of CH_4 at low T_g. Therefore, the model predictions should be considered accurate only above a temperature of ~775 °C. From these results it is concluded that T_g is the most important parameter with respect to syngas composition and it is recommended to operate the FICFB gasifier in the temperature range 850-950 °C in order to maximise H_2 and CO and to minimise CO_2 and H_2O.

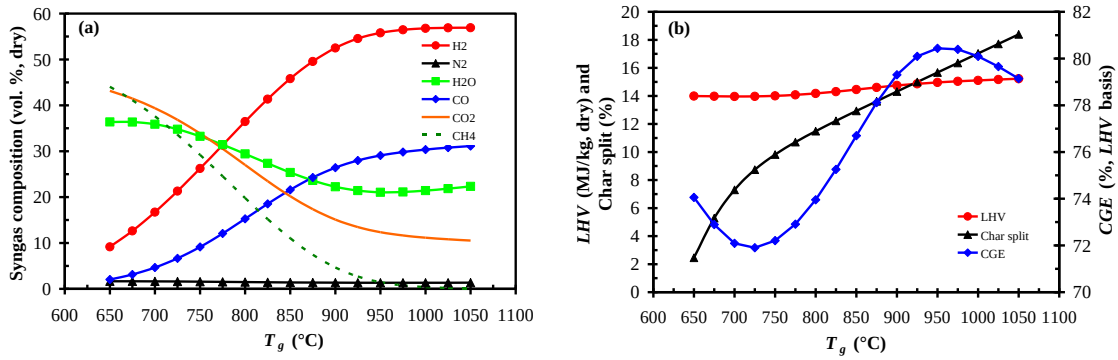

Figure 4.2 Effect of gasification temperature on (a) syngas composition and (b) syngas LHV, gasifier CGE and char split fraction

Figure 4.2 (b) displays how T_g affects the LHV of the syngas, gasifier *CGE* and the char split fraction (i.e. the percentage of char sent to the CZ of the gasifier). The heating value, *CGE* and char split are all on a mass basis. The LHV is calculated from the dry gas composition and the *CGE* is determined using LHV values for both syngas and biomass fuel. It is shown in Figure 4.2 (b) that T_g has significant influence on all three of the performance indicators. LHV increases from 13.99 to 15.23 MJ/kg over the T_g range. The char split fraction climbs from 2.45% to 18.39% (the higher the T_g the greater the amount of char combusted to achieve the desired T_g). Gasifier *CGE* rises and falls over the T_g range; with a maximum at 950 °C and a minimum at 725 °C (80.44% and 71.9%). These results reiterate what was stated above; the gasifier should be operated in the T_g range 850-950 °C in order to maximise *CGE* and produce a high energy content syngas with high H_2 and CO.

Figure 4.3 compares the temperature sensitivity analysis results to results reported in the literature for three different FICFB models [12, 111, 134]. From Figure 4.3 (a) it can be seen that there is fairly good agreement with results reported elsewhere. The same trends; increases in H_2 and CO and decreases in CH_4 and CO_2 are seen. There is better agreement with the results of Fiorenza et al. [134] than the results of Schuster et al. [12]. This was expected as the model developed by Schuster et al. is of the pure equilibrium type and consequently will over-predict H_2 and CO and under-predict CH_4 and CO_2. At high temperature (above 950 °C) there is better agreement between the results; the higher the temperature the closer to equilibrium. Differences in the results may be attributed to differences in conditions and model inputs, e.g. biomass composition, STBR, etc. Emami Taba et al. analysed the results of numerous works on gasification and concluded that H_2 and CO rise while CH_4 and CO_2 fall with temperature [282]. They state that temperature is the most significant process parameter.

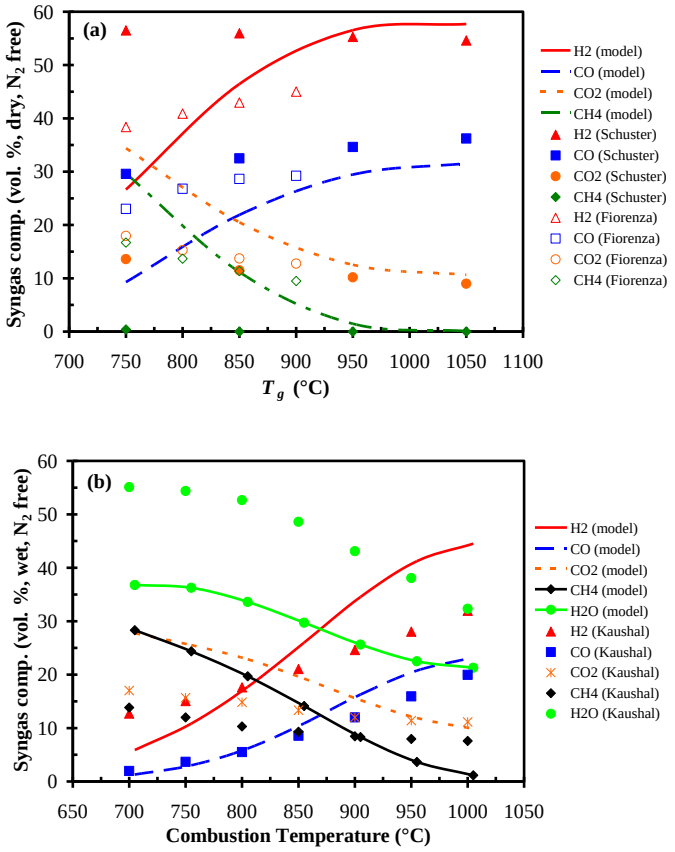

Figure 4.3 Temperature sensitivity analysis results verification

Figure 4.3 (b) displays how wet syngas composition varies with combustion temperature (recall combustion temperature = T_g + 55 °C). The results of this model show fairly good agreement with the work of Kaushal et al. [111]. The greatest discrepancy exists for H_2O content. However, the H_2O content reported in the literature varies widely for FICFB models. For example, Schuster et al. predicted a H_2O content of ~18 vol. % at 850 °C [12], Pröll et al. reported 33.3 vol. % at 850 °C [5] and finally in another article by Kaushal et al. the level of H_2O was given as only 9 vol. % at 883 °C [283].

Biomass moisture content

Biomass moisture content (mass basis) was found to have little impact on syngas composition, e.g. the H_2 content increased only 3.27 pp from 44.76% to 48.03% over

the moisture range 5-40% and this was the second highest change (H_2O content increased by 3.73 pp). The STBR was held constant at the base case value of 0.75 during this sensitivity analysis.

The effect of increasing moisture content on LHV of the syngas, gasifier *CGE* and the char split fraction is illustrated in Figure 4.4. Moisture content has little effect on LHV (depends on the gas composition). However, it was found to have a very strong influence on *CGE* (decreases from 94.28% at 5% moisture to 53.24% at 40% moisture). This influence on *CGE* may be explained by the increase in char split fraction with rising moisture (9.5-20.17% across the moisture range). Greater char split fraction results in less char being gasified, which in turn means less syngas is produced by the gasifier. *CGE* depends on both the syngas LHV and mass flow rate; it is the drop in syngas mass flow rate that causes the dramatic reduction in *CGE* for high moisture content. Based on these results the biomass moisture content proved to be the most significant parameter regarding gasifier *CGE* and therefore should be as low as possible, i.e. the biomass fuel should be dried prior to use in the gasifier.

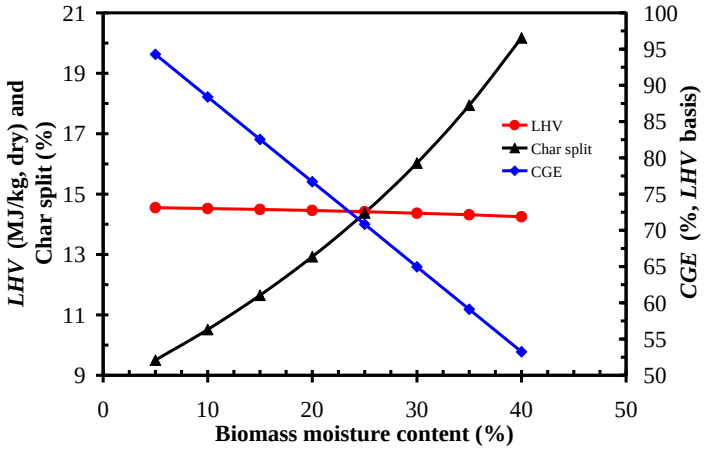

Figure 4.4 Effect of biomass moisture content on syngas LHV, gasifier CGE and char split fraction

The biomass moisture content sensitivity analysis results are compared with published results for two other FICFB models in Figure 4.5 [12, 205]. It is clear from Figure 4.5 (a) that the syngas composition predictions match those of Pröll et al. [205] quite well and as expected the model of Schuster et al. [12] predicts very high H_2 and CO and low CH_4 and CO_2 contents. Referring to Figure 4.5 (b) there is fair agreement with respect to *CGE* between the models. All models predict a strong decreasing trend in *CGE* with increasing moisture content. Any disparity in the results may be due to the STBR. It appears that both Schuster et al. and Pröll et al. held the rate of steam injection to the gasifier constant during this sensitivity analysis and as a result the STBR varies with changes in biomass moisture content. In this work the STBR was held constant by varying steam flow rate as the biomass moisture content changed. This ensured that the influence of biomass moisture alone is seen and not the combined influence of moisture and STBR.

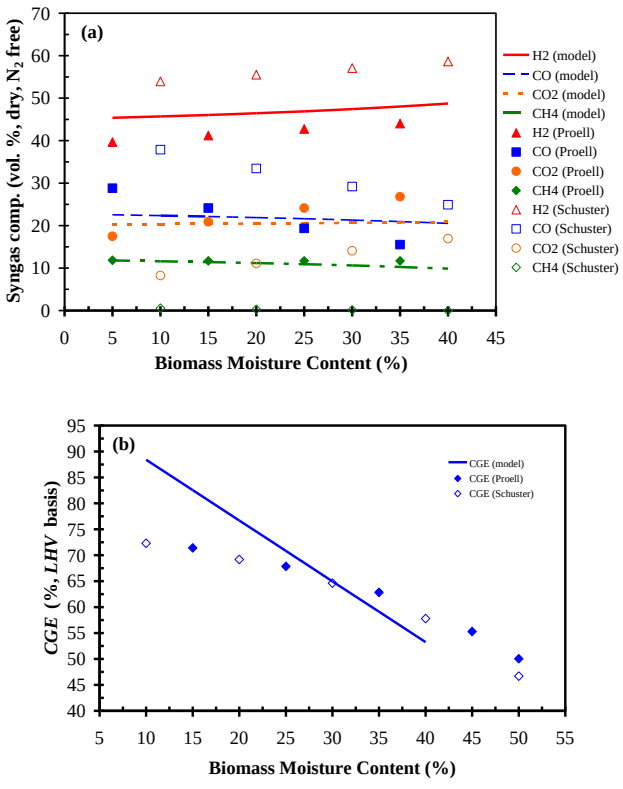

Figure 4.5 Biomass moisture content sensitivity analysis results verification

Steam to biomass ratio

Figure 4.6 (a) depicts the changes in syngas composition in response to variation in STBR (mass basis). It has been reported that the practical range for STBR is 0.5-1 for the FICFB gasifier [5]. It is evident from Figure 4.6 (a) that STBR has little impact on composition above 1.35. Considering this and the reported practical range, the STBR range 0.25-1.35 will now be discussed. Over this range H_2 increases by 25.7 pp; however, on a wet basis (wb) this increase drops to 7.85 pp. It may be more useful to consider the wet gas composition in this analysis as there is such a large increase in H_2O (it rises from 9.26% to 37.6%). CO and CH_4 drop by 17.69 and 15.8 pp respectively (db) and CO_2 increases by 7.27 pp. From these results it is clear that STBR is the second most important parameter in respect of syngas composition. In comparison to the moisture content sensitivity analysis; a much greater mass flow rate of H_2O is fed to the gasifier, which results in a greater impact on gas composition.

From Figure 4.6 (b) it can be seen that STBR has the most significant impact on syngas LHV in comparison to the other sensitivity analyses; however, it is the least important parameter with respect to *CGE*. Gas LHV decreases with STBR because the increase in H_2 is outweighed by the drop in CO and CH_4. The variation in *CGE* may be explained by the fact that at low STBR the LHV is high; however, the syngas mass flow rate is low. Conversely, at high STBR the LHV is low and the syngas mass flow rate is high. These opposing trends result in little change in the *CGE*. In comparison to moisture content, the moisture degrades gasifier *CGE* to a much greater extent. This is due to its low temperature of 25 °C, which leads to higher char combustion than for steam at 450 °C. Considering these findings, it is recommended to operate the gasifier in the range 0.5-1. Operation at higher STBR is not advisable considering the detrimental effect on LHV and the energy that would be required to generate the steam.

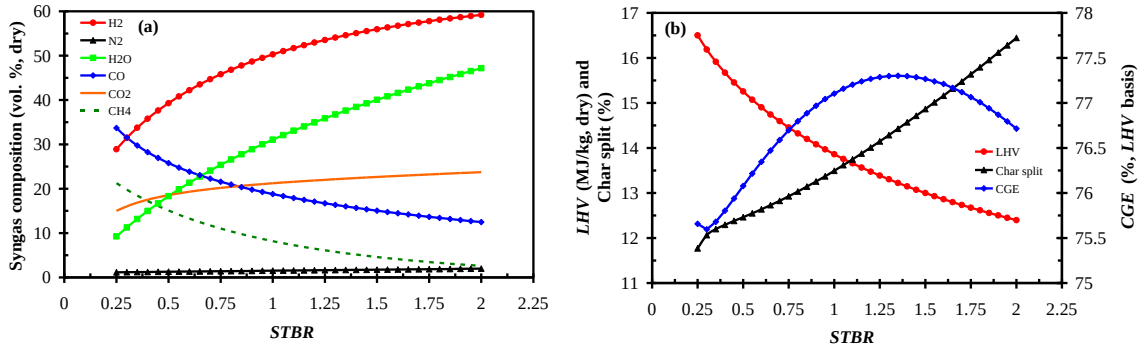

Figure 4.6 Effect of steam to biomass ratio on (a) syngas composition and (b) syngas LHV, gasifier CGE and char split fraction

As displayed in Figure 4.7, the STBR sensitivity results are in accordance with the published results of Fiorenza et al. [134]. Better agreement is seen at the lower STBR values and as before any discrepancy may be attributed to differences in conditions and model inputs.

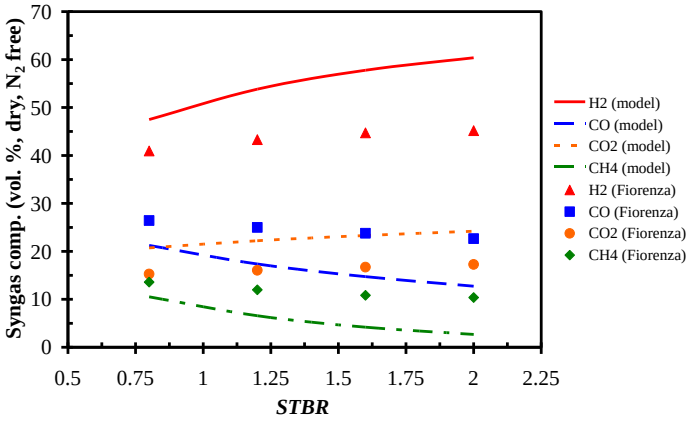

Figure 4.7 Steam to biomass ratio sensitivity analysis results verification

Air-fuel ratio

Syngas composition was found to have a weak dependence on air-fuel ratio (mass basis). The largest change in the combustible gases was an increase from 45.7% to 47% for H_2. Referring to Figure 4.8, syngas LHV remains fairly constant. There is however a substantial decrease in *CGE* with increasing air-fuel ratio (*CGE* drops 3.35 pp). The

decline in *CGE* can be attributed to the increase in char sent to the gasifier CZ and the resulting reduction in syngas mass flow rate. As air-fuel ratio increases the excess air lowers the temperature of the CZ, which in turn affects T_g. In order to maintain T_g at the desired temperature more char must be burned. In conclusion, air-fuel ratio should be as low as possible but high enough to ensure complete combustion of the char.

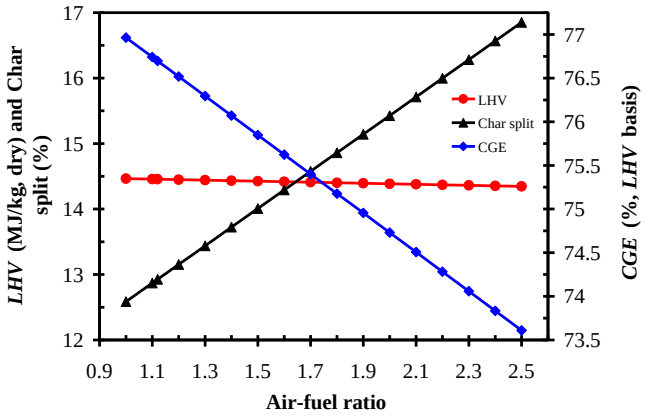

Figure 4.8 Effect of air-fuel ratio on LHV, gasifier CGE and char split fraction

Gasification steam temperature

Syngas composition and LHV remain somewhat unchanged with a rise in steam temperature (150-1000 °C). The elevated temperature does reduce the amount of char required in the gasifier CZ (14.25-10.16%), which has a positive effect on performance. The *CGE* increases from 75.66% to 78.87% (up 3.21 pp). The improvement in performance is only slight; therefore, superheating the steam to high temperature (e.g. 500-1000 °C) is not recommended considering the energy that would be required.

Gasification air temperature

Preheating the combustion air from 25 to 1,025 °C causes slight changes in syngas composition. The largest variation in the combustible gases was a drop from 46.64% to 44.57% for H_2. This negative trend is offset by small increases in both CO and CH_4.

Figure 4.9 shows how syngas LHV increases due to the change in composition and how the char split fraction drops and *CGE* increases. The rise in *CGE* is substantial (5.33 pp) and is as a result of the drop in char split fraction. The amount of char required in the gasifier CZ is lowered with increasing T_a because the sensible heat of the air supplies a greater portion of the heat required by the gasifier. Based on these results, air preheating is more attractive than steam superheating and if waste heat is available, it should be used to increase T_a.

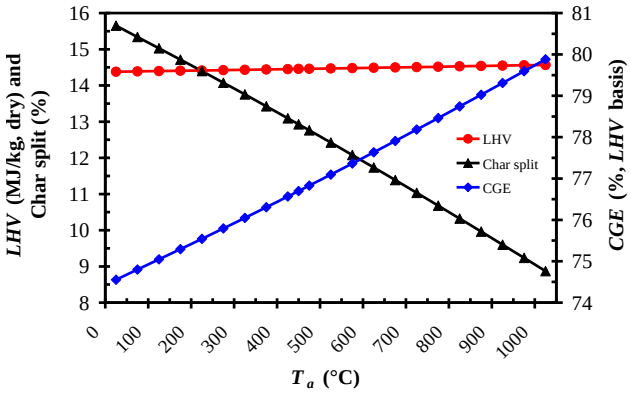

Figure 4.9 Effect of combustion air temperature on LHV, gasifier CGE and char split fraction

4.4 CFB Gasifier Model

The CFB gasifier model is described in this section. CFB technology was selected for reasons discussed previously (see section 3.3.3). The model is based on Gibbs free energy minimisation and the temperature approach method was used to calibrate it against experimental data.

4.4.1 Model Description

Figure 4.10 displays the CFB biomass gasifier Aspen Plus flowsheet. Table 4.4 presents a brief description of the unit operation blocks shown in Figure 4.10. See Figure 3.5 for comparison to the actual system.

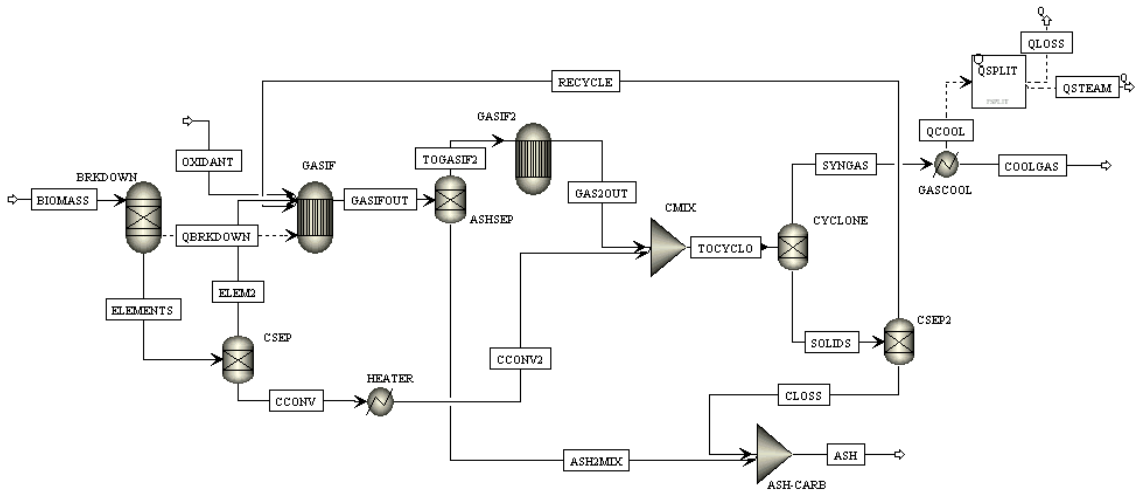

Figure 4.10 CFB gasifier Aspen Plus flowsheet

Table 4.4 Description of CFB gasifier Aspen Plus flowsheet unit operation blocks presented in Figure 4.10

Aspen Plus name	Block ID	Description
RYield	BRKDOWN	Yield reactor – converts the non-conventional stream 'BIOMASS' into conventional components
Sep2	CSEP	Separator – extracts a portion of the carbon contained in the fuel so that it remains un-reacted
	ASHSEP	Separator – separates the inert ash from the gas to allow removal from the system
	CYCLONE	Separator – simulates the CFB cyclone by separating out a specified percentage of the solid carbon
	CSEP2	Separator – extracts a portion of the carbon to simulate carbon loss in the ash, with the rest recycled
RGibbs	GASIF	Gibbs free energy reactor – simulates drying, pyrolysis, partial oxidation and gasification
	GASIF2	Gibbs free energy reactor – restricts chemical equilibrium of the specified reactions to set the syngas composition
Heater	HEATER	Heater – increases the temperature of the un-reacted carbon to the reactor temperature
	GASCOOL	Cooler – simulates syngas cooling to a typical gas cleanup temperature
Mixer	CMIX	Mixer – mixes the un-reacted carbon separated in block 'CSEP' with the syngas
	ASH-CARB	Mixer – mixes the carbon lost with the ash before leaving the system
FSplit	QSPLIT	Splitter – splits the heat available from syngas cooling in 'GASCOOL' into two heat streams with one of them representing the heat lost from the gasifier

The main model assumptions are: isothermal and steady state conditions; 0-D; operation at atmospheric pressure; pressure drops are neglected; char is 100% carbon

(see section 3.3.1); all fuel bound sulphur is converted to H_2S [12, 135, 224]; all fuel bound nitrogen is converted to NH_3 [12, 135, 224, 280]; tar formation is not considered [12, 175]; 2% carbon loss in ash [284]; heat loss from the gasifier is equal to 3% of the total heat input [285-287].

From Figure 4.10, the stream 'BIOMASS' was specified as a non-conventional stream and the ultimate and proximate analyses were inputted (see Table 4.5). The stream thermodynamic condition and mass flow rate were also entered. The block 'BRKDOWN' yields are set by a calculator block, which in turn determines the mass flow of each component in the block outlet stream 'ELEMENTS'.

Table 4.5 Biomass (hemlock wood) composition and heating value

	Unit	Value	Source
Ultimate Analysis (db)			[284]
Carbon	wt. %	51.8	
Hydrogen	wt. %	6.2	
Oxygen	wt. %	40.6	
Nitrogen	wt. %	0.6	
Sulphur	wt. %	0.38	
Chlorine	wt. %	0.0	
Ash	wt. %	0.4	
Proximate Analysis (db)			
Volatile Matter	wt. %	84.8	[94]
Fixed Carbon	wt. %	14.8	Calculated by difference
Ash	wt. %	0.4	[284]
Moisture	wt. %	11.7	[284]
HHV (db)	MJ/kg	20.3	[284]

The function of the next block is to simulate carbon conversion by separating out a specified portion of the carbon from the fuel. Reported carbon conversion for CFB gasifiers in the literature ranged from 90 to 99% [67, 194, 287]. A carbon conversion of 91.9% was used [206], which meant that a split fraction of 0.081 was entered for the solid carbon. Two streams exit this block, 'CCONV', which contains 8.1% of the total carbon entering the gasifier and 'ELEM2', which contains the remaining carbon and all

other fuel components. Before the un-reacted carbon can be mixed with the gas downstream it must be brought up to the gasifier temperature, which is accomplished using the block entitled ‘HEATER’. The un-reacted carbon represents solids contained in the product gas that must be removed by the CFB gasifier cyclone or other solids removal steps downstream. In reality there would also be fly ash and bed material entrained in the gas but these components cannot be modelled in Aspen Plus. Thus, in this model the solid carbon that remains in the syngas represents all solids.

The streams ‘ELEM2’, ‘OXIDANT’ and ‘RECYCLE’ enter the block ‘GASIF’, where pyrolysis, partial oxidation and gasification reactions occur. The mass flow of air entering the reactor is set using a design specification, which varies the oxidant mass flow rate so that a specific gasifier temperature is achieved. Alternatively, the air mass flow is set by a calculator block that calculates the air flow using a user specified equivalence ratio (ER). ER is defined as the ratio of the actual oxidant mass flow rate to the stoichiometric oxidant mass flow rate. Most existing fluidised bed biomass gasifiers operate in the ER range 0.2-0.45 [288]. Ash removal is simulated in the model using the unit operation block ‘ASHSEP’. The material stream ‘TOGASIF2’ is fed to the unit operation block ‘GASIF2’, which is an ‘RGIBBS’ reactor. Equations 3.9-3.11 were specified in the ‘RGIBBS’ reactor and the temperature approach of the reactions were varied until the syngas composition matched experimental data [284].

The next block mixes the un-reacted carbon that was separated upstream with the gas from ‘GASIF2’ and its product stream is fed to a separator that simulates the operation of the CFB gasifier cyclone. The block ‘CYCLONE’ was specified so that it removes 85% of the solid carbon from the gas stream (typical cyclone separation efficiency [281]). The bottom outlet stream from ‘CYCLONE’ with the stream name ‘SOLIDS’ is composed of solid carbon only and is sent to a separator block ‘CSEP2’.

The top outlet stream, which is called ‘SYNGAS’, is composed of all the gases from ‘GASIF2’ and a small amount of solid carbon (15% of the un-reacted carbon). This material stream represents the final output, i.e. the gasifier syngas.

‘CSEP2’ splits the ‘SOLIDS’ stream into a recycle stream ‘RECYCLE’, that is sent back through the gasifier, and another stream named ‘CLOSS’, which represents the carbon lost from the system in the ash. The recycle was added because in a real CFB gasifier, inerts (bed material and fly ash) and un-reacted char are collected in the cyclone and re-injected into the reaction zone of the gasifier via the return leg (see Figure 3.5). The ‘CSEP2’ split fraction is set by a calculator block using the specification that the ash exiting the gasifier contains 2% carbon [284]. The stream ‘CLOSS’ is then mixed with the ash in the block ‘ASH-CARB’.

The stream ‘SYNGAS’ is fed to a cooler entitled ‘GASCOOL’ that cools the gas to the required gas cleanup temperature of 375 °C [120]. The energy that would be lost through cooling could be recovered by generating steam or by supplying heat for air preheating. The heat stream ‘QCOOL’ represents the energy that could be recovered during gas cooling. This stream is fed to ‘QSPLIT’, which is used to split the heat stream ‘QCOOL’ into two heat streams ‘QLOSS’ and ‘QSTEAM’. Two calculator blocks are used, one calculates and sets the amount of heat loss ‘QLOSS’ and the other calculates and sets the amount of heat available for steam generation or air preheating ‘QSTEAM’. The heat loss from the gasifier is assumed to be 3% of the total heat input [285-287].

4.4.2 Model Validation

The model was validated against the experiments of Li et al. [284], which were conducted on a pilot scale air blown biomass CFB gasifier. The fuel used for model

validation was hemlock wood (see Table 4.5). Li et al. [284] reports results for six experimental runs using hemlock wood as input fuel. The input data for three of these runs (run 4, 6 and 7) were entered into the model and the predictions were found to be in good agreement with the reported results. For example, for run number 4 the model predicts the following syngas composition: 3.23% H_2, 72.82% N_2, 8.9% CO, 15.04% CO_2 and 0.01% CH_4 and for the same input data Li et al. [284] reports 3.0% H_2, 68.4% N_2, 9.6% CO, 17.1% CO_2 and 1.9% CH_4. Experimental run number 7 [284], was chosen for a detailed comparison and analysis. The input data for run number 7 were as follows: input fuel stream mass flow = 33.626 kg/h, T_g = 718 °C and gasification pressure = 1.05 bar. Table 4.6 compares the experimental results (run 7) as reported by Li et al. [284] to the model predictions. The model predictions are in good agreement with the experimental data. For example H_2, CO and CO_2 are predicted within 2.5% and N_2 is under-predicted by 6.8%. However, the CH_4 is over-predicted, which causes an error in the calculation of the gas heating value and ultimately the *CGE*. The under or over-prediction of CH_4 is a common problem when modelling gasification. The low T_g (718 °C) results in high CH_4 content but the CH_4 content decreases rapidly with temperature (at ~870 °C the model predicts virtually zero CH_4). This is further discussed in section 4.4.3.

Table 4.6 CFB gasifier model results compared to literature [284]

	Literature (run # 7)	**Model results**
Syngas composition (vol. % db)	H_2 5.5, CO 16.6, CH_4 3.4, CO_2 15, N_2 59.5	H_2 5.53, CO 16.79, CH_4 7.65, CO_2 14.62, N_2 55.42
Syngas HHV (db at 0 °C and 1 atm)	4.82 MJ/m^3	5.87 MJ/m^3
CGE (HHV and mass basis)	71.4%	62.61%

4.4.3 Sensitivity Analyses Results and Discussion

The model described was used to perform sensitivity analyses. The effects of varying ER, T_g, T_a, biomass moisture content and steam injection rate on syngas composition, heating value and *CGE* were investigated. During the sensitivity analyses the model input data was kept the same as for model validation (run 7 input data presented in section 4.4.2), with one parameter being varied at any given time.

Equivalence ratio and gasification temperature

The influence of ER on syngas composition is illustrated in Figure 4.11 (a). T_g depends on the amount of air fed to the gasifier, i.e. it is controlled by ER. As a result, varying ER or T_g will have the same effect on syngas composition, heating value and *CGE*. For this reason only ER is plotted. The corresponding T_g values for each ER are given. In Figure 4.11 (a) the N_2 content is not displayed; its value may be calculated by summing the other components and subtracting this from 100%. N_2 varied between 53% and 61% over the ER/T_g range. The most interesting point from Figure 4.11 (a) is that both H_2 and CO reach a maximum at ER = 0.35 or T_g = 874 °C. After this peak their contents decrease steadily. H_2O increases over the whole range but experiences a small decrease close to the point of maximum H_2 and CO. CO_2 decreases rapidly up to ER = 0.35 and then increases slowly. CH_4 decreases and eventually reaches zero between ER = 0.4-0.45 or T_g = 1046-1195 °C. These trends may be explained as follows:

- The Boudouard reaction (Eq. 3.4) is endothermic; therefore, as T_g rises, so does the amount of CO_2 reacted with char to produce CO. For ERs up to 0.35 sufficient char is available for the Boudouard reaction but for ERs greater than this there is insufficient char, so CO decreases and CO_2 increases.

- The water-gas reaction (Eq. 3.5) is endothermic, which means for increasing ER/T_g CO and H_2 increase and more char and H_2O are consumed.
- The methanation reaction (Eq. 3.6) is exothermic, which means as ER and T_g rise the production of CH_4 decreases, which in turn leaves more H_2 in the gas.
- The CO reacts with O_2 (Eq. 3.7) producing CO_2.
- H_2 reacts with O_2 (Eq. 3.8) producing H_2O. This reaction produces more H_2O than is used up by Eq. 3.5 and 3.10 because its content increases over the whole ER/T_g range. The slight drop in H_2O occurs at ER = 0.34 or T_g = 837 °C. One possible explanation would be that at a sufficiently high temperature Eq. 3.10 begins to consume more H_2O than is produced by Eq. 3.8; however, this trend is short-lived because CH_4 is decreasing rapidly.
- The CO-shift reaction (Eq. 3.9) being exothermic, produces less CO_2 and H_2 at higher temperatures, which means less CO and H_2O are consumed.
- The CH_4 is reduced by the steam-methane reforming reaction (Eq. 3.10). This reaction is endothermic meaning the forward reaction is favoured as temperature increases. Hence, CH_4 and H_2O decrease while H_2 and CO increase.

Fluidised bed biomass gasifiers operate in the T_g range 800-1000 °C, which corresponds to an ER range of 0.33-0.38. ER values higher than 0.3 have to be used to get tar contents below 2 g/m^3 [289]. Taking these points into consideration it is recommended to operate this gasifier at ER = 0.34-0.35 or T_g = 837-874 °C.

The influence of ER on syngas heating value and *CGE* is shown in Figure 4.11 (b). The gas HHV (mass basis) and *CGE* (HHV basis) are plotted against ER. It is evident that the heating value decreases with ER. The HHV is high for low ERs due to the high CH_4 content. The *CGE* increases between ER = 0.29-0.34, reaches a maximum

of 66.1% at ER = 0.34 and then decreases steadily. It is worth noting that the point of maximum *CGE* corresponds to the peak H_2 and CO content in Figure 4.11 (a). The *CGE* for ER = 0.31 as reported by Li et al. [284] is indicated for comparison.

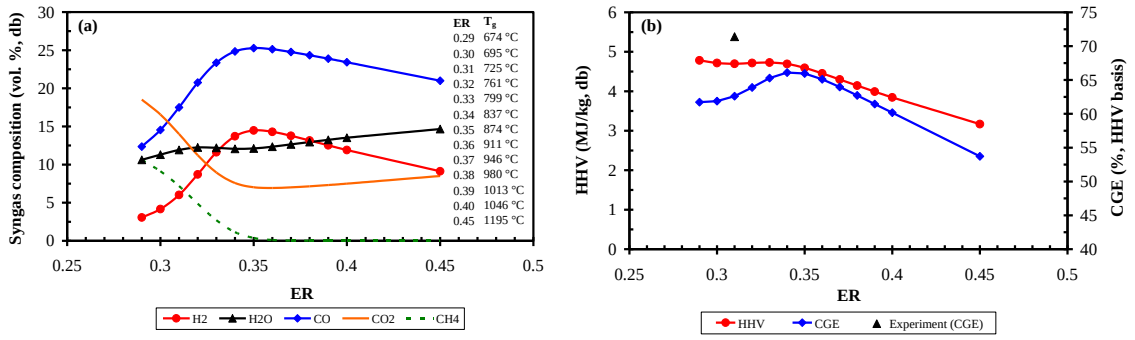

Figure 4.11 Effect of ER on (a) syngas composition and (b) syngas HHV and gasifier CGE (▲: indicates CGE as reported by Li et al. [284])

Gasification air temperature

Air preheating is a means of increasing the conversion efficiency of the gasification process. The sensible heat in the air causes a rise in the gasification temperature, which in turn influences the syngas composition, causing an increase in the production of combustible gases, H_2 and CO. This change in syngas composition affects the gas HHV and hence the gasifier *CGE*. The influence of air preheating on T_g was investigated over the complete ER range. T_g increased almost linearly with T_a for all ERs. It was discovered that a limit on the level of air preheating exists for each ER. As mentioned previously, fluidised bed biomass gasifiers should not be operated over 1,000 °C. It was found that at high ERs air preheating is limited to a low level, e.g. at ER = 0.37 a T_a no more than 114 °C would be recommended because the corresponding T_g = 987 °C whereas for ER = 0.29 the air could in theory be heated to 825 °C as T_g stays below 1,000 °C at 978 °C.

The influence of T_a on syngas composition is shown in Figure 4.12. The syngas composition for ER = 0.29 is plotted against T_a. The gas composition changes reflect the change in T_g. As discussed previously, the rising temperature promotes the products of the endothermic reactions (Eq. 3.4, 3.5 and 3.10) and simultaneously the reactants of the exothermic reactions (Eq. 3.6 and 3.9). The major conclusion drawn from this sensitivity analysis is that T_a has a greater influence on the syngas composition for low ERs. For ER = 0.29 CO and H_2 increase 17.3 and 15.8 percentage points (pp) respectively over the T_a range whereas for ER = 0.34 CO and H_2 rise by only 2.7 and 1.8 pp respectively. It was also found that T_a has a significant impact on composition only up to a certain level, after which additional preheating has little effect. For ER = 0.29 this T_a is high at a value of ~560 °C but for ER = 0.34 it is significantly lower at ~200 °C. This finding agrees with published work [290, 291]. Lucas et al. [290] reported that H_2 rises with increasing air preheat temperature but exhibits no rise between 700 and 830 °C. Yang et al. [291] refers to a critical T_a above which air preheating is no longer efficient if the purpose is to maximise the yield of gaseous products. This critical T_a for CO and H_2 was reported as 530 °C. The results of this work indicate a critical T_a of ~560 °C for ER = 0.29.

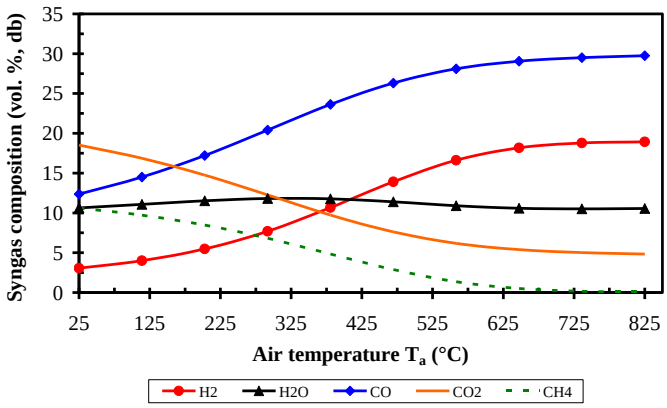

Figure 4.12 Effect of air temperature on syngas composition for ER = 0.29

The influence of air preheating on syngas HHV and *CGE* is shown in Figure 4.13. The gas HHV and *CGE*, Figure 4.13 (a) and (b) respectively, were plotted against T_a for the complete ER range. HHV increases with T_a and the increase is in line with the gas composition change for each ER, i.e. the increase is greater for low ERs than for high ERs (greater change in gas composition for low ERs). The *CGE* trends are in agreement with the changes in gas composition and HHV. T_a has a significant impact on *CGE* at low ER values. Its influence ceases for ERs greater than 0.35. As already seen for gas composition, T_a has a significant effect on *CGE* only up to a certain level, after which additional preheating has little benefit. For ER = 0.29 this T_a is high at a value of ~650 °C but for ER = 0.33 it is significantly lower at ~290 °C. For ER = 0.34, which is a point of interest as it was the point of maximum *CGE* for gasification without air preheating, the *CGE* increases from 66.1 to 67.2% for a T_a of ~110 °C and then increases by a lesser degree to 67.7% for a T_a of ~200 °C.

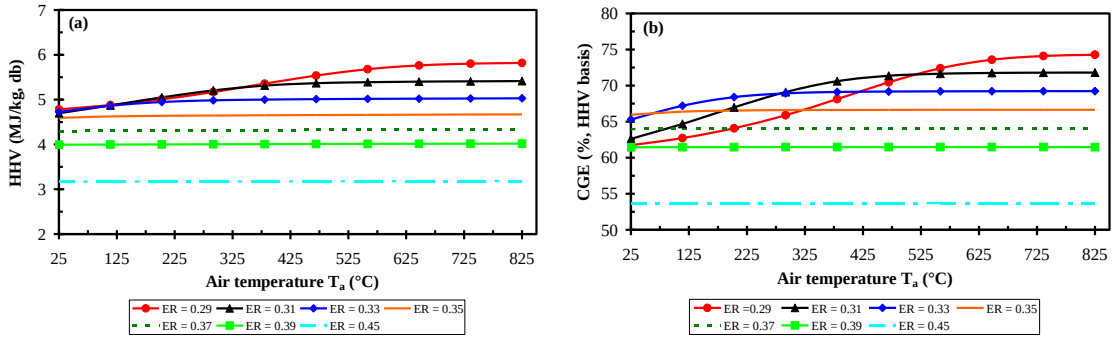

Figure 4.13 Effect of gasification air temperature on (a) syngas HHV and (b) gasifier CGE for complete ER range

Biomass moisture content and steam injection rate

The effect of fuel bound moisture on gasifier performance for ER = 0.34 is shown in Figure 4.14 (a). The moisture level was varied over a realistic range for woody

biomass (5-30%). Increasing the moisture content degrades gasifier performance. Both syngas HHV and gasifier *CGE* reach their maximum level, 5.14 MJ/kg and 73.8% respectively, at the lowest moisture content (5%). The gas heating value and *CGE* decrease over the entire moisture range, for comparison HHV = 3.34 MJ/kg and *CGE* = 44.2% at a moisture content of 30%. These trends are a direct result of changes in the syngas composition with moisture. The rising H_2O content is the main cause for the decline in syngas HHV. CO and CH_4 are shifted and reformed respectively with the additional H_2O decreasing their contents and producing CO_2. There is little change in H_2 content at this ER; however, at lower ERs H_2 content was found to increase with moisture level. Similar performance trends were seen for other ERs but maximum gasifier performance was predicted for an ER range 0.34-0.35.

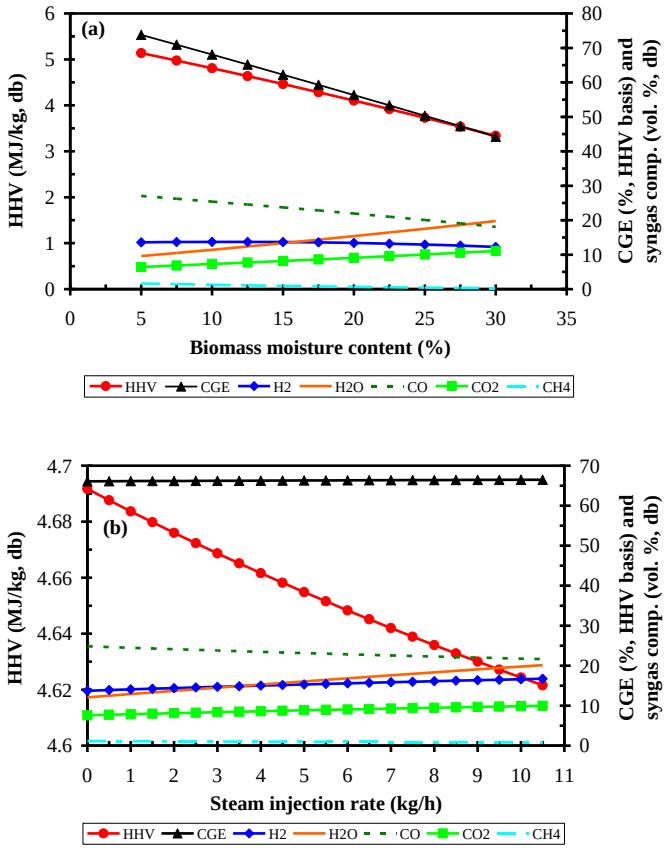

Figure 4.14 Effect of (a) biomass moisture content and (b) steam injection rate on syngas composition, syngas HHV and gasifier CGE for ER = 0.34

The influence of steam injection rate on gasifier performance for ER = 0.34 is illustrated in Figure 4.14 (b). The steam injection rate was varied from 0 to 10.5 kg/h [284]. The syngas HHV decreases only slightly from 4.69 to 4.62 MJ/kg and gasifier *CGE* increases from 66.1% to 66.5%. This small increase in *CGE* is due to higher syngas mass flow rate. As was seen for increasing moisture level, steam injection causes a rise in H_2O content, which results in a lower syngas HHV. CO and CH_4 are shifted and reformed respectively with the additional H_2O decreasing their contents and producing CO_2. The most important effect of steam injection is the rise in H_2 content, in this case H_2 increases by 3 pp (13.7% to 16.7%) over the range of steam injection. The gasifier temperature will decrease with increasing steam injection rate due to the highly endothermic water-gas and reforming reactions (Eq. 3.5 and 3.10). A drop in T_g is undesirable as this would degrade gasifier performance and could lead to high tar yield. Similar performance trends were seen for other ERs but maximum increase in H_2 content was predicted for an ER range of 0.34-0.35.

Although both steam and moisture are chemically equivalent, steam injection has little impact on HHV and *CGE* compared to moisture content. This is due to the difference in temperature between the two; moisture was at room temperature, whereas steam was at a much higher temperature. The results indicate that the biomass should be pre-dried to ensure low moisture content and if a H_2 rich syngas is desired steam injection should be employed. Air preheating should be considered when using high moisture fuels/steam injection because it causes an increase in the gasifier temperature. This would offset the drop in T_g caused by steam injection/high moisture.

4.5 Chapter Summary

This chapter presented two biomass gasifier Aspen Plus models. Both models proved capable of accurately predicting 'real world' gasifier performance, i.e. both models were validated. The following sections summarise the results obtained through application of the models.

4.5.1 DFB Gasifier Model

This section summarises the findings from application of the DFB gasifier model. Refer to section 4.3.3 for a discussion of all results.

- Gasification temperature is the most important parameter with respect to syngas composition; the gasifier should be operated in the range 850 to 950 °C in order to maximise gasifier *CGE* and produce a high energy content syngas with high H_2 and CO.
- Biomass moisture content was found to have little impact on syngas composition and LHV; however, it had a very strong influence on *CGE*. It proved to be the most significant parameter regarding *CGE* and should be as low as possible, i.e. the biomass should be dried prior to use in the gasifier.
- Steam to biomass ratio had the most significant impact on LHV but was the least important parameter with respect to *CGE*. It is recommended to operate the gasifier in the STBR range 0.5 to 1.
- Syngas composition and LHV were found to have weak dependence on air-fuel ratio. There was a substantial decrease in *CGE* with increasing air-fuel ratio. It should be as low as possible but high enough for complete combustion of char.

- Air preheating is more attractive than steam superheating. Steam temperature had little impact on syngas composition and LHV and slight influence on *CGE*. Air temperature had more of an effect on composition, heating value and had significant influence on *CGE*.

4.5.2 CFB Gasifier Model

This section summarises the findings from application of the CFB gasifier model. Refer to section 4.4.3 for a discussion of all results.

- Equivalence ratio and gasification temperature displayed strong influence on syngas composition, heating value and *CGE*. *CGE* reached its maximum at ER = 0.34; therefore, it is recommended to operate the gasifier at ER = 0.34 to 0.35 or T_g = 837 to 874 °C.
- Increasing air temperature had a positive impact on syngas composition, heating value and *CGE*.
- A critical air temperature exists for each ER; it was high for low ER and low for high ER. Air preheating was found to be more effective at low ER and should not be used above an ER of 0.35.
- Increased moisture content degraded performance; therefore, biomass drying should be employed.
- Steam injection increased the H_2 content of the syngas.
- Air preheating should be considered when using high moisture fuels/steam injection because it would offset the drop in T_g.
- CFB gasifiers produce low quality syngas with low energy content, high N_2 and low H_2 content and thus are not attractive for fuel cell applications.

5 SOLID OXIDE FUEL CELL AND COMBINED SYSTEM MODELLING

5.1 Chapter Introduction

In this chapter, the developed SOFC model is described along with validation details and results from sensitivity analyses. Then the various combined system configurations are discussed and compared in relation to plant performance. A number of options for enhancing plant performance are investigated and finally the results from sensitivity analyses of the main operating parameters for the base case system configuration are presented.

5.2 SOFC Model

The SOFC model is described in detail in this section. The tubular SOFC technology was selected (refer to section 3.4.2). The model is of the equilibrium type and is based on Gibbs free energy minimisation. The model performs heat and mass balances and considers ohmic, activation and concentration losses for the voltage calculation. There is no built-in model in Aspen Plus that can represent a SOFC. It is common to develop a complete SOFC stack model in a programming language and link it to Aspen Plus as a subroutine [232]. The subroutine must incorporate complex phenomena making them difficult and time consuming to develop and use. An alternative method proposed by Zhang et al. [232], using existing Aspen Plus unit operation blocks with minimum requirements for linking of a subroutine was used.

5.2.1 Model Description

Model flowsheet

The Aspen Plus flowsheet of the SOFC stack is depicted in Figure 5.1. Table 5.1 presents a brief description of the unit operation blocks shown in Figure 5.1. For comparison to the actual system, refer to Figure 3.14.

The model is based on the following main assumptions: isothermal and steady state operation; 0-D; pressure drops are neglected; adiabatic pre-reformers; reforming and shift reactions reach chemical equilibrium; ion cross over through the electrolyte cannot be modelled in Aspen Plus, therefore the overall oxidation of H_2 (Eq. 3.8) was considered instead of the cell half reactions (Eq. 3.15 and 3.16); only H_2 is reacted electrochemically, it is assumed that CO is shifted to H_2 and CH_4 is reformed to H_2 (see section 3.4.1 for explanation) [4, 230, 232, 292].

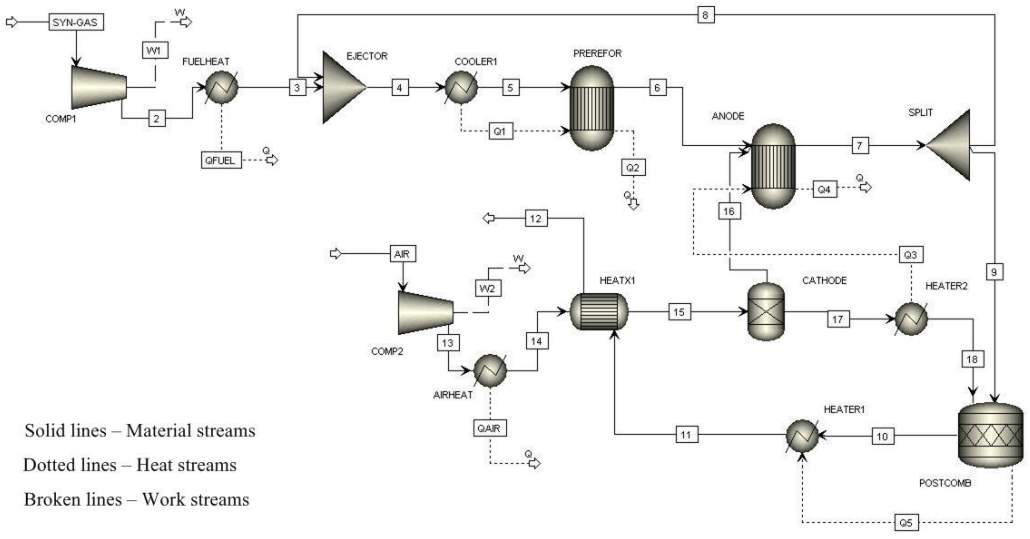

Figure 5.1 SOFC stack Aspen Plus flowsheet

Table 5.1 Description of SOFC stack Aspen Plus flowsheet unit operation blocks presented in Figure 5.1

Aspen Plus name	Block ID	Description
Compr	COMP1	Compressor – increases the pressure of the input fuel to a sufficient level to drive the ejector process
	COMP2	Compressor – increases the pressure of the input oxidant slightly above atmospheric pressure
Heater	FUELHEAT	Heater – preheats the incoming fuel
	AIRHEAT	Heater – preheats the incoming air
	COOLER1	Cooler – decreases the temperature of the mixed fuel to the calculated pre-reforming temperature
	HEATER1	Heater – increases the temperature of the combustion plenum products
	HEATER2	Heater – increases the temperature of the depleted oxidant stream to the SOFC operating temperature
Mixer	EJECTOR	Mixer – simulates mixing of the recycled depleted fuel with fresh fuel in the ejector
RGibbs	PREREFOR	Gibbs free energy reactor – simulates steam reforming of higher hydrocarbons and CH_4 and the shifting of CO to H_2
	ANODE	Gibbs free energy reactor – simulates the reactions occurring at the anode
FSplit	SPLIT	Splitter – splits the depleted fuel into a recycle stream sent to the ejector and a stream sent to the combustion plenum
RStoic	POSTCOMB	Stoichiometric reactor – simulates the complete combustion of the remaining fuel with the depleted oxidant
HeatX	HEATX1	Heat exchanger – simulates preheating of the oxidant through the injector tube wall by the combustion of the depleted fuel
Sep	CATHODE	Separator – separates the O_2 required by the electrochemical reaction

Referring to Figure 5.1, the stream ‘SYN-GAS’ is fed to the ‘COMP1’ block, simulating syngas compression. The discharge pressure was calculated using a pressure ratio of 3 [231]. That is, the syngas is compressed to three times the SOFC operating pressure (P_{SOFC}). Syngas composition, temperature and pressure were entered; its mole flow rate is set by a design specification block and depends on the specified stack power (or for variable power a calculator block sets the mole flow depending on the specified current density). The pressurised syngas is brought up to the preheat temperature in the block ‘FUELHEAT’ and its exit stream enters the ‘EJECTOR’ block, where it is mixed with the recycled depleted fuel (stream 8). The blocks ‘COOLER1’ and ‘PREREFOR’ represent the stack pre-reformers. The purpose of ‘COOLER1’ is to set the pre-reforming temperature. It is calculated by means of a design specification block, which

varies the temperature of 'COOLER1' until the net heat duty of 'PREREFOR' equals zero (i.e. adiabatic). As a result, the gas is cooled simulating the endothermicity of the steam reforming process. Steam reforming (for CH_4 and higher hydrocarbons) and CO-shift reactions (Eq. 3.20 and 3.9), assumed to reach equilibrium at the pre-reforming temperature, were specified in the 'PREREFOR' block.

The pre-reformed fuel (stream 6) is fed to the 'ANODE' block, where the remaining CH_4 is reformed, CO is shifted and H_2 is oxidised. The transfer of ions cannot be modelled in Aspen Plus; therefore, the overall reaction (Eq. 3.8) instead of the cell half reactions (Eq. 3.15 and 3.16) was used in the model. Equations 3.8, 3.9 and 3.20 were specified in the 'ANODE' block and it was assumed that they reach equilibrium at the block temperature (SOFC operating temperature T_{op} = 910 °C). The stream 'AIR' is fed to the 'COMP2' block, the air compressor and its discharge pressure was set to P_{SOFC}. The air stream composition, temperature and pressure were entered. The molar flow rate is set using a design specification block that varies the air flow until the air utilisation factor (U_a) equals 16.7% [7]. The compressed air is brought up to the air preheat temperature in the block 'AIRHEAT' and its exit stream enters 'HEATX1' where it is preheated further by the hot combustion plenum products. The compressed and preheated air (stream 15) enters the 'CATHODE' block, whose function is to separate out the O_2 required for the electrochemical reaction ($nO_{2,consumed}$). The 'CATHODE' block O_2 split fraction ($O_{2,split}$) is set by a calculator block using the following equations:

$$nH_{2,in} = nH_{2,syngas} + 1\left(nCO_{syngas}\right) + 4\left(nCH_{4,syngas}\right) + \ldots \quad \text{Eq. 5.1}$$

$$U_f = \frac{nH_{2,consumed}}{nH_{2,in}} \quad \text{Eq. 5.2}$$

$$nO_{2,consumed} = 0.5nH_{2,consumed}$$ Eq. 5.3

$$O_{2,split} = \frac{nO_{2,consumed}}{nO_{2,in}}$$ Eq. 5.4

$nH_{2,in}$ is calculated, where $nH_{2,syngas}$ is the molar flow rate of H_2 contained in 'SYN-GAS'; 1(nCO_{syngas}) is the molar flow rate of H_2 that could be produced from the CO in 'SYN-GAS'; 4($nCH_{4,syngas}$) is the molar flow rate of H_2 that could be produced from the CH_4 in 'SYN-GAS' and the same applies to the higher hydrocarbons. Next $nH_{2,consumed}$ is determined with known fuel utilisation factor (U_f), a typical value being 0.85 [162]. $nO_{2,consumed}$ is then found using Eq. 5.3 and finally $O_{2,split}$ is calculated using Eq. 5.4. It is worth noting that $O_{2,split}$ is equivalent to U_a. The required O_2 is directed to the 'ANODE' block (stream 16). The temperature of the depleted air (stream 17) must be increased to T_{op}. The heat needed to do this is supplied by the electrochemical reaction and this process was simulated by taking a heat stream (Q3) from 'HEATER2' to 'ANODE'. The temperature of the 'HEATER2' block was specified as 910 °C (i.e. T_{op}). The depleted fuel (stream 7) enters the block 'SPLIT', whose function is to split the stream into a recycle (stream 8) and a stream directed to the combustion plenum. The split fraction of the block is set using a design specification block where it is determined by a specified steam to carbon ratio (STCR), defined as the molar ratio of steam to combustible carbon [293], a typical value being 2.5 [195-197]. Excess steam inhibits carbon deposition (see section 3.5.2). The depleted fuel and oxidant are fed to 'POSTCOMB' where complete combustion of the remaining fuel occurs. The heat generated by the combustion reactions is represented by the heat stream Q5, which is fed to the block 'HEATER1', whose function is to calculate and set the combustion products temperature. Finally, the high temperature combustion products (stream 11)

serve to preheat the incoming air in the 'HEATX1' block. The temperature of the SOFC stack exhaust (stream 12) is also determined.

Voltage calculation

The voltage was calculated by first applying the Nernst equation (Eq. 5.5) to determine the Nernst voltage (V_N) and then subtracting the various losses, including ohmic, activation and concentration losses.

$$V_N = -\frac{\Delta\bar{g}_f}{2 \cdot F} + \frac{R_g \cdot T_{avg}}{2 \cdot F} \ln \frac{P_{H_2} \cdot P_{O_2}{}^{0.5}}{P_{H_2O}} \qquad \text{Eq. 5.5}$$

where $\Delta\bar{g}_f$ is the molar Gibbs free energy of formation (J/mol) at standard pressure (1 bar), 2 represents the number of moles of electrons produced per mole of H_2 fuel reacted, F is the Faraday constant (96,485 C/mol), T_{avg} is the average temperature between the SOFC inlet and outlet streams (K), R_g is the universal gas constant (8.314 J/mol K) and P_i is the partial pressure (in bar) of gaseous component i. For a description of how $\Delta\bar{g}_f$ is calculated, refer to Appendix C. The partial pressures were taken as average values of the anode and cathode inlet and outlet streams. The gas composition changes along the length of the SOFC anode and cathode and thus the Nernst voltage and current vary with axial direction [11]; the 0-D model predicts the outlet gas composition, hence the reason for using the average partial pressure values.

The ohmic loss, which is the voltage loss due to the resistance to electron flow through both electrodes and the interconnection and the resistance to ion flow through the electrolyte, was calculated using Eq. 5.6-5.9. These equations developed by Song et al. [247] take into account realistic electron/ion paths in a tubular SOFC and they have been used in many studies to simulate the ohmic loss for SPGI tubular SOFC systems

[6, 294, 295]. They assumed uniform current density in the circumferential direction and uniform ionic flux in the electrolyte in the radial direction.

Anode: $$V_{Ohm\_A} = \frac{j \cdot \rho_A (A \cdot \pi \cdot D_m)^2}{8 \cdot t_A}$$ Eq. 5.6

Cathode: $$V_{Ohm\_C} = \frac{j \cdot \rho_C (\pi \cdot D_m)^2}{8 \cdot t_C} \cdot A[A + 2(1 - A - B)]$$ Eq. 5.7

Electrolyte: $$V_{Ohm\_E} = j \cdot \rho_E \cdot t_E$$ Eq. 5.8

Interconnection: $$V_{Ohm\_Int} = j \cdot \rho_{Int} (\pi \cdot D_m) \frac{t_{Int}}{w_{Int}}$$ Eq. 5.9

The angle related to the extent of electrical contact is $A\pi$ radians while the angle $B\pi$ radians is related to the interconnection. The resistivity terms (ρ_A, ρ_C, ρ_E and ρ_{Int}) were determined using the temperature dependent relations proposed by Bessette et al. [244], given in Table 5.2. Other terms that appear in Eq. 5.6-5.9 include j the current density (A/m^2), D_m the mean diameter of a cell (m), calculated from the geometry parameters given in Table 5.2, the cell component thickness t (m) and the interconnection width w_{Int} (m). The ohmic loss is especially important for tubular SOFCs as it is the dominant loss due to long current flow paths (see Figure 3.13).

The activation loss due to slow or sluggish kinetics of the electrochemical reaction taking place on the electrodes was determined using the semi-empirical correlations proposed by Achenbach [297], Eq. 5.10 and 5.11. It is the voltage lost as a result of the energy barrier that must be overcome by the reacting species.

Anode: $$\frac{1}{R_{Act\_A}} = \frac{2 \cdot F}{R_g \cdot T_{op}} \cdot k_A \left(\frac{P_{H_2}}{P^0} \right)^m \exp\left(\frac{-E_A}{R_g \cdot T_{op}} \right)$$ Eq. 5.10

Cathode: $$\frac{1}{R_{Act\_C}} = \frac{4 \cdot F}{R_g \cdot T_{op}} \cdot k_C \left(\frac{P_{O_2}}{P^0} \right)^m \exp\left(\frac{-E_C}{R_g \cdot T_{op}} \right)$$ Eq. 5.11

The R_{Act} terms represent specific resistance (Ω m^2) at both anode and cathode. The activation voltage loss V_{Act} was evaluated by multiplying the specific resistance terms by j (A/m^2). The pre-exponential factors k_A and k_C are listed in Table 5.2. The partial pressures P_i (bar) were taken as average values of the anode and cathode inlet and outlet streams (0-D model). P^0 is a reference pressure and was taken as 1 bar; the influence of partial pressure is accounted for by the slope m. The E terms are activation energies and are listed in Table 5.2. The activation voltage loss is less significant in SOFCs compared to other fuel cells due to the high operating temperature.

Table 5.2 SOFC stack model input parameters

Geometry [167, 172, 240, 296]	
Cell length / diameter (m)	1.5 / 0.022
Anode thickness t_A (m)	0.0001
Cathode thickness t_C (m)	0.0022
Electrolyte thickness t_E (m)	0.00004
Interconnection thickness t_{Int} (m)	0.000085
Interconnection width w_{Int} (m)	0.009
Material properties	
Anode resistivity ρ_A (Ω m) [244]	$2.98\times10^{-5}\exp(-1392/T_{op})$
Cathode resistivity ρ_C (Ω m) [244]	$8.114\times10^{-5}\exp(600/T_{op})$
Electrolyte resistivity ρ_E (Ω m) [244]	$2.94\times10^{-5}\exp(10350/T_{op})$
Interconnection resistivity ρ_{Int} (Ω m) [240]	0.025
Ohmic loss [247]	
A / B	0.804 / 0.13
Activation loss [292, 297]	
Pre-exponential factor k_A / k_C (A/m^2)	2.13×10^{8} / 1.49×10^{10}
Slope m	0.25
Activation energy E_A / E_C (J/mol)	110000 / 160000
Concentration loss	
Electrode pore radius r (m) [298]	5×10^{-7}
Electrode porosity ε / tortuosity ξ [241]	0.5 / 5.9

The concentration loss due to mass transfer limitations in the porous electrodes was modelled using Eq. 5.12 and 5.13 for anode and cathode respectively [298].

$$V_{Conc\_A} = -\frac{R_g \cdot T_{op}}{2 \cdot F} \ln\left[\frac{1-\left(R_g \cdot T_{op}/2 \cdot F\right)\left(t_A / D_{An(eff)} \cdot y^0{}_{H_2} \cdot P_{SOFC}\right) j}{1+\left(R_g \cdot T_{op}/2 \cdot F\right)\left(t_A / D_{An(eff)} \cdot y^0{}_{H_2O} \cdot P_{SOFC}\right) j}\right] \quad \text{Eq. 5.12}$$

$$V_{Conc\_C} = -\frac{R_g \cdot T_{op}}{4 \cdot F} \ln\left\{\frac{\left(P_{SOFC}/\delta_{O_2}\right) - \left[\left(P_{SOFC}/\delta_{O_2}\right) - y^0{}_{O_2} \cdot P_{SOFC}\right] \exp\left[\left(R_g \cdot T_{op}/4 \cdot F\right)\left(\delta_{O_2} \cdot t_C / D_{Cat(eff)} \cdot P_{SOFC}\right) j\right]}{y^0{}_{O_2} \cdot P_{SOFC}}\right\} \quad \text{Eq. 5.13}$$

The $y^0{}_i$ terms are gas molar fractions in the bulk flow, taken as average values of the anode and cathode inlet and outlet streams. The only other terms that have not yet been explained are the diffusion coefficient (D) terms and the constant δ_{O2}. The calculation of these terms will now be explained.

Diffusion transport in the electrodes (gases in pores) was considered. Equations 5.12 and 5.13 were derived using Fick's law of diffusion and both ordinary and Knudsen diffusion were considered. Ordinary diffusion occurs when the pore diameter of the material is large in comparison to the mean free path of the gas molecules, whereas Knudsen diffusion occurs when the pores are small. Both types of diffusion were accounted for by calculating effective diffusion coefficients for the anode and cathode. The following equations were used to determine the Knudsen diffusion and effective Knudsen diffusion coefficients for the anode and cathode gases [298]:

$$D_{K,i} = 97r\left(T_{op}/M_i\right)^{0.5} \quad \text{Eq. 5.14}$$

$$D_{K,i(eff)} = D_{K,i}\left(\varepsilon/\xi\right) \quad \text{Eq. 5.15}$$

where subscript i represents the gaseous component (H_2, H_2O, O_2 or N_2), r is the electrode pore radius (m) given in Table 5.2, M_i is the molecular weight (kg/kmol) of the gaseous component, ε is porosity and ξ is tortuosity of the electrodes (Table 5.2).

The most common method for theoretical estimation of ordinary binary diffusion coefficients is the one developed independently by Chapman and Enskog [299]. Todd and Young [300] investigated the performance of four widely used ordinary binary diffusion coefficient estimation techniques, the Chapman-Enskog and Fuller et al. [301] methods among them. From comparing predictions with available experimental data they concluded that the Fuller et al. [301] method, which is by far the simplest, performs best with an estimated mean error of 5%. Based on these findings the Fuller et al. method (Eq. 5.16) was used to calculate the ordinary binary diffusion coefficient for both anode and cathode [301].

$$D_{ik} = \frac{1\times10^{-7} T_{op}^{1.75}\left(1/M_i + 1/M_k\right)^{1/2}}{P\left(v_i^{1/3} + v_k^{1/3}\right)^2} \qquad \text{Eq. 5.16}$$

where subscripts *i* and *k* represent the gaseous components that make up the binary gas mixture (H_2-H_2O at the anode and O_2-N_2 at the cathode), *P* is pressure in atmospheres and *v* is the Fuller diffusion volume, taken as 7.07, 12.7, 16.6 and 17.9 for H_2, H_2O, O_2 and N_2 respectively [301]. Similar to the case of Knudsen diffusion, the effective ordinary diffusion coefficient is given by Eq. 5.17. The overall effective diffusion coefficient for each gas was then calculated using Eq. 5.18 [298].

$$D_{ik(eff)} = D_{ik}\left(\varepsilon/\xi\right) \qquad \text{Eq. 5.17}$$

$$1/D_{i(eff)} = 1/D_{ik(eff)} + 1/D_{K,i(eff)} \qquad \text{Eq. 5.18}$$

Finally, the anode and cathode diffusion coefficients were calculated using Eq. 5.19 and 5.20 and δ_{O2} in Eq. 5.13 was found using Eq. 5.21 [298].

$$D_{An(eff)} = \left(\frac{y^0{}_{H_2O} \cdot P_{SOFC}}{P_{SOFC}} \right) D_{H_2(eff)} + \left(\frac{y^0{}_{H_2} \cdot P_{SOFC}}{P_{SOFC}} \right) D_{H_2O(eff)} \quad \text{Eq. 5.19}$$

$$D_{Cat(eff)} = D_{O_2(eff)} \quad \text{Eq. 5.20}$$

$$\delta_{O_2} = \frac{D_{K,O_2(eff)}}{\left(D_{K,O_2(eff)} + D_{O_2-N_2(eff)} \right)} \quad \text{Eq. 5.21}$$

The concentration loss is low unless the current density is high and the fuel and air concentrations are low, caused by high utilisations (U_f and U_a). Under these conditions the limiting current may be reached reducing the voltage to very low levels.

The actual cell voltage V was calculated using Eq. 5.22, which is simply the Nernst voltage less the sum of the voltage losses.

$$V = V_N - \left(V_{Ohm} + V_{Act} + V_{Conc} \right) \quad \text{Eq. 5.22}$$

The calculations described in this section are carried out using a design specification block, which varies the input fuel flow until the SOFC stack DC power (DC Power = Cell Voltage × Current) equals a specified value (base case: 120 kW). However, for known current (I), as was the case for the current density sensitivity analysis (section 5.2.3), a calculator block determines and sets the input fuel flow using [4, 232]:

$$nH_{2,in} = \frac{I}{2FU_f} \quad \text{Eq. 5.23}$$

$$nFuel_{in} = \frac{nH_{2,in}}{yH_2 + yCO + 4yCH_4 + \ldots} \quad \text{Eq. 5.24}$$

where $nFuel_{in}$ is the input fuel flow (kmol/s) and y_i is the molar fraction of gaseous component i in the input fuel. The voltage and DC power are then calculated.

The Fortran code written to carry out all the calculations described in this section and for determining plant performance of the combined systems (section 5.3) is supplied in Appendix D.

5.2.2 Model Validation

Validation: fuel number one

The model was validated against published data for the SPGI 100 kW CHP SOFC stack operating on natural gas. The model inputs were as follows [231, 232]:

- Natural gas composition (mole fraction): CH_4 0.813, C_2H_6 0.029, C_3H_8 0.004, C_4H_{10} 0.002, N_2 0.143, CO_2 0.009.
- Operating pressure (P_{SOFC}) / ejector pressure ratio: 109,431 Pa / 3.
- Active area: 96.0768 m^2 (1,152 cells).
- Operating / electrodes exhaust temperature (T_{op}): 910 °C.
- Input air / fuel temperature: 630 / 200 °C.
- U_f / U_a / STCR: 0.85 / 0.19 / 1.8.
- Cold and hot stream temperature difference (recuperator 'HEATX1'): 10 °C.
- DC power: 120 kW.
- DC to AC inverter efficiency: 92%.

As seen in Table 5.3, the model results are in good agreement with published work. There is only a slight difference for voltage, current density and efficiency. Zhang et al. [232] used a very different method for calculating the voltage to the one applied in this work. They used semi-empirical correlations developed using a reference polarisation curve (refer to section 3.6.2). Campanari reports a voltage and current

density of 690 mV and 180 mA/cm^2 and a net AC efficiency of 48.5% (LHV basis) [231]. These results compare well with this work. The gross and net SOFC AC efficiencies (LHV basis) are defined as:

$$\eta_{SOFC,gross} = \frac{P_{el,AC}}{nFuel_{in} \cdot LHV_{fuel}} \quad \text{Eq. 5.25}$$

$$\eta_{SOFC,net} = \frac{P_{el,AC} - P_{comp}}{nFuel_{in} \cdot LHV_{fuel}} \quad \text{Eq. 5.26}$$

where $P_{el,AC}$ is the AC power (kW), $nFuel_{in}$ is the molar flow rate of input fuel (kmol/s), LHV_{fuel} is the lower heating value of the input fuel (kJ/kmol) and P_{comp} is the electrical power requirement of the fuel and air compressors (kW).

Table 5.3 SOFC stack model results compared to literature (validation: fuel number one)

	Literature [232]	**Model results**
Voltage (mV)	700	683
Current density (mA/cm^2)	178	182.86
Pre-reforming temperature (K)	809.15	808.25
Pre-reformer CH_4 conversion (%)	25.9	25
Cathode inlet temperature (K)	1094.47	1096.85
Combustion products temperature (K)	1285.5	1285.45
Stack exhaust temperature (K)	1107	1106.85
Anode inlet gas composition (mole %)	H_2 27, CO 5.6, CH_4 10.1, H_2O 27.9, CO_2 23.1, N_2 6.2	H_2 26.9, CO 5.6, CH_4 10.4, H_2O 27.8, CO_2 23.1, N_2 6.2
Anode exhaust gas composition (mole %)	H_2 11.6, CO 7.4, H_2O 50.9, CO_2 24.9, N_2 5.1	H_2 11.6, CO 7.4, H_2O 50.9, CO_2 24.9, N_2 5.1
Cathode exhaust gas composition (mole %)	O_2 17.7, N_2 82.3	O_2 17.7, N_2 82.3
Stack exhaust gas composition (mole %)	H_2O 4.5, CO_2 2.3, O_2 15.9, N_2 77.3	H_2O 4.5, CO_2 2.3, O_2 15.9, N_2 77.3
Gross AC efficiency (LHV) (%)	52	51.28
Net AC efficiency (LHV) (%)	nr[a]	49.15

[a] nr = not reported.

Validation: fuel number two

A second validation of the model was conducted using published data for the SPGI 100 kW CHP SOFC stack operating on natural gas of different composition and with the stack operating at different conditions compared to the first validation. The model inputs for this validation run were as follows [231, 232, 236, 242]:

- Natural gas composition (mass fraction): CH_4 0.938, N_2 0.038, CO_2 0.024.
- Operating pressure (P_{SOFC}) / ejector pressure ratio: 109,431 Pa / 3.
- Active area: 96.0768 m^2 (1,152 cells).
- Operating / electrodes exhaust temperature (T_{op}): 920 °C.
- Input air / fuel temperature: 20 / 200 °C.
- U_f / U_a / STCR: 0.85 / 0.2 / 2.
- DC power: 127.4 kW.
- DC to AC inverter efficiency: 92%.

The temperature and gas composition data (Table 5.4) utilised for the second validation were obtained using a 1-D model, which was validated against experiments carried out on a SPGI 100 kW CHP SOFC stack in Torino, Italy [242]. The Aspen Plus model predictions are in good agreement with the literature data. The largest discrepancies exist for the combustion products temperature and the stack exhaust temperature. Both of these temperatures were taken from the model predictions reported in Verda and Quaglia [242]. The actual experimental temperatures presented in that article match this works model predictions more closely. The measured average combustion products temperature and stack exhaust temperature were 1,297 and 519 K respectively, which compare very well with this work.

Table 5.4 SOFC stack model results compared to literature (validation: fuel number two)

	Literature [236, 242]	**Model results**
Voltage (mV)	661	662.8
Current density (mA/cm^2)	200.6[a]	200.62
Pre-reforming temperature (K)	851.15	815.35
Pre-reformer CH_4 conversion (%)	40	35
Cathode inlet temperature (K)	1155.15	1155.15
Combustion products temperature (K)	1374.15	1299.65
Stack exhaust temperature (K)[b]	552.15	512.85
Anode inlet gas composition (mass %)	H_2 3.16, CO 11.2, CH_4 5.81, H_2O 27.3, CO_2 51.29, N_2 1.24	H_2 2.9, CO 8.3, CH_4 7.4, H_2O 27.4, CO_2 52.8, N_2 1.3
Anode exhaust gas composition (mass %)	H_2 1.39, CO 11.91, H_2O 39.88, CO_2 45.88, N_2 0.94	H_2 1.0, CO 9.2, H_2O 41.2, CO_2 47.7, N_2 0.9
Cathode exhaust gas composition (mass %)	nr[c]	O_2 19.6, N_2 80.4
Stack exhaust gas composition (mass %)	H_2O 3.14, CO_2 3.87, O_2 17.38, N_2 75.62	H_2O 3.0, CO_2 3.7, O_2 17.6, N_2 75.7
Gross AC efficiency (LHV) (%)	48[d]	49.8
Net AC efficiency (LHV) (%)	nr	47.8

[a] Calculated assuming an active area of 96.0768 m^2.

[b] Stack exhaust temperature after preheating cathode air to high level (1155.15 K).

[c] nr = not reported.

[d] Calculated using Eq. 5.25.

5.2.3 Sensitivity Analyses Results and Discussion

The validated model was run using the following syngas composition for wood gasification: 45.8% H_2, 21.6% CO, 10.0% CH_4, 21.2% CO_2, 1.4% N_2 (vol. % db) and 25.7% H_2O (vol. % wb) [5]. This syngas composition is typical of the Güssing FICFB gasifier. Numerous experiments have been carried out at TU Delft using a pilot scale CFB gasifier. The following reported syngas composition for miscanthus gasification has been used in this work: 13.65% H_2, 21.6% CO, 7.5% CH_4, 2.0% C_2H_y, 35.25% CO_2, 13.0% N_2 (vol. % db) [70] and 40% H_2O (vol. % wb) [302]. This miscanthus syngas was produced using a steam-O_2 mixture as fluidising agent. In order to bring the syngas molar composition to 100% the difference was added to N_2 (7%) as it is inert

and because its content was approximated due to measurement difficulties during the experiments [302].

The model inputs were kept the same as described in sections 5.2.1 and 5.2.2 with the following exceptions: fuel gas composition (wood and miscanthus syngas compositions given above); T_{op} = 910 °C; input air temperature = 630 °C; input fuel temperature = 300 °C; U_a = 16.7% and STCR = 2.5. The elevated input fuel and air temperatures are realistic. Syngas would exit a gasifier at ~800 °C; however, its temperature at the entrance to the SOFC stack would depend on the gas cleaning system employed. Warm gas cleaning systems typically operate at a temperature of ~300 °C. The high input air temperature, which is the temperature after the initial preheating step (block 'AIRHEAT' Figure 5.1), is achieved by utilising the stack exhaust (~830 °C).

Comparing operation on wood syngas to natural gas operation (see Table 5.3) at current density = 182.86 mA/cm^2, voltage decreased by 14 mV to 669 mV, DC power dropped 2.43 kW to 117.57 kW and the gross and net SOFC AC efficiency reduced 8.28 and 11.63 percentage points (pp) to 43% and 37.52% respectively. For miscanthus syngas gross and net SOFC AC efficiency reduced 9.63 and 15.9 pp to 41.65% and 33.25% respectively. The relatively large drop in efficiency is attributed to increased input fuel and air flow, which is due to the lower quality of the fuel gas and also decreased electrical power output. For a DC power output of 120 kW the SOFC stack performance on wood syngas was as follows: current density = 188.7 mA/cm^2, cell voltage = 662 mV, $\eta_{SOFC,gross}$ = 42.53% and $\eta_{SOFC,net}$ = 37.04%. These have been identified as realistic design operating conditions with regard to stack performance for operation on wood syngas.

Sensitivity analyses were performed in order to give insight into the influence of the main operating parameters on the system and to investigate off design performance.

The effects of varying current density, STCR, U_f and U_a on SOFC stack performance for both wood and miscanthus syngas fuels were investigated. The model input data was kept the same as presented above with a single parameter varied at any given time.

Current density

Figure 5.2 (a) and (b) displays the voltage characteristics of a single tubular SOFC fed with wood syngas and miscanthus syngas respectively. The predicted voltage characteristics are consistent with well-known phenomena for tubular SOFCs: Nernst voltage = ~0.9 V; ohmic loss is dominant; activation loss is less significant in SOFCs due to high temperature; concentration loss is the least significant but increases rapidly at high current density. Voltage characteristics were found to be better for wood than miscanthus due to greater voltage losses in the miscanthus case. For example, at a typical current density of 190 mA/cm^2 the cell voltage for wood syngas is 0.66 V and for miscanthus syngas it is lower at 0.637 V.

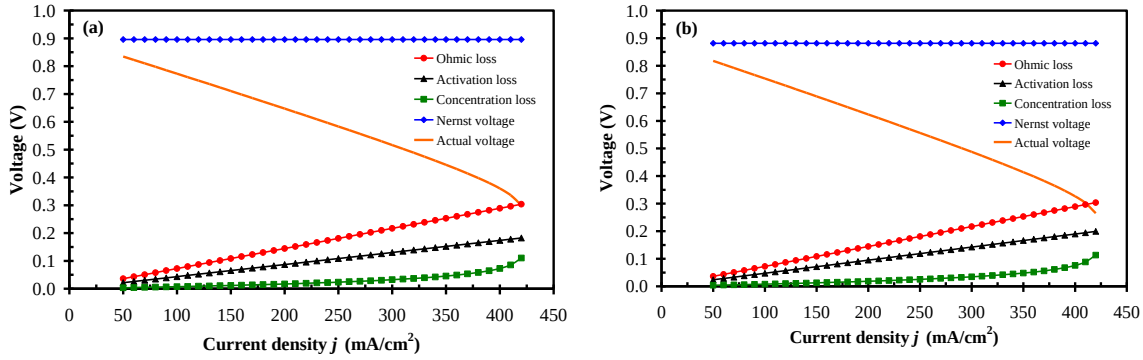

Figure 5.2 SOFC voltage characteristics versus current density for (a) wood syngas and (b) miscanthus syngas

From Figure 5.3 it is evident that current density j has significant influence on the system for both fuels. Increasing j lowers both voltage and efficiency but increases

power. Voltage is reduced as a result of increased losses as shown in Figure 5.2. Efficiency drops substantially (~35 pp for both fuels) due to higher parasitic power and energy input. Power increases to a maximum and then decreases. Fuel cells are usually operated to the left of this peak power. It is desirable with regard to operating costs, to operate the stack at high voltage and efficiency; however, it is also desirable with regard to capital costs, to operate the stack at high power (less SOFCs needed). Therefore, there must be a trade-off between voltage, efficiency and power. These trends and the need for a compromise between efficiency and capital costs match results reported elsewhere [303]. The stack operates with better performance on wood syngas compared to miscanthus syngas. The miscanthus syngas fed to the stack had much lower H_2 and higher CO_2, H_2O and N_2 content than the wood syngas, which caused the reduction in performance. It also meant that a much higher fuel flow rate was required for the miscanthus case. The results for wood syngas over a typical operating j range of 180-200 mA/cm^2, indicate a cell voltage range of 673-648 mV, $\eta_{SOFC,gross}$ range of 43.2-41.6%, $\eta_{SOFC,net}$ range of 37.8-36.1% and an AC power range of 107-114.5 kW.

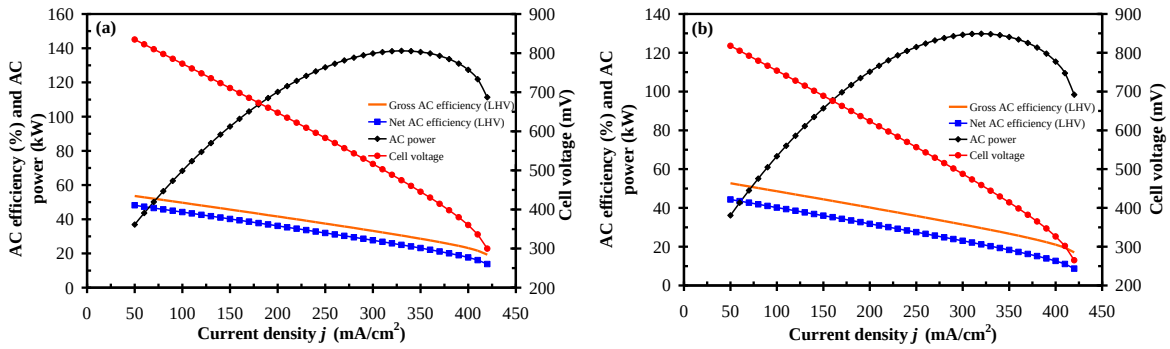

Figure 5.3 Effect of current density on voltage, power and efficiency for (a) wood syngas and (b) miscanthus syngas

Steam to carbon ratio

The effects of varying STCR are displayed in Figures 5.4 and 5.5. Only the results for the wood syngas case are displayed; the same trends were seen for miscanthus syngas. From Figure 5.4 (b) it can be seen that STCR has a substantial impact on the pre-reformer, the inlet temperature increases ~320 K over the STCR range for both fuels (wood and miscanthus) due to the recirculation of more high temperature depleted fuel. As a result the anode temperature rises and causes greater CH_4 conversion (0-92.2% and 0-97% for wood and miscanthus respectively). The high temperature and greater amount of steam available promotes the steam reforming of CH_4 via Eq. 3.10. This reaction is endothermic meaning the forward reaction is favoured as temperature increases. Increasing STCR has a negative impact on voltage and efficiency and increases current density; this is due to the change in anode temperature and gaseous component partial pressures, which decreases the Nernst voltage and increases the voltage losses. It is therefore desirable to operate the stack at low STCR. These results agree well with the literature [275, 303]. Figure 5.5 displays how STCR affects the pre-reformer outlet or anode inlet gas composition. Increasing STCR causes the mole fraction of H_2O and CO_2 to rise, this lowers the mole fraction of H_2 and CO negatively affecting stack performance. The CH_4 content decreases over the STCR range due to the high temperature and greater amount of steam available for reforming.

Considering these results, it is recommended to operate the SOFC stack at low STCR; however, it should be high enough to inhibit carbon deposition (section 3.5.2). Significant carbon deposition is expected for biomass gas at lower temperatures; therefore, steam addition is essential [304].

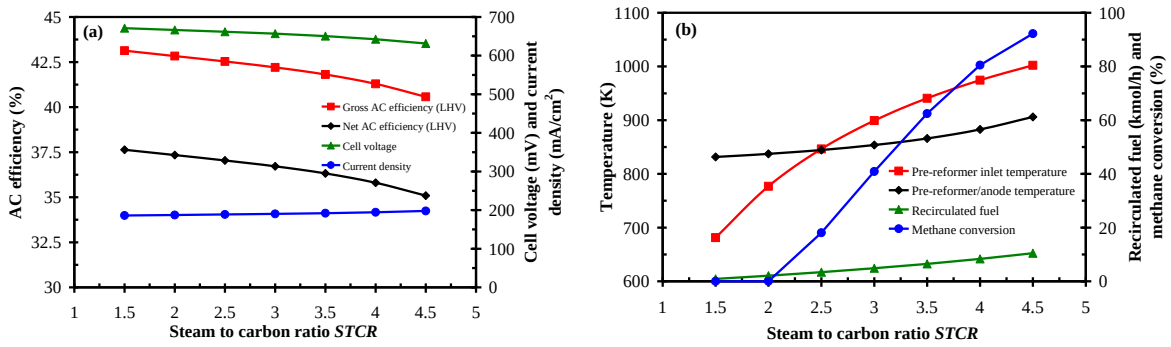

Figure 5.4 Effect of STCR for wood fuel on (a) voltage, efficiency and current density and (b) pre-reformer and recirculated fuel

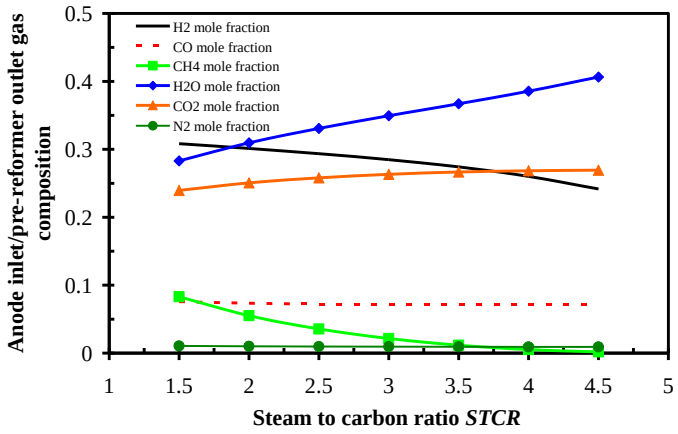

Figure 5.5 Effect of STCR for wood fuel on anode inlet/pre-reformer outlet gas composition

Fuel utilisation factor

The influence of U_f on SOFC stack performance is depicted in Figure 5.6. Only the results for wood fuel are displayed; the same trends were seen for miscanthus fuel. The cell voltage decreases with U_f due to increased voltage losses. The current density increases due to the higher amount of H_2 consumed on the anode (Eq. 5.23 re-arranged: $I = 2FnH_{2,consumed}$). The fuel flow rate required to achieve the desired power (120 kW DC) decreases with U_f. This is because more of the energy contained in the fuel is converted to electricity rather than heat due to the higher H_2 consumed by the

electrochemical reaction. Efficiency was found to be very sensitive to changes in U_f, $\eta_{SOFC,gross}$ and $\eta_{SOFC,net}$ increase by 18.6 and 17.96 pp respectively over the U_f range (a rise of ~17 pp was seen for miscanthus fuel). This is primarily due to the reduced fuel flow rate at high U_f. The decrease in cell voltage and strong influence on efficiency witnessed here is in good agreement with published work [303]. The amount of recirculated fuel decreases with U_f as less fuel needs to be recirculated to meet the specified STCR due to the increased H_2O content in the depleted fuel. As a result of less high temperature depleted fuel being recirculated the pre-reformer/anode temperature drops and thus the CH_4 conversion fraction is lowered. The cathode and stack exhaust temperatures are dependent on the combustion temperature, which is determined by the amount of fuel available to the combustion plenum. At low U_f more of the fuel is available for combustion therefore the temperatures are high and as U_f increases (more fuel energy converted to electricity as opposed to heat) the temperatures decrease. Considering these findings, it is recommended to operate the SOFC stack at high fuel utilisation but below the level where the concentration loss increases to a high degree.

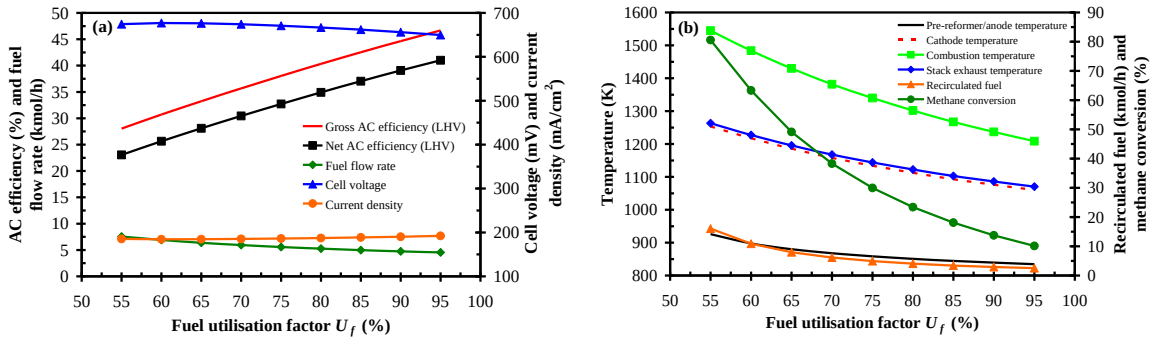

Figure 5.6 Effect of U_f for wood fuel on (a) voltage, efficiency, fuel flow and current density and (b) pre-reformer, stack temperatures and recirculated fuel

Air utilisation factor

The influence of U_a on the system for wood syngas is shown in Figure 5.7. The miscanthus results display the same trends but SOFC performance is lower (lower voltage and efficiency as discussed previously). The cell voltage and gross efficiency decrease with U_a and the current density increases. The influence of U_a is much less significant than that of U_f. The net efficiency rises and reaches a peak value at a U_a of ~20% and then decreases. For this reason SOFCs should be operated in the U_a range: 16 to 20%. As displayed in Figure 5.7 (b) the stack temperatures rise with U_a, the reason being that at high U_a less air is fed to the stack which means less N_2 and excess O_2 for cooling in the combustion plenum.

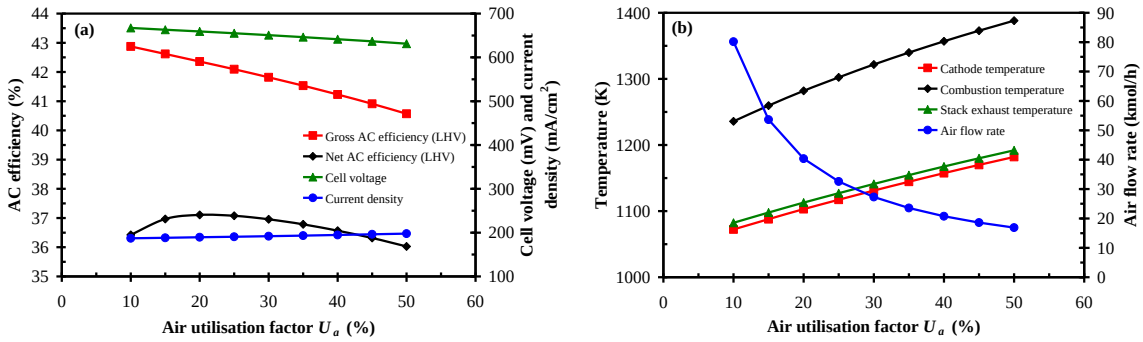

Figure 5.7 Effect of air utilisation factor for wood fuel on (a) voltage, efficiency and current density and (b) stack temperatures and input air flow

5.3 Combined System Models

The combined system models are presented in this section. The DFB gasifier model was integrated with the SOFC model (both described previously); syngas cleaning, heat recovery and balance of plant components were considered (BG-SOFC system). The main aim of this research work was to investigate the feasibility of BG-SOFC systems through thermodynamic modelling and economic analyses. The thermodynamic modelling side of this aim is described in this chapter.

Only the DFB gasifier model was integrated with the SOFC model as the CFB gasifier model produced a syngas that was not attractive for fuel cell applications. It has low energy content (half that of DFB gasifier syngas), high N_2 (forty times that of DFB gasifier syngas) and low H_2 content (over eight times lower). The SOFC model results (section 5.2.3) revealed that H_2, CO_2 and N_2 content affect SOFC performance. SOFC performance dropped significantly while operating on miscanthus syngas compared to wood syngas. The miscanthus syngas contained much lower H_2 and greater amounts of CO_2 and N_2 causing a drop in Nernst voltage and an increase in voltage losses. Comparing to CFB gasifier syngas, miscanthus gas has over twice the H_2 content and lower total inert gases (N_2 + CO_2). Considering these facts, operation on CFB gasifier syngas is not recommended.

5.3.1 Model Description

System 1

The system 1 (base case system) Aspen Plus flowsheet is displayed in Figure 5.8. The system comprises the FICFB gasifier, tubular SOFC stack, syngas cleaning equipment, heat recovery system (syngas cooler, steam generator, air preheaters, etc.) and balance of plant components (compressors, pumps, etc.).

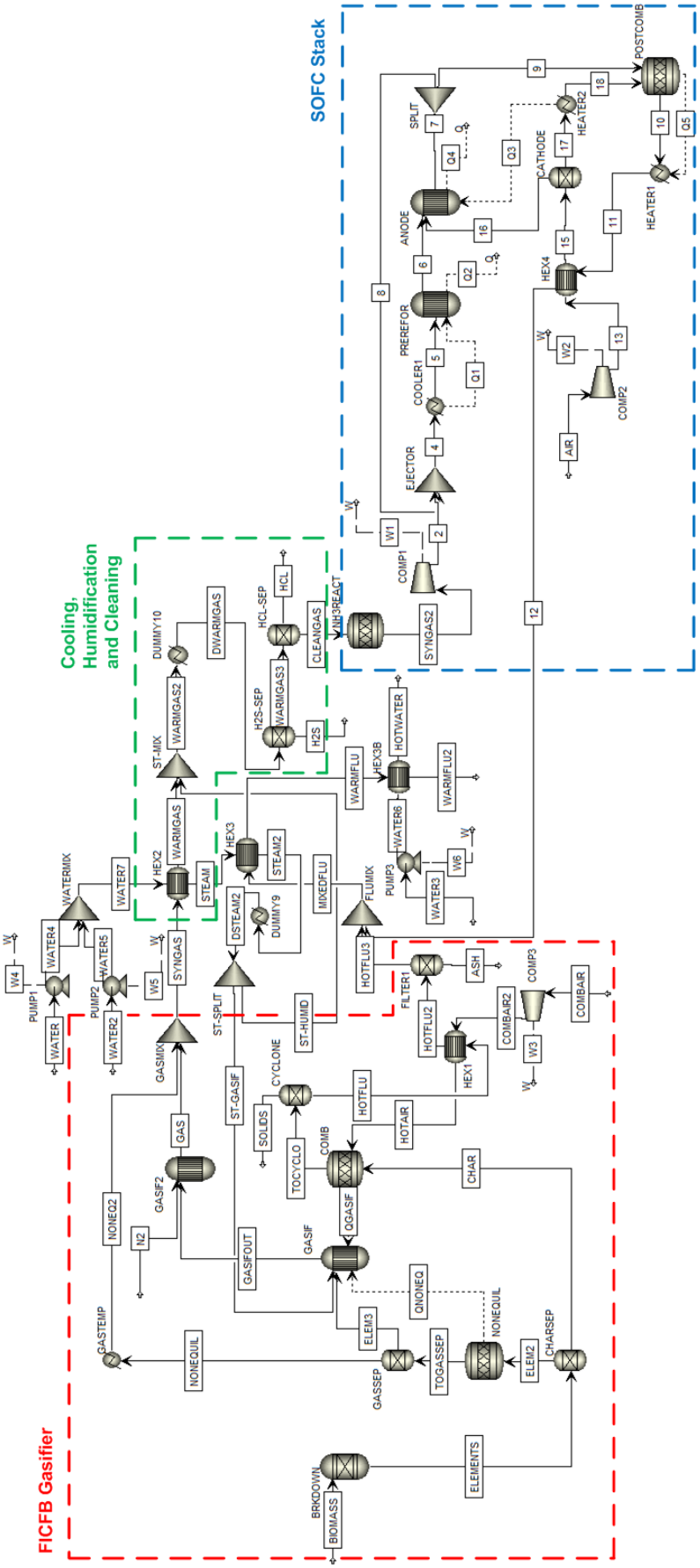

Figure 5.8 System 1 Aspen Plus flowsheet

From Figure 5.8, it is clear that the modelling approach to both the gasifier and the SOFC match the models presented earlier (sections 4.3 and 5.2). It was necessary to make some changes to the layout and model inputs and these will now be explained. The 'BIOMASS' stream mass flow rate is set by one of two ways depending on whether the current density *j* is variable (constant power output) or constant (variable power output). When *j* is variable a design specification block varies the biomass mass flow rate until the DC power equals the desired value (120 kW). Equations 5.1, 5.2 and 5.23 were employed to determine *j* (note: $j = I$ / Active area), after which the voltage and power were calculated (see Fortran code in Appendix D). This calculation sequence was repeated until the DC power was equal to the desired value. For specified *j* a design specification block utilises Eq. 5.23 and 5.24 to determine the syngas flow rate at the SOFC inlet ('SYNGAS2' stream) required to achieve that *j* value. The design specification block varies biomass mass flow rate until this *j* is achieved.

The stream 'COMBAIR' is fed to a Compr block titled 'COMP3', which compresses the combustion air to a pressure of 1.094 bar. All compressors ('COMP1', 'COMP2' and 'COMP3') were assumed to have mechanical and isentropic efficiencies of 95% and 75% respectively. The compressed combustion air enters the combustion air preheater; a HeatX block named 'HEX1'. All heat exchangers ('HEX1', 'HEX2', 'HEX3', 'HEX4' and 'HEX3B') were specified as countercurrent with the shortcut calculation option selected. The 'HEX1' cold stream outlet temperature was set at 450 °C, i.e. the combustion air preheat temperature T_a. The stream 'HOTAIR' is then fed to the CZ of the gasifier (block 'COMB') where char combustion takes place. The only difference here with the DFB model described previously is that the CZ temperature is assumed 70 °C above T_g (55 °C was assumed before). This elevated CZ temperature is still realistic as it falls within the range 40-70 °C reported in the literature [128]. It was

necessary to use this elevated CZ temperature to achieve a T_a of 450 °C by utilising the CZ flue gas at 920 °C in 'HEX1'.

The gasification steam temperature was lowered from 450 °C to 350 °C as it was not possible to heat the steam above 350 °C utilising the heat recovered from the syngas (syngas cooler 'HEX2') and the mixed flue gas (steam superheater 'HEX3'). The DFB gasifier model sensitivity analysis results (section 4.3.3) indicated that gasification steam temperature has little impact on gasifier performance; therefore, the lower temperature is of no great concern. As before, a design specification block is employed to calculate and set the mass flow rate of gasification steam using a STBR. In this model the stream 'WATER' mass flow rate is varied until the STBR equals 0.75.

The 'WATER2' stream mass flow rate is set by a design specification block and is dependent on the STCR required to prevent carbon deposition after syngas cooling and during cleaning. STCR was kept as low as possible at 1.85 due to the SOFC anode recycle, used for syngas preheating, which results in a much greater STCR at the SOFC inlet (SOFC STCR = 4.57). Sensitivity analysis results for the SOFC model (section 5.2.3) shows that SOFC performance drops with rising STCR so it should be kept as low as possible. The pressure of 'WATER' and 'WATER2' is increased to 5 bar using pumps; all pumps ('PUMP1', 'PUMP2' and 'PUMP3') were assumed to have a pump efficiency of 75%. The two streams are then mixed and pass through the syngas cooler where the mixed stream temperature is increased to the saturation temperature (dryness fraction = 65%) and the syngas temperature drops to ~408 °C. This syngas temperature was chosen because the operating temperature of the syngas cleaning equipment is 400 °C and syngas temperature decreases to this after humidification (Mixer block 'ST-MIX'). The saturated steam is superheated to 350 °C by the 'MIXEDFLU' stream in the block 'HEX3'. The mixed steam is split into gasification steam (directed to GZ of the

gasifier) and humidification steam (mixed with syngas to increase STCR to 1.85). This is accomplished using a calculator block that sets the block 'ST-SPLIT' split fraction ('WATER2' stream mass flow rate divided by the mixed water/steam mass flow rate).

The blocks 'PUMP3' and 'HEX3B' represent the district heating system, which was assumed to operate at 120 °C. 'WATER3' mass flow rate is varied until the flue gas is cooled to 130 °C. This gives an indication of the amount of hot water that could be produced. However, for system performance calculations the following equation was used to calculate the maximum recoverable heat (Q), i.e. the heat that could be recovered if the flue gas was cooled to standard temperature:

$$Q = \dot{m}_{flue} \cdot c_{p,flue} \cdot \Delta T \qquad \text{Eq. 5.27}$$

where $\dot{m}_{flue}$ is the flue gas mass flow rate (kg/s), $c_{p,flue}$ is the flue gas specific heat capacity (kJ/kg K) and ΔT is the flue gas temperature minus 25 °C.

The humidified syngas 'WARMGAS2' enters the cleaning system, which consists of H_2S and HCl removal steps. Some cleaning steps are omitted; e.g. the cyclone filter and sintered metal candle filter for particulates and alkali removal. These steps were not modelled as the model does not consider particulates or alkali. Refer to section 3.5.3 for a description of the entire syngas cleaning and reforming system. Warm gas cleaning technologies (operating at ~400 °C) were selected rather than simplistic well proven cold gas cleaning technologies (scrubbers, etc.) because a major advantage of biomass gasifier SOFC integration is that they operate at comparable temperatures and syngas cooling to low temperature would have considerable efficiency penalty. H_2S is removed using a ZnO bed. A value of 0.3 ppmv for H_2S after the ZnO bed has been assumed [121]. HCl content is lowered to 1 ppmv by means of a sodium carbonate bed [121,

168]. The ZnO and sodium carbonate beds were modelled as separators with the split fractions set using two design specification blocks that vary split fraction until H_2S and HCl concentrations equal 0.3 and 1 ppmv respectively in the 'CLEANGAS' stream. Tars were not considered in the model but it was assumed that they would not cause problems as the syngas temperature was maintained above the tar dew point temperature (150-350 °C) [11, 121, 305]. The tars would be catalytically reformed in the SOFC pre-reformers along with the lighter hydrocarbons. STCR must be high enough to prevent carbon deposition in the pre-reformers, SOFC anodes and other plant equipment. NH_3 was not removed as it is considered a fuel (see section 3.5). Conversion of NH_3 in a SOFC is a two stage process: decomposition into nitrogen and hydrogen followed by oxidation of hydrogen to water [201]. The first stage of this process was simulated in the 'NH3REACT' RStoic block, where the reverse NH_3 formation reaction (Eq. 3.11) was specified with 100% NH_3 conversion. The block temperature was set to the cleaning temperature (400 °C) using a calculator block. The second stage of the process occurs within the SOFC stack when the H_2 is converted on the anodes.

An anode recycle is employed to preheat the syngas prior to the SOFC pre-reformers. A design specification block varies the split fraction of the block 'SPLIT' until the temperature of stream 4 equals 800 °C.

The SOFC air mole flow rate (stream 'AIR') was calculated and set using a calculator block and a design specification block. The calculator block determines the O_2 consumed electrochemically ($nO_{2,consumed}$) using Eq. 5.1-5.3; it then sets the 'CATHODE' block O_2 split fraction using Eq. 5.4. The design specification block then varies the 'AIR' stream flow rate until the calculated 'CATHODE' block O_2 split fraction equals the desired U_a value of 16.7%. The cathode air preheat temperature is also 800 °C and it is heated by the combustion products (stream 11) in the HeatX block

'HEX4'. The SOFC stack exhaust stream 12 is then mixed with the CZ flue stream 'HOTFLU3' and serves to superheat steam and heat district heating water (discussed previously in this section).

System performance calculations are performed using the Fortran code given in Appendix D. The SOFC AC efficiency (LHV basis) is determined using Eq. 5.25 presented earlier for the standalone model. In Eq. 5.25 $nFuel_{in} \times LHV_{fuel}$ represents the 'SYNGAS2' stream power (kW). The plant net AC electrical efficiency (LHV basis) and plant net AC CHP efficiency (LHV basis) were calculated as follows:

$$\eta_{el,net} = \frac{P_{el,AC} - P_{parasitic}}{P_{biomass}} \qquad \text{Eq. 5.28}$$

$$\eta_{CHP,net} = \frac{\left(P_{el,AC} - P_{parasitic}\right) + Q}{P_{biomass}} \qquad \text{Eq. 5.29}$$

where $P_{el,AC}$ is AC power (kW) (i.e. DC power × 92%), $P_{parasitic}$ is the total parasitic power (kW) (includes all compressors, 'PUMP1' and 'PUMP2'), $P_{biomass}$ is biomass input power (kW) (i.e. 'BIOMASS' stream mass flow rate × biomass LHV given in Table 4.2) and Q is the maximum recoverable heat calculated using Eq. 5.27.

System 1 performance was lower than anticipated (see Table 5.5) with $\eta_{el,net}$ = 25.3% and $\eta_{CHP,net}$ = 69.53%. Alternative system layouts were investigated in an attempt to increase performance.

System 2

The standalone SOFC model (section 5.2) was run using system 1 conditions and it was discovered that the drop in SOFC performance was due to high SOFC STCR.

The anode recycle, employed for syngas preheating, was identified as the cause. As a result, system 2 with a cathode recycle instead of the anode recycle was investigated.

Only the SOFC stack portion of the Aspen Plus flowsheet is displayed in Figure 5.9; the rest of the flowsheet matches that of system 1 (Figure 5.8). In this system the 'SYNGAS2' stream is compressed to the SOFC stack pressure (1.094 bar) in the block 'COMP1'. The syngas is then preheated to 790 °C in the HeatX block 'HEX5'.

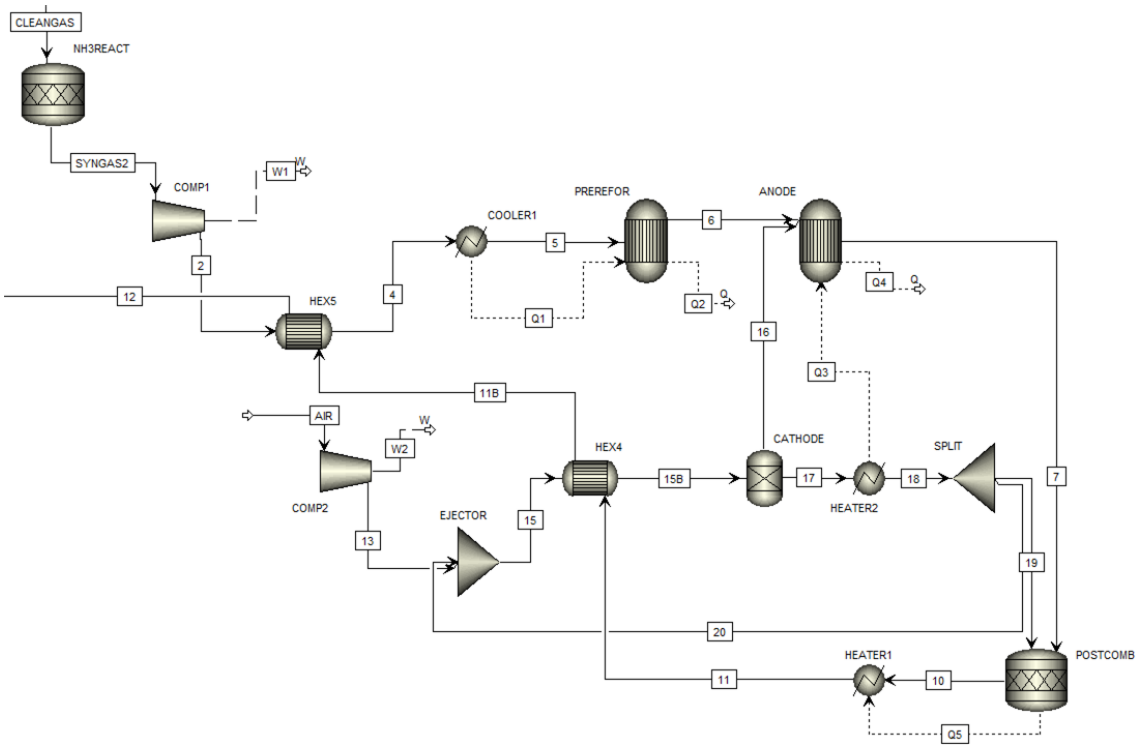

Figure 5.9 System 2 Aspen Plus flowsheet

The syngas preheat temperature is slightly lower than for system 1 as the hot stream (stream 11B) is below 800 °C. On the cathode side 'AIR' enters the 'COMP2' block where it is compressed to three times the SOFC stack pressure in order to drive the cathode recycle process. A design specification block controls the amount of cathode off-gas recycled by varying the split fraction of block 'SPLIT' until the stream 15 temperature = 670 °C. The cathode air temperature is brought up to 800 °C in the

'HEX4' block through heat exchange with the burner exhaust gas (stream 11). 'HEX4' was included in the system 2 model (instead of using the cathode recycle to raise the air temperature to 800 °C) as it simulates preheating of the cathode air in the feed tubes as they pass through the burner and this would still be part of the design even if the anode recycle were replaced by a cathode recycle (see Figure 3.14). All other aspects of the system 2 model match those of the system 1 model.

System 3

For system 3 the anode recycle was replaced with an electric heater for preheating the syngas before feeding to the SOFC stack. The recycle process was removed from the system. Again only the SOFC stack portion of the Aspen Plus flowsheet is displayed in Figure 5.10; the rest of the flowsheet matches that of system 1 (Figure 5.8).

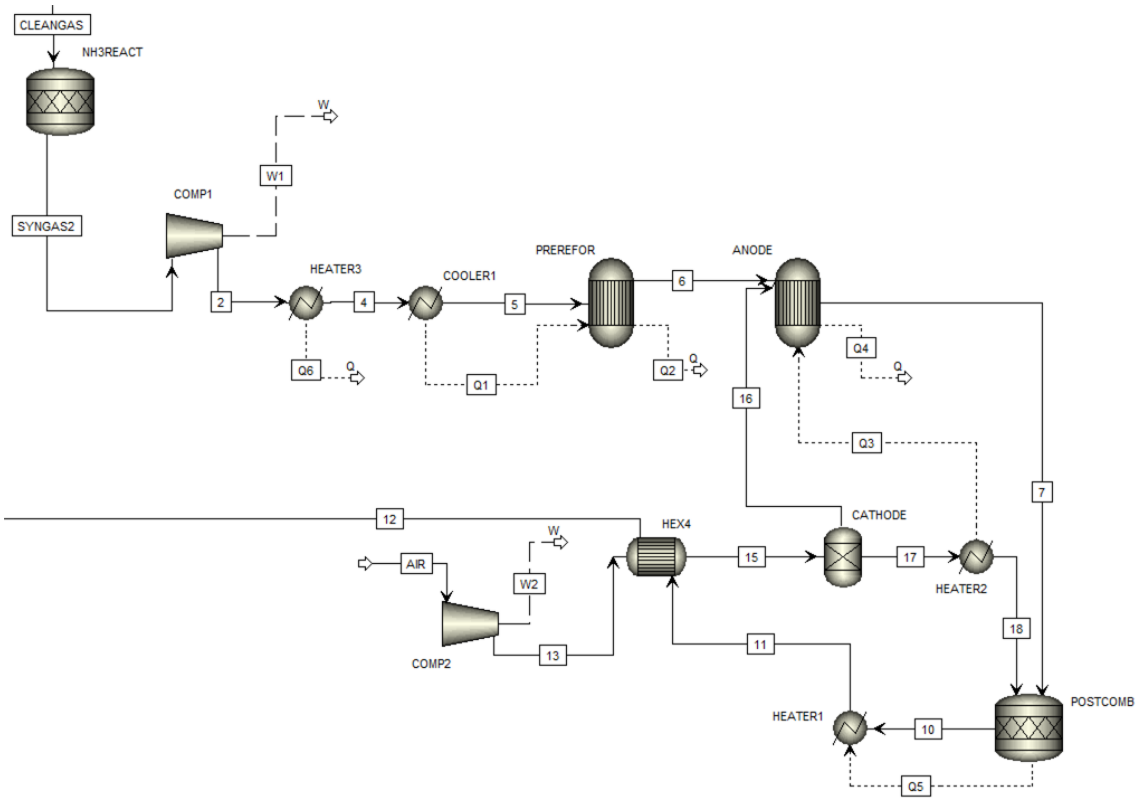

Figure 5.10 System 3 Aspen Plus flowsheet

The ‘SYNGAS2’ stream is fed to block ‘COMP1’ where the pressure of the fuel is raised to 1.094 bar. The syngas is preheated to the SOFC stack inlet temperature of 800 °C by means of an electric heater titled ‘HEATER3’. The power requirement of the electric heater was calculated ($\dot{m}\, c_p \Delta T$), which was subsequently included in the system performance calculations (parasitic power and net efficiencies). All other aspects of the system 3 model match those of the system 1 model.

System 4

Thermal integration of the biomass gasifier and SOFC stack was explored in system 4. The high temperature SOFC flue gas, which contains ~15 vol. % O_2, was split into two streams with one being fed directly to the gasifier CZ for char combustion.

With reference to Figure 5.11, all Aspen Plus unit operation blocks are identical to those of system 1 except for the inclusion of a splitter block ‘SPLIT2’ and the exclusion of the gasifier CZ air preheater ‘HEX1’. Thus there would be cost advantages to this system configuration. The gasifier will operate at lower efficiency compared to system 1 as the ‘OXIDANT’ stream temperature is 100 °C below the CZ air temperature of 450 °C for system 1. The split fraction of block ‘SPLIT2’ is set by a design specification block assuming a value of 8 kg/h for excess O_2 in the CZ exhaust (mean value over the SOFC current density range 100-420 mA/cm^2 for system 1).

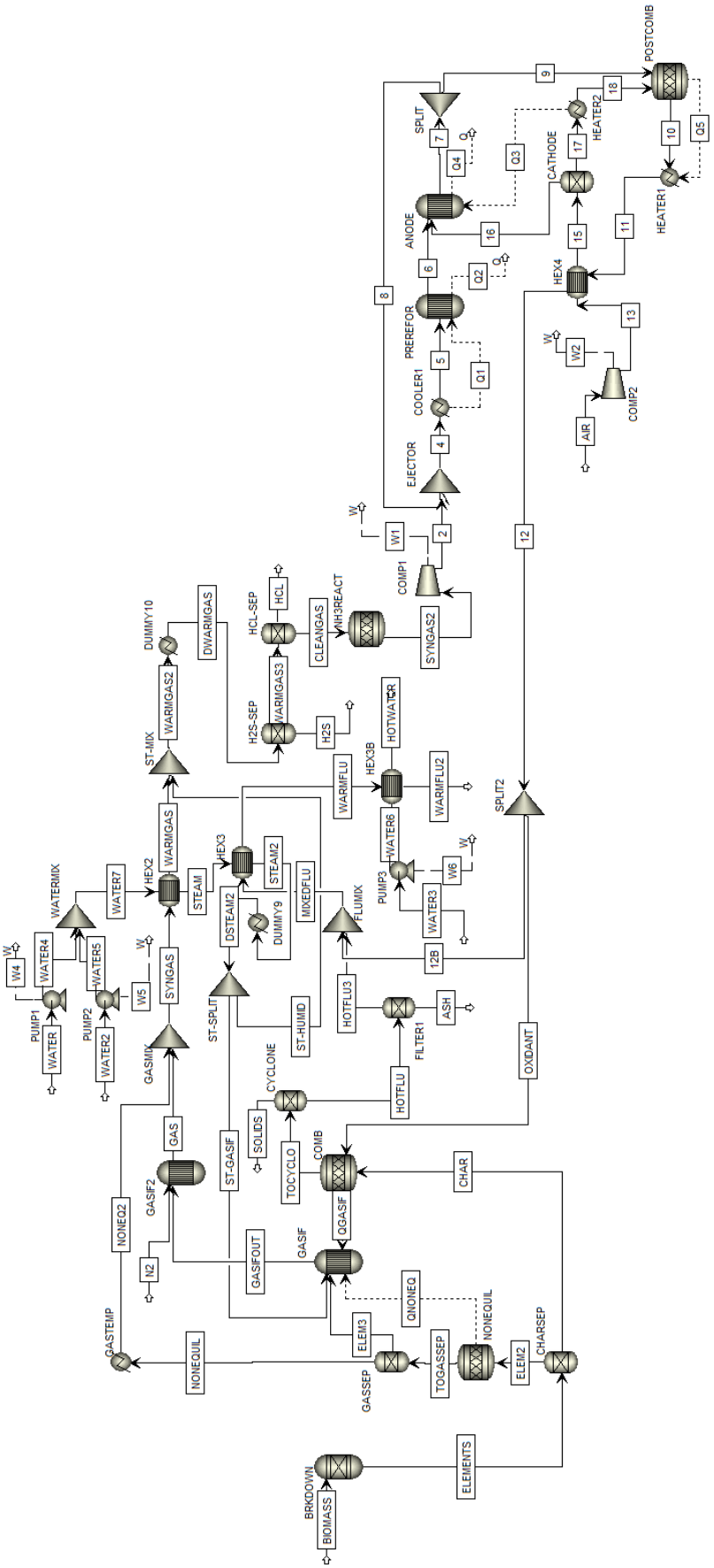

Figure 5.11 System 4 Aspen Plus flowsheet

5.3.2 System Comparison

Table 5.5 compares system performance for a DC power output of 120 kW (110.4 kW AC). The SOFC STCR was much greater for systems 1 and 4 in comparison to systems 2 and 3, caused by the use of an anode recycle for syngas preheating. An SOFC STCR of 2.5 was chosen for systems 2 and 3; this is a realistic level of syngas humidification to prevent carbon deposition problems [195-197] and to ensure adequate steam for reforming of hydrocarbons/tars. A low current density and high cell voltage leads to a high SOFC efficiency. System 3, which has the lowest current density and highest voltage achieves the greatest SOFC efficiency (LHV); followed by systems 2, 1 and 4. These results indicate that the fuel cell performs best without a recycle (system 3) and high SOFC STCR has a significant negative impact for systems 1 and 4.

Biomass input power (explained in section 5.3.1), i.e. the required rate of fuel input to achieve 120 kW DC power output, depends on the efficiency. System 3 has the highest SOFC efficiency and the lowest biomass input power. Syngas power (stream 'SYNGAS', i.e. gasifier outlet) is dependent on biomass input power. Char split (mass basis) changes only for system 4; this rise in char split causes a decrease in syngas LHV and gasifier *CGE* (LHV and mass basis). As discussed in section 5.3.1, the lower temperature of the 'OXIDANT' stream (350 °C) has a negative influence on gasifier performance. In addition, the reduced O_2 content and presence of H_2O and CO_2 and an increase in mass flow passing through the gasifier CZ also affect performance.

Parasitic power (power requirement of pumps, compressors and electric heater) was greatest for system 2, due to high mass flow rate of SOFC air, followed by system 3 and was much lower for systems 1 and 4. This demonstrates that the cathode recycle and electric heater options are both highly energy intensive. Recoverable heat was highest for systems 2 and 4 resulting from high flue gas temperature. Comparing

systems 1 and 3, they have the same 'MIXEDFLU' stream temperature; however, a higher steam demand for system 3 (STCR = 2.5 versus 1.85) leads to lower recoverable heat. Net AC power-to-heat ratio is simply the net AC power output ($P_{el,AC} - P_{parasitic}$) divided by the maximum recoverable heat. A high value is usually desirable as electricity is more often the most valuable and hence the main product of the plant.

The plant net efficiencies calculated using Eq. 5.28 and 5.29 reveal that systems 1 and 4 are more attractive than systems 2 and 3. Systems 2 and 3 have inferior electrical efficiency indicating that the increase in SOFC efficiency is outweighed by the rise in parasitic power making these systems unappealing. The base case system 1 achieves the highest electrical efficiency with a 0.85 percentage point (pp) drop for system 4 resulting from decreased gasifier performance compared to system 1. System 4 exhibits the greatest CHP efficiency and in comparison with other systems there would be cost savings as there is no need for a gasifier oxidant heat exchanger. In contrast, system 2 requires an additional heat exchanger for syngas preheating ('HEX5').

Table 5.5 Comparison of system base case results (120 kW DC power)

Operating Parameter/ Performance Indicator	**System 1**	**System 2**	**System 3**	**System 4**
SOFC STCR	4.57	2.5	2.5	4.63
Current density	1959.19 A/m^2	1908.68 A/m^2	1844 A/m^2	1962.01 A/m^2
Cell voltage	0.638 V	0.654 V	0.677 V	0.637 V
SOFC AC efficiency	41.17%	42.26%	43.74%	41.03%
Biomass input power	350.81 kW	341.74 kW	330.16 kW	363.58 kW
Syngas power	267.41 kW	260.5 kW	251.67 kW	268.29 kW
Char split	13.5%	13.5%	13.5%	16.6%
Syngas LHV (db)	14.43 MJ/kg	14.43 MJ/kg	14.43 MJ/kg	14.35 MJ/kg
Gasifier *CGE*	76.23%	76.23%	76.23%	73.79%
Parasitic power	21.63 kW	30.29 kW	29.91 kW	21.5 kW
Maximum recoverable heat	155.15 kW	162.53 kW	140.14 kW	169.98 kW
Net AC power-to-heat ratio	0.57	0.49	0.57	0.52
Plant net AC electrical efficiency (LHV basis)	25.3%	23.44%	24.38%	24.45%
Plant net AC CHP efficiency (LHV basis)	69.53%	71%	66.82%	71.2%

A detailed discussion in respect of the effect of current density j on system 1 performance (Figures 5.12 and 5.17) is provided in section 5.3.4; in this section the results are discussed regarding system comparison. Referring to Figure 5.12, j was varied from 110 to 420 mA/cm^2. As was seen for the standalone model (section 5.2.3), SOFC voltage and efficiency decrease and power increases to a peak, after which it drops. Increasing j has a strong negative impact on plant performance, net electrical and CHP efficiencies ($\eta_{el,net}$ and $\eta_{CHP,net}$) fall ~23 pp over the j range.

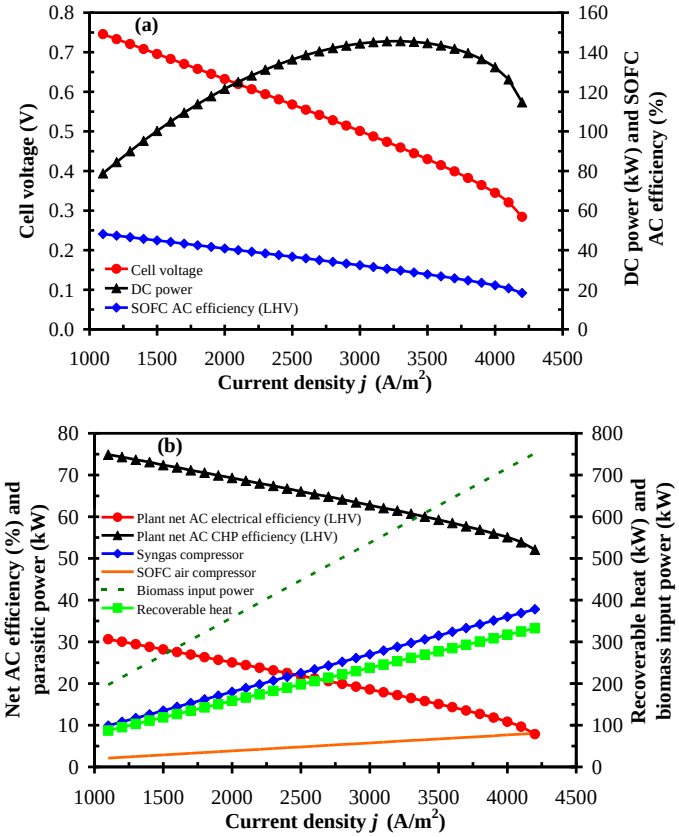

Figure 5.12 Effect of current density on system 1 performance

Figure 5.13 depicts the influence of j on system 2 over the range 115-325 mA/cm^2. In comparison to system 1 results, the same trends exist. The limiting current density is much lower at 325 mA/cm^2. Power drops more rapidly and peak power is below that of system 1 at a lower j (143.2 kW at 285 mA/cm^2 versus 145.6 kW at 330

mA/cm^2). At 325 mA/cm^2 the SOFC efficiency is only 26.6% in contrast to 30.1% for system 1; moreover, the concentration loss (V_{Conc}) was found to be over three orders of magnitude higher for system 2. The increase in V_{Conc} is likely due to the drop in O_2 partial pressure resulting from the cathode recycle. $\eta_{el,net}$ and $\eta_{CHP,net}$ fall from 28.7% to 11.5% and 79.2% to 62.2% respectively over the j range. Over the same j range system 1 $\eta_{el,net}$ and $\eta_{CHP,net}$ drop from 30.3% to 16.9% and 74.6% to 61.1% respectively. Parasitic power is considerably higher than for system 1 over the entire range and Figure 5.13 (b) shows that it is almost exclusively due to the SOFC air compressor. The STCR was only 1.85 for this sensitivity analysis and at higher, more realistic, STCR system 2 performance would degrade. For this reason a STCR sensitivity analysis was carried out for systems 2 and 3 and the results may be found in Appendix E. The results presented here confirm that a cathode recycle is not an attractive alternative to the base case anode recycle system over the entire operating j range.

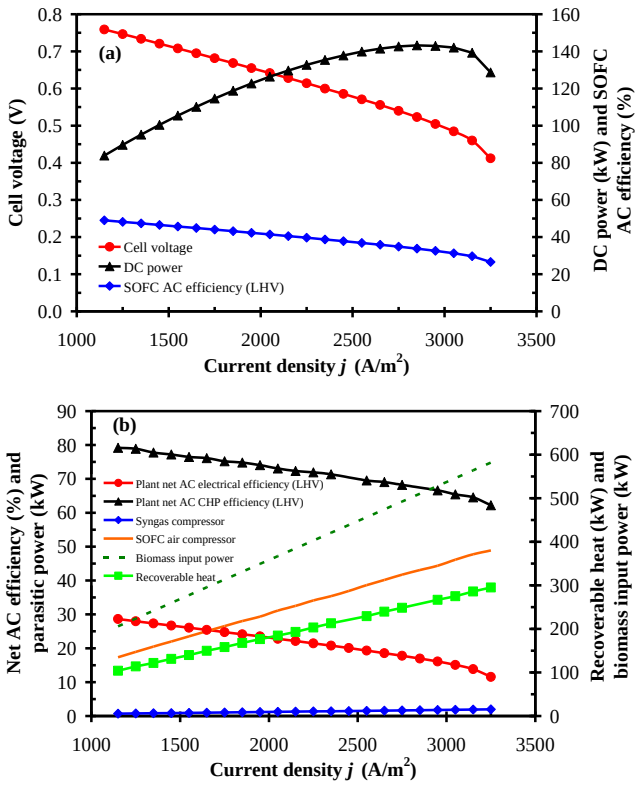

Figure 5.13 Effect of current density on system 2 performance

From Figure 5.14 (a) it is evident that the SOFC stack operates with improved performance for system 3 in comparison to system 1 across the entire j range. For example, the stack achieves a peak power of 156.7 kW at j = 335 mA/cm^2 and operates at higher SOFC efficiency (e.g. $\eta_{SOFC,gross}$ = 19.8% at j = 420 mA/cm^2 versus 18.4% for system 1). Figure 5.14 (b) displays plant performance and it is clear that the improvement in SOFC stack efficiency is outweighed by the increased parasitic power, which leads to lower plant net efficiencies over the complete j range. The increased parasitic power is attributed to the syngas heater. Once again it was deemed necessary to conduct a STCR sensitivity analysis as the STCR was low at 1.85 and the results are provided in Appendix E. These results confirm that an electric heater is not an attractive alternative for syngas preheating over the entire operating j range.

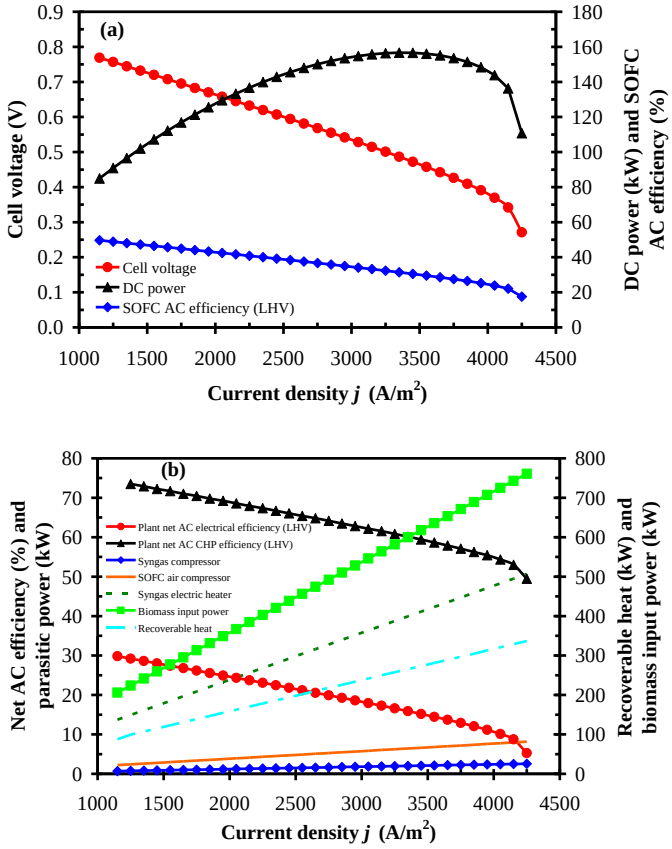

Figure 5.14 Effect of current density on system 3 performance

The effect of increasing j on system 4 performance is illustrated in Figures 5.15 and 5.16. SOFC stack performance Figure 5.15 (a) remains unchanged with reference to system 1. As discussed earlier in this section the gasifier operates at lower efficiency. Increasing j improves the gasifier performance; however, even at the highest j value *CGE* remains below that of system 1 (75.14% versus 76.23%). Lower *CGE* results in higher biomass input power, which in turn decreases $\eta_{el,net}$ for the complete j range (28.8-7.8% for system 4 versus 30.6-7.9% for system 1). Figure 5.15 (b) shows that there is a substantial rise in $\eta_{CHP,net}$ for system 4. This was found to be the result of a higher flue gas temperature as the gasifier CZ flue gas is not used to preheat the CZ air. Based on these results, thermal integration (system 4) was deemed attractive. The modest drop in $\eta_{el,net}$ may be offset by the substantial rise in $\eta_{CHP,net}$ and cost benefit (no 'HEX1').

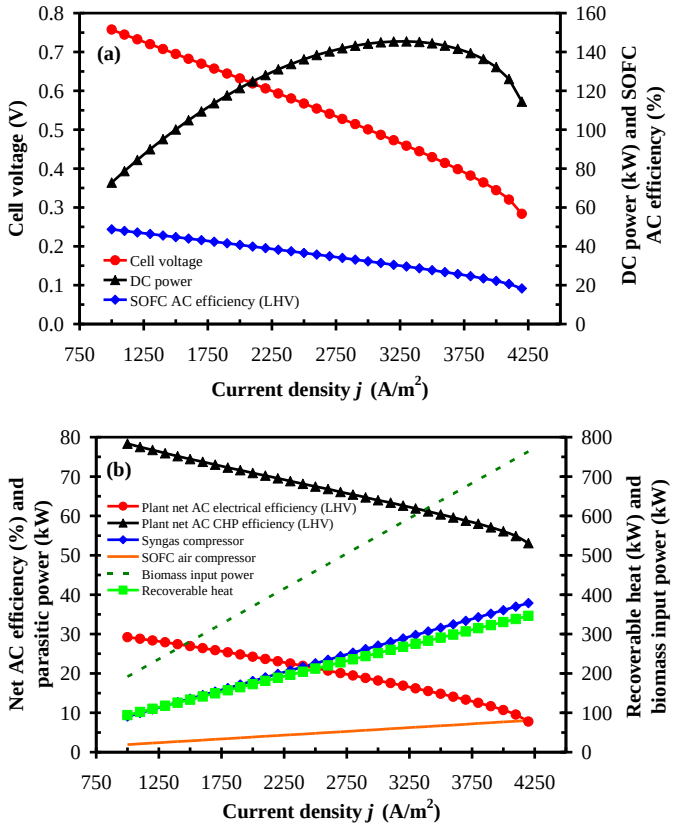

Figure 5.15 Effect of current density on system 4 performance

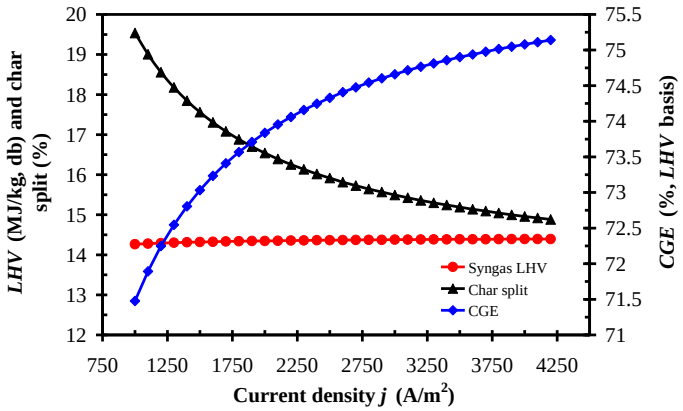

Figure 5.16 Effect of current density on system 4 gasifier performance

The performance of all systems (systems 1-4) was lower than anticipated and therefore potential improvements to the systems were investigated.

5.3.3 System Performance Enhancement

Lowering syngas preheat temperature

Analysis of model results indicated that the elevated SOFC STCR of systems 1 and 4 caused by the anode recycle has a strong negative effect on the performance of those systems. Therefore, it was deemed worthwhile to investigate lowering the syngas preheat temperature (temperature at pre-reformer inlet), which in turn would decrease the SOFC STCR of systems 1 and 4 and in theory boost performance.

All system models (1-4) were run with the syngas preheat temperature reduced from 800 °C to 700 °C and the results are presented in Table 5.6. This drop in preheat temperature caused a reduction in the pre-reformer temperature of ~60 °C in all cases. A drop in temperature of this magnitude should not lead to any thermal gradient problems in the SOFC stack but this would need to be confirmed with the fuel cell manufacturer. Excessive thermal gradients may lead to mechanical failure of the SOFC stack.

Table 5.6 System performance enhancement: effect of lowering syngas preheat temperature (120 kW DC power)

Operating Parameter/ Performance Indicator	**System 1A**	**System 2A**	**System 3A**	**System 4A**
SOFC STCR	2.285	2.285	2.285	2.277
Current density	1843.54 A/m^2	1903.19 A/m^2	1840.06 A/m^2	1842 A/m^2
Cell voltage	0.677 V	0.656 V	0.679 V	0.678 V
SOFC AC efficiency	43.75%	42.38%	43.83%	43.69%
Biomass input power	330.08 kW	340.76 kW	329.46 kW	342.16 kW
Syngas power	251.61 kW	259.76 kW	251.14 kW	251.92 kW
Char split	13.5%	13.5%	13.5%	16.81%
Syngas LHV (db)	14.43 MJ/kg	14.43 MJ/kg	14.43 MJ/kg	14.34 MJ/kg
Gasifier *CGE*	76.23%	76.23%	76.23%	73.63%
Parasitic power	20.34 kW	30.34 kW	22.58 kW	20.18 kW
Maximum recoverable heat	145.78 kW	173.25 kW	141.66 kW	160.25 kW
Net AC power-to-heat ratio	0.62	0.46	0.62	0.56
Plant net AC electrical efficiency (LHV basis)	27.28%	23.5%	26.66%	26.37%
Plant net AC CHP efficiency (LHV basis)	71.45%	74.34%	69.66%	73.2%

In comparison to the base case results (Table 5.5), the SOFC STCR for systems 1A and 4A are far below their base case values. Less depleted fuel needs to be recycled to reach the reduced syngas preheat temperature, which means less H_2O content and thus lower STCR. SOFC STCR was set to 2.285 for systems 2A and 3A so that the results would be comparable to system 1A. The difference in SOFC STCR for system 4A compared to the other systems is miniscule and may be ignored. SOFC performance improves for all systems (compared to Table 5.5 results). Current density drops and voltage and efficiency increase. Systems 1A and 4A experience the largest improvement as a consequence of the dramatic fall in SOFC STCR. It is worth noting that SOFC performance is very similar for systems 1A, 3A and 4A. After further investigation, the slight improvement in SOFC performance for system 2A was discovered to be due to the drop in SOFC STCR from 2.5 to 2.285. Lowering syngas preheat temperature actually decreases SOFC performance. This shows that the increase in performance for

systems 1A and 4A is solely as a result of the reduction in SOFC STCR and not the drop in syngas preheat temperature.

The biomass feed requirement falls for all systems but the drop for systems 2A and 3A was minimal. There was little change in gasifier performance for system 4A (*CGE* fell from 73.79% to 73.63%). System 1A and 4A parasitic power decreases slightly because of lower syngas and SOFC air flow rates. System 3A parasitic power drops significantly (less energy needed to preheat the syngas), which leads to large gains in plant efficiencies. The results re-affirm that the anode recycle is the better option, in comparison to an electric heater, for syngas preheating. Although the gap in performance between the two is narrowed when syngas preheat temperature is lowered. System 3A would be appealing if it was desirable to reduce system complexity, i.e. by removal of the recycle.

Once again Systems 1 and 4 are the most attractive with respect to plant efficiency. System 1A achieves the highest electrical efficiency while system 4A has the greatest CHP efficiency (excluding system 2A, which is not considered due to its very low electrical efficiency). In comparison to the base case results in Table 5.5, system 1 $\eta_{el,net}$ and $\eta_{CHP,net}$ rise 1.98 and 1.92 pp respectively and system 4 $\eta_{el,net}$ and $\eta_{CHP,net}$ increase 1.92 and 2 pp respectively. Based on these results, lowering the syngas preheat temperature in order to improve plant performance is highly recommended.

Lowering syngas and cathode air preheat temperature

The cathode preheat temperature was also lowered to 700 °C from 800 °C in an attempt to increase system 4 gasifier performance. Reducing cathode preheat temperature results in a higher SOFC stack flue gas temperature and therefore gasifier oxidant temperature ('OXIDANT' temperature increases from 351 to 445.6 °C). It will

result in a large temperature difference between cathode outlet and inlet (910 °C – 700 °C = 210 °C), which could cause damaging thermal gradients within the SOFC stack.

Table 5.7 System performance enhancement: effect of lowering syngas and cathode air preheat temperature (120 kW DC power)

Operating Parameter/ Performance Indicator	**System 1B**	**System 2B**	**System 3B**	**System 4B**
SOFC STCR	2.285	2.285	2.285	2.28
Current density	1808 A/m^2	1862.68 A/m^2	1804.8 A/m^2	1807.1 A/m^2
Cell voltage	0.691 V	0.671 V	0.692 V	0.691 V
SOFC AC efficiency	44.61%	43.3%	44.69%	44.57%
Biomass input power	323.71 kW	333.51 kW	323.13 kW	331.15 kW
Syngas power	246.75 kW	254.23 kW	246.32 kW	246.96 kW
Char split	13.5%	13.5%	13.5%	15.6%
Syngas LHV (db)	14.43 MJ/kg	14.43 MJ/kg	14.43 MJ/kg	14.38 MJ/kg
Gasifier *CGE*	76.23%	76.23%	76.23%	74.58%
Parasitic power	19.95 kW	29.55 kW	22.15 kW	19.78 kW
Maximum recoverable heat	189.28 kW	232.88 kW	185.07 kW	198.41 kW
Net AC power-to-heat ratio	0.48	0.35	0.48	0.46
Plant net AC electrical efficiency (LHV basis)	27.94%	24.24%	27.31%	27.37%
Plant net AC CHP efficiency (LHV basis)	86.41%	94.07%	84.58%	87.28%

Comparing the results displayed in Table 5.7 with those in Table 5.6, SOFC performance improves for all systems. SOFC efficiencies for systems 1B, 3B and 4B were within 0.12 pp of each other. Biomass feed requirement decreases for all systems with the drop for system 4B well above the other systems (11.01 kW versus ~6.65 kW). This was found to be attributable to better gasifier performance; the drop in cathode preheat temperature causes the gasifier *CGE* to rise from 73.63% to 74.58%. The increase in *CGE* was found to be due to the higher CZ oxidant temperature of 445.6 °C, which decreases the char required to 15.6%. Once more, systems 1 and 4 perform best; with system 1B achieving the highest $\eta_{el,net}$ and system 4B having the best $\eta_{CHP,net}$ (system 2B excluded due to its low $\eta_{el,net}$). The enormous increase in $\eta_{CHP,net}$ for all systems is caused by the higher flue gas temperature (less heat removed from flue gas to

preheat the cathode air). System 4B experiences the largest rise in $\eta_{el,net}$; 1 pp compared to ~0.68 pp for other systems. As discussed already, this is the result of higher *CGE* and thus lower biomass input power. Considering these results, it appears that lowering the syngas preheat temperature is the better option for enhancing system performance as it has a strong positive impact and it only results in an anode temperature drop of 60 °C and therefore is not as likely to cause damaging temperature gradients within the SOFC stack. Further investigations, such as CFD modelling and lab scale experimentation, would need to be carried out if both options (syngas and cathode preheat temperature reduction) were to be implemented in order to ensure safe operation of the SOFC stack.

An alternative method of increasing system 4 gasifier *CGE* was explored. Rather than lowering cathode preheat temperature, an electric heater was employed to raise the temperature of the CZ oxidant to 450 °C. The results revealed that as expected the *CGE* rose (74.7%); however, plant net electrical efficiency dropped (26.37% to 25.76%) due to the increased parasitic power. Therefore, this approach is not recommended.

5.3.4 Sensitivity Analyses Results and Discussion

The results presented in sections 5.3.2 and 5.3.3 revealed that system 1 has superior performance in comparison to the other system configurations. Therefore, system 1 was chosen to perform sensitivity analyses of the main operating variables. The results presented and discussed in this section were attained using the system 1 model only (exception: system 3 layout employed for cleaning temperature sensitivity at high cleaning temperature 600-700 °C as recycle was not required).

Current density

Figure 5.17 displays the voltage characteristics of a single tubular SOFC. The predicted voltage characteristics are consistent with the results achieved using the

standalone model (section 5.2.3): Nernst voltage = ~0.9 V; ohmic loss is dominant; activation loss is less significant; concentration loss is the least significant but increases rapidly at high current density. Nernst voltage remains constant over the *j* range. All three of the voltage losses rise with increasing *j*.

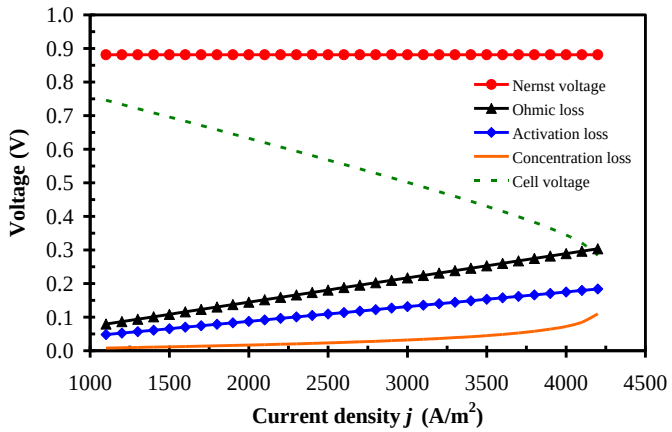

Figure 5.17 SOFC voltage characteristics versus current density for system 1

From Figure 5.12 it is evident that *j* has significant influence on the system. Increasing *j* lowers both voltage (0.746-0.284 V) and SOFC efficiency (48.1-18.4%) but increases DC power (78.8-114.7 kW). Voltage is reduced as a result of increased losses as shown in Figure 5.17. As was seen for the standalone SOFC model, there must be a trade-off between SOFC voltage, efficiency and power. Plant efficiencies fall substantially (~23 pp) due to higher parasitic power and biomass input. It is clear from Figure 5.12 (b) that the parasitic power is dominated by the syngas compressor power requirement. The syngas compressor must compress a gas at 400 °C to three times the SOFC pressure; whereas the SOFC air compressor only raises the air pressure to 1.094 bar and the air inlet temperature is low at 25 °C. The results over a typical operating *j* range of 180-200 mA/cm^2, indicate a cell voltage range of 0.658-0.632 V, $\eta_{el,net}$ range of 26.3-25.1%, $\eta_{CHP,net}$ range of 70.6-69.3% and a DC power range of 113.8-121.5 kW.

Steam to carbon ratio

The effects of varying STCR are depicted in Figure 5.18. From Figure 5.18 (a) it can be seen that STCR has a substantial negative impact on voltage (0.647-0.573 V) and SOFC efficiency (41.8-37%) and increases current density (193-217.9 mA/cm^2), this is due to the change in gaseous component partial pressures (H_2O rises, H_2 and CO fall). This leads to a drop in Nernst voltage (0.887-0.85 V) and an increase in voltage losses. Figure 5.18 (b) shows that more biomass fuel is required to achieve 120 kW DC, which increases parasitic power due to greater mass flow rates, and decreases the plant net efficiencies significantly ($\eta_{el,net}$ down 6.7 pp and $\eta_{CHP,net}$ drops 14.7 pp). Recoverable heat decreases even though the 'MIXEDFLU' stream temperature and mass flow rate increases because the steam requirement rises, lowering the plant flue gas temperature. It is therefore desirable to operate the plant at low STCR.

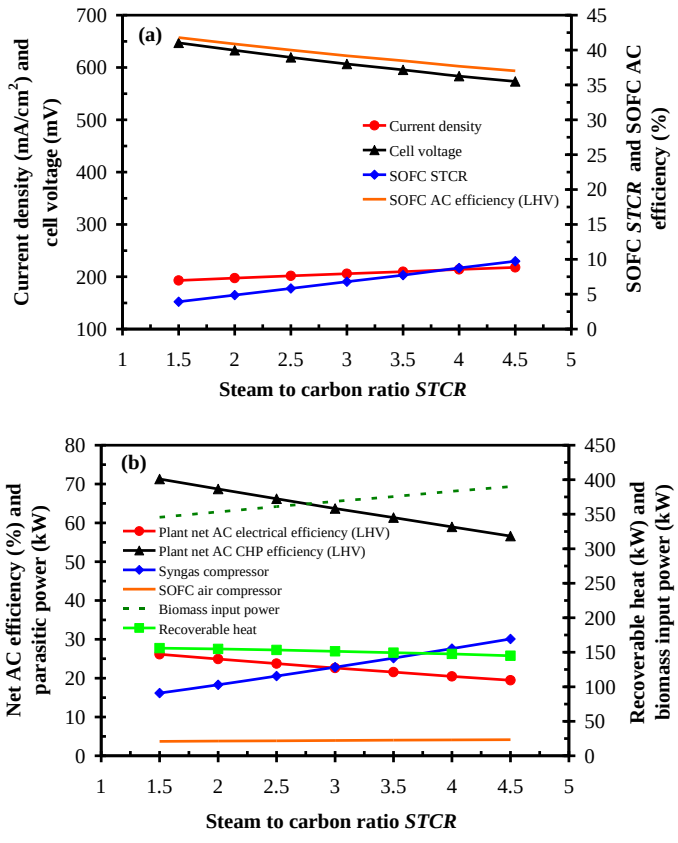

Figure 5.18 Effect of steam to carbon ratio on system 1

Fuel utilisation factor

U_f is limited to 0.85 for this system layout because above this value the temperature of the 'MIXEDFLU' stream is below the required steam temperature of 350 °C making it impossible to raise the gasification/humidification steam at this temperature ('HEX3' Figure 5.8).

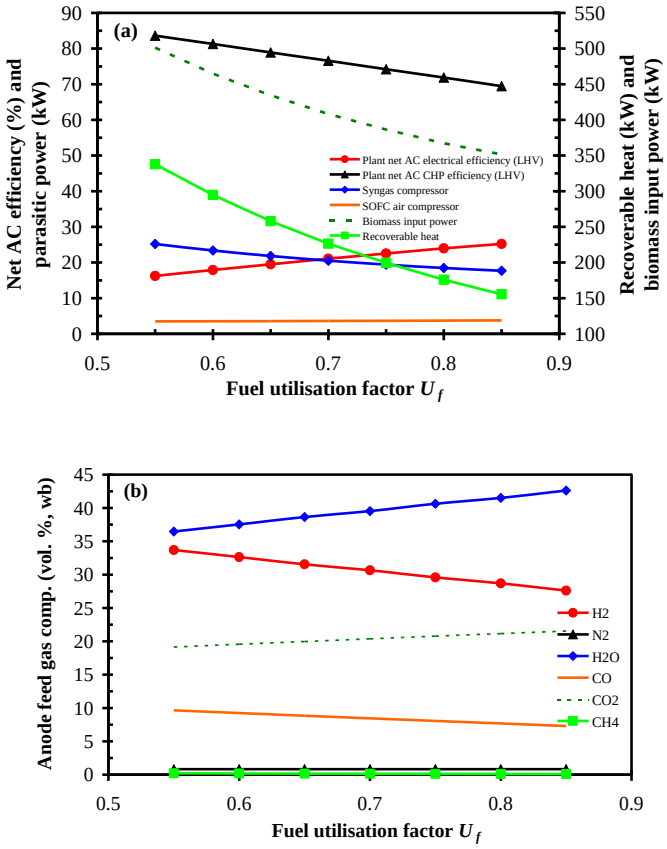

Figure 5.19 Effect of fuel utilisation factor on system 1

The influence of U_f on system 1 performance is illustrated in Figure 5.19. The SOFC performance results can be found in Appendix E. Voltage decreases slightly with U_f due to increased losses and current density increases ~15 mA/cm^2 because of the higher amount of H_2 consumed. $\eta_{SOFC,gross}$ displays a huge increase (28.8-41.1%) attributable to the dramatic drop in the biomass input required to achieve the desired

power (120 kW DC). This is because more of the energy contained in the fuel is converted to electricity rather than heat as explained earlier in section 5.2.3 for the standalone SOFC model. Plant efficiencies were very sensitive to changes in U_f, $\eta_{el,net}$ increased by 9 pp and $\eta_{CHP,net}$ dropped 14.2 pp. The increase in $\eta_{el,net}$ was primarily due to the reduced biomass input at high U_f. At low U_f more of the fuel is available for combustion therefore the SOFC stack flue temperature is high and as U_f increases the temperature drops, thus lowering the recoverable heat and $\eta_{CHP,net}$. The influence of U_f on anode feed gas composition is shown in Figure 5.19 (b). Higher U_f results in greater levels of H_2O and CO_2 and lower H_2 and CO. This causes the slight drop in cell voltage (~15 mV). It is recommended to operate the SOFC stack at high U_f as it is usually desirable to run the plant at high $\eta_{el,net}$ rather than high $\eta_{CHP,net}$. These results reveal U_f as an extremely important operating parameter as it can change the mode of operation of the plant (focus on electricity or heat). The net power-to-heat ratio increases from 0.24 to 0.57 over the U_f range.

Air utilisation factor

Similarly to U_f, U_a is limited to 0.16 for this system as below this value the temperature of the 'MIXEDFLU' is below the required steam temperature of 350 °C. The influence of U_a on system 1 is shown in Figure 5.20. The cell voltage and SOFC efficiency decrease but only slightly with U_a and the current density increases marginally. Plant net electrical efficiency remains fairly constant over the U_a range. Conversely, there is a significant drop in $\eta_{CHP,net}$ due to an increase in biomass input and decrease in recoverable heat. Parasitic power does not have much effect on plant efficiencies because the syngas compressor power shows a small rise, which is offset by a fall in the SOFC air compressor power for increasing U_a. Recoverable heat decreases

with U_a due to the drop in mass flow rate of the flue gas stream regardless of its rise in temperature caused by the reduction in excess air (cooling) in the SOFC burner.

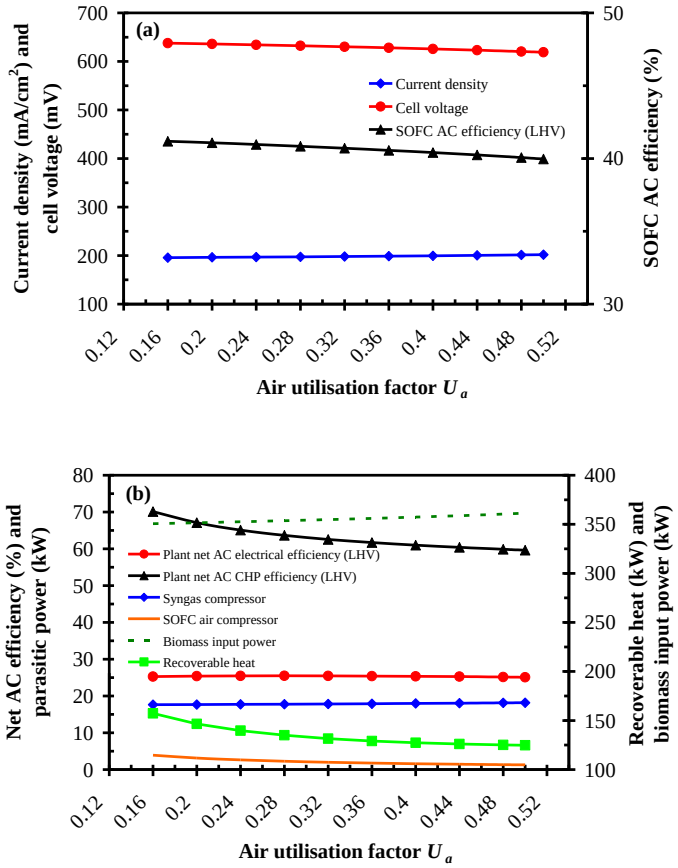

Figure 5.20 Effect of air utilisation factor on system 1

Gasification temperature

T_g was varied from 775 to 1,050 °C; 775 °C is the minimum T_g considering the steam temperature requirement of 350 °C. The results with regard to the influence of T_g on syngas composition at gasifier exit match those presented in section 4.3.3 for the standalone FICFB gasifier model, i.e. H_2 and CO rise and H_2O, CO_2 and CH_4 decrease with rising T_g. These results are presented in Appendix E. Figure 5.21 (a) displays how T_g affects the LHV of the syngas, gasifier *CGE* and the char split fraction. It is evident that T_g has significant influence on gasifier performance. LHV increases from 14.1 to

15.2 MJ/kg and the char split fraction climbs from 11.3% to 19%. Gasifier *CGE* rises from 72.5%, reaches a peak of 79.9% at 950 °C and falls to 78.6%. Therefore, it is concluded that increasing T_g has a favourable influence on gasifier performance.

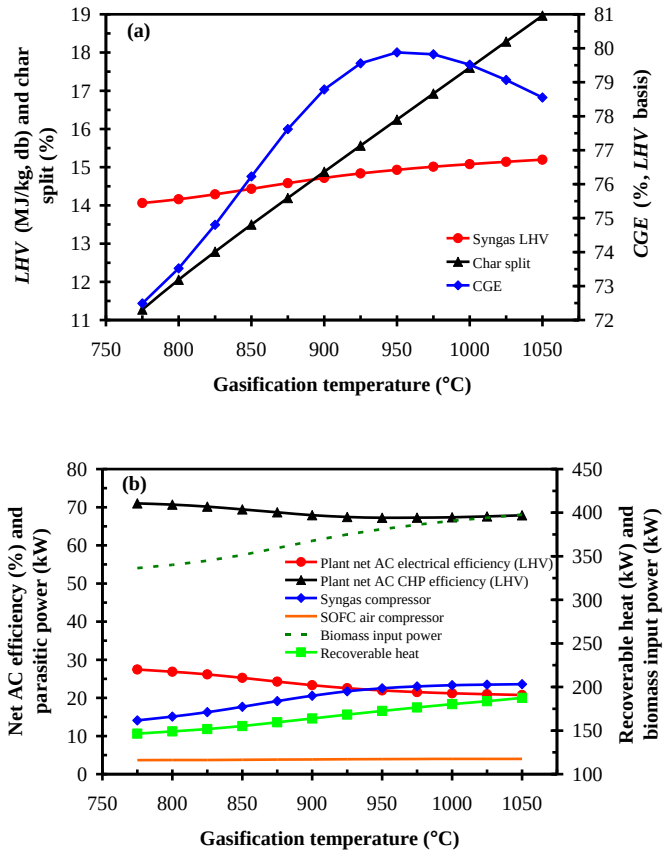

Figure 5.21 Effect of gasification temperature on system 1

A somewhat surprising conclusion is drawn from analysis of the SOFC stack and overall plant performance results; these results suggest that T_g should be kept as low as possible. This was surprising considering the gasifier performance drops with decreasing T_g. A possible explanation is given below after discussion of the SOFC and plant performance results. The SOFC efficiency fell significantly over the T_g range (see Appendix E). From Figure 5.21 (b) it can be seen that T_g has a considerable negative impact on $\eta_{el,net}$ (down 6.7 pp) and a lesser influence on $\eta_{CHP,net}$ (down 3.1 pp). These

trends can be explained by the fact that biomass input climbs from 336.5 kW to 397.8 kW and parasitic power also rises due to higher mass flow rates.

Further investigation revealed that the SOFC performance degradation was caused by the stack pre-reformers. When the low CH_4 content syngas, obtained at high T_g, is fed to the pre-reformers, the conditions favour the reverse CO-shift reaction (Eq. 3.9). This reaction is favoured because of the rising pre-reformer temperature (586.4-822.4 °C), which is due to the low level of CH_4 reforming (endothermic). With reference to Figure 5.22, the H_2O content in the anode feed gas increases with T_g. The only explanation for this is the occurrence of the reverse CO-shift reaction in the pre-reformers because the only other possible source of this H_2O is the recycle stream and its flow rate drops with T_g. The increased H_2O content at the anode inlet leads to lower SOFC stack performance.

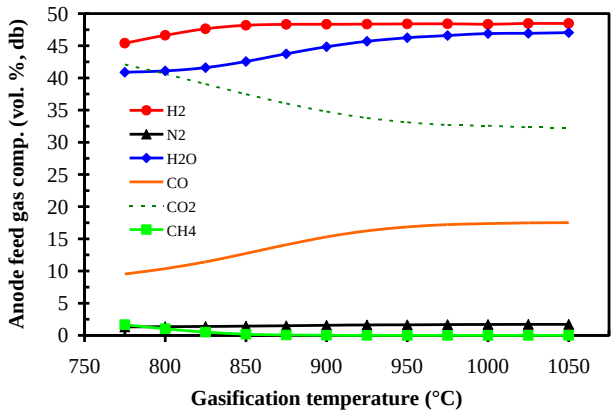

Figure 5.22 Effect of gasification temperature on system 1 anode feed gas composition

The results suggest that T_g should be kept as low as possible with respect to SOFC stack and overall plant performance. However, a low T_g would lead to high tar levels in the syngas, which could cause severe damage to the SOFC stack. Considering these findings, it is recommended to operate the gasifier in the T_g range 850-900 °C in order

to produce a high energy content syngas with high H_2 and CO, to achieve acceptable gasifier *CGE*, to ensure a safe level of tars for conversion in the SOFC stack and to achieve reasonable plant efficiency.

Biomass moisture content

Biomass moisture content was found to have little impact on syngas composition. The effect of increasing moisture content on LHV of the syngas, gasifier *CGE* and the char split fraction is illustrated in Figure 5.23. It has little effect on LHV (depends on the gas composition). However, it was found to have a very strong influence on *CGE* (decreases from 93.6% at 5% moisture to 64.7% at 30% moisture). This influence on *CGE* may be explained by the increase in char split fraction with rising moisture (10.2-16.5%). Moisture content had little effect on SOFC stack performance (current, voltage and $\eta_{SOFC,gross}$ remained fairly constant). Figure 5.23 (b) reveals that moisture has a strong unfavourable effect on the plant net efficiencies ($\eta_{el,net}$ down 9.8 pp and $\eta_{CHP,net}$ drops 18.6 pp). At low moisture content of 5% the predicted efficiencies are very high at 31.2% and 80.7% for $\eta_{el,net}$ and $\eta_{CHP,net}$ respectively. As parasitic power remains constant, the change in plant efficiencies is due to the rise in biomass input power (285.1-414.8 kW).

Based on these results, the biomass moisture content is an operating parameter of extreme importance and should be as low as possible, i.e. the biomass fuel should be dried prior to use in the gasifier. At sufficient scale, investment in a biomass dryer is recommended as it is prohibitively expensive to purchase biomass that has been dried to low moisture (< ~15 wt. %). Irish forest wood chip (50% moisture) was quoted as 70 €/t (2010 €), increasing to 110 €/t (2010 €) for 35% moisture (see section 6.3) [76, 306, 307].

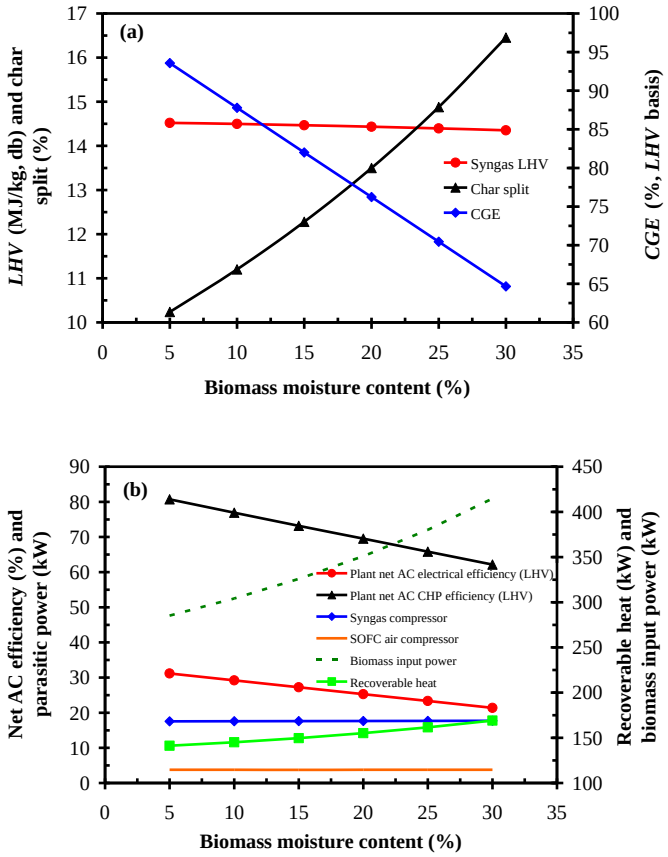

Figure 5.23 Effect of biomass moisture content on system 1

Steam to biomass ratio

Figure 5.24 (a) depicts the changes in syngas composition in response to variation in STBR. Over the STBR range H_2 increases by 11.1 pp; however, on a wet basis this increase drops to 2.5 pp. It may be more useful to consider the wet gas composition in this analysis as there is a large increase in H_2O (18.4% to 31.3%). CO and CH_4 drop by 7 pp (db) and CO_2 increases by 2.7 pp. From Figure 5.24 (b) it can be seen that STBR has a significant impact on syngas LHV (15.2-13.8 MJ/kg); however, it has little influence on *CGE* (75.8-76.4%). Gas LHV decreases with STBR because the increase in H_2 is outweighed by the drop in CO and CH_4. STBR had a limited impact on SOFC stack performance ($\eta_{SOFC,gross}$ fell by 1.39 pp) and plant net efficiencies ($\eta_{el,net}$ down 1 pp and $\eta_{CHP,net}$ drops 1.3 pp). These results are provided in Appendix E. The drop in

plant efficiencies can be attributed to a small rise in parasitic power and biomass feed requirement.

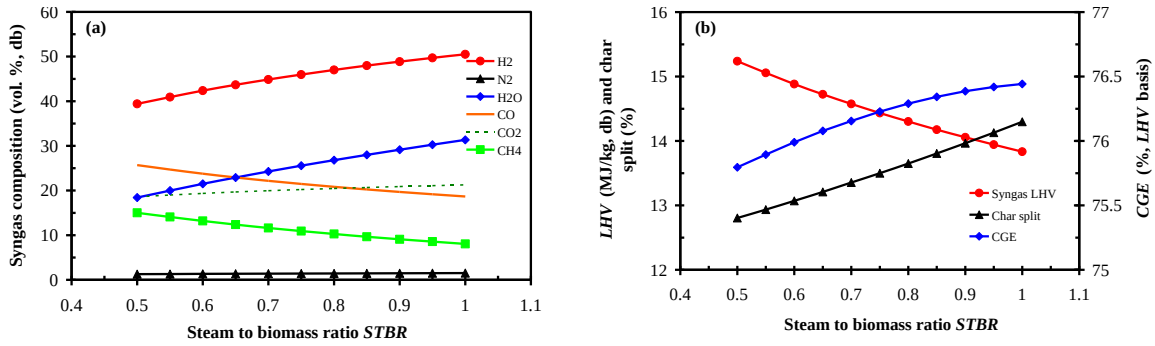

Figure 5.24 Effect of steam to biomass ratio on system 1

Considering these findings, it is recommended to operate the gasifier at low STBR. However, it should not be lower than 0.5 as there must be sufficient steam supplied to the gasifier for bed fluidisation.

Air-fuel ratio

Syngas composition was found to have a weak dependence on air-fuel ratio. With reference to Figure 5.25 (a), syngas LHV remains fairly constant. There is however a substantial decrease in *CGE* with increasing air-fuel ratio (*CGE* drops 3.5 pp). As air-fuel ratio increases the excess air lowers the temperature of the CZ, which in turn affects T_g. In order to maintain T_g at the desired temperature more char must be burned (13.2-17.6%). Figure 5.25 (b) shows that $\eta_{el,net}$ drops 1.4 pp and $\eta_{CHP,net}$ rises 2.2 pp. These trends are caused by significant increases in biomass feed rate and recoverable heat (~20 kW in both cases). Parasitic power remains almost constant (note the gasifier air compressor power rises to only 0.53 kW). Air-fuel ratio has no impact on SOFC performance. In conclusion, air-fuel ratio should be as low as possible.

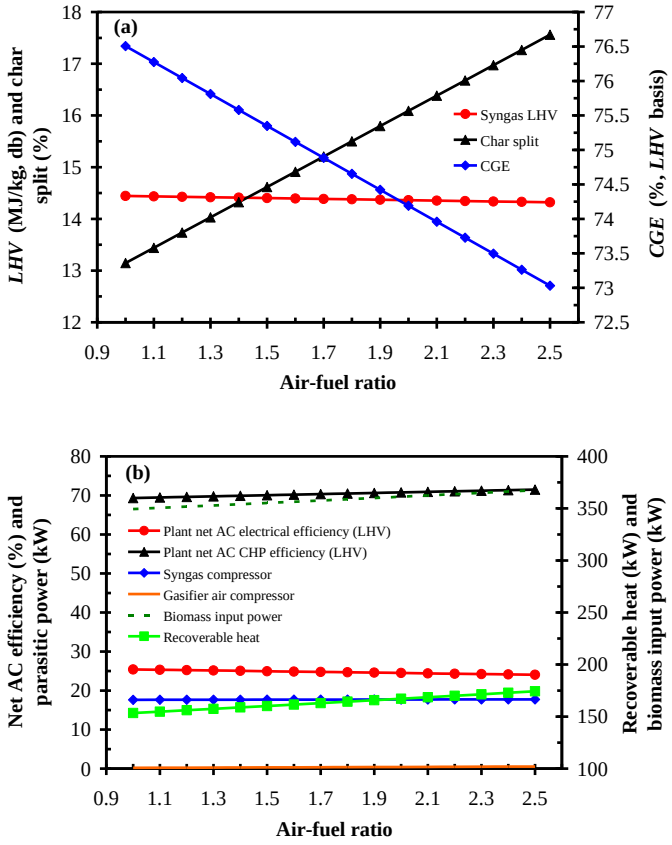

Figure 5.25 Effect of air-fuel ratio on system 1

Gasification steam temperature

Syngas composition and LHV remain somewhat unchanged with a rise in steam temperature (160-350 °C). Referring to Figure 5.26 (a), the elevated temperature does reduce the amount of char required in the gasifier CZ (14.3-13.5%), which has a positive effect on performance. The *CGE* increases from 75.58% to 76.23% (up 0.65 pp). It is evident from Figure 5.26 (b) that increasing steam temperature has minimal effect on plant performance. $\eta_{el,net}$ rises 0.24 pp and $\eta_{CHP,net}$ drops 0.43 pp; these trends are due to small decreases in biomass input and recoverable heat. The steam temperature had no effect on SOFC performance (voltage, efficiency, etc.).

Considering these results, it may be desirable to simplify the plant and achieve cost savings by removing the steam superheater ('HEX3') from the system. That would

mean the steam would be fed to the gasifier at 154 °C with dryness fraction ~60%. This would lower gasifier *CGE* but only slightly and the drop in *CGE* could possibly be recouped through elevated CZ air preheating (see results below).

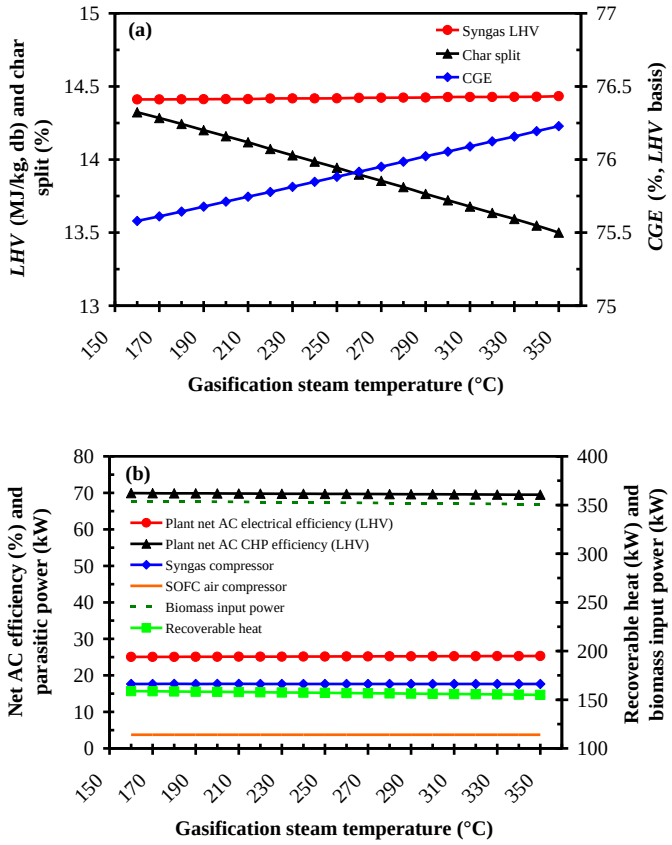

Figure 5.26 Effect of gasification steam temperature on system 1

Gasification air temperature

The gasifier CZ air was preheated from 25 to 650 °C; 650 °C being the maximum allowable preheat temperature so as to ensure gasification/humidification steam could be generated at 350 °C ('MIXEDFLU' stream temperature and 'HEX3'). Preheating the combustion air caused slight changes in syngas composition. Figure 5.27 (a) shows how syngas LHV increases due to the change in composition and how the char split fraction drops and *CGE* increases. The rise in *CGE* is substantial (3.1 pp) and is as a result of the

drop in char split fraction (16.1-12.1%). Figure 5.27 (b) displays the variation in the plant net efficiencies. $\eta_{el,net}$ and $\eta_{CHP,net}$ were found to have a weak dependence on gasification air temperature; increasing 1.1 and decreasing 2.1 pp respectively. The parasitic power requirement remains constant. Recoverable heat drops as a consequence of the greater amount of heat removed from the CZ flue gas for preheating the air. Finally, biomass input power falls ~18 kW, causing the increase in $\eta_{el,net}$. The air temperature had no effect on SOFC performance (voltage, efficiency, etc.).

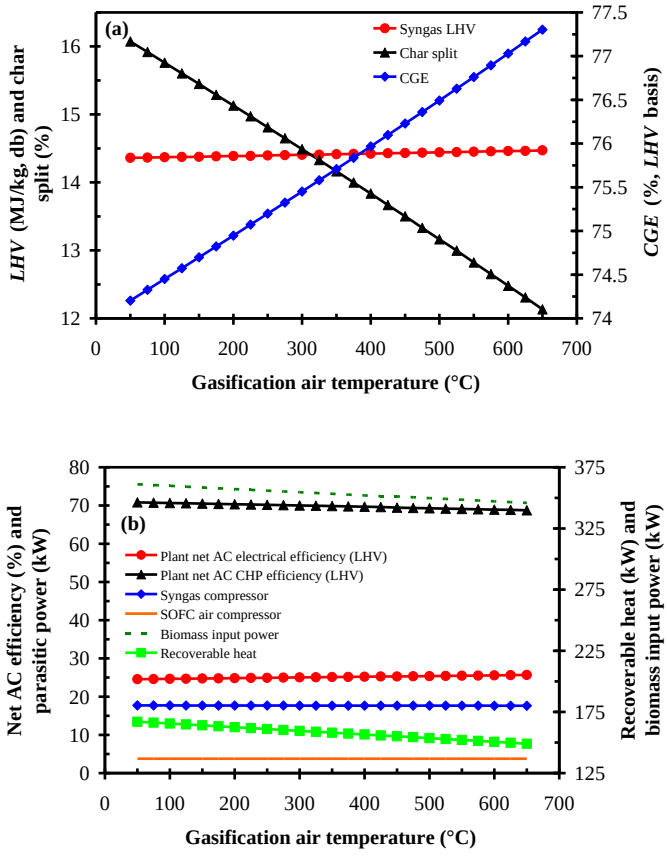

Figure 5.27 Effect of gasification air temperature on system 1

Based on these results, it is concluded that gasification air preheating is more attractive than gasification steam superheating. Over the temperature range 160-350 °C,

air preheating raises $\eta_{el,net}$ and *CGE* 0.37 and 1 pp respectively, whereas steam superheating increases $\eta_{el,net}$ and *CGE* only 0.24 and 0.65 pp respectively.

Cleaning temperature

Cleaning temperature will be a function of the type of technology employed but for the purposes of this investigation a temperature range of 400-700 °C was assumed. The base case system 1 configuration was employed for the cleaning temperature range of 400-500 °C but for higher temperatures (600 °C and 700 °C) system 3 plant layout was utilised as the anode recycle was no longer a practical method for syngas preheating. The 'COMP1' block power requirement to compress the syngas at 600-700 °C to three times the SOFC pressure was too high and made cleaning at high temperature unattractive (high parasitic power reduced $\eta_{el,net}$). In addition, the syngas temperature after compression was above 800 °C; making the anode recycle redundant (purpose of recycle was to raise syngas temperature to 800 °C). The use of an electric heater for syngas preheating as in system 3 was more efficient for these temperatures. At 600-700 °C when the system 3 configuration was employed the STCR was increased to 2.285 in order to make results comparable with the system 1 results (at 400-500 °C).

The effect of raising the operating temperature of the syngas cleaning system on SOFC stack and plant performance is illustrated in Figure 5.28. SOFC stack performance improves with $\eta_{SOFC,gross}$ increasing from 41.2% to 44%. This rise was due to a drop in required biomass feed and a rise in cell voltage (0.637-0.68 V). The change in voltage is caused by an increase in Nernst voltage (due to variation in anode feed gas composition discussed later) and a fall in voltage losses. Plant net efficiencies display a strong dependence on cleaning temperature. $\eta_{el,net}$ increases 5 pp (25.3% to 30.3%) and $\eta_{CHP,net}$ fell 2.5 pp (69.5% to 67%). For 500 °C, the rise in electrical efficiency is put

down to the drop in SOFC STCR (less depleted fuel needs to be recycled to achieve the preheat temperature) and the resulting improved SOFC stack performance and also the fall in biomass input power. For 600-700 °C, the improvement in $\eta_{el,net}$ is due to the fall in parasitic power; i.e. the syngas compressor power requirement decreases from ~18 kW to ~1.65 kW (syngas is compressed to 1.094 bar instead of 3.282 bar). Contrasting the results at 600 °C and 700 °C the rise in $\eta_{el,net}$ is because of the reduction in syngas electric heater power (11.82-5.19 kW). The decrease in $\eta_{CHP,net}$ is caused by a significant drop in recoverable heat (155-120.5 kW). Less heat can be recovered at high cleaning temperature as less heat is taken from the syngas cooling section of the plant, which leads to more heat being removed from the 'MIXEDFLU' stream for steam generation in the 'HEX3' block.

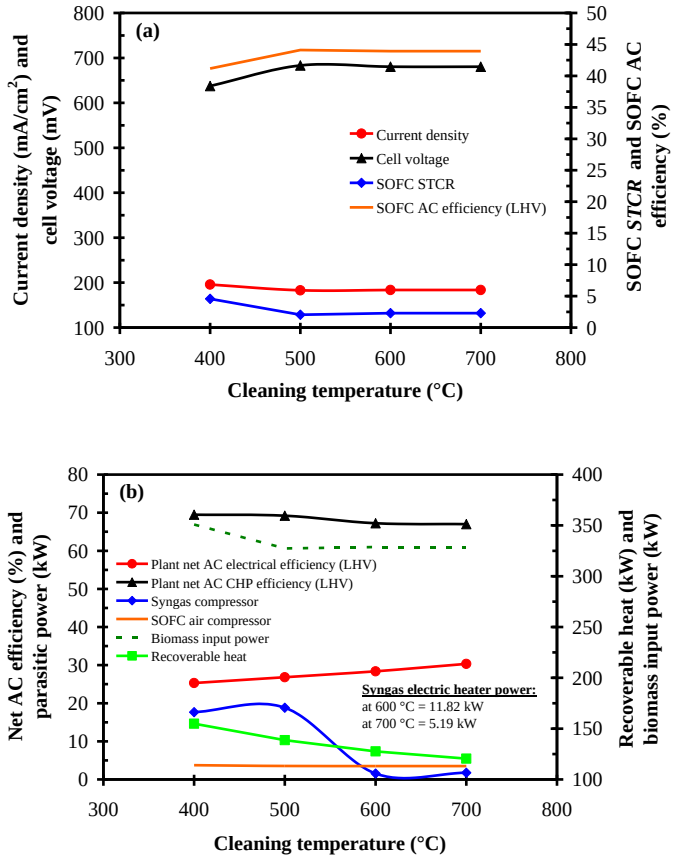

Figure 5.28 Effect of cleaning temperature on system performance

Figure 5.29 shows the impact of cleaning temperature on anode feed gas composition. The cause of the changes in composition is the change in SOFC STCR. At 400 °C SOFC STCR = 4.57 and H_2O and CO_2 are high, which results in low H_2 and CO. For 500-700 °C, SOFC STCR is lower (2.04-2.285), which leads to higher H_2 and CO and lower H_2O and CO_2. CH_4 increases with cleaning temperature (0.1% to 2%) because its conversion in the pre-reformers drops due to the reduction in H_2O at lower SOFC STCR. These changes in composition lead to better SOFC stack performance.

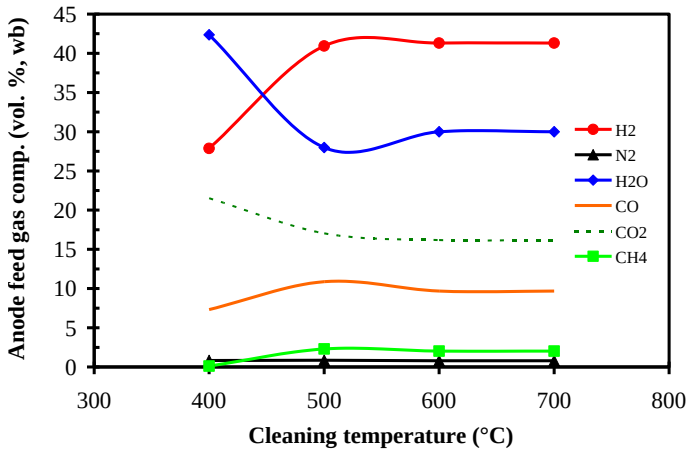

Figure 5.29 Effect of cleaning temperature on anode feed gas composition

In conclusion, high temperature syngas cleaning appears to be very attractive as it offers the potential to reduce plant complexity (no need for an anode recycle) and improves the performance of the SOFC stack and net electrical efficiency of the plant significantly. However, there are limits on the currently available cleaning technologies (see section 3.5.1). The maximum operating temperature for HCl removal to 1 ppmv in a sodium carbonate bed is 600 °C [168]. The maximum operating temperature for H_2S removal to < 1 ppmv in a ZnO bed is ~400 °C [8, 11, 168]. Research efforts should continue in order to increase the temperature of syngas cleaning so that the improvements in efficiency predicted here may be realised. Finally, for a cleaning

temperature of 700 °C and a syngas preheat temperature of 700 °C (lowered from 800 °C) the electric heater power requirement of 5.19 kW could be eliminated, resulting in a further increase in $\eta_{el,net}$ (30.3% to ~31.9%). This demonstrates the great potential that BG-SOFC systems have for achieving high operating efficiency. In contrast, biomass combustion based technologies achieve low electrical efficiencies at small scale (20-25%).

Plant scale

System 1 was scaled up to 500 kWe and 1 MWe power output. These relatively small scales were selected for a number of reasons:

- SPGI tubular SOFC technology has low power density and power-to-weight ratio [162], meaning plants based on this technology will have large footprint (section 3.4). Considering this, ~2 MWe output is considered the upper limit.
- There is a lack of large heat loads in Ireland (see chapter two) and if the plant is to be operated in CHP mode the scale should be limited to ~1 MWe.
- The under-developed biomass supply chain in Ireland limits scale.

The 500 kWe system consists of four 120 kW DC stacks and the 1 MWe system comprises eight stacks. To account for this the SOFC stack active area, assumed to be 96.0768 m^2 (1,152 cells) for the base case system 1, was multiplied by four and eight giving active areas of 384.3072 m^2 (4,608 cells) and 768.6144 m^2 (9,216 cells) for the 500 kWe and 1 MWe scales respectively.

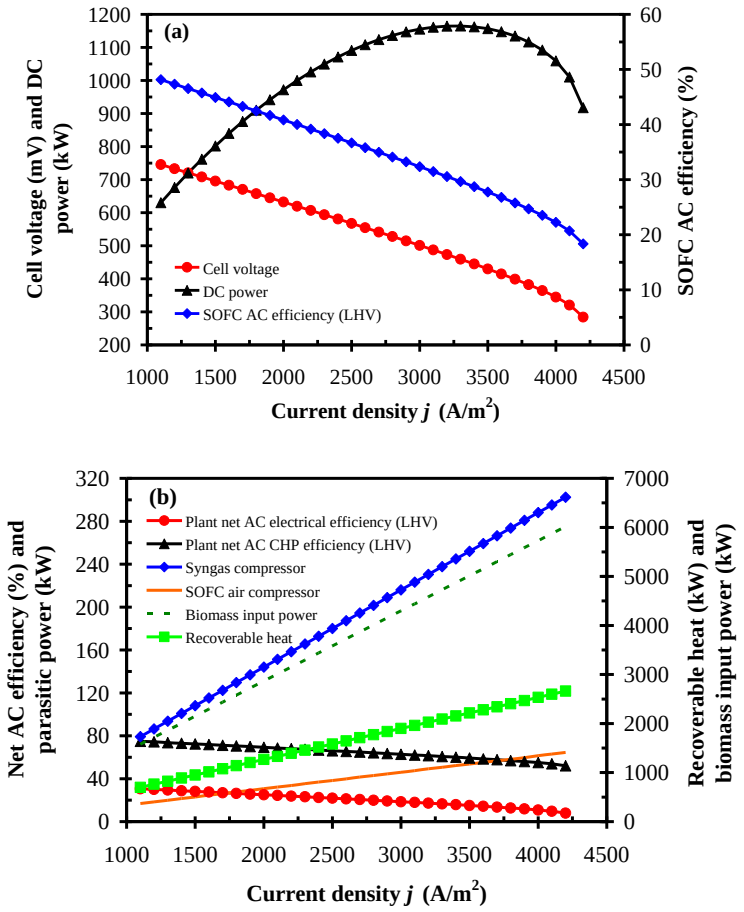

Figure 5.30 1 MWe scale system performance

The results for the 1 MWe system are given in Figure 5.30. The cell voltage and SOFC efficiency results are identical to those of the base case system. The DC power values are eight orders of magnitude higher across the entire *j* range, e.g. the peak power = 1,164.8 kW (eight times the base case system value of 145.6 kW) and also occurs at *j* = 330 mA/cm^2. The same may be said regarding the plant performance results, where parasitic power, biomass input power and recoverable heat are all eight times their values for the base case scale and net efficiencies are equivalent over the complete *j* range. Analogous results were obtained for the 500 kWe system; the difference between the two scales is that mass flow rates and power levels, etc., were four orders of magnitude greater than the base case system (see Appendix E).

5.4 Chapter Summary

The SOFC and combined system (BG-SOFC system) Aspen Plus models were described in this chapter. Four system configurations were investigated; system 1 (base case with anode recycle), system 2 (cathode recycle), system 3 (no recycle with an electric heater used for syngas preheating) and system 4 (thermal integration). The sections that follow summarise the results obtained through application of the models. Refer to sections 5.2 and 5.3 for a discussion of all results.

5.4.1 SOFC Model

This section summarises the findings from application of the SOFC model. Refer to section 5.2 for a discussion of all results.

- SOFC stack performance degraded significantly for operation on wood and miscanthus syngas in comparison to natural gas.
- Better performance was seen for wood syngas than miscanthus syngas.
- Cell voltage decreased with increasing current density *j* due to higher voltage losses.
- Voltage and efficiency dropped, power increased to a maximum and then decreased. Therefore, a trade-off must be made between voltage, efficiency and power regarding *j*.
- Steam to carbon ratio should be as low as possible but high enough to inhibit carbon deposition.
- Fuel utilisation factor should be high at ~85% and air utilisation factor should be ~16% to 20%.

5.4.2 Combined System Models: System Comparison

The four system configurations were compared in terms of performance (see section 5.3.2).

- The SOFC stack performs best without a recycle (i.e. system 3 layout).
- The cathode recycle and electric heater options (systems 2 and 3 respectively) were found to be energy intensive and had very high parasitic power requirement.
- Regarding plant net efficiencies ($\eta_{el,net}$ and $\eta_{CHP,net}$), systems 1 and 4 were more attractive than systems 2 and 3.
- System 4 experienced a drop in gasifier performance leading to lower $\eta_{el,net}$ in comparison to system 1; however, this would be offset by the rise in $\eta_{CHP,net}$ and cost savings (no need for the gasifier CZ oxidant heat exchanger).
- The same trends were seen for the *j* sensitivity analysis for all systems.
- The limiting *j* value was much lower for system 2 compared to system 1 and power output dropped more rapidly with a reduced peak power at a lower *j*. Parasitic power was considerably higher over the entire *j* range. A cathode recycle is not an attractive alternative to the base case anode recycle system.
- The SOFC stack operated at higher efficiency for system 3; however, this was outweighed by increased parasitic power, which led to lower $\eta_{el,net}$ and $\eta_{CHP,net}$ over the complete *j* range. An electric heater is not an attractive alternative for syngas preheating.
- The SOFC stack performance remained unchanged for system 4 with reference to system 1. System 4 gasifier performance was lower over the entire *j* range; however, there was a substantial increase in $\eta_{CHP,net}$. This and the cost savings make thermal integration attractive.

5.4.3 Combined System Models: System Performance Enhancement

Potential improvements to the system configurations were investigated (see section 5.3.3).

Lowering syngas preheat temperature

- Reduction in syngas preheat temperature resulted in an acceptable anode inlet/outlet temperature difference for all systems.
- Lowering the syngas preheat temperature was an effective method to decrease SOFC STCR for systems 1 and 4.
- SOFC stack performance improved for all systems and systems 1A, 3A and 4A SOFC stack performance were very similar.
- The increase in performance for systems 1A and 4A was solely due to the reduction in SOFC STCR and not the drop in syngas preheat temperature.
- System 3A parasitic power dropped substantially; however, the anode recycle was still more efficient for syngas preheating (compared to electric heater).
- System 3A would be appealing if it was desirable to reduce plant complexity (removal of the recycle).
- System 1A achieved the highest $\eta_{el,net}$ while system 4A had the greatest $\eta_{CHP,net}$.
- Lowering the syngas preheat temperature is highly recommended.

Lowering syngas and cathode air preheat temperature

- Reduction in cathode air preheat temperature resulted in a large cathode inlet/outlet temperature difference for all systems, which could cause damaging thermal gradients within the SOFC stack.

- SOFC stack performance improved for all systems and systems 1B, 3B and 4B SOFC stack performance were almost identical.
- System 4B displayed better gasifier performance (higher CZ oxidant temperature).
- There was an enormous increase in $\eta_{CHP,net}$ for all systems.
- System 1B achieved the highest $\eta_{el,net}$ while system 4B had the greatest $\eta_{CHP,net}$.
- In comparison, syngas preheat temperature reduction was superior in terms of system performance enhancement as it had a strong positive impact and it resulted in an acceptable anode inlet/outlet temperature difference.

5.4.4 Combined System Models: Sensitivity Analyses Results and Discussion

Combined system models were employed to investigate the influence of the main operating parameters on system performance (refer to section 5.3.4).

- System 1 because it had superior performance to the other system configurations was chosen to perform sensitivity analyses of the main operating parameters.
- Nernst voltage remained constant over the j range. All three of the voltage losses rose with increasing j. There must be a trade-off between voltage, efficiency and power regarding j. $\eta_{el,net}$ and $\eta_{CHP,net}$ fell substantially with j.
- STCR had a substantial negative impact on SOFC efficiency and plant net efficiencies. It is therefore desirable to operate the plant at low STCR.
- U_f is limited to 0.85 for system 1. SOFC efficiency displayed a huge increase with rising U_f. $\eta_{el,net}$ and $\eta_{CHP,net}$ were very sensitive to variation in U_f; $\eta_{el,net}$ increased and $\eta_{CHP,net}$ decreased with increasing U_f. It is recommended to operate the SOFC

stack at high U_f. U_f can change the mode of operation of the plant as it has a very strong influence on the net power-to-heat ratio.

- U_a is limited to 0.16 for system 1. Rising U_a led to slight decreases in voltage and SOFC efficiency. $\eta_{el,net}$ remained fairly constant; conversely, there was a significant drop in $\eta_{CHP,net}$.
- T_g should be above 775 °C. T_g had a very strong impact on syngas composition and LHV. Increasing T_g had a favourable influence on gasifier performance and LHV; *CGE* increased to a peak and then fell. SOFC and overall plant performance results suggest that T_g should be kept as low as possible. SOFC efficiency, $\eta_{el,net}$ and $\eta_{CHP,net}$ fell significantly with rising T_g. As a low T_g would lead to high tar levels, it is recommended to operate the gasifier in the range 850 to 900 °C.
- Biomass moisture content had little impact on syngas composition and LHV but very strong influence on *CGE*. It had little effect on SOFC stack performance but had a strong unfavourable effect on the plant net efficiencies. The results indicated that moisture is of extreme importance and should be as low as possible.
- STBR had significant impact on syngas composition and LHV but little influence on *CGE*. It had a limited impact on SOFC stack performance and plant net efficiencies. It is recommended to operate the gasifier at low STBR.
- Syngas composition and LHV had a weak dependence on air-fuel ratio; however, *CGE* dropped substantially over the range. Air-fuel ratio had no impact on SOFC performance, but $\eta_{el,net}$ fell and $\eta_{CHP,net}$ rose with increasing air-fuel ratio. It should be kept as low as possible.
- Gas composition and LHV remained unchanged with a rise in gasification steam temperature; however, *CGE* increased slightly. There was minimal effect on plant

net efficiencies and no effect on SOFC performance. It may be desirable with regard to plant simplification and cost savings to remove the steam superheater.

- Gasifier CZ air preheat temperature is limited to 650 °C. Preheating the air caused slight changes in syngas composition and increased LHV and *CGE*. $\eta_{el,net}$ and $\eta_{CHP,net}$ had weak dependence but experienced a small increase and decrease respectively. Air temperature had no effect on SOFC performance. Gasification air preheating was more attractive than gasification steam superheating.
- The anode recycle is not a practical method of syngas preheating for cleaning temperatures of 600 to 700 °C and the system 3 layout should be employed. SOFC stack performance improved with increasing cleaning temperature and plant net efficiencies displayed strong dependence; $\eta_{el,net}$ increased and $\eta_{CHP,net}$ fell. High temperature cleaning appears to be very attractive as it offers the potential to reduce plant complexity (no need for recycle) and improves performance significantly. However, there are limits on the currently available cleaning technologies. Research efforts should continue in order to increase the temperature of syngas cleaning.
- High cleaning temperature in conjunction with reduced syngas preheat temperature offer further increases in $\eta_{el,net}$. This demonstrates the great potential that BG-SOFC systems have for achieving high operating efficiency.
- For a scale of 1 MWe, the mass flow rates, power levels, etc., were eight orders of magnitude greater than system 1 base case results. The performance indicators such as plant net efficiency, SOFC efficiency, etc., were equal to the base case values. Analogous results were obtained for the 500 kWe system; the difference between the two scales was that mass flow rates and power levels, etc., were four orders of magnitude greater than the base case system.

6 ENGINEERING ECONOMIC MODELLING

6.1 Chapter Introduction

A technical analysis of a power generation or CHP system alone is not sufficient to make informed decisions on whether to proceed with a project; an economic analysis is always necessary. The preceding chapter presented results from the technical analysis of the investigated BG-SOFC systems. This chapter provides details on the developed engineering economic model and presents results and findings through its application.

A description of the methodology employed to conduct the economic analysis of the BG-SOFC systems is provided. Then the engineering economic model is presented including explanation of all model inputs and assumptions. The results and findings from various sensitivity analyses are presented and discussed in the final section.

6.2 Methodology

There are numerous methods available to perform economic analysis of power generation and CHP systems. Some frequently applied methods include the simple payback period, internal rate of return, net present value (*NPV*) and levelised cost of electricity (*LCoE*) [308]. The *LCoE* method was applied in this research work. This method is an economic assessment of the cost of the system including all costs over its lifetime: initial investment, operating and maintenance (O&M), cost of fuel and cost of capital. The *LCoE* is the minimum price at which the electricity must be sold for the project to break-even [309]. With reference to Eq. 6.1, *NPV* will equal zero at the break-even point (net revenue over the project lifetime must equal the initial investment for the project to break-even). The *NPV*, which is defined as the present value (*PV*) of net

cash inflows generated by the project minus the initial investment, is given by the following equation [310]:

$$NPV = \left[\frac{R_0}{(1+DR)^0} + \frac{R_1}{(1+DR)^1} + \ldots \frac{R_z}{(1+DR)^z} \right] - CapEx \qquad \text{Eq. 6.1}$$

where R_0 is the net revenue for the first period, R_1 for the second, etc., *DR* is the discount rate (%) and *CapEx* is the initial capital expenditure for the project (i.e. the initial investment). *DR* considers risk as well as interest rates and inflation; it is the time value of money. The *NPV* accounts for the time value of money by using discounted cash inflows [310]. A positive *NPV* indicates a worthwhile investment; a project having a negative *NPV* would be rejected. Equation 6.1 can be re-written as [311]:

$$NPV = (CoE \cdot PV_{el}) - PV_{costs} \qquad \text{Eq. 6.2}$$

where *CoE* is the cost of electricity, PV_{el} is the present value of electricity output (MWh) over the project lifetime and PV_{costs} is the present value of net costs (i.e. the gross costs, made up of *CapEx*, fuel cost and O&M costs, minus revenue from the sale of heat). PV_{el} and PV_{costs} are determined using the general *PV* equation:

$$PV_x = \sum_{z=0}^{15} \left[\frac{x}{(1+DR)^z} \right] \qquad \text{Eq. 6.3}$$

where *x* represents the parameter (in this case electricity output or net costs) to be converted to present values and *z* is the time period (i.e. year zero, one, two, etc.). To obtain an expression for *LCoE*, Eq. 6.2 is re-arranged and *NPV* set to zero, which gives:

$$LCoE = \frac{PV_{costs}}{PV_{el}} \qquad \text{Eq. 6.4}$$

When the *LCoE* method is employed the *NPV* will equal zero (as explained above) and the internal rate of return will equal the employed discount rate. Calculating the simple payback period, which is the ratio of initial investment to the net revenue per period, will give a duration less than the assumed project lifetime even though it is clear that the true payback period will be equal to the project lifetime because the *LCoE* method assumes that the project breaks even. The reason for this disparity between predicted and true payback period is that the simple payback period method does not consider the decreasing value of money with time.

6.3 Engineering Economic Model

A Microsoft Excel spreadsheet model was developed to compute the *LCoE* of the investigated BG-SOFC CHP systems. The model is capable of calculating the *LCoE* for other CHP technologies as shown in section 6.4. The model was based on the following assumptions:

- Construction year is 2012 (to suit available economic data).
- Plant lifetime of fifteen years [175, 176, 200, 256, 312].
- No degradation in power output over the plant lifetime.
- Plant scale has no impact on the *LCoE*.
- Labour, utilities and overheads included in assumed O&M costs.
- Plant equipment depreciation neglected; however, salvage value of equipment was not considered.
- No equipment grants; Irish CHP Deployment Programme ended in 2011 [313].

Referring to Figure 6.1, the model was designed in such a way that the *LCoE* depends on the BG-SOFC system performance (i.e. the net AC electrical efficiency). This was accomplished through the calculation of the heat rate, which is equal to 3,600 divided by the net AC electrical efficiency. Heat rate is defined as the energy needed to produce 1 kWh of electricity (note: 1 kWh = 3,600 kJ). This heat rate was then employed to determine the biomass fuel energy input, which in turn affects the cost associated with the biomass fuel and *LCoE*. System 1 base case performance results (Table 5.5) were used as inputs for the base case engineering economic model. The discount rate was set at 10% [256, 314, 315]. Reported values ranged between 5% and 15% [316-320]. Net electricity output is computed using the system performance data. Appropriate capacity factors for electricity and heat were specified (CF_{el} = 80% and CF_{heat} = 50%). Multiplying the assumed capacity factors by the number of hours in a year gives the plant annual operating hours (using CF_{el}) and the number of hours that the plant operates in CHP mode (using CF_{heat}). A CF_{el} of 80% was chosen considering experience at the Güssing CHP plant (BG-gas engine) [321]. In addition, Brammer and Bridgwater [100] and Jin et al. [266] assumed this value for BG-gas engine and BG-SOFC systems respectively. CF_{heat} is significantly lower because generally heat cannot be sold during summer (unless the heat is used for an industrial process). The heat sale price was taken as 40 €/MWh [258]. This is conservative considering the high price of domestic heat in Ireland; 87.20 €/MWh (excluding carbon tax) assuming 75% gas boiler efficiency and using the average natural gas price reported by the SEAI [306]. As discussed in chapter two, there is no district heating network in Ireland and therefore no feed in tariff exists.

Figure 6.1 Spreadsheet engineering economic model (base case)

Construction year = 2012 (to suit available economic data)

System performance

Net AC electrical efficiency (LHV)	25.3%	
AC power (gross)	110.4	kWe
Parasitic power	21.63	kWe
Recoverable heat	155.15	kWth

Economic model inputs

Discount rate	10%	
Electricity output (net)	0.08877	MWe
CF (electricity)	80%	
Heat output	0.15515	MWth
Heat sale price	40	€/MWh
CF (heat)	50%	
Hours per year	8760	
Heat Rate (net LHV)	14229.25	kJ/kWh
CapEx	6,365,108	€/MWe
Fuel cost	9.68	€/GJ
O&M (4% of CapEx)	22,601.23	€

Calculations

Year	**0**	**1**	**2**	**3**	**4**	**5**	**6**	**7**	**8**	**9**	**10**	**11**	**12**	**13**	**14**	**15**
Energy input/output																
Annual Electricity Output (MWh)	0.00	622.10	622.10	622.10	622.10	622.10	622.10	622.10	622.10	622.10	622.10	622.10	622.10	622.10	622.10	622.10
Annual Heat Output (MWh)	0.00	679.56	679.56	679.56	679.56	679.56	679.56	679.56	679.56	679.56	679.56	679.56	679.56	679.56	679.56	679.56
Biomass input (GJ)	0.00	8852.02	8852.02	8852.02	8852.02	8852.02	8852.02	8852.02	8852.02	8852.02	8852.02	8852.02	8852.02	8852.02	8852.02	8852.02
Costs (€)																
CapEx	565030.64	0.00	0.00	0.00	0.00	0.00	**232143.14**	0.00	0.00	0.00	0.00	**232143.14**	0.00	0.00	0.00	0.00
Biomass	0.00	85668.72	85668.72	85668.72	85668.72	85668.72	85668.72	85668.72	85668.72	85668.72	85668.72	85668.72	85668.72	85668.72	85668.72	85668.72
O&M	0.00	22601.23	22601.23	22601.23	22601.23	22601.23	22601.23	22601.23	22601.23	22601.23	22601.23	22601.23	22601.23	22601.23	22601.23	22601.23
Gross Costs (€)	€565,030.64	€108,269.94	€108,269.94	€108,269.94	€108,269.94	€108,269.94	€340,413.09	€108,269.94	€108,269.94	€108,269.94	€108,269.94	€340,413.09	€108,269.94	€108,269.94	€108,269.94	€108,269.94
Heat Revenue (€)	€0.00	€27,182.28	€27,182.28	€27,182.28	€27,182.28	€27,182.28	€27,182.28	€27,182.28	€27,182.28	€27,182.28	€27,182.28	€27,182.28	€27,182.28	€27,182.28	€27,182.28	€27,182.28
Net Costs (€)	€565,030.64	€81,087.66	€81,087.66	€81,087.66	€81,087.66	€81,087.66	€313,230.81	€81,087.66	€81,087.66	€81,087.66	€81,087.66	€313,230.81	€81,087.66	€81,087.66	€81,087.66	€81,087.66

PV of costs	€1,394,193.36	
PV of electricity	4,731.74	MWh
LCoE	294.65	€/MWh
NPV	€0.00	

There is great uncertainty regarding the cost of SOFCs given that the technology is still in development and there is no established market. In view of this a number of different prices were utilised in the model. The lowest of these, 1,170 US$/kWe (2002 $), was reported by Autissier et al. for the SPGI 220 kWe SOFC-GT system [322]. Two other prices, 4,600 US$/kWe (2007 $) and 3,000 US$/kWe (2009 $), were published by the California Stationary Fuel Cell Collaborative [323]. This report was compiled through interviews with fuel cell manufacturers and the prices represent an average cost for all fuel cells on the market (i.e. all fuel cell technologies). These costs were converted to 2012 figures using the Chemical Engineering Plant Cost Index (CEPCI) [324]. This method has been widely applied for adjusting costs of biomass/coal gasification and SOFC plants [100, 258, 273, 325, 326]. The following annual average CEPCI values were used in the calculations: 395.6 (year 2002), 525.4 (year 2007), 521.9 (year 2009) and 584.6 (year 2012). To convert the costs, the historical prices were multiplied by the ratio CEPCI (year 2012) over the applicable historical CEPCI value. For example for 1,170 US$/kWe (2002 $), this was multiplied by the factor (584.6/395.6) giving a 2012 price of 1,729 US$/kWe. The final step was to convert US$ to € and this was done utilising an average exchange rate for 2012 of 1.285 [327]. The calculated prices for the SOFC stack *CapEx* are shown in Figure 6.6. It should be noted that all specific costs (€/kWe) reported here were assumed to be the installed cost including balance of plant components. Two companies (Repotec Renewable Power Technologies and Ortner Anlagen) that supply Güssing CHP type plants were contacted and they provided cost estimates between 4,500 and 5,000 €/kWe (includes syngas cleaning system and gas engine, etc.) [328, 329]. The average specific cost of 4,750 €/kWe was used for the model. 1,000 €/kWe was subtracted (assumed high end gas engine cost) and the relevant SOFC stack cost was added in its place giving a rough

estimate for the specific cost of the BG-SOFC CHP system. For the base case, the SOFC stack cost of 2,615 €/kWe was added to 3,750 €/kWe, giving a system cost of 6,365 €/kWe (as seen in Figure 6.1).

Table 6.1 Biomass fuel price conversion

Year	**CPI**[a]	**Forest Wood Chip 50% Moisture (€/t)**	**Forest Wood Chip 35% Moisture (€/t)**	**Energy Crop (lower) 20% Moisture (€/t)**	**Energy Crop (average) 20% Moisture (€/t)**	**Energy Crop (upper) 20% Moisture (€/t)**
2005	2.5%	-	-	75.10	105.10	135.10
2006	4.0%	-	-	78.10	109.30	140.50
2007	4.9%	-	-	81.93	114.66	147.39
2008	4.1%	-	-	85.29	119.36	153.43
2009	-4.5%	-	-	81.45	113.99	146.53
2010	-1.0%	70.00	110.00	80.64	112.85	145.06
2011	2.6%	71.82	112.86	82.73	115.78	148.83
2012	1.7%	**73.04**	**114.78**	**84.14**	**117.75**	**151.36**

[a] [88]

The fuel cost was calculated on a €/GJ basis (LHV) using quoted prices from the biomass supply industry (forest wood chip) and prices reported in literature (willow wood chip and miscanthus). Irish forest wood chip was between 70 and 110 €/t (2010 €), depending on moisture content (50% to 35%) [76, 306, 307]. These quoted prices were converted to 2012 € employing the consumer price index (CPI) method as shown in Table 6.1. Energy crop prices (willow chips and miscanthus) fell into the range of 75.10 to 135.10 €/t (2005 €) delivered [86, 89]. These prices were converted to an energy basis (€/GJ) using published LHV values for Sitka spruce, willow wood chips and miscanthus [94], accounting for moisture content. These prices are presented in Figure 6.7 (section 6.4).

With reference to the calculations section of the spreadsheet shown in Figure 6.1, annual electricity output in MWh is equal to net electricity output (MWe) multiplied by the plant operating hours (CF_{el} × 8,760 hours). Annual heat output is calculated in a similar fashion using heat output (MWth) and CF_{heat}. Biomass energy input (GJ) is the product of the annual electricity output and the heat rate.

CapEx for year zero represents the initial capital investment and is equal to the specific plant cost (6,365 €/kWe for base case) multiplied by the net electricity output. There are some additional *CapEx* costs in year six and eleven. These costs are incurred because the SOFC stack life is 40,000 operating hours [176] and therefore it is necessary to replace the SOFC stack during these years. The cost of SOFC stack replacement was calculated using the assumed specific cost (€/kWe) and net electricity output. It should be noted that even though these costs are labelled as *CapEx*, they are not considered part of the plant initial investment and therefore their *PV* is considered in the *LCoE* calculation. The biomass costs were determined by simply multiplying the biomass energy input (GJ) by the fuel cost (€/GJ). O&M costs were computed assuming they were equal to 4% of the initial *CapEx* [100, 258, 266, 293, 312]. The sum of these three costs gives the annual gross costs from which the heat revenue (product of annual heat output in MWh and heat sale price) is subtracted giving the yearly net costs.

Finally, Eq. 6.3 and 6.4 are employed to calculate the *PV* of net costs and electricity output (MWh) and the *LCoE*. As expected, Eq. 6.2 gives a *NPV* of zero. It is clear that the engineering economic model described here is based on a large number of assumptions, which means there will be high uncertainty with any results; therefore, the results may be considered indicative only.

6.4 Results and Discussion

The model inputs and results displayed in Figure 6.1 are considered the base case engineering economic model conditions. Recall, the base case BG-SOFC system 1 performance results (Table 5.5) were used as inputs. The computed *LCoE* for these conditions is 294.65 €/MWh, which is very high and well above the 2012 Irish renewable energy feed in tariff (REFIT) for small scale biomass CHP (≤ 1.5 MWe 143.64 €/MWh) [61]. This result implies that the CHP system is far from commercially viable. The contribution of each cost to this *LCoE* value is shown in Figure 6.2. From the figure it is clear that lowering the *CapEx* or fuel cost will have considerable effect on the *LCoE*.

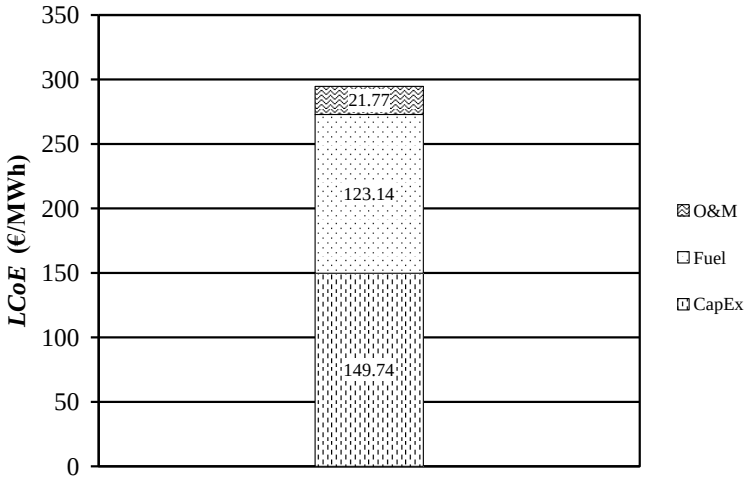

Figure 6.2 Cost contributions to LCoE (base case)

As discussed previously, there is a high level of uncertainty with the engineering economic model and it was therefore deemed appropriate to carry out sensitivity analyses of model inputs and other investigations such as best case scenario (based on findings from sensitivity analyses) and technology comparison (gas engine, ORC, steam turbine, etc.).

Discount rate

As mentioned previously, reported values for the discount rate ranged between 5% and 15%. A sensitivity analysis for this range was conducted and the results are displayed in Figure 6.3. *LCoE* was found to be very sensitive to the assumed *DR*, increasing 61.30 €/MWh over the *DR* range of 5 to 15%. The rise in *LCoE* is caused by decreases in PV_{el} and PV_{costs}. This investigation clearly demonstrates the level of uncertainty in the engineering economic model. Projects based on BG-SOFC technology would be regarded as high risk; therefore, the relatively high assumed *DR* of 10% can be considered realistic.

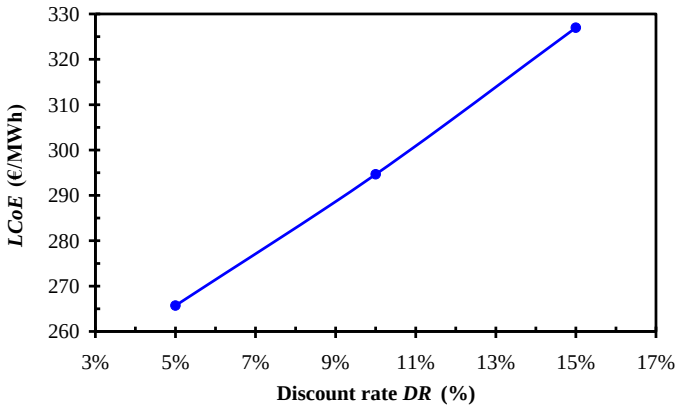

Figure 6.3 Effect of discount rate on LCoE

Electricity and heat capacity factors

Figure 6.4 (a) depicts the effects of CF_{el} on the economics of the system. CF_{el} was assumed to have no impact on SOFC stack replacement years (i.e. replacements still take place in years six and eleven). The assumption is valid even at CF_{el} = 70%, at this capacity factor the first SOFC stack could last until year seven; however, a second replacement would still be needed in year twelve. As the plant lifetime is fixed at fifteen years there would be no benefit in changing the replacement years and therefore they

were held constant. Annual electricity output in MWh increases with CF_{el} as the plant operates for a greater amount of hours in the year. Biomass fuel costs also rise, again due to the increase in operating hours. It is clear that CF_{el} has significant influence on *LCoE* (drops ~40 €/MWh over CF_{el} range) and should be as high as possible. CF_{el} is limited by plant availability, which depends on equipment maintenance requirements. Higher CF_{el} (~90%) may be feasible for BG-SOFC plants in comparison to BG-gas engine technology as SOFCs have no moving parts and require less maintenance [320, 330].

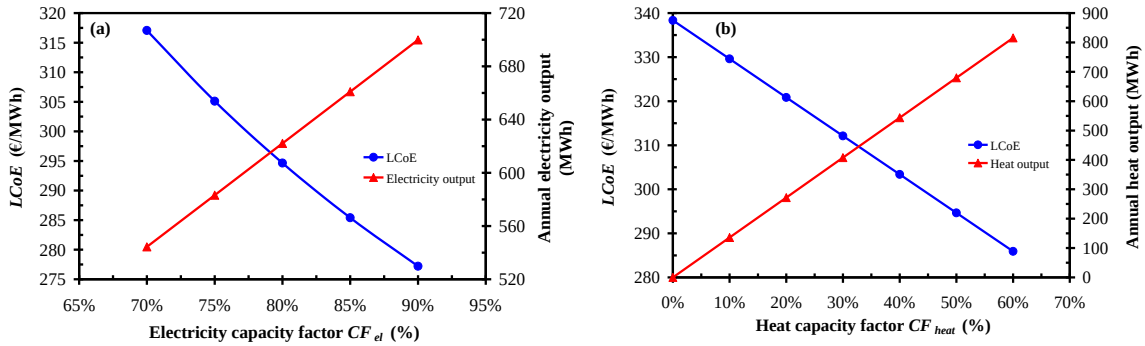

Figure 6.4 Effect of (a) electricity capacity factor on LCoE and annual electricity output and (b) heat capacity factor on LCoE and annual heat output

Figure 6.4 (b) reveals the importance of heat revenue, which depends on CF_{heat}, in terms of the commercial viability of the plant. If the plant operates in electricity only mode (i.e. CF_{heat} = 0%), *LCoE* is very high at 338.30 €/MWh. CF_{heat} should be as high as possible but is dependent upon the heat requirements of the customer.

Heat sale price

Both PV_{costs} and *LCoE* decrease linearly with increasing heat sale price, as shown in Figure 6.5. As the annual revenue from the sale of heat rises (€13,591 to €54,365 for

heat sale price of 20 and 80 €/MWh respectively), PV_{costs} decrease. *LCoE* experiences a substantial drop of 65.50 €/MWh over the heat sale price range. These results convey the importance of a high heat sale price on CHP plant economics.

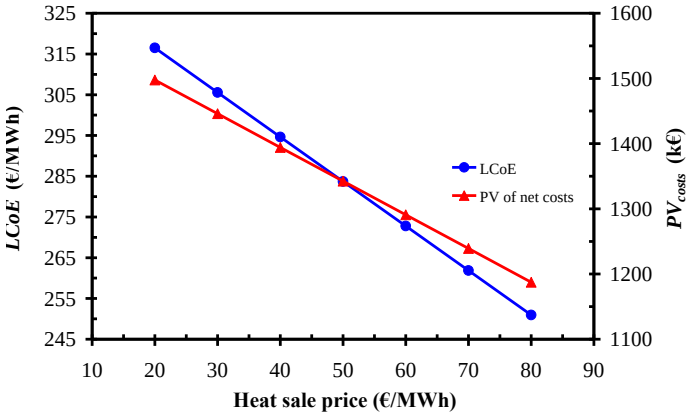

Figure 6.5 Effect of heat sale price on LCoE and present value of net costs

SOFC stack *CapEx*

The *LCoE* results from the SOFC stack *CapEx* sensitivity analysis are displayed in Figure 6.6. This sensitivity analysis was carried out because of the uncertainty regarding the cost of SOFCs. The first three specific cost values were chosen as described in section 6.3. The lowest specific cost of 1,000 €/kWe was included in the investigation as it is typical for a high end gas engine and should be a realistic cost target for SOFC developers. The results show that SOFC stack *CapEx* has enormous significance with respect to *LCoE* (difference of 124.20 €/MWh between highest and lowest *CapEx*). This analysis demonstrates the importance of lowering SOFC manufacturing costs in order to improve SOFC based power/CHP plant economics.

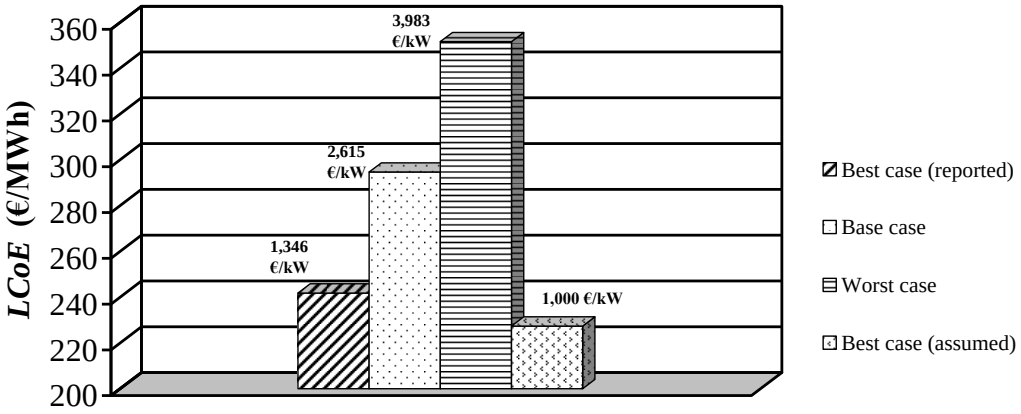

Figure 6.6 Effect of SOFC stack CapEx on LCoE

SOFC stack lifetime

A major goal of the fuel cell industry is to increase the lifetime of their cells, i.e. reduce fuel cell degradation with time. Since the SOFC stack accounts for 41.1% of the initial plant *CapEx*, it was deemed appropriate to examine the effect of stack lifetime on plant economics. The model was run assuming an increased stack lifetime of 84,000 hours [11] (base case lifetime = 40,000 hours). This meant that the SOFC stack required replacement only once during the plant lifetime (in year eleven) and this led to a reduction in net costs and *LCoE* (dropped from 294.65 to 266.95 €/MWh). Theoretically, plant lifetime could be extended beyond fifteen years (> 20 years) if fuel cell lifetime could be increased. In conclusion, extending SOFC stack lifetime is very attractive in view of its impact on *LCoE* and the possibility of extending plant lifetime.

Fuel cost

The €/GJ prices given in Figure 6.7 were calculated for Irish forest wood chip and energy crops (willow wood chip and miscanthus), as detailed in section 6.3. The low price for forest wood chip would not be feasible in practice due to the high moisture content (50%). The wood chip would need to be dried prior to gasification, which would only be commercially viable for a large scale plant. There are three prices for

each energy crop as a price range is reported in the literature (refer to section 6.3). The model was run for each fuel price and the *LCoE* was plotted. It is evident from Figure 6.7 that energy crops have potential to lower the *LCoE*. The average energy crop prices correspond to the high moisture forest wood chip price. The price of forest wood chip is increasing, the SEAI report an average price of 127 €/t (35% moisture) for Ireland in 2013 [306]. This translates to 10.71 €/GJ, which results in *LCoE* = 309.31 €/MWh. In Germany, which has a well-established biomass supply market, the price is also fairly high at 96.76 €/t (35% moisture) in 2013 [331]. Assuming the LHV is the same as for Irish forest wood chip, this leads to a price of 8.16 €/GJ and *LCoE* = 273.03 €/MWh.

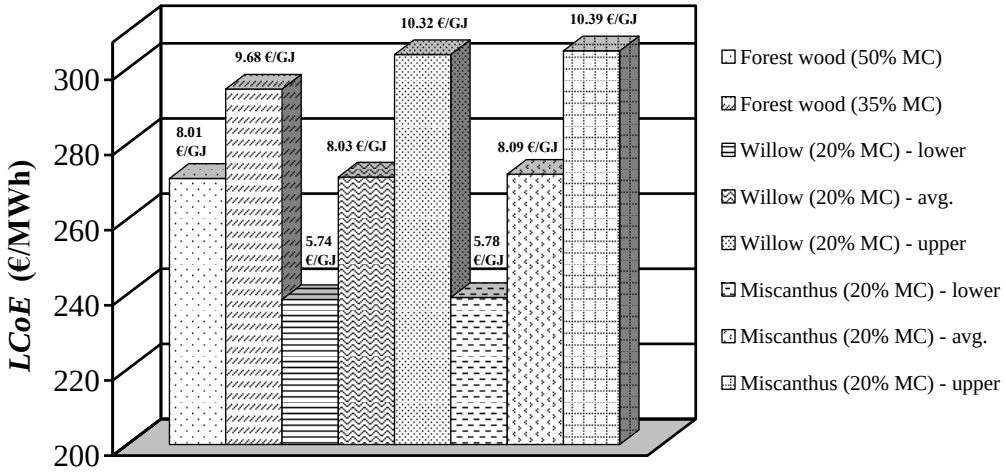

Figure 6.7 Effect of Irish biomass prices on LCoE

Figure 6.8 presents economic results for a theoretical fuel cost range of 4 to 10 €/GJ. Both PV_{costs} and *LCoE* show a strong increasing linear trend with rising fuel cost. *LCoE* rises 85.10 €/MWh over the assumed fuel cost range. The main finding from this investigation is that a reduction in the price of biomass would greatly improve the economics of BG-SOFC systems and for this reason energy crops should be investigated further as a fuel for biomass plants.

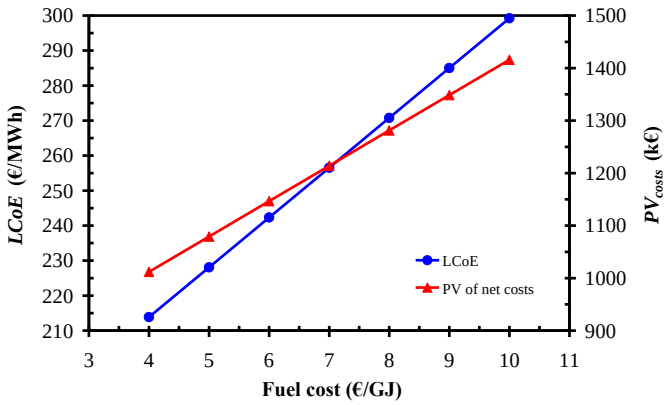

Figure 6.8 Effect of fuel cost on LCoE and present value of net costs

Operating and maintenance costs

As explained in section 6.3, O&M costs were calculated as a percentage of initial *CapEx*. The investigated range was 2% to 6%. As anticipated, an increase in O&M costs leads to increases in both PV_{costs} and *LCoE*.

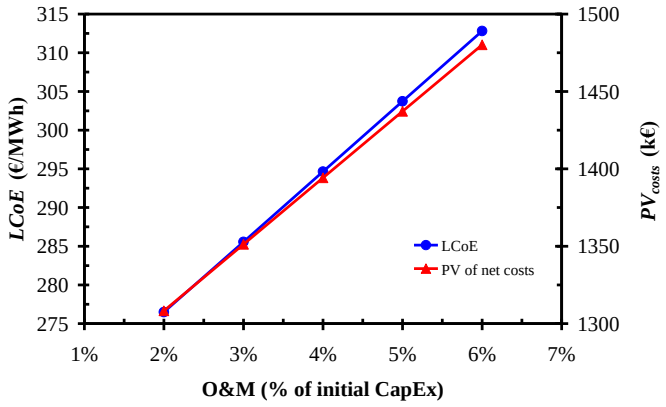

Figure 6.9 Effect of operating and maintenance costs on LCoE and present value of net costs

System performance

The results of the system performance sensitivity analysis are illustrated in Figure 6.10. Performance results (net AC electrical efficiency, AC power, parasitic power and

recoverable heat) for systems 1, 4, 1A and 4A presented previously in Tables 5.5 and 5.6 were entered into the engineering economic model. Two other cases were investigated; system 3 performance at a cleaning temperature of 700 °C and system 1 performance at a biomass moisture content of 5% (section 5.3.4). The latter two cases, although unrealistic, were included to confirm that system performance has little impact on *LCoE* (these cases have very high net AC electrical efficiencies above 30%). The greatest difference in *LCoE* between the realistic (i.e. achievable) systems was only 7.40 €/MWh (system 4 versus system 1A). The net AC electrical efficiencies for systems 4 and 1A were 24.45% and 27.28% respectively. This substantial difference in performance has minimal impact on plant economics. In conclusion, the results indicate that system performance has only a limited positive effect on *LCoE*; therefore, costs (*CapEx* and fuel costs) must decrease for BG-SOFC systems to become economically competitive. *CapEx* would vary with each system configuration (e.g. system 4 does not require a gasification air heat exchanger) but the engineering economic model developed here does not take this into account.

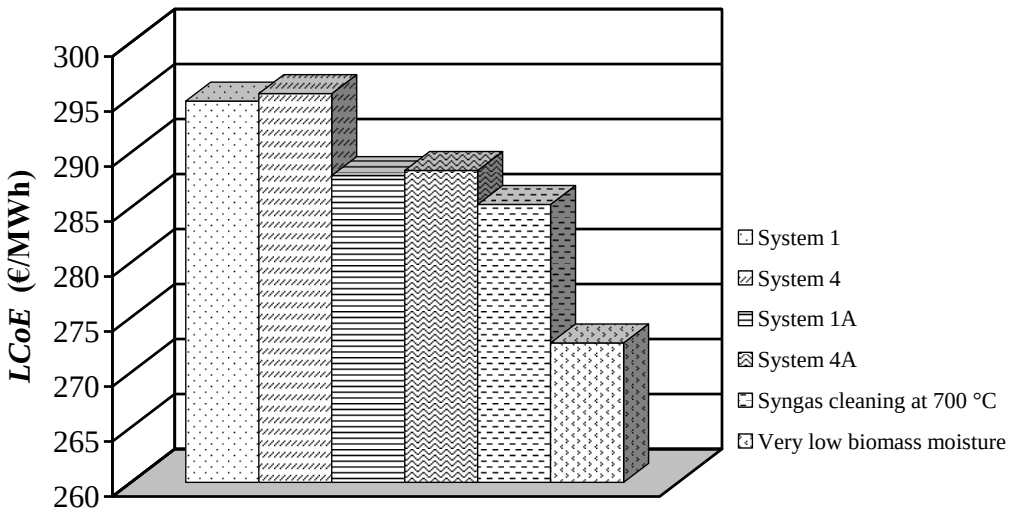

Figure 6.10 Effect of BG-SOFC system performance on LCoE

Finally, comparing system 1 and system 4 results (1A versus 4A also) it is evident that thermal integration of the gasifier and SOFC has very little negative impact on *LCoE* even though there is a drop in system performance. This reiterates the findings reported in section 5.3 regarding the attractiveness of thermal integration.

Best case scenario

This sensitivity analysis was conducted to identify the conditions necessary for the investigated CHP technology to become commercially viable. Figure 6.11 displays the required engineering economic model inputs and important results. System 1A performance data was selected as it is considered the most achievable of the high efficiency system modifications presented in section 5.3. The discount rate and capacity factors were left at their base case values. Heat sale price was increased to 60 €/MWh, which is high but still below the Irish domestic natural gas heat price (section 6.3). A more favourable *CapEx* of 4,500 €/kWe was assumed. This figure stems from the lowest quoted price for a Güssing CHP type plant (4,500 €/kWe including gas engine) and the lowest investigated SOFC stack price of 1,000 €/kWe. A low biomass fuel price of 6 €/GJ was chosen. O&M costs remained at the base case 4% of initial *CapEx* and it was assumed that only one SOFC stack replacement was needed during the lifetime of the plant. The calculated *LCoE* of 145.78 €/MWh is below the Irish 2014 REFIT of 146.812 €/MWh [61]. The results from this analysis reveal that the fuel cost is the determining factor regarding *LCoE*. Even with high system performance, high heat sale price and lower *CapEx* the fuel price must be low at 6 €/GJ in order to achieve a *LCoE* just below the current Irish REFIT.

Net AC electrical efficiency (LHV)	27.3%	
AC power (gross)	110.4	kWe
Parasitic power	20.34	kWe
Recoverable heat	145.78	kWth
Discount rate	10%	
Electricity output (net)	0.09006	MWe
CF (electricity)	80%	
Heat output	0.14578	MWth
Heat sale price	60	€/MWh
CF (heat)	50%	
Heat Rate (net LHV)	13196.48	kJ/kWh
CapEx	€4,500,000.00	€/MWe
Fuel cost	6	€/GJ
O&M (4% of CapEx)	16,210.80	€
Annual Electricity Output (MWh)	631.14	
Annual Heat Output (MWh)	638.52	
Biomass input (GJ)	8328.83	
PV of costs	€699,820.00	
PV of electricity	4800.50	MWh
LCoE	145.78	€/MWh

Figure 6.11 Best case scenario model inputs and results

Technology comparison and model verification

This investigation was carried out to check the accuracy of the engineering economic model by comparing its results with published results (based on actual CHP plant data) [127] and to contrast the economic performance of different CHP technologies. Input data for each technology (excluding BG-SOFC) was taken from the paper by Bolhàr-Nordenkampf et al. [127] with some data based on assumptions. The data displayed in italics in Figure 6.12 was published by Bolhàr-Nordenkampf et al. [127]. Net electrical efficiency was calculated using Eq. 5.28 and the heat rate was determined as described in section 6.3 (both highlighted in Figure 6.12). The remaining data not in italics were assumed values.

	BG-SOFC		Güssing CHP Plant		Fixed Bed Gasification		ORC		Stirling Engine		Steam Turbine	
Biomass input power	350.81	kWth	*8000*	kWth	*2000*	kWth	*8000*	kWth	*900*	kWth	*17000*	kWth
AC power (gross)	110.4	kWe	*2000*	kWe	*580*	kWe	*1130*	kWe	*50*	kWe	*2700*	kWe
Parasitic power	21.63	kWe	*300*	kWe	*100*	kWe	*180*	kWe	*30*	kWe	*260*	kWe
Recoverable heat	155.15	kWth	*4500*	kWth	*720*	kWth	*6100*	kWth	*800*	kWth	*12000*	kWth
Net AC electrical efficiency (LHV)	25.30	%	21.25	%	24	%	11.88	%	2.22	%	14.35	%
Heat Rate (net LHV)	14,229.25	kJ/kWh	16,941.18	kJ/kWh	15,000.00	kJ/kWh	30,303.03	kJ/kWh	162,162.16	kJ/kWh	25,087.11	kJ/kWh
CapEx	6,365,108.07	€/MWe	4,750,000.00	€/MWe	*5,172,000.00*	€/MWe	*4,630,000.00*	€/MWe	*8,784,000.00*	€/MWe	*2,637,000.00*	€/MWe
O&M (% of CapEx)	4	%	5	%	4	%	2	%	2	%	2	%

Figure 6.12 Technology comparison and model verification input data

The BG-SOFC system performance data, *CapEx* and O&M match those of the base case (Figure 6.1). The *CapEx* value assumed for the Güssing CHP plant is the average specific cost (4,750 €/kWe) quoted by suppliers of Güssing CHP type plants (see section 6.3). Appropriate O&M percentages for the technologies (other than BG-SOFC) were selected based on O&M cost data reported in Bolhàr-Nordenkampf et al. [127]. Discount rate, capacity factors, heat sale price and fuel cost were all held constant at the base case values assumed in this work for the BG-SOFC systems (refer to section 6.3). Plant lifetime was set at fifteen years.

The model results for each technology show fairly good agreement with Bolhàr-Nordenkampf et al. [127]. Any discrepancy could be put down to differences in model inputs (e.g. a much higher fuel cost was assumed in this research work). It is clear from Figure 6.13 that the BG-SOFC technology is the most expensive (apart from Stirling engine technology, which is by far the most expensive). As expected, the most developed technology (steam turbine) was the least expensive. It is interesting to note that the Güssing CHP, fixed bed gasification and ORC technologies all achieve comparable *LCoE* values.

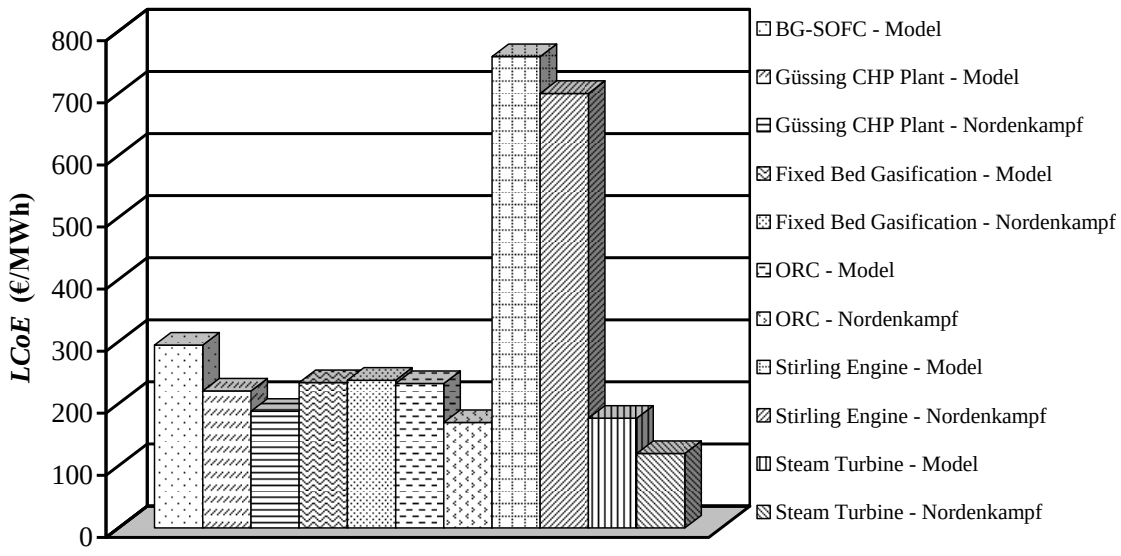

Figure 6.13 Technology comparison and model verification

6.5 Chapter Summary

This chapter presented the developed spreadsheet based engineering economic model. This section summarises the findings from application of the model.

- It was necessary to base the engineering economic model on a large number of assumptions; therefore, the results are considered indicative only.
- Economic results for base case conditions revealed BG-SOFC CHP systems to be far from commercially viable in an Irish context.
- *LCoE* was found to be very sensitive to discount rate.
- Both electricity and heat capacity factors should be as high as possible to improve plant economics. They are limited, however, by plant availability and user heat requirements.
- Heat revenue and thus heat sale price was found to be of utmost importance with respect to CHP plant economics.
- SOFC stack capital investment requirement was shown to have enormous impact on *LCoE* and therefore fuel cell developers need to lower manufacturing costs.
- SOFC stack lifetime extension was deemed very attractive in view of its influence on *LCoE* and the possibility of extending plant lifetime.
- Biomass fuel cost was discovered to be critical to the commercial viability of these plants. Energy crops have great potential in this regard.
- BG-SOFC system performance had only a limited positive effect on *LCoE*. This revealed that costs (*CapEx* and fuel costs) must decrease if these systems are to become economically competitive.
- Thermal integration between the SOFC and gasifier had very little negative impact on *LCoE* and therefore is attractive.

- Biomass fuel cost was identified as the determining factor regarding plant commercial viability.
- The predictions of the engineering economic model compared well with results published elsewhere for various CHP technologies [127].
- BG-SOFC technology was the most expensive of the investigated CHP technologies (excluding Stirling engine technology).

7 CONCLUSIONS AND FURTHER RESEARCH

7.1 Chapter Introduction

The overall aim and objectives stated in chapter one were achieved; therefore, the research project may be deemed successful. This chapter provides a summary of the conclusions drawn from analysis of the model results including the standalone and combined system technical models (chapters four and five) and the engineering economic model (chapter six). Firstly, the main findings of the research work are given. Then areas of possible further research are identified and briefly discussed and finally an outlook is presented.

7.2 Main Findings

The main finding from application of the technical models of the BG-SOFC systems is that biomass gasification and solid oxide fuel cell technologies are ideally matched and when integrated have the potential to achieve very high efficiencies (even at small scale). This makes these systems very attractive compared to traditional biomass combustion based systems (only efficient at large scale). High efficiency at small scale is important as scale is limited by biomass supply logistics. CHP plants based on BG-SOFC technology can contribute significantly to Irish and EU energy efficiency and high efficiency CHP targets.

Regarding the economic analysis of these systems, they are not currently commercially viable. Capital costs and biomass fuel prices must fall dramatically if these systems are ever to become competitive with traditional fossil fuel power generation.

If biomass CHP is to make any significant contribution in Ireland the government must provide financial supports for its deployment, for installation of district heating networks to provide large heat loads, provide financial incentives to Irish farmers to grow energy crops and to private forest owners to encourage thinning, which would increase the availability of biomass and thus stimulate a drop in biomass prices. Other major findings include:

- Heat revenue and thus heat sale price is of utmost importance with respect to CHP plant economics.
- Biomass fuel cost is critical to the commercial viability of these plants. Energy crops have great potential in this regard.
- Thermal integration between the SOFC and gasifier leads to a slight drop in plant performance (electrical) but has very little negative impact on levelised cost of electricity and therefore is attractive.
- High temperature cleaning appears to be very attractive as it offers the potential to reduce plant complexity (no need for recycle) and improves performance significantly. Research efforts on hot gas cleaning should continue.
- A cathode recycle or electric heater is not an attractive alternative to the base case anode recycle system for syngas preheating.
- Steam to carbon ratio (STCR) has substantial negative impact on SOFC efficiency and plant net efficiencies. It is therefore desirable to operate at low STCR. With an anode recycle, the only way to achieve this is to reduce the syngas preheat temperature.
- Fuel utilisation factor can change the mode of operation of the plant as it has a very strong influence on the net power-to-heat ratio.

- Biomass moisture has a strong unfavourable effect on the plant net efficiencies. Moisture content is of extreme importance and should be as low as possible.
- Gasification air preheating is more attractive than gasification steam superheating.

In view of the main findings, construction of a biomass gasification plant in Ireland based on proven technologies; such as the FICFB gasifier and gas engine technologies installed at the Güssing CHP plant, is recommended. Biomass supply agreements should be made with local farmers (willow chips) and a district heating system should be installed. The successful completion of a project such as this could stimulate major growth in the bioenergy industry in Ireland.

7.3 Further Research

7.3.1 DFB Gasifier Model

Other researchers have claimed that it is possible to elevate the cold gas efficiency (*CGE*) of the FICFB gasifier from ~78% to ~89% using a pyrolysis pre-treatment step [221]. It is recommended to investigate this further through both simulation and experimental work as an increase in *CGE* of this magnitude would improve BG-SOFC system performance greatly.

The FICFB gasifier model developed in this research work neglected heat loss and as a consequence no additional/supplemental fuel was required to achieve the specified gasification temperature (i.e. fuel in addition to the char burned in the gasifier combustion zone). Experience with the real world gasifier has shown that additional fuel in the form of a syngas recycle is needed; however, in a recent article it was reported that the Güssing CHP plant gasifier requires no additional fuel for gasifier

temperatures ≤ 820 °C [136]. This could be explored through extension of the model developed here.

Furthermore, heat streams connecting the 'GASIF2' and 'GASTEMP' unit operation blocks to 'GASIF' (Figure 4.1, Figure 5.8, etc.) should be included. Inclusion of these heat streams may affect the amount of char required to achieve the specified gasification temperature (additional/supplemental fuel may be needed). This model limitation also applies to the CFB gasifier model (Figure 4.10 blocks 'HEATER' and 'GASIF2').

7.3.2 SOFC Model

A straightforward method for calculating the SOFC ohmic voltage loss was applied in this work. A much more complex but potentially more accurate method known as the equivalent circuit approach could be used [11, 240, 332]. It involves the calculation of an equivalent resistance for the SOFC components (electrodes, electrolyte and interconnection). Equivalent resistance is dependent on geometry (thickness and current flow length) and material resistivity. Investigating this may be worthwhile as the ohmic loss was found to be the most important voltage loss for tubular SOFCs.

The SOFC model could be adapted to explore other SOFC designs, such as the flattened and delta tubular SOFCs or planar SOFCs. Less operational data is available for these other designs but they are expected to have superior performance to the traditional tubular SOFCs.

CFD modelling of the SOFC stack could be employed to explore the feasibility of the performance improvement options investigated in section 5.3.3 (i.e. reduction in syngas and cathode air preheat temperatures). The CFD model would reveal the preheat temperature limits as it would display the temperature gradients within the stack.

7.3.3 Combined System Models

The predictive capability of the combined system models could be improved by simulating the gas cleanup process in more detail. The chemical reactions that occur during H_2S and HCl removal were not modelled. The processes were modelled using Aspen Plus separator blocks. If these processes were modelled in more detail, it would be possible to predict the required flow rate of adsorbent.

7.3.4 Engineering Economic Model

As BG and SOFC technologies become better established, more reliable and detailed economic data will become available and it will be possible to reduce the level of uncertainty and develop comprehensive engineering economic models.

The model could be extended to take plant scale into consideration in its calculations. Specific costs tend to decrease with increasing scale.

The engineering economic model could be integrated with the Aspen Plus models to enable the automatic transfer of BG-SOFC system performance data for the economic calculations. This would make the models more robust and would simplify economic analyses of various system layouts.

7.3.5 General Work

It is recommended to include exergy calculations in the Aspen Plus models (i.e. second law of thermodynamics analysis). Aspen Plus does not calculate the exergy of streams as there is no Aspen Plus variable that represents exergy and therefore it must be calculated manually. This could be done within Aspen Plus using Fortran code or using another computer program and linking it to the Aspen Plus models.

Full optimisation studies of the investigated BG-SOFC system configurations could be carried out.

A major drawback of tubular SOFC systems is the low power-to-weight ratio and therefore large plant footprint. A possible solution would be to install small scale SOFC CHP units in homes replacing conventional natural gas boilers. These units could then be fuelled by syngas from centralised biomass gasification plants that feed the gas into the natural gas network. This would also solve the district heating network problem in Ireland. This alternative approach should be researched in an Irish context.

7.4 Outlook

The potential for bioenergy in Ireland is exceptional and yet its contribution to date has been miniscule. Biomass gasification is regarded by many as the enabling technology for modern biomass use. It offers the possibility of conversion to electricity, heat, transport fuels and chemicals and therefore can contribute to all of Ireland's renewable energy targets. It is hoped that energy policy makers will consider the findings and recommendations of research work such as this and in doing so implement policies that will remove the barriers to bioenergy and encourage the efficient utilisation of biomass resources. The many social and economic benefits, discussed throughout the thesis, associated with bioenergy would then be realised.

REFERENCES

[1] Seitarides T, Athanasiou C, Zabaniotou A. Modular biomass gasification-based solid oxide fuel cells (SOFC) for sustainable development. Renewable and Sustainable Energy Reviews 2008;12:1251.

[2] Cordiner S, Feola M, Mulone V, Romanelli F. Analysis of a SOFC energy generation system fuelled with biomass reformate. Applied Thermal Engineering 2007;27:738.

[3] Fryda L, Panopoulos KD, Kakaras E. Integrated CHP with autothermal biomass gasification and SOFC-MGT. Energy Conversion and Management 2008;49:281.

[4] Panopoulos KD, Fryda LE, Karl J, Poulou S, Kakaras E. High temperature solid oxide fuel cell integrated with novel allothermal biomass gasification: Part I: Modelling and feasibility study. Journal of Power Sources 2006;159:570.

[5] Pröll T, Rauch R, Aichernig C, Hofbauer H. Coupling of biomass steam gasification and an SOFC-gas turbine hybrid system for highly efficient electricity generation. ASME Turbo Expo: Power for Land, Sea, and Air. Vienna, Austria; 2004.

[6] Sucipta M, Kimijima S, Song TW, Suzuki K. Biomass solid oxide fuel cell-microgas turbine hybrid system: Effect of fuel composition. Journal of Fuel Cell Science and Technology 2008;5:041006.

[7] Suwanwarangkul R, Croiset E, Pritzker MD, Fowler MW, Douglas PL, Entchev E. Modelling of a cathode-supported tubular solid oxide fuel cell operating with biomass-derived synthesis gas. Journal of Power Sources 2007;166:386.

[8] Toonssen R. Sustainable power from biomass. The Netherlands: TU Delft; 2010.

[9] Bang-Møller C, Rokni M. Thermodynamic performance study of biomass gasification, solid oxide fuel cell and micro gas turbine hybrid systems. Energy Conversion and Management 2010;51:2330.

[10] Di Carlo A, Bocci E, Naso V. Process simulation of a SOFC and double bubbling fluidized bed gasifier power plant. International Journal of Hydrogen Energy 2013;38:532.

[11] Nagel F-P. Electricity from wood through the combination of gasification and solid oxide fuel cells: systems analysis and Proof-of-concept. Switzerland: ETH Zurich; 2008.

[12] Schuster G, Loffler G, Weigl K, Hofbauer H. Biomass steam gasification - an extensive parametric modeling study. Bioresource Technology 2001;77:71.

[13] Basu P, Kaushal P. Modeling of Pyrolysis and Gasification of Biomass in Fluidized Beds: A Review. Chemical Product and Process Modeling 2009;4:1.

[14] Sasaki K, Hori Y, Kikuchi R, Eguchi K, Ueno A, Takeuchi H, et al. Current-Voltage Characteristics and Impedance Analysis of Solid Oxide Fuel Cells for Mixed H2 and CO Gases. Journal of The Electrochemical Society 2002;149:A227.

[15] World Energy Outlook. IEA/OECD; 2013.

[16] Dept. Communications, Marine and Natural Resources. Government White Paper: Delivering a Sustainable Energy Future for Ireland. 2007.

[17] Dept. Communications, Energy and Natural Resources. National Renewable Energy Action Plan IRELAND. 2010.

[18] Situation Analysis and Role of Biomass Gasification (BMG) Technologies in Future Energy Needs. IEA Bioenergy; 2007.

[19] Martini S, Kleinhappl M, Hofbauer H. Kopplung von Biomassevergasung mit SOFC-Brennstoffzellensystemen. DGMK 2008. Germany; 2008.

[20] Martini S, Kleinhappl M, Hofbauer H. High Temperature Gas Treatment for Clean Gas Applications. 4th International Freiberg Conference on IGCC & XtL Technologies. Dresden, Germany; 2010.

[21] Martini S, Kleinhappl M, Zeisler J. SOFC field tests with biomass gasification derived product gas for the evaluation of stationary BIG-SOFC-CHP concepts. 2012.

[22] Howley M, Gallachóir B, Dennehy E. Energy in Ireland Key Statistics 2009. SEAI; 2009.

[23] Dennehy E, Howley M, Gallachoir B, Barriscale A. Renewable Energy in Ireland–2010 Update. SEAI; 2010.

[24] European Commission. Directive 2009/28/EC on the promotion of the use of energy from renewable sources. Official Journal of the European Union 2009.

[25] European Commission. EU Climate and Energy Package. Available at: http://ec.europa.eu/. Accessed May 2010.

[26] Eurostat Press Office. Eurostat News Release 103/2010. Available at: http://epp.eurostat.ec.europa.eu/. Accessed May 2010.

[27] Howley M, Gallachóir B, Dennehy E. Energy in Ireland 1990 - 2008. SEAI; 2009.

[28] European Commission. EU energy and transport in figures: statistical pocketbook: Luxembourg: Office for Official Publications of the European Communities; 2010.

[29] Dept. of the Environment, Heritage and Local Government. National Climate Change Strategy (Ireland) 2007-2012. 2007.

[30] Dept. of Communications, Marine and Natural Resources. BioEnergy Action Plan for Ireland. 2007.

[31] Dept. of Communications, Energy and Natural Resources. Maximising Ireland's Energy Efficiency, The National Energy Efficiency Action Plan 2009 – 2020. 2009.

[32] EirGrid. Generation Adequacy Report 2010-2016. 2009.

[33] Edenderry Power Plant website. Available at: http://www.edenderrypower.ie/. Accessed April 2010.

[34] Connected and Contracted Generators. Available at: http://www.eirgrid.com/. Accessed May 2010.

[35] EirGrid Monthly Electricity Statistics Update-April 2010. Available at: http://www.eirgrid.com/. Accessed April 2010.

[36] Endesa Ireland. Available at: http://www.tarbertpowerproject.com/. Accessed May 2010.

[37] ESB Moneypoint Environmental Retrofit Project. Available at: http://www.esb.ie/. Accessed April 2010.

[38] Reilly J. The Co-Firing Market for Biomass, National Forestry Conference. 2010.

[39] CER. Treatment of Small, Renewable and Low Carbon Generators outside the Group Processing Approach (CER/09/099). 2009.

[40] Eirgrid. Gate 3 ITC Programme Final Results Scheduled Firm Access Quantities. 2010.

[41] EirGrid. Grid 25 A Strategy for the Development of Ireland's Electricity Grid for a Sustainable and Competitive Future. 2010.

[42] Dept. of Communications, Energy and Natural Resources and Dept. of Enterprise, Trade and Investment. All Island Grid Study. 2008.

[43] Energy Policies of IEA Countries: Ireland 2007 Review: OECD/IEA; 2007.

[44] Single Electricity Market Operator. Available at: http://www.sem-o.com/. Accessed April 2010.

[45] Teagasc. Available at: http://www.teagasc.ie/. Accessed January 2010.

[46] European Commission. Biomass action plan COM(2005) 628. Official Journal of the European Union 2005.

[47] European Commission. The Renewable Energy Progress Report COM(2009) 192. Official Journal of the European Union 2009.

[48] European Commission. The Renewable Energy Progress Report SEC(2009) 503. Official Journal of the European Union 2009.

[49] O'Rourke F, Boyle F, Reynolds A. Renewable energy resources and technologies applicable to Ireland. Renewable and Sustainable Energy Reviews 2009;13:1975.

[50] Climate and Energy Ministry. National Renewable Energy Action Plan DENMARK. 2010.

[51] Dept. of Communications, Energy and Natural Resources. National Renewable Energy Action Plan IRELAND: First Progress Report. 2012.

[52] EPA. Ireland's Greenhouse Gas Emissions Projections 2010-2020. 2010.

[53] European Environment Agency. Annual European Union greenhouse gas inventory 1990–2008 and inventory report 2010. 2010.

[54] Dept. of Environment, Heritage and Local Government. Carbon Budget 2010. 2010.

[55] EPA. Ireland's Greenhouse Gas Emission Projections 2012-2030. 2013.

[56] Dennehy E, Barriscale A, Howley M, Ó'Gallachóir B. Combined Heat and Power in Ireland 2010 Update. SEAI; 2010.

[57] European Commission. Directive 2004/8/EC on the promotion of cogeneration based on a useful heat demand in the internal energy market. Official Journal of the European Union 2004.

[58] Dennehy E, Fanning E, Howley M. Combined Heat and Power in Ireland 2012 Update. SEAI; 2012.

[59] European Commission. Europe can save more energy by combined heat and power generation COM(2008) 771. Official Journal of the European Union 2008.

[60] Ó Cléirigh B. Combined Heat and Power (CHP) Potential in Ireland. SEAI; 2009.

[61] Dept. of Communications, Energy and Natural Resources. Available at: http://www.dcenr.gov.ie/. Accessed February 2014.

[62] Ceres Power. Available at: http://www.cerespower.com/. Accessed March 2010.

[63] van den Broek R, Teeuwisse S, Healion K, Kent T, van Wijk A, Faaij A, et al. Potentials for electricity production from wood in Ireland. Energy 2001;26:991.

[64] Knaggs G, O'Driscoll E. Woodflow for the Republic of Ireland for 2008. COFORD; 2009.

[65] de Jong W. Nitrogen compounds in pressurised fluidised bed gasification of biomass and fossil fuels. The Netherlands: TU Delft; 2005.

[66] McKendry P. Energy production from biomass (part 1): overview of biomass. Bioresource Technology 2002;83:37.

[67] Prins M. Thermodynamic analysis of biomass gasification and torrefaction. The Netherlands: Technische Universiteit Eindhoven; 2005.

[68] Norheim A. Experimental investigation of Solid Oxide Fuel Cells using biomass gasification producer gases. Trondheim: Norwegian University of Science and Technology; 2005.

[69] Higman C, van der Burgt M. Gasification. Burlington, MA, USA: Gulf Professional Publishing; 2003.

[70] Siedlecki M, van der Nat K, Simeone E, de Jong W. The first results of gas and solids characterization obtained during steam-oxygen gasification of biomass in a 100kWth CFB gasifier. World Renewable Energy Congress IX. Florence, Italy; 2006.

[71] SEAI. Co-Firing with Biomass. 2003.

[72] Cengel YA, Boles MA, Kanoglu M. Thermodynamics: An Engineering Approach (SI units). 7th ed. UK: McGraw-Hill; 2011.

[73] COFORD. Maximising the Potential of Wood Use for Energy Generation in Ireland. 2003.

[74] Dept. of Communications, Marine and Natural Resources. Bioenergy in Ireland. 2004.

[75] SEAI. Bioenergy News (Issue 4). 2009.

[76] O'Toole D. Private Communication, Biomass Business Development Manager, Coillte, Ireland. 2010.

[77] Coillte Website. Available at: http://www.coillte.ie/. Accessed March 2010.

[78] Phillips H, Redmond J, Mac Siúrtáin M, Nemesova A. Roundwood production from private sector forests 2009-2028: a geospatial forecast. COFORD; 2009.

[79] Knaggs G, O'Driscoll E. An overview of the Irish wood-based biomass sector in 2007-2009. COFORD; 2010.

[80] Clare Local Development Company and Teagasc. County Clare Wood Energy Project: Step by Step Guide to Selling Your Timber for Wood Energy 2008.

[81] Gillespie J. Fostering Our Indigenous Forestry Sector. Department of Agriculture, Fisheries and Food 2010.

[82] Coillte. Timber Production Forecast 2006-2010. 2006.

[83] Lynn M. Roundwood supply and demand forecasts and infrastructural requirements COFORD; 2010.

[84] Crowley T. Coillte's Business Expand Beyond Timber. Coillte; 2009.

[85] Stanley B. Biomass 2010 Fuelling the Future. Coillte; 2010.

[86] Styles D, Jones MB. Current and future financial competitiveness of electricity and heat from energy crops: A case study from Ireland. Energy Policy 2007;35:4355.

[87] Wickham J, Rice B, Finnan J, McConnon R. A review of past and current research on short rotation coppice in Ireland and abroad. COFORD; 2010.

[88] Central Statistics Office. Available at: http://www.cso.ie/en/statistics/. Accessed May 2010.

[89] Styles D, Thorne F, Jones MB. Energy crops in Ireland: An economic comparison of willow and Miscanthus production with conventional farming systems. Biomass and Bioenergy 2008;32:407.

[90] Teagasc. Energy Crops Manual. 2010.

[91] Billet harvesting, drying and processing of willow short rotation coppice for the wood energy market in the UK. SWS Forestry Services.

[92] Dept. of Agriculture, Fisheries and Food. Planting and Growing Miscanthus: Best practice guidelines for growing miscanthus under the Bioenergy Scheme. 2009.

[93] Kofman PD. Units, conversion factors and formulae for wood for energy. COFORD; 2010.

[94] ECN. Phyllis Database. Available at: https://www.ecn.nl/phyllis2/. Last accessed April 2014.

[95] COFORD. Forestry and Wood Update. August 2010.

[96] Girvin S, Ó'Riain G, Wilson M. A bioenergy mapping & modelling tool as applied in Ireland. Innovation for Sustainable Production. Bruges; 2010, p. 85.

[97] Basu P. Biomass gasification and pyrolysis: practical design and theory. Brulington, MA: Academic; 2010.

[98] Cummer KR, Brown RC. Ancillary equipment for biomass gasification. Biomass and Bioenergy 2002;23:113.

[99] Brammer JG, Bridgwater AV. Drying technologies for an integrated gasification bio-energy plant. Renewable and Sustainable Energy Reviews 1999;3:243.

[100] Brammer JG, Bridgwater AV. The influence of feedstock drying on the performance and economics of a biomass gasifier–engine CHP system. Biomass and Bioenergy 2002;22:271.

[101] Ståhl M, Granström K, Berghel J, Renström R. Industrial processes for biomass drying and their effects on the quality properties of wood pellets. Biomass and Bioenergy 2004;27:621.

[102] Zhang L, Xu C, Champagne P. Overview of recent advances in thermo-chemical conversion of biomass. Energy Conversion and Management 2010;51:969.

[103] Kirkels AF, Verbong GPJ. Biomass gasification: Still promising? A 30-year global overview. Renewable and Sustainable Energy Reviews 2011;15:471.

[104] Biotricity straw fired biomass plant. Available at: http://www.ecoseed.org/. Accessed November 2013.

[105] Babu S. Observations on the current status of biomass gasification. IEA Bioenergy; 2005.

[106] Nieminen M. Technology Brief: Fluidized bed gasification, gas cleaning, and fuel gas utilization systems. IEA Bioenergy; 2004.

[107] Austermann S, Whiting K. Commercial Assessment: Advanced Conversion Technology (Gasification) for Biomass Projects. Juniper; 2007.

[108] Moreea-Taha R. Modelling and simulation for coal gasification. IEA Coal Research; 2000.

[109] Demirbas A. Carbonization ranking of selected biomass for charcoal, liquid and gaseous products. Energy Conversion and Management 2001;42:1229.

[110] Bridgwater AV. Progress in thermochemical biomass conversion. Oxford: Blackwell Science; 2001.

[111] Kaushal P, Proell T, Hofbauer H. Application of a detailed mathematical model to the gasifier unit of the dual fluidized bed gasification plant. Biomass and Bioenergy 2011;35:2491.

[112] Pickett MM. Modeling The Performance And Emissions Of British Gas/Lurgi-Based Integrated Gasification Combined Cycle Systems. Civil Engineering. Raleigh, NC: North Carolina State University; 2000.

[113] Olofsson I, Nordin A, Söderlind U. Initial review and evaluation of process technologies and systems suitable for cost-efficient medium-scale gasification for biomass to liquid fuels. Umeå: Energy Technology & Thermal Process Chemistry, University of Umeå; 2005.

[114] Iliuta I, Leclerc A, Larachi F. Allothermal steam gasification of biomass in cyclic multi-compartment bubbling fluidized-bed gasifier/combustor – New reactor concept. Bioresource Technology 2010;101:3194.

[115] Knoef H. Technology Brief: Fixed-bed gasification. IEA Bioenergy; 2003.

[116] Henriksen U, Ahrenfeldt J, Jensen TK, Gøbel B, Bentzen JD, Hindsgaul C, et al. The design, construction and operation of a 75 kW two-stage gasifier. Energy 2006;31:1542.

[117] IEA Task 33 Thermal Gasification Facilities Database. Available at: http://www.ieatask33.org/content/thermal_gasification_facilities. Accessed December 2013.

[118] Siedlecki M. On the gasification of biomass in a steam-oxygen blown CFB gasifier with the focus on gas quality upgrading. The Netherlands: TU Delft; 2011.

[119] Rollins ML, Reardon L, Nichols D, Lee P, Moore M, Crim M, et al. Economic Evaluation of CO2 Sequestration Technologies Task 4, Biomass Gasification-Based Processing. NETL; 2002.

[120] Ståhl K. Värnamo Demonstration Plant – A demonstration plant for biofuel-fired combined heat and power generation based on pressurized gasification. The Demonstration Programme 1996-2000. European Commission, Swedish Energy Agency, Sydkraft AB; 2001.

[121] Zwart R. Gas Cleaning: Downstream Biomass Gasification-Status Report: ECN; 2009.

[122] Corella J, Toledo JM, Molina G. A Review on Dual Fluidized-Bed Biomass Gasifiers. Industrial & Engineering Chemistry Research 2007;46:6831.

[123] Göransson K, Söderlind U, He J, Zhang W. Review of syngas production via biomass DFBGs. Renewable and Sustainable Energy Reviews 2011;15:482.

[124] FICFB Gasification Technology. Available at: http://ficfb.at/. Accessed December 2013.

[125] Hofbauer H, Rauch R, Bosch K, Koch R, Aichernig C. Biomass CHP Plant Güssing - A Success Story. Expert Meeting on Pyrolysis and Gasification of Biomass and Waste Strasbourg, France; 2002.

[126] Hofbauer H, Rauch R, Loeffler G, Kaiser S, Fercher E, Tremmel H. Six years experience with the FICFB-gasification process. 12th European conference and Technology exhibition on biomass for energy, Industry and Climate Protection. Amsterdam; 2002, p. 982.

[127] Bolhar-Nordenkampf M, Hofbauer H. Gasification demonstration plants in Austria IV International Slovak Biomass Forum. Bratislava; 2004, p. 227.

[128] Pröll T, Rauch R, Aichernig C, Hofbauer H. Fluidized Bed Steam Gasification of Solid Biomass - Performance Characteristics of an 8 MWth Combined Heat and Power Plant. International Journal of Chemical Reactor Engineering 2007;5:1.

[129] Pröll T, Hofbauer H. Development and Application of a Simulation Tool for Biomass Gasification Based Processes. International Journal of Chemical Reactor Engineering 2008;6:1.

[130] Hofbauer H, Rauch R. Hydrogen-Rich Gas From Biomass Steam Gasification (Contract JOR3CT970196). 2001.

[131] Rauch R. Indirect Gasification - Workshop at IEA Bioenergy Task 32 and Task 33 Meeting. TU Wien; October 2010.

[132] IEA Bioenergy Annual Report 2009. IEA; 2010.

[133] Hofbauer H. Biomass Steam Gasification Industrial Experience and Future Prospects TU Wien; 2008.

[134] Fiorenza G, Canonaco J, Blasi A, Braccio G. Biomass steam gasification at the Trisaia dual fluidized bed pilot plant: experimental results and optimization

analysis of process variables. Zero Emission Power Generation Workshop. Gebze, Turkey; 2007, p. 1.

[135] Kern S, Pfeifer C, Hofbauer H. Gasification of wood in a dual fluidized bed gasifier: Influence of fuel feeding on process performance. Chemical Engineering Science 2013;90:284.

[136] Kirnbauer F, Wilk V, Hofbauer H. Performance improvement of dual fluidized bed gasifiers by temperature reduction: The behavior of tar species in the product gas. Fuel 2013;108:534.

[137] Rauch R, Hrbek J. Country Report Austria - IEA Bioenergy Task33 Meeting. TU Wien; November 2013.

[138] Sharma V. Research and Development Activities on Biofuels (ENEA Research Centre Trisaia). ENEA Trisaia; 2011.

[139] Bain R. United States Country Report - IEA Bioenergy, Task 33. NREL; 2011.

[140] van der drift B. Biomass gasification in the Netherlands - IEA Bioenergy, Task 33. ECN; 2013.

[141] Kolb T. Country Activities Germany. IEA Bioenergy; November 2013.

[142] Maniatis K. Progress in Biomass Gasification: An Overview. In: Bridgwater AV, editor. Progress in Thermochemical Biomass Conversion: Blackwell Publishing; 2001.

[143] IEA Bioenergy Task 33 Meeting Minutes. IEA Bioenergy; November 2009.

[144] Jewulski J, Stepien M, Blesznowski M, Nanna F. Slip stream testing with a SOFC unit at Güssing and Trisaia plants. 2010.

[145] Gasification 2010 Worldwide Database US DOE and NETL; 2010.

[146] Akunuri NV. Modeling The Performance, Emissions, And Costs Of Texaco Gasifier-Based Integrated Gasification Combined Cycle Systems. Civil Engineering. Raleigh, NC: North Carolina State University; 1999.

[147] Llano P. Biomass co-gasification tests in Elcogas IGCC power plant. IEA Bioenergy; November 2009.

[148] Ståhl K, Waldheim L, Morris M, Johnsson U, Gårdmark L. Biomass IGCC at Värnamo, Sweden – Past and Future. CA, USA: Stanford University; 2004.

[149] Sweden Country Report - IEA Task 33. IEA Bioenergy; 2008.

[150] Waldheim L. GREVE, ARBRE and CHRISGAS - IEA Task 33 Worskhop. TPS Termiska Processer AB; 2006.

[151] Spliethoff H. Power generation from solid fuels. Heidelberg: Springer; 2010.

[152] Bain R. DOE Gasification Demonstrations. NREL; November 2009.

[153] Carbona. Research & Technology Development Needs to Improve Gasification Plant Operation IEA Task 33 Workshop; November 2009.

[154] IEA Bioenergy Task 33 Meeting Minutes. IEA Bioenergy; October 2010.

[155] Hofbauer H, Rauch R. Gasification Survey Country: Austria. IEA Bioenergy; 2008.

[156] Finland Country Report - IEA Task 33. IEA Bioenergy; 2008.

[157] Kwant KW, Knoef H. Status of gasification in countries participating in the IEA and gasnet activity, August 2004. IEA Bioenergy; 2004.

[158] Babu S. Thermal Gasification of Biomass Work Shop No. 1: Perspectives on Biomass Gasification. IEA Bioenergy; 2006.

[159] Hansen M. Thermal Biomass Gasification in Denmark IEA Bioenergy Task 33; November 2013.

[160] Van der Drift A, Boerrigter H. Synthesis gas from biomass for fuels and chemicals. ECN Biomass, Coal and Environmental Research; 2006.

[161] Hajimolana SA, Hussain MA, Daud WMAW, Soroush M, Shamiri A. Mathematical modeling of solid oxide fuel cells: A review. Renewable and Sustainable Energy Reviews 2011;15:1893.

[162] Singhal SC, Kendall K. High-temperature solid oxide fuel cells: fundamentals, design and applications. Oxford: Elsevier Advanced Technology; 2003.

[163] Fuel cell handbook. 7th ed: US Department of Energy and NETL; 2004.

[164] Sequeira CAC, Brito PSD, Mota AF, Carvalho JL, Rodrigues LFFTTG, Santos DMF, et al. Fermentation, gasification and pyrolysis of carbonaceous residues towards usage in fuel cells. Energy Conversion and Management 2007;48:2203.

[165] Song C. Fuel processing for low-temperature and high-temperature fuel cells: Challenges, and opportunities for sustainable development in the 21st century. Catalysis Today 2002;77:17.

[166] Singhal SC. Solid oxide fuel cells for stationary, mobile, and military applications. Solid State Ionics 2002;152-153:405.

[167] Singhal SC. Advances in solid oxide fuel cell technology. Solid State Ionics 2000;135:305.

[168] Aravind PV, de Jong W. Evaluation of high temperature gas cleaning options for biomass gasification product gas for Solid Oxide Fuel Cells. Progress in Energy and Combustion Science 2012;38:737.

[169] Larminie J, Dicks A. Fuel cell systems explained. 2nd ed. Chichester: Wiley; 2003.

[170] O'Hayre R, Cha S, Colella W, Prinz F. Fuel cell fundamentals. 2nd ed. Hoboken, N.J.: John Wiley & Sons; 2009.

[171] Holtappels P, Stimming U. Solid Oxide Fuel Cells (SOFC). In: Vielstich W, Lamm A, Gasteiger HA, editors. Handbook of fuel cells: fundamentals technology and applications. Chichester: Wiley; 2003.

[172] Williams MC, Strakey JP, Singhal SC. U.S. distributed generation fuel cell program. Journal of Power Sources 2004;131:79.

[173] Karl J, Frank N, Hohenwarter U, Karellas S, Saule M. Conversion of Syngas From Biomass in Solid Oxide Fuel Cells. Journal of Fuel Cell Science and Technology 2009;6:021005.

[174] Benson S. Fuel cells: use with coal and other solid fuels. IEA Coal Research; 2001.

[175] Molino A, Giordano G, Motola V, Fiorenza G, Nanna F, Braccio G. Electricity production by biomass steam gasification using a high efficiency technology and low environmental impact. Fuel 2013;103:179.

[176] Meyer L, Tsatsaronis G, Buchgeister J, Schebek L. Exergoenvironmental analysis for evaluation of the environmental impact of energy conversion systems. Energy 2009;34:75.

[177] Siemens Power Generation SFC-200 System Summary. Available at: http://www.powergeneration.siemens.com. Accessed June 2007.

[178] George RA. Status of tubular SOFC field unit demonstrations. Journal of Power Sources 2000;86:134.

[179] Yokokawa H, Sakai N. History of high temperature fuel cell development. In: Vielstich W, Lamm A, Gasteiger HA, editors. Handbook of fuel cells: fundamentals technology and applications. Chichester: Wiley; 2003.

[180] Minh NQ, Singhal C, Williams M. Solid Oxide Fuel Cells: Development Activities, Trends and Technological Challenges. ECS Transactions 2009;17:211.

[181] McPhail S, Leto L, Boigues-Muñoz C. The Yellow Pages of SOFC Technology - International Status of SOFC deployment 2012-2013. IEA and ENEA; 2013.

[182] Saito T, Abe T, Fujinaga K, Miyao M, Kuroishi M, Hiwatashi K, et al. Development of Tubular SOFC at TOTO. Proceedings-Electrochemical Society: Electrochemical Society; 2005.

[183] Yokokawa H, Watanabe T, Ueno A, Hoshino K. Investigation on Degradation in Long-Term Operations of Four Different Stack/Modules. ECS Transactions 2007;7:133.

[184] Tomida K, Nishiura M, Koga S, Miyamoto K, Teramoto Y, Yoshida S, et al. Development of SOFC-GT Combined Cycle System with Tubular Type Cell Stack Mitsubishi Heavy Industries; 2010.

[185] Kobayashi Y, Ando Y, Nishiura M, Tomida K, Kishizawa H, Matake N. Next-Generation SOFC-Combined Power Generation System (High Efficiency Hybrid Power Generation System) Mitsubishi Heavy Industries Technical Review 2013;50:42.

[186] Office of Fossil Energy - Fuel Cell Program Annual Report US DOE, NETL and SECA; 2007.

[187] Pierre J. Siemens Energy, 11th Annual SECA Workshop. 2010.

[188] In brief - Siemens to sell off SOFC business. Fuel Cells Bulletin 2008;2008:5.

[189] Liu M, van der Kleij A, Verkooijen AHM, Aravind PV. An experimental study of the interaction between tar and SOFCs with Ni/GDC anodes. Applied Energy 2013;108:149.

[190] Lorente E, Millan M, Brandon NP. Use of gasification syngas in SOFC: Impact of real tar on anode materials. International Journal of Hydrogen Energy 2012;37:7271.

[191] Gariglio M, De Benedictis F, Santarelli M, Calì M, Orsello G. Experimental activity on two tubular solid oxide fuel cell cogeneration plants in a real industrial environment. International Journal of Hydrogen Energy 2009;34:4661.

[192] Pereira EG, da Silva JN, de Oliveira JL, Machado CS. Sustainable energy: A review of gasification technologies. Renewable and Sustainable Energy Reviews 2012;16:4753.

[193] Colpan CO, Fung AS, Hamdullahpur F. Modeling of an integrated two-stage biomass gasifier and solid oxide fuel cell system. Biomass and Bioenergy 2012;42:132.

[194] Stevens DJ. Hot Gas Conditioning: Recent Progress With Larger-Scale Biomass Gasification Systems. Pacific Northwest National Laboratory, Richland, Washington: NREL, US DOE; 2001.

[195] Hofmann P, Schweiger A, Fryda L, Panopoulos KD, Hohenwarter U, Bentzen JD, et al. High temperature electrolyte supported Ni-GDC/YSZ/LSM SOFC operation on two-stage Viking gasifier product gas. Journal of Power Sources 2007;173:357.

[196] Hofmann P, Panopoulos KD, Fryda LE, Schweiger A, Ouweltjes JP, Karl J. Integrating biomass gasification with solid oxide fuel cells: Effect of real product gas tars, fluctuations and particulates on Ni-GDC anode. International Journal of Hydrogen Energy 2008;33:2834.

[197] Hofmann P, Panopoulos KD, Aravind PV, Siedlecki M, Schweiger A, Karl J, et al. Operation of solid oxide fuel cell on biomass product gas with tar levels > 10 g Nm−3. International Journal of Hydrogen Energy 2009;34:9203.

[198] Torres W, Pansare SS, Goodwin Jr JG. Hot gas removal of tars, ammonia, and hydrogen sulfide from biomass gasification gas. Catalysis reviews 2007;49:407.

[199] Meng X, de Jong W, Pal R, Verkooijen AHM. In bed and downstream hot gas desulphurization during solid fuel gasification: A review. Fuel Processing Technology 2010;91:964.

[200] Brown D, Gassner M, Fuchino T, Maréchal F. Thermo-economic analysis for the optimal conceptual design of biomass gasification energy conversion systems. Applied Thermal Engineering 2009;29:2137.

[201] Fuerte A, Valenzuela RX, Escudero MJ, Daza L. Ammonia as efficient fuel for SOFC. Journal of Power Sources 2009;192:170.

[202] Schweiger A, Hohenwarter U. Small scale hot gas cleaning device for SOFC utilization of woody biomass product gas. Proc. 15th European Biomass Conference Exhibition. Berlin, Germany; 2007.

[203] Dayton D. A review of the literature on catalytic biomass tar destruction. NREL; 2002.

[204] Aravind P, Ouweltjes J, De Heer E, Woudstra N, Rietveld G. Impact of Biosyngas and its components on SOFC Anodes. Electrochemical Society Proceedings; 2005, p. 1459.

[205] Pröll T, Hofbauer H. H2 rich syngas by selective CO2 removal from biomass gasification in a dual fluidized bed system — Process modelling approach. Fuel Processing Technology 2008;89:1207.

[206] Li X. Biomass gasification in a circulating fluidized bed. Canada: The University of British Columbia; 2003.

[207] Milne T, Evans R, Abatzoglou N. Biomass gasifier "tars": their nature, formation, and conversion. NREL; 1998.

[208] Koppatz S, Pfeifer C, Rauch R, Hofbauer H, Marquard-Moellenstedt T, Specht M. H2 rich product gas by steam gasification of biomass with in situ CO2 absorption in a dual fluidized bed system of 8 MW fuel input. Fuel Processing Technology 2009;90:914.

[209] Singh D, Hernández-Pacheco E, Hutton PN, Patel N, Mann MD. Carbon deposition in an SOFC fueled by tar-laden biomass gas: a thermodynamic analysis. Journal of Power Sources 2005;142:194.

[210] Suwanwarangkul R, Croiset E, Entchev E, Charojrochkul S, Pritzker MD, Fowler MW, et al. Experimental and modeling study of solid oxide fuel cell operating with syngas fuel. Journal of Power Sources 2006;161:308.

[211] Mermelstein J, Millan-Agorio M, Brandon N. The Impact and Mitigation of Carbon Formation on Ni-YSZ Anodes from Biomass Gasification Tars. ECS Transactions 2009;17:111.

[212] Chen T, Li T, Miao H, Wang WG, Wu Y. Operation of Ni-YSZ Anode Supported Solid Oxide Fuel Cell on Different Simulated Syngas. ECS Transactions 2009;25:1905.

[213] Dekker N, Ouweltjes J, Rietveld B. Conversion of Simulated Biogas in a SOFC: The Effect of Organic Compounds. ECS Transactions 2007;7:1465.

[214] Negro SO, Suurs RAA, Hekkert MP. The bumpy road of biomass gasification in the Netherlands: Explaining the rise and fall of an emerging innovation system. Technological Forecasting and Social Change 2008;75:57.

[215] Baron S, Brandon N, Atkinson A, Steele B, Rudkin R. The impact of wood-derived gasification gases on Ni-CGO anodes in intermediate temperature solid oxide fuel cells. Journal of Power Sources 2004;126:58.

[216] Costa-Nunes O, Gorte RJ, Vohs JM. Comparison of the performance of Cu–CeO2–YSZ and Ni–YSZ composite SOFC anodes with H2, CO, and syngas. Journal of Power Sources 2005;141:241.

[217] Saule M, Franka N, Hofmannb P, Ouweltjesc JP, Schweigerd A, Karla J. Operation of Solid Oxide Fuel Cells with Syngas from Biomass. H2expo; 2006.

[218] de Souza-Santos ML. Solid fuels combustion and gasification: modeling, simulation, and equipment operation. New York: Marcel Dekker; 2004.

[219] Puig-Arnavat M, Bruno JC, Coronas A. Review and analysis of biomass gasification models. Renewable and Sustainable Energy Reviews 2010;14:2841.

[220] Gómez-Barea A, Leckner B. Modeling of biomass gasification in fluidized bed. Progress in Energy and Combustion Science 2010;36:444.

[221] Gassner M, Maréchal F. Thermodynamic comparison of the FICFB and Viking gasification concepts. Energy 2009;34:1744.

[222] Abdelouahed L, Authier O, Mauviel G, Corriou JP, Verdier G, Dufour A. Detailed Modeling of Biomass Gasification in Dual Fluidized Bed Reactors under Aspen Plus. Energy & Fuels 2012;26:3840.

[223] He J, Göransson K, Söderlind U, Zhang W. Simulation of biomass gasification in a dual fluidized bed gasifier. Biomass Conversion and Biorefinery 2012;2:1.

[224] De Kam MJ, Vance Morey R, Tiffany DG. Biomass Integrated Gasification Combined Cycle for heat and power at ethanol plants. Energy Conversion and Management 2009;50:1682.

[225] Cohce MK, Rosen MA, Dincer I. Efficiency evaluation of a biomass gasification-based hydrogen production. International Journal of Hydrogen Energy 2011;36:11388.

[226] Bove R, Ubertini S. Modeling solid oxide fuel cell operation: Approaches, techniques and results. Journal of Power Sources 2006;159:543.

[227] Bove R, Ubertini S. Modeling solid oxide fuel cells: methods, procedures and techniques: Springer; 2008.

[228] Kakaç S, Pramuanjaroenkij A, Zhou XY. A review of numerical modeling of solid oxide fuel cells. International Journal of Hydrogen Energy 2007;32:761.

[229] Wang K, Hissel D, Péra MC, Steiner N, Marra D, Sorrentino M, et al. A Review on solid oxide fuel cell models. International Journal of Hydrogen Energy 2011;36:7212.

[230] Costamagna P, Magistri L, Massardo AF. Design and part-load performance of a hybrid system based on a solid oxide fuel cell reactor and a micro gas turbine. Journal of Power Sources 2001;96:352.

[231] Campanari S. Thermodynamic model and parametric analysis of a tubular SOFC module. Journal of Power Sources 2001;92:26.

[232] Zhang W, Croiset E, Douglas PL, Fowler MW, Entchev E. Simulation of a tubular solid oxide fuel cell stack using AspenPlusTM unit operation models. Energy Conversion and Management 2005;46:181.

[233] Calise F, Palombo A, Vanoli L. Design and partial load exergy analysis of hybrid SOFC–GT power plant. Journal of Power Sources 2006;158:225.

[234] Leone P, Santarelli M, Cali M. Model and Simulation of a SOFC CHP Plant Fuelled with Hydrogen. ECS Transactions 2007;5:553.

[235] Milewski J, Miller A, Sałaciński J. Off-design analysis of SOFC hybrid system. International Journal of Hydrogen Energy 2007;32:687.

[236] Cali M, Santarelli MGL, Leone P. Design of experiments for fitting regression models on the tubular SOFC: Screening test, response surface analysis and optimization. International Journal of Hydrogen Energy 2007;32:343.

[237] Akkaya AV, Sahin B, Huseyin Erdem H. Exergetic performance coefficient analysis of a simple fuel cell system. International Journal of Hydrogen Energy 2007;32:4600.

[238] Akkaya AV, Sahin B, Erdem HH. Thermodynamic model for exergetic performance of a tubular SOFC module. Renewable Energy 2009;34:1863.

[239] Suwanwarangkul R, Croiset E, Pritzker MD, Fowler MW, Douglas PL, Entchev E. Mechanistic modelling of a cathode-supported tubular solid oxide fuel cell. Journal of Power Sources 2006;154:74.

[240] Campanari S, Iora P. Definition and sensitivity analysis of a finite volume SOFC model for a tubular cell geometry. Journal of Power Sources 2004;132:113.

[241] Calise F, d'Accadia MD, Palombo A, Vanoli L. One-dimensional model of a tubular solid oxide fuel cell. Journal of Fuel Cell Science and Technology 2008;5:021014.

[242] Verda V, Calí Quaglia M. Solid oxide fuel cell systems for distributed power generation and cogeneration. International Journal of Hydrogen Energy 2008;33:2087.

[243] Hirano A, Suzuki M, Ippommatsu M. Evaluation of a New Solid Oxide Fuel Cell System by Non-isothermal Modeling. Journal of The Electrochemical Society 1992;139:2744.

[244] Bessette NF, Wepfer WJ, Winnick J. A mathematical model of a solid oxide fuel cell. Journal of the Electrochemical Society 1995;142:3792.

[245] Haynes C, Wepfer WJ. 'Design for power' of a commercial grade tubular solid oxide fuel cell. Energy Conversion and Management 2000;41:1123.

[246] Li P-W, Suzuki K. Numerical Modeling and Performance Study of a Tubular SOFC. Journal of The Electrochemical Society 2004;151:A548.

[247] Song TW, Sohn JL, Kim JH, Kim TS, Ro ST, Suzuki K. Performance analysis of a tubular solid oxide fuel cell/micro gas turbine hybrid power system based on a quasi-two dimensional model. Journal of Power Sources 2005;142:30.

[248] Bharadwaj A, Archer DH, Rubin ES. Modeling the performance of a tubular solid oxide fuel cell. Journal of Fuel Cell Science and Technology 2005;2:38.

[249] Sánchez D, Chacartegui R, Muñoz A, Sánchez T. Thermal and electrochemical model of internal reforming solid oxide fuel cells with tubular geometry. Journal of Power Sources 2006;160:1074.

[250] Sucipta M, Kimijima S, Suzuki K. Performance analysis of the SOFC-MGT hybrid system with gasified biomass fuel. Journal of Power Sources 2007;174:124.

[251] Sucipta M, Kimijima S, Suzuki K. Solid Oxide Fuel Cell-Micro Gas Turbine Hybrid System Using Natural Gas Mixed with Biomass Gasified Fuel. Journal of The Electrochemical Society 2008;155:B258.

[252] Barzi YM, Ghassemi M, Hamedi MH. Numerical analysis of start-up operation of a tubular solid oxide fuel cell. International Journal of Hydrogen Energy 2009;34:2015.

[253] Nagel FP, Schildhauer TJ, Biollaz S, Wokaun A. Performance comparison of planar, tubular and Delta8 solid oxide fuel cells using a generalized finite volume model. Journal of Power Sources 2008;184:143.

[254] Hernández-Pacheco E, Singh D, Hutton PN, Patel N, Mann MD. A macro-level model for determining the performance characteristics of solid oxide fuel cells. Journal of Power Sources 2004;138:174.

[255] Zabaniotou A. Agro-residues implication in decentralized CHP production through a thermochemical conversion system with SOFC. Sustainable Energy Technologies and Assessments 2014;6:34.

[256] Omosun AO, Bauen A, Brandon NP, Adjiman CS, Hart D. Modelling system efficiencies and costs of two biomass-fuelled SOFC systems. Journal of Power Sources 2004;131:96.

[257] Nagel FP, Schildhauer TJ, Biollaz SMA. Biomass-integrated gasification fuel cell systems - Part 1: Definition of systems and technical analysis. International Journal of Hydrogen Energy 2009;34:6809.

[258] Nagel FP, Schildhauer TJ, McCaughey N, Biollaz SMA. Biomass-integrated gasification fuel cell systems – Part 2: Economic analysis. International Journal of Hydrogen Energy 2009;34:6826.

[259] Aravind PV, Woudstra T, Woudstra N, Spliethoff H. Thermodynamic evaluation of small-scale systems with biomass gasifiers, solid oxide fuel cells with Ni/GDC anodes and gas turbines. Journal of Power Sources 2009;190:461.

[260] Arteaga-Pérez LE, Casas-Ledón Y, Pérez-Bermúdez R, Peralta LM, Dewulf J, Prins W. Energy and exergy analysis of a sugar cane bagasse gasifier integrated to a solid oxide fuel cell based on a quasi-equilibrium approach. Chemical Engineering Journal 2013;228:1121.

[261] Bang-Møller C, Rokni M, Elmegaard B, Ahrenfeldt J, Henriksen UB. Decentralized combined heat and power production by two-stage biomass gasification and solid oxide fuel cells. Energy 2013;58:527.

[262] Pierobon L, Rokni M, Larsen U, Haglind F. Thermodynamic analysis of an integrated gasification solid oxide fuel cell plant combined with an organic Rankine cycle. Renewable Energy 2013;60:226.

[263] Morandin M, Maréchal F, Giacomini S. Synthesis and thermo-economic design optimization of wood-gasifier-SOFC systems for small scale applications. Biomass and Bioenergy 2013;49:299.

[264] Colpan CO, Hamdullahpur F, Dincer I, Yoo Y. Effect of gasification agent on the performance of solid oxide fuel cell and biomass gasification systems. International Journal of Hydrogen Energy 2010;35:5001.

[265] Sadhukhan J, Zhao Y, Shah N, Brandon NP. Performance analysis of integrated biomass gasification fuel cell (BGFC) and biomass gasification combined cycle (BGCC) systems. Chemical Engineering Science 2010;65:1942.

[266] Jin H, Larson E, Celik F. Performance and cost analysis of future, commercially mature gasification-based electric power generation from switchgrass. Biofuels, Bioproducts and Biorefining 2009;3:142.

[267] Athanasiou C, Coutelieris F, Vakouftsi E, Skoulou V, Antonakou E, Marnellos G, et al. From biomass to electricity through integrated gasification/SOFC system-optimization and energy balance. International Journal of Hydrogen Energy 2007;32:337.

[268] Athanasiou C, Vakouftsi E, Coutelieris FA, Marnellos G, Zabaniotou A. Efficiencies of olive kernel gasification combined cycle with solid oxide fuel cells (SOFCs). Chemical Engineering Journal 2009;149:183.

[269] Craig KR, Mann MK. Cost and Performance Analysis of Biomass-Based Integrated Gasification Combined-Cycle (BIGCC) Power Systems. NREL, US DOE; 1996.

[270] de Jong W, Unal O, Andries J, Hein KRG, Spliethoff H. Biomass and fossil fuel conversion by pressurised fluidised bed gasification using hot gas ceramic filters as gas cleaning. Biomass and Bioenergy 2003;25:59.

[271] Mathieu P, Dubuisson R. Performance analysis of a biomass gasifier. Energy Conversion and Management 2002;43:1291.

[272] Prins MJ, Ptasinski KJ, Janssen FJJG. More efficient biomass gasification via torrefaction. Energy 2006;31:3458.

[273] Zhu Y. Evaluation Of Gas Turbine And Gasifier-Based Power Generation System. Civil, Construction, and Environmental Engineering. Raleigh, NC: North Carolina State University; 2004.

[274] Kuchonthara P, Bhattacharya S, Tsutsumi A. Combination of thermochemical recuperative coal gasification cycle and fuel cell for power generation. Fuel 2005;84:1019.

[275] Cocco D, Tola V. Externally reformed solid oxide fuel cell-micro-gas turbine (SOFC-MGT) hybrid systems fueled by methanol and di-methyl-ether (DME). Energy 2009;34:2124.

[276] Kuchonthara P, Bhattacharya S, Tsutsumi A. Combinations of solid oxide fuel cell and several enhanced gas turbine cycles. Journal of Power Sources 2003;124:65.

[277] Sudiro M, Zanella C, Bertucco A, Bressan L, Fontana M. Dual-bed gasification of petcoke: model development and validation. Energy & Fuels 2010;24:1213.

[278] Ramzan N, Ashraf A, Naveed S, Malik A. Simulation of hybrid biomass gasification using Aspen plus: A comparative performance analysis for food, municipal solid and poultry waste. Biomass and Bioenergy 2011;35:3962.

[279] AspenTech. Aspen Plus Help Files.

[280] Wilk V, Hofbauer H. Conversion of fuel nitrogen in a dual fluidized bed steam gasifier. Fuel 2013;106:793.

[281] Zhang R, Basu P. A simple model for prediction of solid collection efficiency of a gas-solid separator. Powder Technology 2004;147:86.

[282] Emami Taba L, Irfan MF, Wan Daud WAM, Chakrabarti MH. The effect of temperature on various parameters in coal, biomass and CO-gasification: A review. Renewable and Sustainable Energy Reviews 2012;16:5584.

[283] Kaushal P, Proll T, Hofbauer H. Model development and validation: Co-combustion of residual char, gases and volatile fuels in the fast fluidized combustion chamber of a dual fluidized bed biomass gasifier. Fuel 2007;86:2687.

[284] Li XT, Grace JR, Lim CJ, Watkinson AP, Chen HP, Kim JR. Biomass gasification in a circulating fluidized bed. Biomass and Bioenergy 2004;26:171.

[285] Donolo G, Simon GD, Fermeglia M. Steady state simulation of energy production from biomass by molten carbonate fuel cells. Journal of Power Sources 2006;158:1282.

[286] Corella J, Toledo JM, Molina G. Calculation of the conditions to get less than 2 g tar/Nm3 in a fluidized bed biomass gasifier. Fuel Processing Technology 2006;87:841.

[287] Hughes WE. Biomass Integrated- Gasification / Gas Turbine Power Generation In Zimbabwe. Mechanical and Aerospace Engineering. USA: Princeton University; 1998.

[288] Corella J, Sanz A. Modeling circulating fluidized bed biomass gasifiers. A pseudo-rigorous model for stationary state. Fuel Processing Technology 2005;86:1021.

[289] Sanz A, Corella J. Modeling circulating fluidized bed biomass gasifiers. Results from a pseudo-rigorous 1-dimensional model for stationary state. Fuel Processing Technology 2006;87:247.

[290] Lucas C, Szewczyk D, Blasiak W, Mochida S. High-temperature air and steam gasification of densified biofuels. Biomass and Bioenergy 2004;27:563.

[291] Yang W, Ponzio A, Lucas C, Blasiak W. Performance analysis of a fixed-bed biomass gasifier using high-temperature air. Fuel Processing Technology 2006;87:235.

[292] Hofmann P, Panopoulos KD, Fryda LE, Kakaras E. Comparison between two methane reforming models applied to a quasi-two-dimensional planar solid oxide fuel cell model. Energy 2009;34:2151.

[293] Santin M, Traverso A, Magistri L, Massardo A. Thermoeconomic analysis of SOFC-GT hybrid systems fed by liquid fuels. Energy 2010;35:1077.

[294] Song TW, Sohn JL, Kim TS, Ro ST. Performance characteristics of a MW-class SOFC/GT hybrid system based on a commercially available gas turbine. Journal of Power Sources 2006;158:361.

[295] Komatsu Y, Kimijima S, Szmyd JS. Performance analysis for the part-load operation of a solid oxide fuel cell-micro gas turbine hybrid system. Energy 2010;35:982.

[296] Calise F, Dentice d' Accadia M, Vanoli L, von Spakovsky MR. Full load synthesis/design optimization of a hybrid SOFC-GT power plant. Energy 2007;32:446.

[297] Achenbach E. Three-dimensional and time-dependent simulation of a planar solid oxide fuel cell stack. Journal of Power Sources 1994;49:333.

[298] Chan SH, Khor KA, Xia ZT. A complete polarization model of a solid oxide fuel cell and its sensitivity to the change of cell component thickness. Journal of Power Sources 2001;93:130.

[299] Arpino F, Massarotti N. Numerical simulation of mass and energy transport phenomena in solid oxide fuel cells. Energy 2009;34:2033.

[300] Todd B, Young JB. Thermodynamic and transport properties of gases for use in solid oxide fuel cell modelling. Journal of Power Sources 2002;110:186.

[301] Fuller EN, Schettler PD, Giddings JC. A new method for prediction of binary gas-phase diffusion coefficients. Industrial and Engineering Chemistry 1966;58:19.

[302] Siedlecki M. Private Communication, Delft University of Technology, Delft, The Netherlands. 2009.

[303] Calise F, Dentice d'Accadia M, Palombo A, Vanoli L. Simulation and exergy analysis of a hybrid Solid Oxide Fuel Cell (SOFC)-Gas Turbine System. Energy 2006;31:3278.

[304] Sasaki K, Teraoka Y. Equilibria in Fuel Cell Gases. Journal of The Electrochemical Society 2003;150:A878.

[305] van der Meijden CM. Development of the MILENA gasification technology for the production of Bio-SNG. The Netherlands: Eindhoven University of Technology; 2010.

[306] Commercial and domestic fuel cost comparison. http://www.seai.ie/Publications/Statistics_Publications/Fuel_Cost_Comparison/. Accessed November 2013.

[307] Clearpower Bioenergy Solutions, Private Communication, Ireland. 2010.

[308] Newnan DG, Eschenbach T, Lavelle JP. Engineering economic analysis. 10th ed. New York; Oxford: Oxford University Press; 2009.

[309] The Irish Academy of Engineering. Review of Ireland's Energy Policy. 2009.

[310] Net Present Value Equation. Available at: http://accountingexplained.com/managerial/capital-budgeting/npv. Accessed November 2013.

[311] Cleveland CJ, Ayres RU. Encyclopedia of energy. Amsterdam; Boston: Elsevier Academic Press; 2004.

[312] Franzoni A, Magistri L, Traverso A, Massardo AF. Thermoeconomic analysis of pressurized hybrid SOFC systems with CO2 separation. Energy 2008;33:311.

[313] CHP Deployment Programme. Available at: https://www.seai.ie/Grants/CHP/. Accessed April 2014.

[314] Nouni MR, Mullick SC, Kandpal TC. Biomass gasifier projects for decentralized power supply in India: A financial evaluation. Energy Policy 2007;35:1373.

[315] Adams T, Barton P. High-efficiency power production from natural gas with carbon capture. Journal of Power Sources 2010;195:1971.

[316] Börjesson M, Ahlgren EO. Biomass gasification in cost-optimized district heating systems—A regional modelling analysis. Energy Policy 2010;38:168.

[317] Buragohain B, Mahanta P, Moholkar VS. Biomass gasification for decentralized power generation: The Indian perspective. Renewable and Sustainable Energy Reviews 2010;14:73.

[318] Fahlén E, Ahlgren EO. Assessment of integration of different biomass gasification alternatives in a district-heating system. Energy 2009;34:2184.

[319] Kumbaroğlu G, Madlener R, Demirel M. A real options evaluation model for the diffusion prospects of new renewable power generation technologies. Energy Economics 2008;30:1882.

[320] López PR, González MG, Reyes NR, Jurado F. Optimization of biomass fuelled systems for distributed power generation using Particle Swarm Optimization. Electric Power Systems Research 2008;78:1448.

[321] Rauch R. Biomass CHP Güssing - Biomass Steam Gasification (IEA Bioenergy Task 33 Meeting). TU Wien and Bioenergy 2020+; November 2009.

[322] Autissier N, Palazzi F, Marechal F, Van Herle J, Favrat D. Thermo-economic optimization of a solid oxide fuel cell, gas turbine hybrid system. Journal of fuel cell science and technology 2007;4:123.

[323] White Paper Summary of Interviews with Stationary Fuel Cell Manufacturers. California Stationary Fuel Cell Collaborative; 2008.

[324] Chemical Engineering Magazine CEPCI. Available at: http://www.che.com/pci/. Accessed November 2013.

[325] Wetterlund E, Söderström M. Biomass gasification in district heating systems – The effect of economic energy policies. Applied Energy 2010;87:2914.

[326] Arsalis A. Thermoeconomic modeling and parametric study of hybrid SOFC–gas turbine–steam turbine power plants ranging from 1.5 to 10 MWe. Journal of Power Sources 2008;181:313.

[327] European Central Bank foreign exchange rates. Available at: http://www.ecb.europa.eu/stats/exchange/. Accessed November 2013.

[328] Ortner Anlagen, Private Communication, Austria. 2010.

[329] Repotec Renewable Power Technologies, Private Communication, Austria. 2010.

[330] Klein J, Rednam A. Comparative Costs of California Central Station Electricity Generation Technologies: Final Staff Report. California energy commission; 2007.

[331] CARMEN (Germany) Fuel Price Indices. Available at: http://www.carmen-ev.de/infothek/preisindizes/. Accessed November 2013.

[332] Calise F, D'Accadia MD, Palombo A, Vanoli L. A Detailed One Dimensional Finite-Volume Simulation Model of a Tubular SOFC and a Pre-Reformer. International Journal of Thermodynamics 2007;10:87.

[333] UNECE/FAO. Joint Wood Energy Enquiry 2008 Background Data Analysis 2009.

[334] Knaggs G, O'Driscoll E. Estimated woodflow for the Republic of Ireland for 2006 COFORD; 2008.

[335] Nuon. Welcome at the Nuon Power Buggenum IGCC Willem-Alexander Power Plant IEA Task 33; 2009.

[336] Van der Drift A. Status of biomass gasification. ERA-NET workshop on gasification. Amsterdam; 2008.

[337] Higman C. European coal gasification projects. Presentation at FutureGen Workshop. Tokyo; 2008.

[338] Nuon Website. Available at: http://www.nuon.com/. Accessed June 2011.

[339] NETL Gasifipedia. Available at: http://www.netl.doe.gov/research/coal/energy-systems/gasification/gasifipedia/sasol. Accessed March 2014.

[340] Higman C, van der Burgt M. Gasification. 2nd ed. Gulf Professional; 2008.

[341] Bengtsson S. VVBGC demonstration plant activities at Värnamo. Biomass and Bioenergy 2011;35, Supplement 1:S16.

[342] Bengtsson S, Zethraeus B. Clean Hydrogen-rich Synthesis gas, Publishable Final Activity Report. 2010.

[343] Piterou A, Shackley S, Upham P. Project ARBRE: Lessons for bio-energy developers and policy-makers. Energy Policy 2008;36:2044.

[344] Pang S, Li J. BIGCC system for New Zealand: an overview and perspective. 2006.

[345] Waldheim L, Carpentieri E. Update on the progress of the Brazilian wood BIG-GT demonstration project. Journal of engineering for gas turbines and power 2001;123:525.

[346] Babu S. Biomass gasification for hydrogen production–process description and research needs. IEA Bioenergy; 2002.

[347] Paisley M, Farris M, Black J, Irving J, Overend R. Preliminary operating results from the Battelle/FERCO gasification demonstration plant in Burlington, Vermont, USA. 1st World conference on biomass for energy and industry. Seville, Spain; 2000.

[348] Barker N. Country status report: United Kingdom IEA Bioenergy Task 33; 2006.

[349] Upham P. Applying environmental-behaviour concepts to renewable energy siting controversy: Reflections on a longitudinal bioenergy case study. Energy Policy 2009;37:4273.

[350] Skjoldborg B. Optimisation of I/S Skive District Heating Biomass Gasification Plant. IEA Bioenergy Task 33; October 2010.

[351] Rauch R, Hofbauer H, Bosch K, Siefert I, Aichernig C, Tremmel H, et al. Steam gasification of biomass at CHP plant Guessing-Status of the demonstration plant. 2nd world conference and technology exhibition on biomass for energy, industry and climate protection. Rome, Italy; 2004.

[352] Hannula I. Finnish Country Summary – Biomass Gasification in 2013 IEA Bioenergy Task 33; November 2013.

[353] Isaksson J. Metso Presentation at IEA Bioenergy Task 33 Meeting. November 2009.

[354] Rogers GFC, Mayhew YR. Thermodynamic and transport properties of fluids: SI units. 5th ed: Oxford: Blackwell; 1995.

APPENDIX A: Wood Use in Ireland

The UNECE/FAO collected and compiled data on wood use for energy by member states [333]. The share of wood fuel sources (i.e. direct, indirect, PCRW and unspecified) was reported. Direct supply is defined as wood that enters the energy market directly from the forest/farm, e.g. pulpwood and SRC willow. Indirect supply is defined as wood that has been processed or wood wastes due to processing, e.g. sawmill residues and wood pellets. PCRW is defined as waste wood after at least one life cycle, e.g. pallets. The unspecified wood source refers to wood that was used for energy with its origin unknown. The share of wood fuel sources for the fifteen countries that supplied data (Ireland included) was as follows: Direct 43%, Indirect 53%, PCRW 3% and Unspecified 1%. For Ireland alone, the contribution of direct wood supply was much lower at 12.6%; however, this figure is expected to increase in the near future due to the thinning of private forests. In addition, indirect wood supply was higher at 60.6% with the remaining 26.8% of wood used for energy stemming from PCRW. Ireland's wood energy consumption is low in comparison to the majority of other member states, even on a per capita and contribution to total energy consumption basis. The report also presented wood energy data in terms of users. The users were classified as follows:

- Power and Heat – Defined as a plant that generates electricity, heat or both (CHP) as their primary activity, therefore auto producers that generate electricity and/or heat wholly/partly for their own use to support their primary activity are excluded.
- Industrial – Defined as auto producers, which includes mainly the wood processing industry, e.g. sawmills and panel board mills.
- Residential – Defined as domestic households.

- Other – Defined as any other sector, e.g. agriculture, commercial/services and transport.

The share of wood fuel for energy by user for the fifteen countries that supplied data (Ireland included) was as follows: Power and heat 18%, Industrial 43%, Residential 38% and Other 1%. For Ireland the largest user of wood for energy purposes was the industrial users (71%), followed by the residential users (24%) and other users (5%), with no contribution from power and heat users. These figures were based on 2007 data, i.e. prior to wood co-firing at the Edenderry peat power plant. Wood consumption by power and heat producers experienced an annual growth rate of ~19% between 2005 and 2007 (no contribution from Ireland). By 2011 the commercial power and heat sector could become the most important consumer of woody biomass for energy generation [333].

Table A.1 presents data regarding the contribution of renewables to Ireland's TPER in 2008. The total contribution of 581 ktoe matches the data that was presented in section 2.2. The renewable energy source titled 'other' represents landfill gas, biogas, solar, geothermal and biofuel. Biomass, in this case wood and tallow/MBM, accounts for a relatively large portion of the total renewable contribution (31%), with wood alone accounting for 22%. This however, only translates into 1.13% of Ireland's TPER for biomass or 0.81% for wood alone. The majority of the biomass renewable contribution is in the form of thermal energy (RES-H), with the bulk of this RES-H stemming from and being utilised within the wood processing industry.

Table A.1 Contribution of renewables to TPER for 2008 [79]

Renewable Energy Source		ktoe		%		% TPER
Wind		207		36		1.31
Biomass		178		31		1.13
of which:						
Wood	128		22		0.81	
Tallow/MBM	50		9		0.32	
Hydro		83		14		0.53
Other		113		19		0.71
Total		**581**		**100**		**3.68**

It has been reported that the use of woody biomass for energy production in the wood processing industry declined in 2008 compared to 2007, as a consequence of reduced activity due to the downturn in the construction industry [79]. On the contrary, woody biomass use has increased in the residential and commercial heating markets and in the electricity generation market (co-firing at Edenderry). The overall result was a rise in wood use for energy generation from 569,000 m^3 (roundwood equivalent) in 2007 to 586,000 m^3 (roundwood equivalent) in 2008 [79].

Figure A.1 illustrates woodflow within the wood processing industry in Ireland for the year 2008. The total roundwood harvest plus imports was 2,272,000 m^3 (overbark), with 90% supplied by Coillte and the balance originating from private forests and imports. The total roundwood is divided into categories according to size:

- Large Sawlog – Logs that have a diameter greater than 20 cm; typically used to produce timber for the construction industry.
- Small Sawlog/Palletwood – Logs that have a diameter of 14 to 20 cm; used in the packaging industry and to produce garden furniture and fencing.
- Small Diameter Logs – Generally the top section of the tree with a diameter between 7 and 14 cm and can be divided into sub categories, including pulpwood and stakewood. Pulpwood is the main raw material used for the manufacture of

panel board. Small sawlog may be downgraded to pulpwood on the basis of poor quality [71]. Stakewood is defined as straight lengths of small diameter logs suitable for the fencing market.

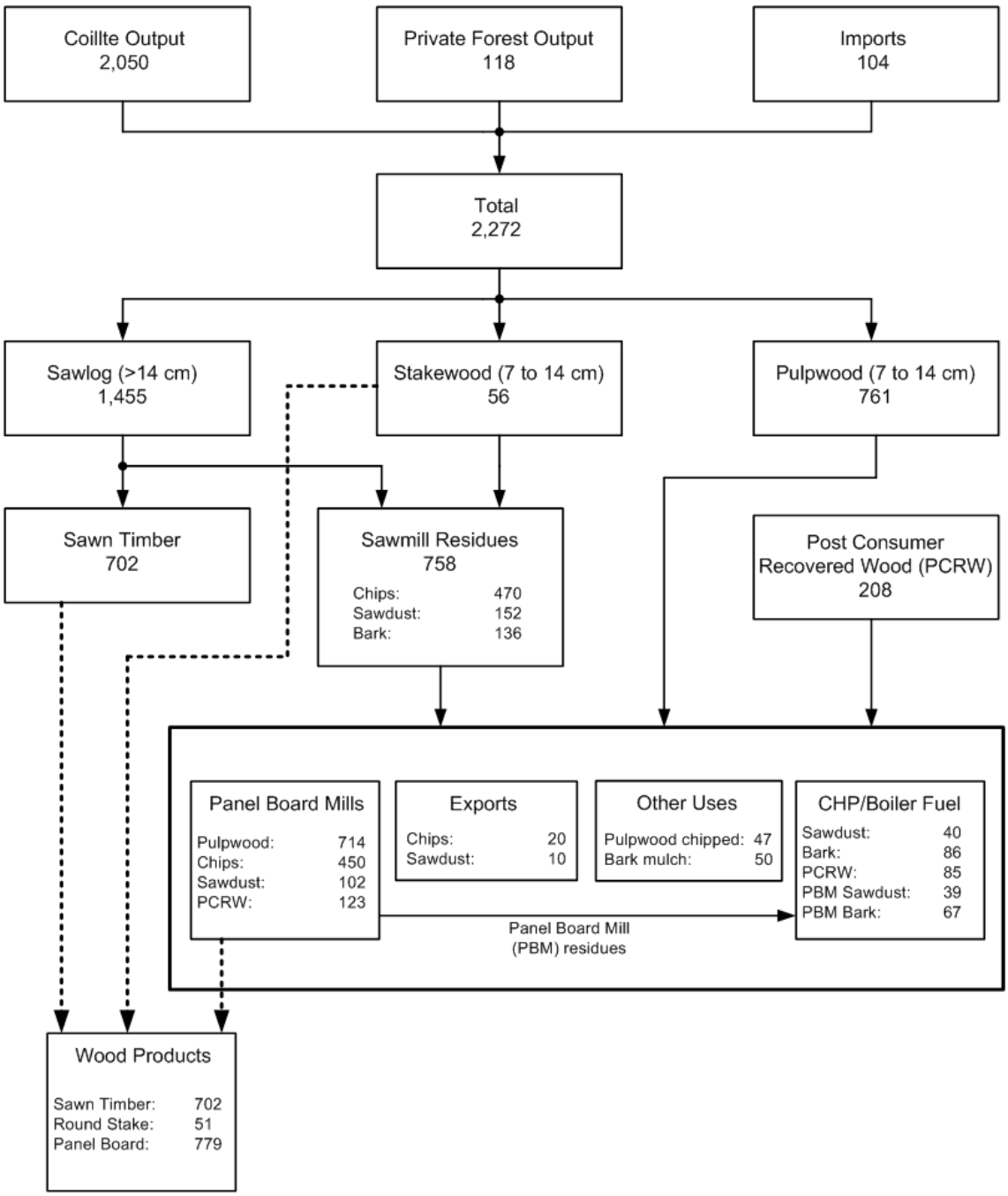

Figure A.1 Ireland's woodflow for 2008 (000 m^3 overbark) [64]

The sawlog is processed in sawmills, which produce sawn timber and wood wastes known as sawmill residues (chip, sawdust and bark). The processing of stakewood also produces residues. The sawmill residues, pulpwood and PCRW are utilised as raw material for the panel board mills, exported, or used for energy purposes or horticulture. As shown in Figure A.1, the bulk of the pulpwood is processed in the panel board mills with a small amount being chipped for energy purposes. The majority of the wood chip, sawdust and PCRW are also processed in the panel board mills with lower amounts being either exported or used for energy purposes. The CHP/Boiler Fuel shown in Figure A.1 includes only the wood utilised for energy within the wood processing industry, i.e. any wood used at the Edenderry peat power station or for fuelling residential/commercial heating systems is not included.

In comparison to previous years, the scale of wood processing has declined. The wood processing industry is heavily dependent on construction and the economic downturn has led to a drop in the demand for wood products. In 2006, when construction activity in Ireland peaked (96,419 house completions compared to 51,724 in 2008 and 20,000 in 2009 [64]), the total roundwood harvest plus imports reached 3,154,000 m^3 (overbark) [334]. Therefore, the wood processing industry has experienced a decline in production of ~30% in two years. In 2008 the output from private forests dropped by ~70% on 2007 levels. This suggests that there has not been sufficient uptake of wood energy in Ireland and therefore no incentive exists to encourage private forest owners to carry out thinning operations and increase production. The wood energy market is considered key to the development of the private forest sector.

APPENDIX B: Gasification plants – additional details

IGCC technology for coal was demonstrated at several locations in the 1990s in Europe and the USA. The following plants were part of those demonstrations and are being operated commercially at the moment [151]:

- Nuon Buggenum 250 MWe coal IGCC plant (Netherlands), which uses Shell entrained flow gasification technology. The plant was demonstrated successfully from 1993 to 1998 and has been operated commercially since (7,500 hours per year) [335]. The plant achieves an efficiency of 43%. Co-gasification tests with biomass started in 2001 and by 2008 15 wt. % co-gasification was normal. The plant has been ready for 30 wt. % co-gasification since 2006 [154, 336]. This IGCC plant closed in April 2013 for financial reasons [140].
- Elcogas Puertollano 300 MWe coal IGCC plant (Spain), which uses Prenflo entrained flow gasification technology. The plant has been operating as a coal IGCC since 1998 with an efficiency of 45% [151]. Co-gasification tests with biomass started in 2007 and as of September 2009 a total of 3,661 tonnes of olive oil waste has been co-gasified [147]. The technical viability of co-gasification up to 10 wt. % has been demonstrated.
- Wabash River 250 MWe coal IGCC plant (USA), which uses E-Gas entrained flow gasification technology (ConocoPhillips). The power plant operates with an efficiency of 39.9% [151].
- Polk County 250 MWe coal IGCC plant (USA), which uses GE entrained flow gasification technology (formerly Texaco technology). The power plant operates with an efficiency of 38% [151].

Other IGCC plants of interest include: Vresova 400 MWe coal IGCC (Sasol-Lurgi gasification technology) Czech Republic, ISAB Energy 512 MWe refinery residue IGCC (GE) Italy, Sarlux 550 MWe refinery residue IGCC (GE) Italy, api Energia 250 MWe refinery residue IGCC (GE) Italy, Agip 250 MWe refinery residue IGCC (Shell) Italy, Pernis 110 MWe refinery residue IGCC (Shell) the Netherlands and SVZ Schwarze Pumpe 75 MWe MSW/coal IGCC (Siemens, BGL and Lurgi gasifiers) Germany [145, 337]. The SVZ Schwarze Pumpe facility ceased operation in 2007 due to economic reasons [337].

There are numerous large gasification projects in the planning and construction stages, many of which are located in China and the USA. In China the focus is on the production of chemicals [145]. In contrast, in the USA about half of the new gasification facilities will produce electricity as primary product. Projects of interest include: Nuon Magnum 1,200 MWe coal/biomass IGCC (Shell) and natural gas CCGT the Netherlands, Powerfuel 900 MWe coal IGCC (Shell) UK and Edwardsport 618 MWe coal IGCC (GE) USA [145, 337]. It has been reported that Nuon has postponed the IGCC phase of the Magnum project until at least 2020 due to insufficient support for unproven onshore carbon capture and storage [338].

Electricity and heat production is most relevant to this work; however, the scale and experience gained through the operation of the Sasol coal-to-liquid fuel facilities in South Africa make them pertinent. The first Sasol plant ‘Sasol I’ was built in the 1950s in an area that became known as Sasolburg (South Africa) and it converted coal to liquid fuel via FT synthesis. The plant used 17 Lurgi fixed bed gasifiers, which were retired in 2004 in favour of natural gas reformers [339]. The Sasol II and III coal-to-liquid fuel plants were constructed in the 1980s in an area that became known as

Secunda (South Africa). These plants are very large, 7,000 MWth of syngas each, and use a total of 80 Sasol-Lurgi fixed bed gasifiers [145, 339].

IGCC technology has been applied to biomass conversion. The world's first complete biomass IGCC plant was built in Värnamo (Sweden) during the period 1991 to 1993 [119, 120, 148, 149]. This plant is discussed in detail due to its significance in the advancement of BG technology; it has been described as the most significant technical accomplishment in BG [158]. The plant operated over the period 1993 to 1999 and is regarded as a very successful demonstration project [69, 105, 149]. The accumulated operating experience amounts to ~8,500 hours of gasification with more than 3,600 hours of GT operation on syngas [142, 149]. The gasification technology was developed jointly by Foster Wheeler and Sydkraft (now E.ON Sverige) under the name Bioflow; it is a pressurised air blown CFB gasifier. The plant produced 6 MWe of electricity which was exported to the grid (4.2 MWe GT and 1.8 MWe ST) as well as 9 MWth of heat for the district heating system of Värnamo, from a total fuel input of 18 MWth. The aim of the project was to demonstrate the integration of BG and combined cycle technology and not to implement a fully optimised plant; this along with the relatively small scale explains the moderate electrical efficiency of 32%. The gasifier was integrated with a gas cooler (350-400 °C), hot gas filter and a combined cycle (GT, HRSG and ST) as shown in Figure B.1.

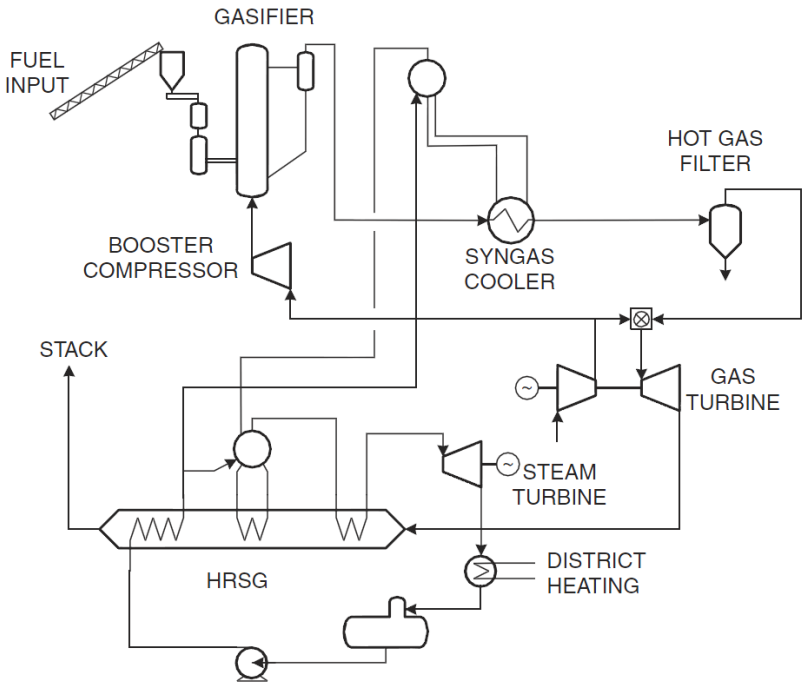

Figure B.1 Flow diagram of Värnamo IGCC plant [340]

Some problems occurred in the hot gas filtration system where some of the ceramic candles broke. The reason was found to be mechanical fatigue due to micro cracking in the filter elements; therefore, sintered metal candles were installed [142]. The new filter candles were operated for more than 2,500 hours without problems and investigations carried out post demonstration indicated that there was no degradation [149]. Fuels including wood chip, bark, forest residues (branches, tree tops, etc.), sawdust (pellets), willow (pellets), straw (pellets) and refuse derived fuel (pellets) were processed without any major operating problems. All emissions were very low with the exception of NO_x, which was due to the fuel bound nitrogen being converted to NH_3 in the gasifier and then to NO_x in the GT combustion chamber [120]. Ståhl recommended that NO_x emissions be reduced by employing a SCR system [120]. The demonstration programme concluded in 2000 and the plant was mothballed as it was not economical to operate [149]. Financial support would be required to make it economically viable

[120]. Furthermore, it has been suggested that the capacity was too small for commercial operation [157]. Sydkraft recommends capacities of between 30 and 70 MWe for future plants and predict electrical efficiencies above 40% [120]. It was concluded that the technology performed very well and had high fuel flexibility with low emissions compared to conventional biomass conversion technologies [120].

The Värnamo facility was acquired by Växjö Värnamo Biomass Gasification Centre for the purpose of performing test work/demonstration activities within the CHRISGAS project (2004-2010) [341]. It was reactivated in 2005 and hot testing was carried out in 2007 [158, 341]. The primary aim of the project was to demonstrate an energy efficient and cost effective method to produce H_2 rich gas from biomass suitable for conversion to liquid fuels [342]. Planned plant modifications included: conversion of pressurised air blown gasifier to O_2 and steam blown gasifier, installation of a new hot gas filter, reformer and water-gas shift unit [149]. These modifications were not carried out due to funding issues. The required funding was approved with the condition that there would be strong industrial involvement, which could not be realised in the project timeframe [341]. As a result the project objectives were shifted towards performing research work at university pilot plants (located at TU Delft and KTH) [342].

In addition, three biomass IGCC projects were funded under the European Commission's THERMIE Programme; ARBRE (UK), Energy Farm/Bioelettrica (Italy) and Biocycle (Denmark) [119, 343, 344]. The ARBRE project began in 1993 with construction of the plant from 1998 to 2001 and commissioning to mid 2002 [105, 149]. The ARBRE company went into liquidation in 2002 with only 448 hours of gasification and 5 hours of GT operation [150]. The plant capacity was 8 MWe (25 MWth fuel input) with an efficiency of 30% and operated on short rotation forestry fuel (willow). It

was of TPS design, which consisted of the atmospheric pressure TPS CFB air blown gasifier, a catalytic tar cracker (second CFB reactor similar in size to the gasifier), gas cooling and cleaning, gas compression and combined cycle [142]. It has been reported that the project failed due to the following events: bankruptcy of the contractor, which led to significant delays in plant construction; technical problems (complex system never demonstrated before); and the withdrawal of the main company for commercial strategy reasons (change in ownership and management at the company) [343]. A positive aspect of the project was the successful development of an energy crop fuel supply chain; a large coal power plant purchased the willow fuel for co-firing after the ARBRE project failed [91, 343]. A similar larger scale project was planned for Brazil (TPS technology), which was to be fuelled by wood and bagasse (sugar cane waste) [119, 149, 345]. The project commenced in 1993 with planned operation by 2001. The project was dropped by the World Bank, the main funding body, in 2001 [119]. The Energy Farm/Bioelettrica project (12 MWe biomass IGCC) faced many technical and non-technical issues. The gasification technology was changed from the Lurgi atmospheric pressure CFB to the pressurised Carbona BFB and the project was eventually cancelled in 2003 [157, 344]. The Biocycle project (Carbona biomass IGCC) was cancelled at an early stage due to difficulty in finding a suitable customer and a sufficient amount of reasonably priced biomass [119, 344].

Another BG project of importance is the BCL/FERCO demonstration plant in Vermont (USA). The 200 t/d wood gasifier was coupled to the McNeil power station (50 MWe biomass combustion) with the produced gas being fired in the existing boiler [346]. The gasifier was the Silvagas DFB. Construction began in 1996 and was completed in late 1997; followed by an extended start-up period from 1998 to 1999 [347]. The first operation in full steam gasification mode was August 1999. It has been

reported that the extended start-up period was not due to problems with the gasification technology but as a result of low availability of the McNeil plant and problems with auxiliary equipment (materials handling, solids separation and gas scrubbing) [347]. The project was to be completed in phases: design, construction and operation with syngas fired in the boiler and finally a combined cycle would be installed and tested [119, 157, 347]. The facility was never converted to biomass IGCC. FERCO were involved in the 22 MWe biomass IGCC WINBEG project (UK) announced in 2003 [348]. The facility planning application was rejected in April 2006; the main reason was excessive biomass transport distances due to the large scale of the plant. Many bioenergy studies in the UK have argued for much smaller scale CHP projects [349].

The GTI Renugas pressurised BFB biomass gasifier was demonstrated in Hawaii (USA) in the 1990s at a 100 t/d bagasse fuelled plant. The plant consisted of the Renugas gasifier, bagasse feeding system, high temperature ceramic filter and flare [65, 152]. The demonstration programme was to be carried out in phases: design, construction and operation of the gasifier (gas flared); integration with a high temperature ceramic filter and GT; O_2 blown mode for methanol production (air blown in normal operation) [119]. There was limited success with gasification and hot gas filtration; serious problems were encountered in handling/feeding of the bagasse fuel [105]. The project was terminated in 1997 without completion of the second and third phases. The Renugas technology was licensed to Tampella Power in 1989 and together with Vattenfall they evaluated the application of biomass IGCC (through their subsidiary Enviropower) [119, 149]. The project was known as VEGA IGCC and they planned on constructing a 60 MWe demonstration plant by 1996; however, the plant was not realised due to poor economics. To aid in the development of biomass IGCC, Enviropower commissioned the 15 MWth 100 t/d biomass fuelled Renugas pilot plant

in Tampere (Finland) in 1993 [65, 105, 119]. The main plant components were as follows: feeding system; high pressure air blown BFB gasifier; hot gas filter and boiler. Over 5,000 tonnes of biomass has been tested at the facility, including wood chips, forest residues, paper mill wastes, willow and straw [119]. In 1997 Enviropower was restructured and a new company Carbona was formed; Carbona now hold the rights to the Renugas technology in Europe. As discussed previously, Carbona were involved in two of the failed European biomass IGCC projects (Biocycle and Energy Farm/Bioelettrica). Recently, they have constructed a BG CHP plant in Skive (Denmark). This plant is commercial and was built as an extension to an existing biomass combustion district heating facility [69]. The plant thermal input is ~20 MWth (wood pellets with wood chips planned in the future) and it is designed to output ~6 MWe and ~11.5 MWth (district heating). The plant comprises the low pressure (~2 bar) air blown Carbona (Renugas) BFB gasifier, biomass feeding system, catalytic tar cracker, gas cooler, filter and scrubber, three gas engines/two gas boilers [153]. The project was proposed in 2001 with construction commencing in 2005 and commissioning during 2007 and 2008; as of April 2010 the gas engines have operated for 10,730 hours [350]. During 2010 the plant ran at 70% output and 50% availability. Stable operation of the plant has been achieved from 2012 with availability of 70% [159].

The Güssing CHP plant (Austria) is considered one of the most successful BG plants in the world as it has operated since 2002 (commercially after a two year demonstration phase). The total plant operating hours was above 44,000 as of 2008 [133] with plant availability greater than 90% [131]. The construction period was September 2000 to 2001 with start-up of the gasifier in November 2001 [125]. The facility including the gas engine was operational by April 2002 [351]. The plant utilises

8 MWth of wood chip fuel to produce 2 MWe of electricity by means of a gas engine (GE Jenbacher J620) and 4.5 MWth of heat [128]. The configuration of the plant is shown in Figure B.2.

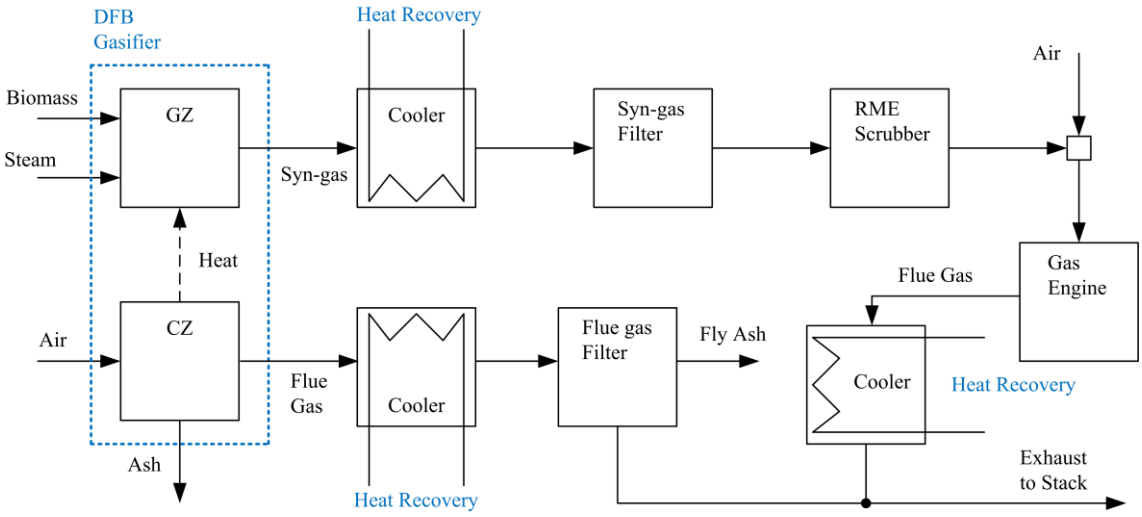

Figure B.2 Flow diagram of Güssing CHP plant

The biomass syngas is produced using a FICFB steam gasifier. Recall, this gasifier operates with two separate zones, the combustion zone (CZ) and gasification zone (GZ). Char is combusted with air in the CZ and heat is transferred to the GZ via circulating bed material. This heat drives the endothermic steam gasification reactions which produce the syngas. Refer to section 3.3.2 for a detailed description of the FICFB gasifier. The raw syngas is cooled and then passed through a filter. Tar, NH_3 and HCl are removed by means of a RME scrubber after which the cold clean syngas is mixed with air and fed to the gas engine [128]. The FICFB gasifier CZ flue gas is cooled then filtered to remove fly ash and mixed with the cooled engine flue gas. The mixed flue gas is directed to the plant stack. Heat is recovered at all stages of cooling to cover air preheating, steam generation and district heating requirements. There are several research projects, which use syngas slip streams at the facility: production of FT diesel,

SNG production and conversion of the gas in a SOFC [137, 351]. The electrical efficiency of the plant is ~25% [128]. Inclusion of an ORC and integrated biomass dryer should increase efficiency to ~34% [131]. The Oberwart plant is similar to the Güssing plant with regards to the gasifier, cooling and cleaning but includes two gas engines, an ORC and a biomass drying unit, which results in higher electrical efficiency [155].

A 60 MWth wood/refuse derived fuel gasifier (atmospheric pressure air blown CFB) has been in operation at a coal fired CHP plant (167 MWe and 240 MWth) in Lahti Finland since 1998 [119, 156]. It is a simple system (no fuel drying or gas cleaning) with syngas co-fired in the existing coal boiler (15% co-firing). This project is considered very successful and operates ~7,000 hours per year (shut down during summer due to low heat demand). Two new gasifiers were installed at the plant in 2012 (80 MWth each) including a gas cleaning unit to lower emissions [352]. A similar gasification system (to the first Lahti plant) was installed in Zeltweg Austria but closed in 2001 because the coal power station was shut down [157]. In addition, a 50 MWth unit (atmospheric pressure air blown CFB) was built in Ruien Belgium and has been operating since 2003 [157]. Another co-firing type BG plant was built in Geertruidenberg Netherlands at the Amer coal fired CHP plant [140]. This plant was scheduled to begin operating on demolition wood in 2000. The original plan was to install an extensive gas cleaning system (cyclones, gas cooler, bag filter and scrubber); however, after facing technical problems the cleaning system was simplified to a gas cooler and cyclones [140, 142, 336]. It operates ~5,000 hours per year and gas cooling remains a problem [140, 154]. It is hoped that these simple co-firing type plants will open up the market for more complex and efficient BG systems [157].

The Greve-in-Chianti refuse derived fuel gasification facility in Italy was in commercial operation from 1993 to 2004 [149, 157]. TPS licensed their technology

(atmospheric pressure air blown CFB) to Ansaldo. The syngas was produced by two 15 MWth CFB gasifiers, passed through cyclones and was fed to a boiler with power generation by ST (6.7 MWe) or to a cement kiln. The plant faced problems (fuel supply and boiler fouling) and therefore operated intermittently [150]. It was shut down in 2004 because a new large scale waste-to-energy facility was built in the region [149]. The Värö gasifier (35 MWth Metso atmospheric pressure CFB) has been in operation since 1987. It appears to be the only lime kiln gasifier (installed during the 1980s) to be still in operation [105, 149]. The Foster Wheeler lime kiln gasifiers (Pietarsaari in Finland, Norrsundet and Karlsborg in Sweden) appear to have been decommissioned over the period 2004 to 2008. Recently, hot gas filter tests were carried out at the Värö plant [353].

Harboøre district heating plant went into service in 1993 with a Vølund updraft fixed bed gasifier (5 MWth) supplying gas to a boiler utilising wood chip as fuel [105, 159]. The facility was converted to a CHP plant in 2000 when two gas engines (1.4 MWe) and a gas cleaning system were installed [159]. As of 2006 the plant operates 8,000 hours per year [336]. Another gas engine based BG facility is the Kokemäki CHP plant in Finland. The Novel updraft fixed bed gasifier is employed, which is being marketed by the company that developed the Bioneer gasification process in the 1980s [105, 158]. The plant consists of the gasifier, biomass dryer, tar reformer, gas cooler, filter, scrubber and three gas engines [156]. The plant output is 1.4 MWe and 4.3 MWth from 7.2 MWth of wood fuel. Construction finished in April 2005 with commissioning in 2006. The current status of the plant is unknown and has been reported to be ‘on hold’ [117].

APPENDIX C: Description of calculation of molar Gibbs free energy of formation

The MATLAB code below was used to plot temperature against $\Delta\bar{g}_f$ for the H_2 oxidation reaction (Eq. 3.8) and obtain a fifth degree polynomial. The polynomial was used in the Aspen Plus models to predict $\Delta\bar{g}_f$ at any temperature. An Excel spreadsheet model was developed to calculate $\Delta\bar{g}_f$ over the temperature range 1062-1182 K. With the use of published thermodynamic tables [354], specific molar enthalpy ($\bar{h}_f$) and entropy ($\bar{s}$) values for H_2, O_2 and H_2O were found through interpolation for each temperature (temperature range = 1062-1182 K, increments of 5 K). $\Delta\bar{g}_f$ values for each temperature were computed using the following equations [163, 169]:

$$\Delta\bar{g}_f = \Delta\bar{h}_f - T\Delta\bar{s} \quad \text{Eq. C.1}$$

$$\Delta\bar{h}_f = (1)\bar{h}_{f,H2O} - \left[(1)\bar{h}_{f,H2} + (0.5)\bar{h}_{f,O2}\right] \quad \text{Eq. C.2}$$

$$\Delta\bar{s} = (1)\bar{s}_{H2O} - \left[(1)\bar{s}_{H2} + (0.5)\bar{s}_{O2}\right] \quad \text{Eq. C.3}$$

$\Delta\bar{h}_f$ is the molar enthalpy of formation and is equal to the difference between $\bar{h}_f$ of the chemical reaction products and reactants (multiplying each $\bar{h}_f$ value by the number of moles for that product or reactant). $\Delta\bar{s}$ is the molar entropy and is calculated in a similar manner. T in Eq. C.1 is simply temperature in Kelvin. The term $T\Delta\bar{s}$ represents unavailable energy resulting from the entropy change within the system (i.e. energy converted to heat instead of electricity) [163]. The temperatures and corresponding $\Delta\bar{g}_f$ values were then plotted in MATLAB and the basic fitting tool was employed to obtain the polynomial.

MATLAB code

```
% This mfile plots Gibbs free energy of formation against temperature for the H2
oxidation reaction
% with the objective of generating a fifth degree polynomial using the MATLAB basic
fitting tool
% G. F. C. Rogers and Y. R. Mayhew, Thermodynamic and Transport Properties of
Fluids, Blackwell Publishing, Oxford UK (1995).

Tavg = [1062, 1067, 1072, 1077, 1082, 1087, 1092, 1097, 1102, 1107, 1112, 1117,
1122, 1127, 1132, 1137, 1142, ...
   1147, 1152, 1157, 1162, 1167, 1172, 1177, 1182]

Delta_gf = [-189221.7629, -188944.2105, -188666.3944, -188388.3145, -188109.9709,
-187831.3635, ...
   -187552.4924, -187273.3575, -186993.9589, -186714.2965, -186434.3704, -
186154.1805, -185873.7269, ...
   -185593.0095, -185312.0284, -185030.7835, -184749.2749, -184467.5025, -
184185.4664, -183903.1665, ...
   -183620.6029, -183337.7755, -183054.6844, -182771.3295, -182487.7109]

plot (Tavg, Delta_gf, '-r^')
```

Polynomial

```
delta_gf = (-6.78E-19*Tavg**5)+(-1.33E-12*Tavg**4)+(5.97E-09*
+          Tavg**3)+(0.0052649*Tavg**2)+(44.288*Tavg)-2.422E+05
```

APPENDIX D: Fortran code for voltage and system performance calculations

The Fortran code below applies to all system configurations (system 1-4) and also the standalone SOFC model (section 5.2). For system 3, the electrical heater power requirement was included in the net efficiency calculations, etc., and for system 4 the 'COMP3' power requirement was omitted.

Two codes are presented, one for variable current density (i.e. constant power) and the other for specified current density (i.e. variable power). For variable current density models the code below was used as a design specification block. The block varies the biomass input mass flow rate until the DC power equals the desired value (120 kW, 500 kW or 1 MW). Equations 5.1, 5.2 and 5.23 were employed to determine the current density, after which the voltage and power were calculated. This calculation sequence was repeated until the DC power was equal to the desired value. For specified current density models the code was implemented using a calculator block in conjunction with a design specification block to set the biomass input mass flow rate. The design specification block utilised Eq. 5.23 and 5.24 for this purpose and the calculation sequence was repeated until the syngas flow rate (at SOFC inlet) was equal to that required to achieve the specified current density.

Variable current density

Aspen Plus Variables

POWER	Stream-Var Stream=POWER Substream=MIXED Variable=MOLE-FLOW Units=kmol/hr
UF	Stream-Var Stream=UF Substream=MIXED Variable=MOLE-FLOW Units=kmol/hr
H2	Mole-Flow Stream=SYNGAS2 Substream=MIXED Component=H2 Units=kmol/hr
CO	Mole-Flow Stream=SYNGAS2 Substream=MIXED Component=CO Units=kmol/hr
CH4	Mole-Flow Stream=SYNGAS2 Substream=MIXED Component=CH4 Units=kmol/hr
C2H6	Mole-Flow Stream=SYNGAS2 Substream=MIXED Component=C2H6 Units=kmol/hr
C3H8	Mole-Flow Stream=SYNGAS2 Substream=MIXED Component=C3H8 Units=kmol/hr
C4H10	Mole-Flow Stream=SYNGAS2 Substream=MIXED Component=C4H10 Units=kmol/hr
YH2EN	Mole-Frac Stream=6 Substream=MIXED Component=H2

YH2EX	Mole-Frac Stream=7 Substream=MIXED Component=H2
YH2OEN	Mole-Frac Stream=6 Substream=MIXED Component=H2O
YH2OEX	Mole-Frac Stream=7 Substream=MIXED Component=H2O
YO2EN	Mole-Frac Stream=15 Substream=MIXED Component=O2
YO2EX	Mole-Frac Stream=18 Substream=MIXED Component=O2
PSOFC	Stream-Var Stream=7 Substream=MIXED Variable=PRES Units=bar
GH2	Mass-Flow Stream=SYNGAS Substream=MIXED Component=H2 Units=kg/hr
GCO	Mass-Flow Stream=SYNGAS Substream=MIXED Component=CO Units=kg/hr
GCH4	Mass-Flow Stream=SYNGAS Substream=MIXED Component=CH4 Units=kg/hr
GC2H6	Mass-Flow Stream=SYNGAS Substream=MIXED Component=C2H6 Units=kg/hr
GC3H8	Mass-Flow Stream=SYNGAS Substream=MIXED Component=C3H8 Units=kg/hr
GC4H10	Mass-Flow Stream=SYNGAS Substream=MIXED Component=C4H10 Units=kg/hr
GCO2	Mass-Flow Stream=SYNGAS Substream=MIXED Component=CO2 Units=kg/hr
GN2	Mass-Flow Stream=SYNGAS Substream=MIXED Component=N2 Units=kg/hr
TOP	Stream-Var Stream=7 Substream=MIXED Variable=TEMP Units=C
TEMPA	Stream-Var Stream=6 Substream=MIXED Variable=TEMP Units=C
TEMPC	Stream-Var Stream=16 Substream=MIXED Variable=TEMP Units=C
COMP1	Work-Power Stream=W1 Units=Watt
COMP2	Work-Power Stream=W2 Units=Watt
COMP3	Work-Power Stream=W3 Units=Watt
ZLHV	NC-Param Variable=HCOMB ID1=WOOD ID2=1 Element=1
BIOMAS	Stream-Var Stream=BIOMASS Substream=NC Variable=MASS-FLOW Units=kg/hr
CPMX	Stream-Prop Stream=WARMFLU Prop-Set=THERMAL Units=kJ/kg-K
FLUE	Stream-Var Stream=WARMFLU Substream=MIXED Variable=MASS-FLOW Units=kg/hr
FLUET	Stream-Var Stream=WARMFLU Substream=MIXED Variable=TEMP Units=C
PUMP1	Work-Power Stream=W4 Units=Watt
PUMP2	Work-Power Stream=W5 Units=Watt
AREA	Stream-Var Stream=AREA Substream=MIXED Variable=MASS-FLOW Units=kg/hr

Fortran code

```
C     Varies inlet fuel flow until the electrical power equals the specified value.
C     Current calculated using H2consumed eqn., voltage calculated by
C     subtracting ohmic, activation and concentration losses from the Nernst voltage.
C     Electrical power then calculated using P = VI

C     Constants:

C     Interconnection resistivity 'ohm metre'
      Rho_int = 0.025
C     Song et al. constants A and B and pi
      A = 0.804
      B = 0.13
      pi = 3.141592654
C     Mean SOFC diameter 'm'
      Dm = 0.01966
C     SOFC component thickness 'm'
      ta = 0.0001
      tc = 0.0022
      te = 0.00004
      tint = 0.000085
C     SOFC interconnection width 'm'
      wint = 0.009
C     Faraday's constant 'C/mol' and molar gas constant 'J/mol K'
      F = 96485.0
      Rg = 8.314
C     Pre-exponential factors 'A/m^2'
C     Note: z is used in front of some constant and variable names so
C     they will be treated as real double precision numbers and not integers (integers letters I to N)
```

```
      zka = 213000000.0
      zkc = 14900000000.0
      Pref = 1.0
      zm = 0.25
C     Activation energy 'J/mol'
      Ea = 110000.0
      Ec = 155000.0
C     Molecular weights of gases & Fuller diffusion volumes, avg
C     electrode pore radius 'm', porosity & tortuosity
      zMH2 = 2.016
      zMH2O = 18.015
      zMO2 = 31.998
      zMN2 = 28.014
      vH2 = 7.07
      vH2O = 12.7
      vO2 = 16.6
      vN2 = 17.9
      r = 0.0000005
      eps = 0.5
      xi = 5.9

C     Calculations

C     Current density 'A/m^2' calculation
      H2consumed = UF*(H2 + CO + 4.0*CH4 + 7.0*C2H6 +
     +            10.0*C3H8 + 13.0*C4H10)
      zI = 2.0*F*(H2consumed*1000.0/3600.0)
      zj = zI / AREA

      Write(NTERM,10)
      10  Format('The current is (A)')
      Write(NTERM,*) zI

      Write(NTERM,20)
      20  Format('The current density is (A/m^2)')
      Write(NTERM,*) zj

C     Nernst voltage 'Volts' calculation
C     Inlet/outlet gas component average mole fractions
      yH2avg = (YH2EN + YH2EX) / 2.0
      yO2avg = (YO2EN + YO2EX) / 2.0
      yH2Oavg = (YH2OEN + YH2OEX) / 2.0
      Tavg = ((((TEMPA+TEMPC)/2.0)+TOP)/2.0)+273.15
C     Molar Gibbs free energy of formation 'J/mol' for H2 oxidation reaction
      delta_gf = (-6.78E-19*Tavg**5)+(-1.33E-12*Tavg**4)+(5.97E-09*
     +           Tavg**3)+(0.0052649*Tavg**2)+(44.288*Tavg)-2.422E+05

      VN = (-delta_gf/(2.0*F))+((Rg*Tavg)/(2.0*F))*DLOG(((yH2avg*
     +      PSOFC)*(yO2avg*PSOFC)**0.5)/(yH2Oavg*PSOFC))

      Write(NTERM,30)
      30  Format('The Nernst voltage is (Volts)')
      Write(NTERM,*) VN

C     Ohmic loss (Volts) calculated using Song et al. eqns
      Top = TOP + 273.15
      Rho_a = 0.0000298*DEXP(-1392.0/Top)
      Rho_c = 0.00008114*DEXP(600.0/Top)
      Rho_e = 0.0000294*DEXP(10350.0/Top)
      Vohm_a = (zj*Rho_a*(A*pi*Dm)**2)/(8.0*ta)
```

```
      Vohm_c = ((zj*Rho_c*(pi*Dm)**2)*A*(A+2.0*(1.0-A-B))) / (8.0*tc)
      Vohm_e = zj*Rho_e*te
      Vohm_int = (zj*Rho_int*(pi*Dm)*tint) / wint
      Vohm = Vohm_a + Vohm_c + Vohm_e + Vohm_int

      Write(NTERM,40)
      40  Format('The ohmic loss is (Volts)')
      Write(NTERM,*) Vohm

C     Activation loss (Volts) calculated using Achenbach eqns

      x = ((2.0*F)/(Rg*Top))*(zka)*((yH2avg*PSOFC/Pref)**zm)
     +     *(DEXP(-Ea/(Rg*Top)))
      y = ((4.0*F)/(Rg*Top))*(zkc)*((yO2avg*PSOFC/Pref)**zm)
     +     *(DEXP(-Ec/(Rg*Top)))
      Ract_a = 1.0/x
      Ract_c = 1.0/y
      Vact_a = zj*Ract_a
      Vact_c = zj*Ract_c
      Vact = Vact_a + Vact_c

      Write(NTERM,50)
      50  Format('The activation loss is (Volts)')
      Write(NTERM,*) Vact

C     Concentration loss (Volts) calculated using Chan et al. eqns

C     Diff coeffs 'm^2/s' using Fuller et al. method
      Ppa = PSOFC*100000.0
      DH2H2O = (0.0000001*Top**1.75*(1.0/zMH2+1.0/zMH2O)**0.5)/((Ppa/
     +         101325.0)*(vH2**(1.0/3.0)+vH2O**(1.0/3.0))**2)
      DH2H2O_eff = DH2H2O*(eps/xi)
      DO2N2 = (0.0000001*Top**1.75*(1.0/zMO2+1.0/zMN2)**0.5)/((Ppa/
     +         101325.0)*(vO2**(1.0/3.0)+vN2**(1.0/3.0))**2)
      DO2N2_eff = DO2N2*(eps/xi)

      Write(NTERM,60)
      60  Format('The DO2N2_eff is (m^2/s)')
      Write(NTERM,*) DO2N2_eff

      DH2k = 97.0*r*(Top/zMH2)**0.5
      DH2k_eff = DH2k*(eps/xi)
      DH2Ok = 97.0*r*(Top/zMH2O)**0.5
      DH2Ok_eff = DH2Ok*(eps/xi)
      DO2k = 97.0*r*(Top/zMO2)**0.5
      DO2k_eff = DO2k*(eps/xi)
      DH2_eff = 1.0/((1.0/DH2H2O_eff)+(1.0/DH2k_eff))
      DH2O_eff = 1.0/((1.0/DH2H2O_eff)+(1.0/DH2Ok_eff))
      DO2_eff = 1.0/((1.0/DO2N2_eff)+(1.0/DO2k_eff))

      Write(NTERM,70)
      70  Format('The DH2_eff is (m^2/s)')
      Write(NTERM,*) DH2_eff

      Write(NTERM,80)
      80  Format('The DH2O_eff is (m^2/s)')
      Write(NTERM,*) DH2O_eff

      Write(NTERM,90)
      90  Format('The DO2_eff is (m^2/s)')
```

```
      Write(NTERM,*) DO2_eff

      Write(NTERM,100)
  100 Format('The DO2k_eff is (m^2/s)')
      Write(NTERM,*) DO2k_eff

      Da_eff = ((yH2Oavg*Ppa)*DH2_eff+(yH2avg*Ppa)*DH2O_eff)/Ppa
      Dc_eff = DO2_eff
      DelO2 = DO2k_eff/(DO2k_eff+DO2N2_eff)

      Write(NTERM,110)
  110 Format('The Da_eff is (m^2/s)')
      Write(NTERM,*) Da_eff

      Write(NTERM,120)
  120 Format('The DelO2 is')
      Write(NTERM,*) DelO2

      Vconc_a = -((Rg*Top)/(2.0*F))*DLOG((1.0-((Rg*Top)/(2.0*F))*
     +      (ta/(Da_eff*yH2avg*Ppa))*zj)/(1.0+((Rg*Top)/
     +      (2.0*F))*(ta/(Da_eff*yH2Oavg*Ppa))*zj))
      Vconc_c = -((Rg*Top)/(4.0*F))*DLOG((((Ppa/DelO2)-((Ppa/DelO2)-
     +      (yO2avg*Ppa))*DEXP(((Rg*Top)/(4.0*F))*((DelO2*tc)/
     +      (Dc_eff*Ppa))*zj))/(yO2avg*Ppa)))
      Vconc = Vconc_a + Vconc_c

      Write(NTERM,130)
  130 Format('The concentration loss is (Volts)')
      Write(NTERM,*) Vconc

C     Actual voltage is given by the Nernst voltage minus the sum of the three losses

      V = VN - (Vohm + Vact + Vconc)

      Write(NTERM,140)
  140 Format('The SOFC voltage is (Volts)')
      Write(NTERM,*) V

C     The SOFC DC power 'Watts' is then calculated
      PDC = V*zI

      Write(NTERM,150)
  150 Format('The SOFC DC Power is (Watts)')
      Write(NTERM,*) PDC

C     SOFC AC electrical efficiency
C     DC-AC inverter efficiency assumed 92%

C     Fuel energy in (kW) calculation, data from Cengel & Boles 6th edition, LHV (kJ/kmol)
      zNRGIN = ((H2*241920.0)+(CO*282931.3)+(CH4*802952.15)
     +      +(C2H6*1428926.4)+(C3H8*2043454.98)
     +      +(C4H10*2637040.51))/3600.0

      Eta1 = ((PDC*0.92/1000.0) / zNRGIN)*100.0

      Write(NTERM,160)
  160 Format('The SOFC AC efficiency is (%)')
      Write(NTERM,*) Eta1

C     Plant gross electrical efficiency
```

```
      Eta2 = ((PDC*0.92/1000.0)/((BIOMAS/3600.0)*(ZLHV/1000.0)))*100.0

      Write(NTERM,170)
      170  Format('The plant gross electrical efficiency is (%)')
      Write(NTERM,*) Eta2

C     Plant net electrical efficiency: considering parasitic power
      Eta3 = (((PDC*0.92/1000.0)-((COMP1+COMP2+COMP3+PUMP1+PUMP2)/
     +       1000.0))/((BIOMAS/3600.0)*(ZLHV/1000.0)))*100.0

      Write(NTERM,180)
      180  Format('The plant net electrical efficiency is (%)')
      Write(NTERM,*) Eta3

C     Recoverable heat (kW): Q = m cp DeltaT
      Q = (FLUE/3600.0)*CPMX*(FLUET-25.0)

      Write(NTERM,190)
      190  Format('The useful heat is (kW)')
      Write(NTERM,*) Q

C     Plant gross CHP (overall) efficiency
      Eta4 = (((PDC*0.92/1000.0) + Q) /
     +       ((BIOMAS/3600.0)*(ZLHV/1000.0)))*100.0

      Write(NTERM,200)
      200  Format('The plant gross CHP efficiency is (%)')
      Write(NTERM,*) Eta4

C     Plant net CHP (overall) efficiency
      Eta5 = ((((PDC*0.92/1000.0)-((COMP1+COMP2+COMP3+PUMP1+PUMP2)
     +       /1000.0)) + Q)/((BIOMAS/3600.0)*(ZLHV/1000.0)))*100.0

      Write(NTERM,210)
      210  Format('The plant net CHP efficiency is (%)')
      Write(NTERM,*) Eta5

C     The plant gross power to heat ratio
      PHRATIO = (PDC*0.92/1000.0) / Q

      Write(NTERM,220)
      220  Format('The plant gross power to heat ratio is')
      Write(NTERM,*) PHRATIO

C     The plant net power to heat ratio
      PHRATIO2 = ((PDC*0.92/1000.0)-((COMP1+COMP2+COMP3+PUMP1+PUMP2)
     +          /1000.0))/Q

      Write(NTERM,230)
      230  Format('The plant net power to heat ratio is')
      Write(NTERM,*) PHRATIO2

C     SYNGAS energy (kW) calculation, data from Cengel & Boles 6th edition, LHV (kJ/kg)
      SYNGAS = ((GH2*120000.0)+(GCO*10100.0)+(GCH4*50050.0)
     +       +(GC2H6*47520.0)+(GC3H8*46340.0)
     +       +(GC4H10*45370.0))/3600.0

      zLHV2 = (SYNGAS/((GH2 + GCO + GCH4 + GCO2 + GN2)/3600))/1000

      Write(NTERM,240)
```

```
      240  Format('The SYNGAS power is (kW)')
      Write(NTERM,*) SYNGAS

      Write(NTERM,250)
      250  Format('The SYNGAS dry LHV is (MJ/kg)')
      Write(NTERM,*) zLHV2

      Write(NTERM,260)
      260  Format('The SYNGAS2 power is (kW)')
      Write(NTERM,*) zNRGIN

C     The DFB gasifier Cold Gas Efficiency (CGE)
      CGE = (SYNGAS / ((BIOMAS/3600.0)*(ZLHV/1000.0)))*100.0

      Write(NTERM,270)
      270  Format('The Cold Gas Efficiency (CGE) is (%)')
      Write(NTERM,*) CGE

C     Biomass power (kW)
      FUEL = (BIOMAS/3600.0)*(ZLHV/1000.0)

      Write(NTERM,280)
      280  Format('The Biomass fuel power is (kW)')
      Write(NTERM,*) FUEL
```

Specified current density

Aspen Plus Variables

YH2EN	Mole-Frac Stream=6 Substream=MIXED Component=H2
YH2EX	Mole-Frac Stream=7 Substream=MIXED Component=H2
YH2OEN	Mole-Frac Stream=6 Substream=MIXED Component=H2O
YH2OEX	Mole-Frac Stream=7 Substream=MIXED Component=H2O
YO2EN	Mole-Frac Stream=15 Substream=MIXED Component=O2
YO2EX	Mole-Frac Stream=18 Substream=MIXED Component=O2
PSOFC	Stream-Var Stream=7 Substream=MIXED Variable=PRES Units=bar
TOP	Stream-Var Stream=7 Substream=MIXED Variable=TEMP Units=C
TEMPA	Stream-Var Stream=6 Substream=MIXED Variable=TEMP Units=C
TEMPC	Stream-Var Stream=16 Substream=MIXED Variable=TEMP Units=C
COMP1	Work-Power Stream=W1 Units=Watt
COMP2	Work-Power Stream=W2 Units=Watt
ZJ	Stream-Var Stream=J Substream=MIXED Variable=MOLE-FLOW Units=kmol/hr
H2	Mole-Flow Stream=SYNGAS2 Substream=MIXED Component=H2 Units=kmol/hr
CO	Mole-Flow Stream=SYNGAS2 Substream=MIXED Component=CO Units=kmol/hr
CH4	Mole-Flow Stream=SYNGAS2 Substream=MIXED Component=CH4 Units=kmol/hr
C2H6	Mole-Flow Stream=SYNGAS2 Substream=MIXED Component=C2H6 Units=kmol/hr
C3H8	Mole-Flow Stream=SYNGAS2 Substream=MIXED Component=C3H8 Units=kmol/hr
C4H10	Mole-Flow Stream=SYNGAS2 Substream=MIXED Component=C4H10 Units=kmol/hr
GH2	Mass-Flow Stream=SYNGAS Substream=MIXED Component=H2 Units=kg/hr
GCO	Mass-Flow Stream=SYNGAS Substream=MIXED Component=CO Units=kg/hr
GCH4	Mass-Flow Stream=SYNGAS Substream=MIXED Component=CH4 Units=kg/hr
GC2H6	Mass-Flow Stream=SYNGAS Substream=MIXED Component=C2H6 Units=kg/hr
GC3H8	Mass-Flow Stream=SYNGAS Substream=MIXED Component=C3H8 Units=kg/hr
GC4H10	Mass-Flow Stream=SYNGAS Substream=MIXED Component=C4H10 Units=kg/hr
GCO2	Mass-Flow Stream=SYNGAS Substream=MIXED Component=CO2 Units=kg/hr
GN2	Mass-Flow Stream=SYNGAS Substream=MIXED Component=N2 Units=kg/hr
COMP3	Work-Power Stream=W3 Units=Watt
ZLHV	NC-Param Variable=HCOMB ID1=WOOD ID2=1 Element=1

BIOMAS	Stream-Var Stream=BIOMASS Substream=NC Variable=MASS-FLOW Units=kg/hr
CPMX	Stream-Prop Stream=WARMFLU Prop-Set=THERMAL Units=kJ/kg-K
FLUE	Stream-Var Stream=WARMFLU Substream=MIXED Variable=MASS-FLOW Units=kg/hr
FLUET	Stream-Var Stream=WARMFLU Substream=MIXED Variable=TEMP Units=C
PUMP1	Work-Power Stream=W4 Units=Watt
PUMP2	Work-Power Stream=W5 Units=Watt
AREA	Stream-Var Stream=AREA Substream=MIXED Variable=MASS-FLOW Units=kg/hr

Fortran code

```
C     Voltage calculated by subtracting ohmic, activation and concentration losses from the
C     Nernst voltage.
C     Electrical power then calculated using P = VI

C     Constants:

C     Interconnection resistivity 'ohm metre'
      Rho_int = 0.025
C     Song et al. constants A and B and pi
      A = 0.804
      B = 0.13
      pi = 3.141592654
C     Mean SOFC diameter 'm'
      Dm = 0.01966
C     SOFC component thickness 'm'
      ta = 0.0001
      tc = 0.0022
      te = 0.00004
      tint = 0.000085
C     SOFC interconnection width 'm'
      wint = 0.009
C     Faraday's constant 'C/mol' and molar gas constant 'J/mol K'
      F = 96485.0
      Rg = 8.314
C     Pre-exponential factors 'A/m^2'
C     Note: z is used in front of some constant and variable names so
C     they will be treated as real double precision numbers and not integers (integers letters I to N)
      zka = 213000000.0
      zkc = 14900000000.0
      Pref = 1.0
      zm = 0.25
C     Activation energy 'J/mol'
      Ea = 110000.0
      Ec = 155000.0
C     Molecular weights of gases & Fuller diffusion volumes, avg
C     electrode pore radius 'm', porosity & tortuosity
      zMH2 = 2.016
      zMH2O = 18.015
      zMO2 = 31.998
      zMN2 = 28.014
      vH2 = 7.07
      vH2O = 12.7
      vO2 = 16.6
      vN2 = 17.9
      r = 0.0000005
      eps = 0.5
      xi = 5.9

C     Calculations
```

```
C       Current 'A' calculation
        zj = ZJ
        zI = zj*AREA

        Write(NTERM,10)
        10  Format('The current is (A)')
        Write(NTERM,*) zI

        Write(NTERM,20)
        20  Format('The current density is (A/m^2)')
        Write(NTERM,*) zj

C       Nernst voltage 'Volts' calculation
C       Inlet/outlet gas component average mole fractions
        yH2avg = (YH2EN + YH2EX) / 2.0
        yO2avg = (YO2EN + YO2EX) / 2.0
        yH2Oavg = (YH2OEN + YH2OEX) / 2.0
        Tavg = ((((TEMPA+TEMPC)/2.0)+TOP)/2.0)+273.15
C       Molar Gibbs free energy of formation 'J/mol' for H2 oxidation reaction
        delta_gf = (-6.78E-19*Tavg**5)+(-1.33E-12*Tavg**4)+(5.97E-09*
     +          Tavg**3)+(0.0052649*Tavg**2)+(44.288*Tavg)-2.422E+05

        VN = (-delta_gf/(2.0*F))+((Rg*Tavg)/(2.0*F))*DLOG(((yH2avg*
     +     PSOFC)*(yO2avg*PSOFC)**0.5)/(yH2Oavg*PSOFC))

        Write(NTERM,30)
        30  Format('The Nernst voltage is (Volts)')
        Write(NTERM,*) VN

C       Ohmic loss (Volts) calculated using Song et al. eqns
        Top = TOP + 273.15
        Rho_a = 0.0000298*DEXP(-1392.0/Top)
        Rho_c = 0.00008114*DEXP(600.0/Top)
        Rho_e = 0.0000294*DEXP(10350.0/Top)

        Vohm_a = (zj*Rho_a*(A*pi*Dm)**2)/(8.0*ta)
        Vohm_c = ((zj*Rho_c*(pi*Dm)**2)*A*(A+2.0*(1.0-A-B))) / (8.0*tc)
        Vohm_e = zj*Rho_e*te
        Vohm_int = (zj*Rho_int*(pi*Dm)*tint) / wint
        Vohm = Vohm_a + Vohm_c + Vohm_e + Vohm_int

        Write(NTERM,40)
        40  Format('The ohmic loss is (Volts)')
        Write(NTERM,*) Vohm

C       Activation loss (Volts) calculated using Achenbach eqns

        x = ((2.0*F)/(Rg*Top))*(zka)*((yH2avg*PSOFC/Pref)**zm)
     +     *(DEXP(-Ea/(Rg*Top)))
        y = ((4.0*F)/(Rg*Top))*(zkc)*((yO2avg*PSOFC/Pref)**zm)
     +     *(DEXP(-Ec/(Rg*Top)))
        Ract_a = 1.0/x
        Ract_c = 1.0/y
        Vact_a = zj*Ract_a
        Vact_c = zj*Ract_c
        Vact = Vact_a + Vact_c

        Write(NTERM,50)
        50  Format('The activation loss is (Volts)')
        Write(NTERM,*) Vact
```

```
C       Concentration loss (Volts) calculated using Chan et al. eqns
C       Diff coeffs 'm^2/s' using Fuller et al. method
        Ppa = PSOFC*100000.0
        DH2H2O = (0.0000001*Top**1.75*(1.0/zMH2+1.0/zMH2O)**0.5)/((Ppa/
     +       101325.0)*(vH2**(1.0/3.0)+vH2O**(1.0/3.0))**2)
        DH2H2O_eff = DH2H2O*(eps/xi)
        DO2N2 = (0.0000001*Top**1.75*(1.0/zMO2+1.0/zMN2)**0.5)/((Ppa/
     +       101325.0)*(vO2**(1.0/3.0)+vN2**(1.0/3.0))**2)
        DO2N2_eff = DO2N2*(eps/xi)

        Write(NTERM,60)
        60  Format('The DO2N2_eff is (m^2/s)')
        Write(NTERM,*) DO2N2_eff

        DH2k = 97.0*r*(Top/zMH2)**0.5
        DH2k_eff = DH2k*(eps/xi)
        DH2Ok = 97.0*r*(Top/zMH2O)**0.5
        DH2Ok_eff = DH2Ok*(eps/xi)
        DO2k = 97.0*r*(Top/zMO2)**0.5
        DO2k_eff = DO2k*(eps/xi)
        DH2_eff = 1.0/((1.0/DH2H2O_eff)+(1.0/DH2k_eff))
        DH2O_eff = 1.0/((1.0/DH2H2O_eff)+(1.0/DH2Ok_eff))
        DO2_eff = 1.0/((1.0/DO2N2_eff)+(1.0/DO2k_eff))

        Write(NTERM,70)
        70  Format('The DH2_eff is (m^2/s)')
        Write(NTERM,*) DH2_eff

        Write(NTERM,80)
        80  Format('The DH2O_eff is (m^2/s)')
        Write(NTERM,*) DH2O_eff

        Write(NTERM,90)
        90  Format('The DO2_eff is (m^2/s)')
        Write(NTERM,*) DO2_eff

        Write(NTERM,100)
        100  Format('The DO2k_eff is (m^2/s)')
        Write(NTERM,*) DO2k_eff

        Da_eff = ((yH2Oavg*Ppa)*DH2_eff+(yH2avg*Ppa)*DH2O_eff)/Ppa
        Dc_eff = DO2_eff
        DelO2 = DO2k_eff/(DO2k_eff+DO2N2_eff)

        Write(NTERM,110)
        110  Format('The Da_eff is (m^2/s)')
        Write(NTERM,*) Da_eff

        Write(NTERM,120)
        120  Format('The DelO2 is')
        Write(NTERM,*) DelO2

        Vconc_a = -((Rg*Top)/(2.0*F))*DLOG((1.0-((Rg*Top)/(2.0*F))*
     +       (ta/(Da_eff*yH2avg*Ppa))*zj)/(1.0+((Rg*Top)/
     +       (2.0*F))*(ta/(Da_eff*yH2Oavg*Ppa))*zj))
        Vconc_c = -((Rg*Top)/(4.0*F))*DLOG((((Ppa/DelO2)-((Ppa/DelO2)-
     +       (yO2avg*Ppa))*DEXP(((Rg*Top)/(4.0*F))*((DelO2*tc)/
     +       (Dc_eff*Ppa))*zj))/(yO2avg*Ppa)))
        Vconc = Vconc_a + Vconc_c
```

```
      Write(NTERM,130)
      130  Format('The concentration loss is (Volts)')
      Write(NTERM,*) Vconc

C     Actual voltage is given by the Nernst voltage minus the sum of the three losses

      V = VN - (Vohm + Vact + Vconc)

      Write(NTERM,140)
      140  Format('The SOFC voltage is (Volts)')
      Write(NTERM,*) V

C     The SOFC DC power 'Watts' is then calculated
      PDC = V*zI

      Write(NTERM,150)
      150  Format('The SOFC DC Power is (Watts)')
      Write(NTERM,*) PDC

C     SOFC AC electrical efficiency
C     DC-AC inverter efficiency assumed 92%

C     Fuel energy in (kW) calculation, data from Cengel & Boles 6th edition, LHV (kJ/kmol)
      zNRGIN = ((H2*241920.0)+(CO*282931.3)+(CH4*802952.15)
     +        +(C2H6*1428926.4)+(C3H8*2043454.98)
     +        +(C4H10*2637040.51))/3600.0

      Eta1 = ((PDC*0.92/1000.0) / zNRGIN)*100.0

      Write(NTERM,160)
      160  Format('The SOFC AC efficiency is (%)')
      Write(NTERM,*) Eta1

C     Plant gross electrical efficiency
      Eta2 = ((PDC*0.92/1000.0)/((BIOMAS/3600.0)*(ZLHV/1000.0)))*100.0

      Write(NTERM,170)
      170  Format('The plant gross electrical efficiency is (%)')
      Write(NTERM,*) Eta2

C     Plant net electrical efficiency: considering parasitic power
      Eta3 = (((PDC*0.92/1000.0)-((COMP1+COMP2+COMP3+PUMP1+PUMP2)/
     +       1000.0))/((BIOMAS/3600.0)*(ZLHV/1000.0)))*100.0

      Write(NTERM,180)
      180  Format('The plant net electrical efficiency is (%)')
      Write(NTERM,*) Eta3

C     Recoverable heat (kW): Q = m cp DeltaT
      Q = (FLUE/3600.0)*CPMX*(FLUET-25.0)

      Write(NTERM,190)
      190  Format('The useful heat is (kW)')
      Write(NTERM,*) Q

C     Plant gross CHP (overall) efficiency
      Eta4 = (((PDC*0.92/1000.0) + Q) /
     +        ((BIOMAS/3600.0)*(ZLHV/1000.0)))*100.0

      Write(NTERM,200)
```

```
      200  Format('The plant gross CHP efficiency is (%)')
      Write(NTERM,*) Eta4

C     Plant net CHP (overall) efficiency
      Eta5 = ((((PDC*0.92/1000.0)-((COMP1+COMP2+COMP3+PUMP1+PUMP2)
     +       /1000.0)) + Q)/((BIOMAS/3600.0)*(ZLHV/1000.0)))*100.0

      Write(NTERM,210)
      210  Format('The plant net CHP efficiency is (%)')
      Write(NTERM,*) Eta5

C     The plant gross power to heat ratio
      PHRATIO = (PDC*0.92/1000.0) / Q

      Write(NTERM,220)
      220  Format('The plant gross power to heat ratio is')
      Write(NTERM,*) PHRATIO

C     The plant net power to heat ratio
      PHRATIO2 = ((PDC*0.92/1000.0)-((COMP1+COMP2+COMP3+PUMP1+PUMP2)
     +           /1000.0))/Q

      Write(NTERM,230)
      230  Format('The plant net power to heat ratio is')
      Write(NTERM,*) PHRATIO2

C     SYNGAS energy (kW) calculation, data from Cengel & Boles 6th edition, LHV (kJ/kg)
      SYNGAS = ((GH2*120000.0)+(GCO*10100.0)+(GCH4*50050.0)
     +       +(GC2H6*47520.0)+(GC3H8*46340.0)
     +       +(GC4H10*45370.0))/3600.0

      zLHV2 = (SYNGAS/((GH2 + GCO + GCH4 + GCO2 + GN2)/3600))/1000

      Write(NTERM,240)
      240  Format('The SYNGAS power is (kW)')
      Write(NTERM,*) SYNGAS

      Write(NTERM,250)
      250  Format('The SYNGAS dry LHV is (MJ/kg)')
      Write(NTERM,*) zLHV2

      Write(NTERM,260)
      260  Format('The SYNGAS2 power is (kW)')
      Write(NTERM,*) zNRGIN

C     The DFB gasifier Cold Gas Efficiency (CGE)
      CGE = (SYNGAS / ((BIOMAS/3600.0)*(ZLHV/1000.0)))*100.0

      Write(NTERM,270)
      270  Format('The Cold Gas Efficiency (CGE) is (%)')
      Write(NTERM,*) CGE

C     Biomass power (kW)
      FUEL = (BIOMAS/3600.0)*(ZLHV/1000.0)

      Write(NTERM,280)
      280  Format('The Biomass fuel power is (kW)')
      Write(NTERM,*) FUEL
```

APPENDIX E: Combined system models – additional results

System comparison

The system 2 STCR sensitivity analysis results are displayed in Figure E.1. The trends match those of system 1 (section 5.3.4) but the results are incomparable as the actual SOFC STCR was considerably greater for system 1 due to the anode recycle (system 1 SOFC STCR range: 3.92-9.72 versus system 2 SOFC STCR range: 1.5-4.5). SOFC performance decreases with increasing STCR owing to a drop in Nernst voltage and an increase in voltage losses. The net plant efficiencies both degrade due to the rise in the biomass feed requirement. The decrease in $\eta_{CHP,net}$ is mainly put down to a fall in recoverable heat caused by a greater humidification steam requirement (9.07-76.03 kg/h over STCR range).

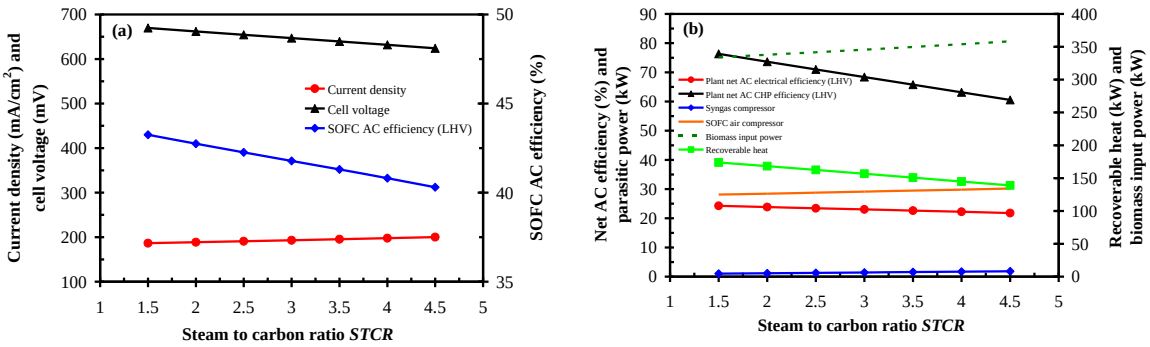

Figure E.1 Effect of steam to carbon ratio on system 2 performance

Figure E.2 shows the system 3 STCR sensitivity analysis results. The trends match those of system 1 (section 5.3.4) but the results are incomparable as discussed above for system 2. $\eta_{el,net}$ drops dramatically due to the rapid increase in syngas heater power requirement. Similar to system 2, $\eta_{CHP,net}$ falls because of the rise in humidification steam (8.82-73.2 kg/h over STCR range).

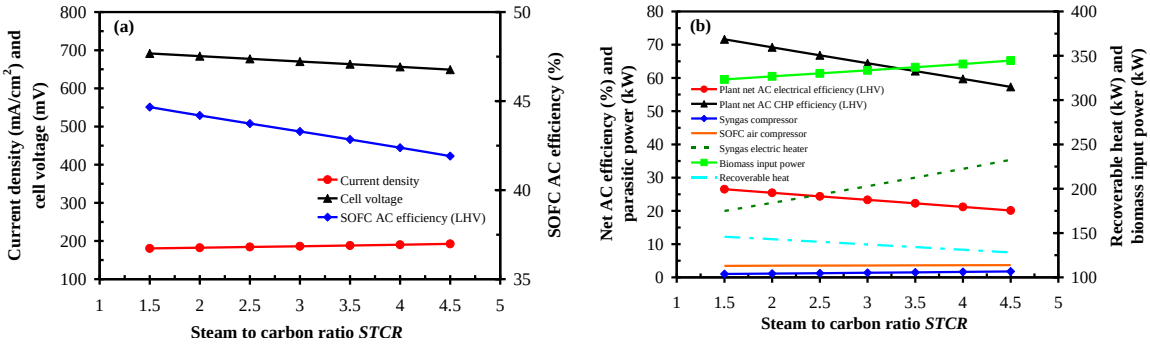

Figure E.2 Effect of steam to carbon ratio on system 3 performance

Fuel utilisation factor

The SOFC performance results for changing U_f are given in Figure E.3. Refer to section 5.3.4 for comments. The SOFC STCR increases from 3.18 to 4.63 due to the rising H_2O content in the recirculated depleted fuel.

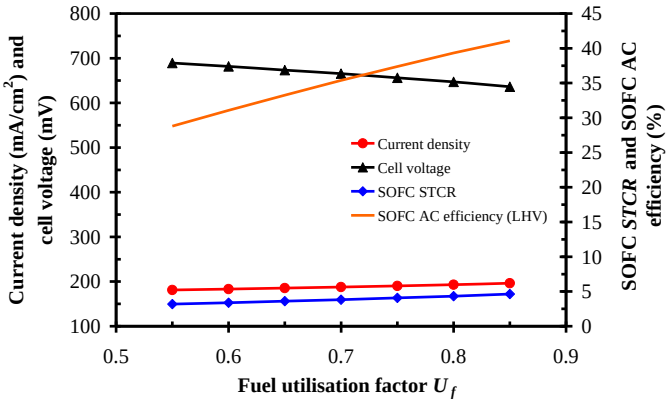

Figure E.3 Effect of fuel utilisation factor on system 1 SOFC performance

Gasification temperature

Figure E.4 shows that T_g has a very strong impact on syngas composition. Over the T_g range H_2 increases 25.4 pp (31.5% to 56.9%) and CO rises 19 pp (12% to 31%). Both CH_4 and CO_2 decrease; CH_4 drops from 24.4% to 0.1% and CO_2 from 30.5% to 10.6%. A reduction in the level of H_2O in the syngas is seen (31.7-22.6%). T_g has little

impact above 950 °C. The variation in syngas composition with T_g with regard to the chemical reactions occurring within the gasifier was discussed in section 4.3.3.

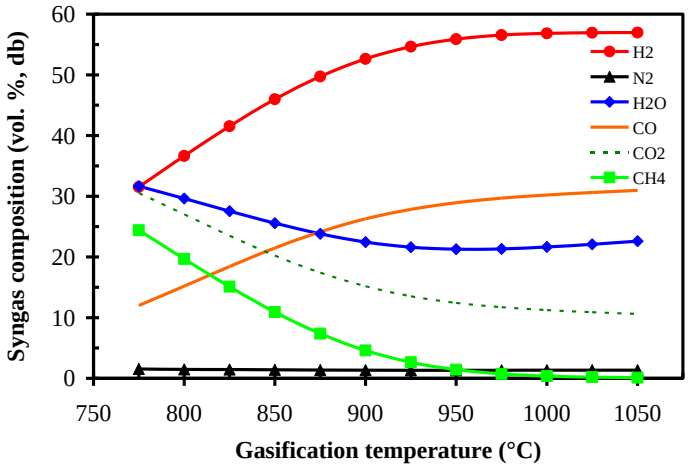

Figure E.4 Effect of gasification temperature on system 1 syngas composition

Figure E.5 depicts the effect that T_g has on SOFC stack performance. Performance degraded with rising temperature. The current increased, voltage dropped and efficiency showed a marked reduction (~10 pp).

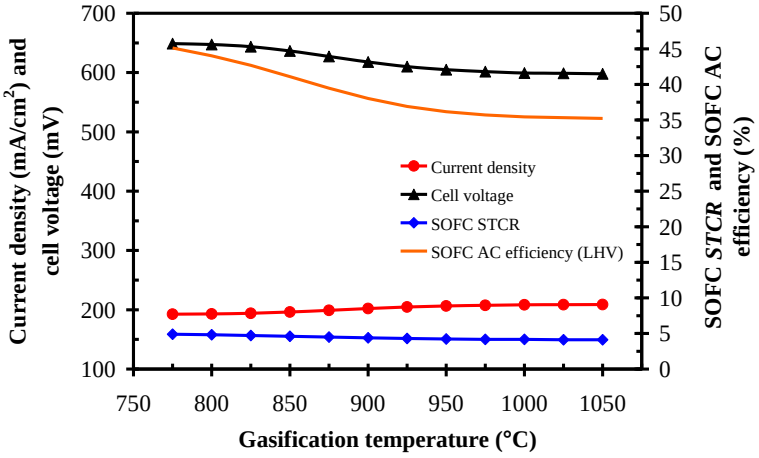

Figure E.5 Effect of gasification temperature on system 1 SOFC performance

Steam to biomass ratio

The influence of STBR on SOFC stack and overall plant performance is displayed in Figure E.6.

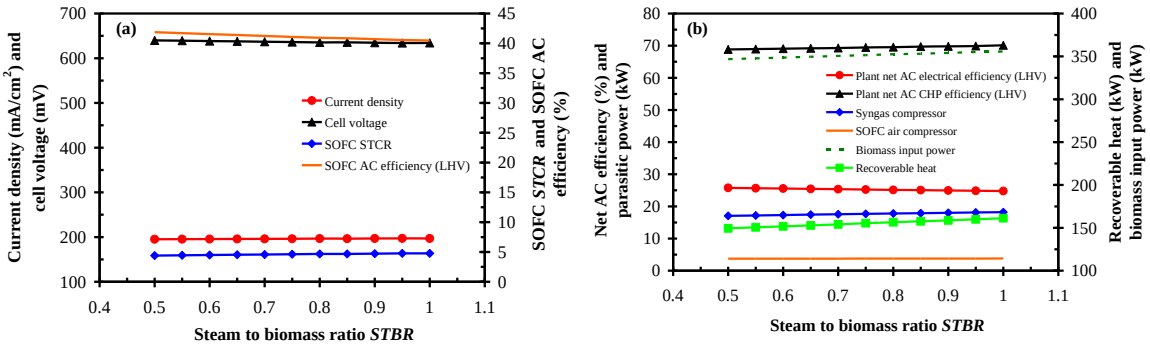

Figure E.6 Effect of steam to biomass ratio on system 1 SOFC stack and plant performance

Plant scale

The results for the scaled up 500 kWe system are given in Figure E.7. Compared to the base case system 1 results, the mass flow rates, power levels, etc., are four orders of magnitude greater. The performance indicators such as plant net efficiency, SOFC efficiency, etc., are equal to the base case system 1 values.

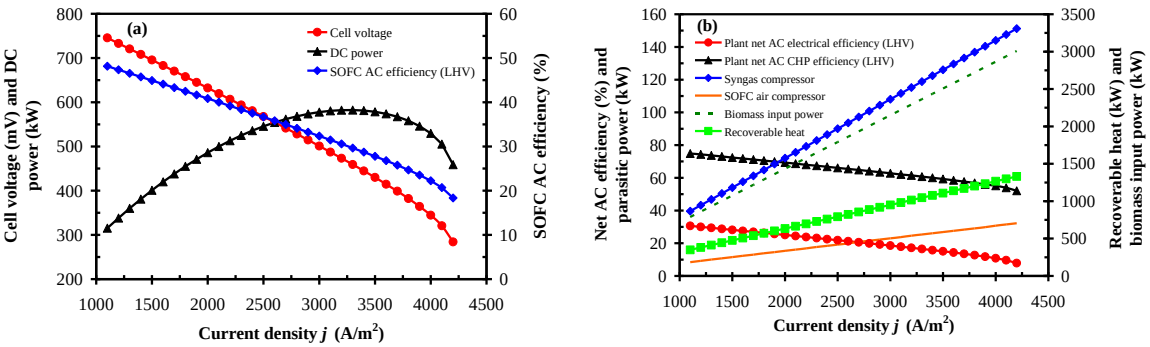

Figure E.7 500 kWe scale system performance